To the Graduate Council:

I am submitting herewith a dissertation written by John Robert Dees, entitled "An Experimental Study of Structure Development During Melt Spinning of Polyethylene Fiber." I recommend that it be accepted in partial fulfillment of the requirements for the degree of Doctor of Philosophy, with a major in Chemical Engineering.

J. E. Spruiell

J. E. Spruiell, Major Professor

We have read this dissertation
and recommend its acceptance:

Edward S. Clark

Joseph J. Cerra

James L. White

James F. Kinstle

Accepted for the Council:

Hilton A. Smith

Vice Chancellor
Graduate Studies and Research

AN EXPERIMENTAL STUDY OF STRUCTURE DEVELOPMENT DURING MELT SPINNING OF POLYETHYLENE FIBER

A Dissertation

Presented to

the Graduate Council of

The University of Tennessee

In Partial Fulfillment

of the Requirements for the Degree

Doctor of Philosophy

by

John Robert Dees

June 1974

To

Bomar and Retha Ellen Dees

1146684

ACKNOWLEDGEMENTS

There are many people who in some way assisted in the completion of this dissertation and the research preceding it. While it is not possible to mention everyone involved, there are several persons who deserve special mention and recognition for their efforts.

I am indebted to my adviser Dr. J. E. Spruiell for his guidance and patience throughout this work. I am also indebted to Dr. J. L. White for suggesting this area of research and supporting it with his continuing interest.

The capable assistance of the personnel of the Machine Shop and Electrical Shop of the Chemical and Metallurgical Engineering Department is gratefully acknowledged. This research depended heavily on these men for installation and maintenance of several major equipment components.

Financial assistance was provided by the National Science Foundation, the Chemical and Metallurgical Engineering Department, and Monsanto Textiles Company. This support is gratefully acknowledged. I am also grateful to Monsanto for the use of its Technical Center computer facilities and other services during the analysis of data and writing of this dissertation. The work of my fellow employees who multilithed this dissertation is gratefully acknowledged.

I am especially indebted to Dr. J. H. Saunders, R. L. Ballman, and J. B. McKoy, Jr. for their patience, support, and encouragement during the data analysis and writing stages.

The work of Carole Rainwater in typing and assisting in preparation of the final copy is gratefully acknowledged.

I wish to also acknowledge the many students and faculty members who made my stay at the University an enjoyable and stimulating experience.

Without the continuous support of my family this work would not have been possible. To my wife Jo Ann and my daughters Sheron and Kathy I express my greatest love and appreciation.

ABSTRACT

The development of crystallinity, orientation, and morphology during the melt spinning of linear polyethylene fiber was investigated. A moveable screw extruder spinning machine was constructed to facilitate examination of the spinning fiber from the spinneret to a point 175 cm down the spinline. The spinning machine was positioned over a rotating anode x-ray generator to allow direct x-ray diffraction studies on the moving filament. Filament diameter, temperature, and tension were also measured.

Eight sets of process conditions were examined by obtaining filament diameter, temperature, and wide angle x-ray diffraction patterns at numerous positions along the spinline. The x-ray patterns were analyzed by scanning microdensitometer and computer to obtain percent crystallinity and crystalline orientation functions. Analysis of experimental data produced values of filament velocity, velocity gradient, density, stress, and elongational viscosity as functions of distance from the spinneret. Crystallization rates and crystallization rate constants were calculated from x-ray crystallinity data. Density, birefringence, tensile properties, wide and small angle x-ray diffraction patterns, pole figures, and electron micrographs were obtained on final fibers.

Observed crystallization rates were several orders of magnitude higher than rates observed in quiescent melts at the same temperatures. Crystallization began at an initially high rate at a point near the maximum velocity gradient in the fiber and continued

at decreasing rates further down the spinline. Crystallization rates increased with increasing takeup stress in spinning.

Orientation along the spinline was essentially the same as that observed in the final fiber at low and high takeup velocities. At intermediate velocities (100 to 200 m/min) the orientation decreased down the spinline. This change was attributed to an increase in lamellar twisting as crystallization progressed.

Spinline stress was found to have an important role in crystallization kinetics and development of morphology in the spinning fiber. Final fiber properties correlated well with crystalline orientation as obtained by x-ray diffraction methods.

TABLE OF CONTENTS

CHAPTER		PAGE
I.	INTRODUCTION	1
II.	LITERATURE SURVEY	5
	Crystallization in Polymers	5
	Morphological Features of Polymer Crystallization	5
	Nucleation in Polymer Crystallization	9
	Strain Induced Crystallization	12
	Fiber Melt Spinning	15
	Rheology of Spinning	15
	Heat Transfer	18
	Structure Development	21
	Experimental Studies of Structure Development .	21
	Theory of Structure Development	23
III.	THEORY	28
	Continuity Equation and Momentum Balance on the Fiber	28
	Continuity Equation	29
	Momentum Equation	30
	Heat Balance on a Spinning Fiber	35
	Structure Development in a Spinning Fiber	37
	Crystallization Kinetics	37
	Orientation During Melt Spinning	41
IV.	EXPERIMENTAL EQUIPMENT, MATERIALS, AND PROCEDURES . .	44
	Equipment	44
	Melt Spinning Equipment	44

CHAPTER PAGE

Rigaku-General Electric Rotating Anode X-Ray Generator 48

Rothschild Tensiometer 49

Hastings-Raydist Match-Temp Pyrometer 49

Photographic Equipment 50

Tech/Ops Microdensitometer 51

Small Angle X-Ray Scattering Equipment 53

Pole Figure Equipment 53

Scanning Electron Microscope 53

Instron Tensile Tester 54

Density Gradient Columns 54

Birefringence Microscope 54

Computers 54

Materials 55

Data Collecting Procedures 55

V. DATA ANALYSIS 58

Calculation of Crystallinity and Orientation from X-Ray Diffraction Patterns 58

Crystallinity 58

Orientation Functions 62

Empirical Equation Used for Data Smoothing 62

Mechanical Aspects of the Spinning Process 64

Velocity and Velocity Gradient 64

Force Balance 67

Rheological and Time Scale Calculations 68

CHAPTER PAGE

Analysis of Crystallinity Data 69

Crystallization Rate 69

Crystallization Rate Constants and Avrami Index 71

VI. RESULTS AND DISCUSSION 74

Filament Diameter, Velocity, and Temperature Profiles 75

Spinline Stress and Elongational Viscosity 85

Development of Crystallinity 88

Development of Crystalline Orientation 99

Small Angle X-Ray Scattering 107

Scanning Electron Microscopy 110

Birefringence, Tensile Properties, and the Role of Spinline Stress 112

Morphological Model for Melt Spun Linear Polyethylene Fiber 117

VII. CONCLUSIONS AND RECOMMENDATIONS 122

Conclusions 122

Diameter, Velocity, and Temperature 122

Elongational Viscosity and Stress 123

Crystallization 124

Orientation, Morphology, and Mechanical Properties 124

Recommendations 125

LIST OF REFERENCES 128

APPENDICES 135

A. Experimental Data 136

B. Computer Programs 173

C. Equipment Operating Instructions 200

VITA 224

LIST OF TABLES

TABLE		PAGE
I.	Spinning Conditions for Linear Polyethylene Samples	74
II.	Final Fiber Deniers	77
III.	Crystallization of Tenite Linear Polyethylene in Differential Scanning Calorimetry	84
IV.	Ultimate Crystallinity Developed During Spinning	91
V.	Crystallization Half Time During Spinning	96
VI.	Long Periods of Spun Fibers	109
VII.	Spinning Run Conditions	136
VIII.	Constants for Empirical Diameter Versus Distance Equation	137
IX.	Constants for Empirical Velocity Versus Distance Equation	138
X.	Constants for Empirical Crystallinity Versus Distance Equation	139
XI.	Run PE01 Experimental Distance, Diameter, and Temperature Data	140
XII.	Run PE02 Experimental Distance, Diameter, and Temperature Data	141
XIII.	Run PE03 Experimental Distance, Diameter, and Temperature Data	142
XIV.	Run PE04 Experimental Distance, Diameter, and Temperature Data	143
XV.	Run PE05 Experimental Distance, Diameter, and Temperature Data	144
XVI.	Run PE06 Experimental Distance, Diameter, and Temperature Data	145
XVII.	Run PE07 Experimental Distance, Diameter, and Temperature Data	146

TABLE		PAGE
XVIII.	Run PE08 Experimental Distance, Diameter, and Temperature Data	147
XIX.	Run PE09 Experimental Distance, Diameter, and Temperature Data	148
XX.	PE01 Calculated Spinline Data	149
XXI.	PE02 Calculated Spinline Data	150
XXII.	PE03 Calculated Spinline Data	151
XXIII.	PE04 Calculated Spinline Data	152
XXIV.	PE05 Calculated Spinline Data	153
XXV.	PE06 Calculated Spinline Data	154
XXVI.	PE07 Calculated Spinline Data	155
XXVII.	PE08 Calculated Spinline Data	156
XXVIII.	PE09 Calculated Spinline Data	157
XXIX.	Distance Versus Time of Travel from the Spinneret	158
XXX.	PE01 Spinline Forces	159
XXXI.	PE02 Spinline Forces	160
XXXII.	PE03 Spinline Forces	161
XXXIII.	PE04 Spinline Forces	162
XXXIV.	PE05 Spinline Forces	163
XXXV.	PE06 Spinline Forces	164
XXXVI.	PE07 Spinline Forces	165
XXXVII.	PE08 Spinline Forces	166
XXXVIII.	PE09 Spinline Forces	167
XXXIX.	PE01 Distance Versus Measured Crystallinity . .	168
XXXX.	PE02 Distance Versus Measured Crystallinity . .	168

TABLE		PAGE
XXXXI.	PE03 Distance Versus Measured Crystallinity . .	169
XXXXII.	PE04 Distance Versus Measured Crystallinity . .	169
XXXXIII.	PE05 Distance Versus Measured Crystallinity . .	170
XXXXIV.	PE06 Distance Versus Measured Crystallinity . .	170
XXXXV.	PE07 Distance Versus Measured Crystallinity . .	171
XXXXVI.	PE08 Distance Versus Measured Crystallinity . .	171
XXXXVII.	PE09 Distance Versus Measured Crystallinity . .	172

LIST OF FIGURES

FIGURE		PAGE
1.	Diagram Illustrating the Proposed Fringed Micelle Structure of Semicrystalline Polymers	6
2.	Schematic Diagram of a Portion of a Lamellar Crystallite with the Polymer Chains in a Regularly Folded Array	6
3.	Proposed Overall Picture of Polymer Structure for Melt Crystallized Sample Showing Interrelation of Various Morphological Units within a Developing Spherulite	8
4.	Incremental Volume Element in Fiber at Position X . . .	29
5.	Schematic of Experimental Equipment	45
6.	Photograph of Moveable Spinning Extruder and Rotating Anode X-Ray Generator	46
7.	Schematic of Wide Angle X-Ray Diffraction Pattern of Polyethylene	59
8.	Diffracted Intensity Versus 2Θ Angle Along the Equator of a Polyethylene WAXS Pattern	60
9.	Schematic of Diffraction Pattern Showing Angles 2Θ and Ψ	61
10.	Types of Curves Described by the Function $y = A \exp\left(B\left(\frac{x-C}{D}\right)^E\right) + F$	65
11.	Filament Diameter Versus Distance from Spinneret . . .	76
12.	Velocity as a Function of Distance from the Spinneret .	78
13.	Velocity Gradient as a Function of Distance from the Spinneret	79
14.	Fiber Surface Temperature Versus Distance from the Spinneret	81
15.	Temperature of Plateau in the Temperature Profile Versus Takeup Velocity	83
16.	Tensile Stress in Spinning Filament as a Function of Distance from the Spinneret	86

FIGURE		PAGE
17.	Typical Plot for Crystallinity Versus Distance from Spinneret	89
18.	Crystallinity Versus Distance from Spinneret Comparison of Results for Several Runs	90
19.	Crystallinity Versus Time After Leaving Spinneret Showing the Effect of Increasing Takeup Velocity at Constant Mass Flow Rate	92
20.	Crystallinity Versus Time from Start of Crystallization Showing the Effect of Changing the Mass Flow Rate	93
21.	Crystallization Rates Versus Temperature as Calculated from Fitted Crystallinity Versus Distance Functions	95
22.	Plot of Crystallization Rate at the Half Time Versus Spin Line Tension	98
23.	Crystallization Rate Constants Calculated from Equation (108) with an Exponent of One and Plotted Versus Temperature	100
24.	Plot of Phase Transformation Data as $-\ell n\,(1-\theta)$ Versus Time	101
25.	Slopes of the $-\ell n\,(1-\theta)$ Versus Time Plots Shown Plotted Against Takeup Stress in the Spinline . . .	102
26.	Pole Density Distributions for the 200 and 020 Reflections at Takeup Velocities of 50 m/min, 200 m/min, and 556 m/min	104
27.	Crystalline Orientation Functions Versus Takeup Velocity	105
28.	Variation of Crystalline Orientation Functions Along Spinline for Takeup Velocities of 50 m/min, 100 m/min, and 556 m/min	106
29.	Pinhole SAXS Patterns for a Low Takeup Velocity (50 m/min, PE03) and a Relatively High Takeup Velocity (400 m/min, PE06)	108
30.	Scanning Electron Micrographs of the Surface Texture of Polyethylene Fibers Spun with Takeup Velocities of 50 m/min and 556 m/min	111

FIGURE PAGE

31. Birefringence of Fiber Versus Stress During Spinning 113

32. Tensile Strength and Elongation to Break Versus c-axis Crystalline Orientation Function 115

33. Young's Modulus Versus c-Axis Crystalline Orientation Function 116

34. Morphological Model of Structures Developed in As-Spun Polyethylene Fiber 118

35. Design Drawing for Four Hole Spinneret 204

LIST OF SYMBOLS

a	Material constant in orientation equation.
A	Fiber cross sectional area.
$A(\theta)$	Optical constant in orientation equation.
$A,B,C,D,E,F,$	Constants in empirical equation.
C_p	Specific heat.
$\frac{dV}{dx}$	Velocity gradient.
d	Fiber diameter.
$Ei(x)$	Integral exponential function.
f	An orientation factor.
F_{ext}	External takeup force
F_x	Force at point x.
F_{rheo}	Rheological force.
F_{grav}	Gravity force.
F_{inert}	Inertia force.
F_{drag}	Air drag force.
F_{surf}	Surface tension force.
g	Gravity constant.
h	Heat transfer coefficient.
ΔH	Enthalpy of fusion.
$k(T)$	Isothermal crystallization rate constant.
$K[T(t)]$	Isothermal crystallization rate constant used in nonisothermal equations.
L	Length of spinline; position of takeup unit on spinline.
$\dot{M}$	Rate of momentum change.

n	Avrami exponent.
Δn	Birefringence.
$\dot{N}$	Nucleation rate.
R	Cooling parameter.
S	Deformation ratio
t	Time.
T	Temperature.
T_a	Ambient temperature.
T_g	Glass transition temperature.
T_m	Melting temperature.
$v(t,\tau)$	Volume of crystal at time t that started growing at time τ.
V	Fiber velocity.
$w(t,\tau)$	Weight of crystal at time t that began growing at time τ.
W	Mass flow rate.
x,y,z	Axes of rectangular coordinate system.
X	Mass fraction.
X_∞	Mass fraction transformed at time $t=\infty$.
X'	Ficticious fraction of material transformed.
$\alpha_{\parallel}$, $\alpha_{\perp}$	Average polarizabilities per unit volume of the crystal parallel to and perpendicular to the c-axis.
η	Average refractive index.
η_e	Trouton viscosity.
θ	Degree of transformation.
Θ	Bragg angle in x-ray diffraction.
ρ_a	Density of amorphous polymer.

ρ_c	Density of crystalline polymer.
ρ_L	Density of molten polymer.
σ_d	Air drag coefficient.
σ_L	Takeup stress.
σ_s	Surface tension of fiber.
τ	Relaxation time.
τ_{xx}	Stress on x plane in x direction.

CHAPTER I

INTRODUCTION

In recent years the production rate of synthetic fibers has exceeded a billion pounds per year. The commercial success of synthetic fiber manufacturing processes has been enhanced by the works of investigators using scientific approaches to develop an understanding of the complexities of the spinning process. One aspect which is still the subject of intensive research is that of structure development in synthetic fibers during melt spinning of high molecular weight materials such as polyamides, polyesters, and polyolefins. This dissertation details a study of synthetic fiber structure development. Its goal is an experimental investigation of the development of crystallinity, orientation, and morphology during melt spinning of fibers and the interpretation of experimentally observed phenomena in terms of existing theories.

Since man-made polymers were successfully commercialized in the first half of this century, they have become some of the most important materials used by man. In fact, they are now found in almost every phase of our daily lives. Polymer production for use in fibers, films, and fabricated parts has steadily increased through the years, and the growth trend continues.

Little was known about the properties of the first polymeric substances synthesized in the laboratory. To gain an understanding of the properties of these materials, scientists began investigating polymers from a variety of viewpoints. From these first efforts research has continuously expanded, and our knowledge of polymers has

increased rapidly. Topics which were unknown fifty years ago now comprise a sizeable part of the chemistry curricula in many universities, and entire university departments now exist to expand and teach the knowledge of polymer science.

As new applications were found for polymers, industry was quick to invent special techniques for manufacturing new products. An outstanding example of such a case is the use of polymers to manufacture synthetic fibers. Techniques for spinning fibers were developed and improved through the years to the point that a major segment of industry is now devoted solely to synthetic fiber manufacture.

Formation of a fiber by spinning consists of the extrusion of suitable material in melt or solution form through a small orifice and the solidification of the extruded strand. The idea for the process was borrowed from nature. This process is, in principle, like that used by a spider to spin its web or by a silkworm to wind its cocoon. The first recorded spinning of synthetic fiber was by Count de Chardonnet of France in the 1880's, who made fiber by extruding strands of nitrocellulose dissolved in a solution of alcohol and ether (112). The product became known as Chardonnet silk. This solution spinning process was used for other modified cellulose fibers and was the forerunner of modern wet spinning processes.

The synthesis of high polymers by Carothers (19) in the late 1920's opened the modern era of synthetic fibers. Several polymeric materials were found to have properties that were desirable in a fiber. The techniques developed for making fibers from polymers included wet and dry spinning processes, which are variations of

solution spinning developed from Chardonnet's original process, and melt spinning of polymers having sufficient thermal stability. Improvement of these early processes led to the techniques now used to make synthetic fibers from a variety of materials.

Empirical development of the spinning process improved it rapidly in the early years of fiber production. However, a continuing pursuit for a basic understanding of the phenomena occurring in the spinning process has led, in recent years, to considerable fundamental research and the development of theories to explain several of these phenomena both individually and in the combination occurring in spinning. To date these researches have been moderately successful; a quantitative description of many of the phenomena found in fiber spinning has been achieved.

The first attempt at a quantitative description of spinning was begun by Ziabicki and Kedzierska (115, 116, 120, 121, 122, 123, 124, 125) in the late 1950's. They used the framework of continuum mechanics to formulate the governing equations of mass, momentum, and energy conservation. From this beginning investigators have expanded the work to include several features of modern commercial processes. Their efforts have made possible a quantitative description of the momentum and heat transfer phenomena occurring in spinning. Within certain operating limits it is now possible to quantitatively predict heat transfer coefficients and interrelationships between fiber velocity, diameter, tensile stress, and temperature.

However, there are still parts of the spinning process which are incompletely understood. In particular, quantitative integration

of the various phenomena into a coherent model of the process is lacking. One of the major areas where information, understanding, and theoretical analysis are needed is the nonisothermal crystallization under molecular orientation which occurs during spinning. The research presented in this dissertation is directed toward a fuller understanding of this important part of melt spinning. In a more ambitious vein it is hoped that this research will eventually lead to a quantitative description of the melt spinning process.

The experimental approach used in this research was a direct examination of a steady-state fiber spinning process. A melt spinning apparatus was assembled to provide controlled, reproducible spinning conditions with an equipment configuration that permitted direct x-ray, temperature, and photographic examination of the critical fiber forming zone in the spinline. Various spinning conditions were studied to observe the effect of process variables on the development of structure in the fiber.

CHAPTER II

LITERATURE SURVEY

The literature dealing with crystallization during melt spinning is limited. Before beginning a review of the literature bearing directly on this subject, it would be well to present a brief summary of crystallization in polymers. Hence the first section of this survey deals with that subject. The second section is a discussion of melt spinning with emphasis on the development of structure during the fiber spinning process. The material presented in the first section is intended to serve as a background for a subsequent discussion of melt spinning.

A. CRYSTALLIZATION IN POLYMERS

Morphological Features of Polymer Crystallization

Early investigators of polymer crystallization used the fringed micelle model which assumed the polymer consisted of small crystallites, or micelles, connected by macromolecules to the surrounding amorphous material as shown schematically in Figure 1. Alfrey and Mark (3) used such a model as a basis for their statistical treatment of polymer crystallization in 1942. This model was not adequate, however, to describe the details of polymer structure. Single polymer crystals grown from solution gave directly observable evidence of a folded chain lamellar structure as shown in Figure 2. This evidence along with the discovery of spherulitic structure in polymers altered the approaches to theoretical analysis.

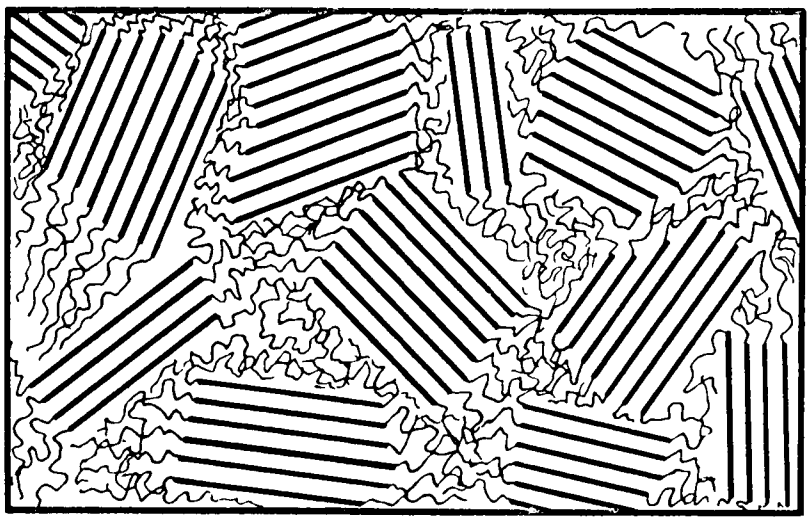

Figure 1. Diagram Illustrating the Proposed Fringed Micelle Structure of Semicrystalline Polymers.

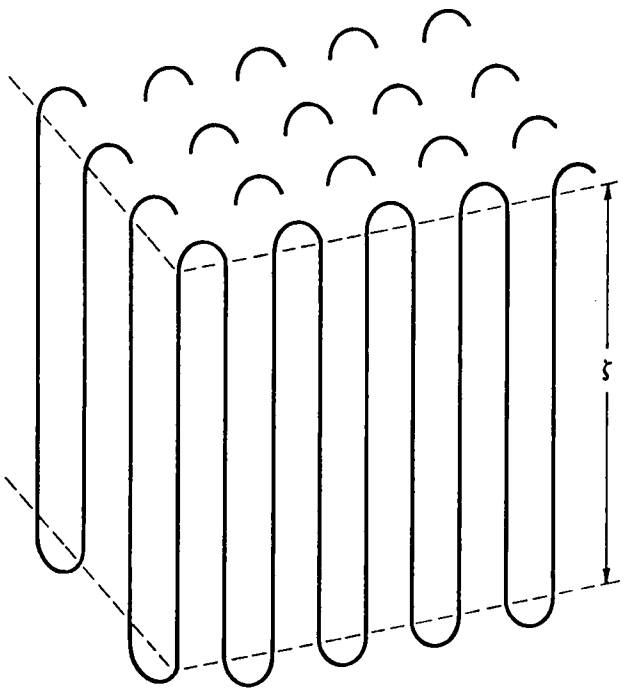

Figure 2. Schematic Diagram of a Portion of a Lamellar Crystallite With the Polymer Chains in a Regularly Folded Array.

The spherulite is the single most important morphological unit present in bulk polymer samples crystallized from the melt. It has been extensively investigated from the standpoint of its structure (41, 51, 53, 86) and the kinetics of its growth (18, 42, 63). Crystallites, microfibrils, fibrils, and dendrites have been observed in various polymers. These were often found as components of the larger spherulites. Even "granular" crystalline structure has been described as consisting of spherulites with suboptic dimensions. In his review of polymer morphology Sharples (93) presented the spherulite as a spherical structure consisting of branched fibrils radiating from a central nucleus as shown schematically in Figure 3. Each fibril consists of crystallites having folded chain structures with the molecule axes perpendicular to the fibril axes. The molecule axes were thus perpendicular to the spherulite radius.

Detailed models and mechanisms for spherulite growth were developed by Price (86), Keith (51, 53), and Gornick (32). The theory of folded chain lamellar growth in polymers was incorporated into a growth theory for spherulites by Hoffman (41), and expansion of theories based on the lamellar model have been made by Price (87), Frank and Tosi (28), and Binsbergen (14).

Crystallization kinetics of high polymers has been treated theoretically using the approach originally developed by Avrami (5, 6, 7) for nonpolymers. He derived the equation

$$X = 1 - e^{-kt^n}$$

where X is the mass fraction of transformed material, t is time, k is a crystallization rate constant and n is the Avrami exponent. Similar derivations were made by Johnson and Mehl (45), and Evans (25).

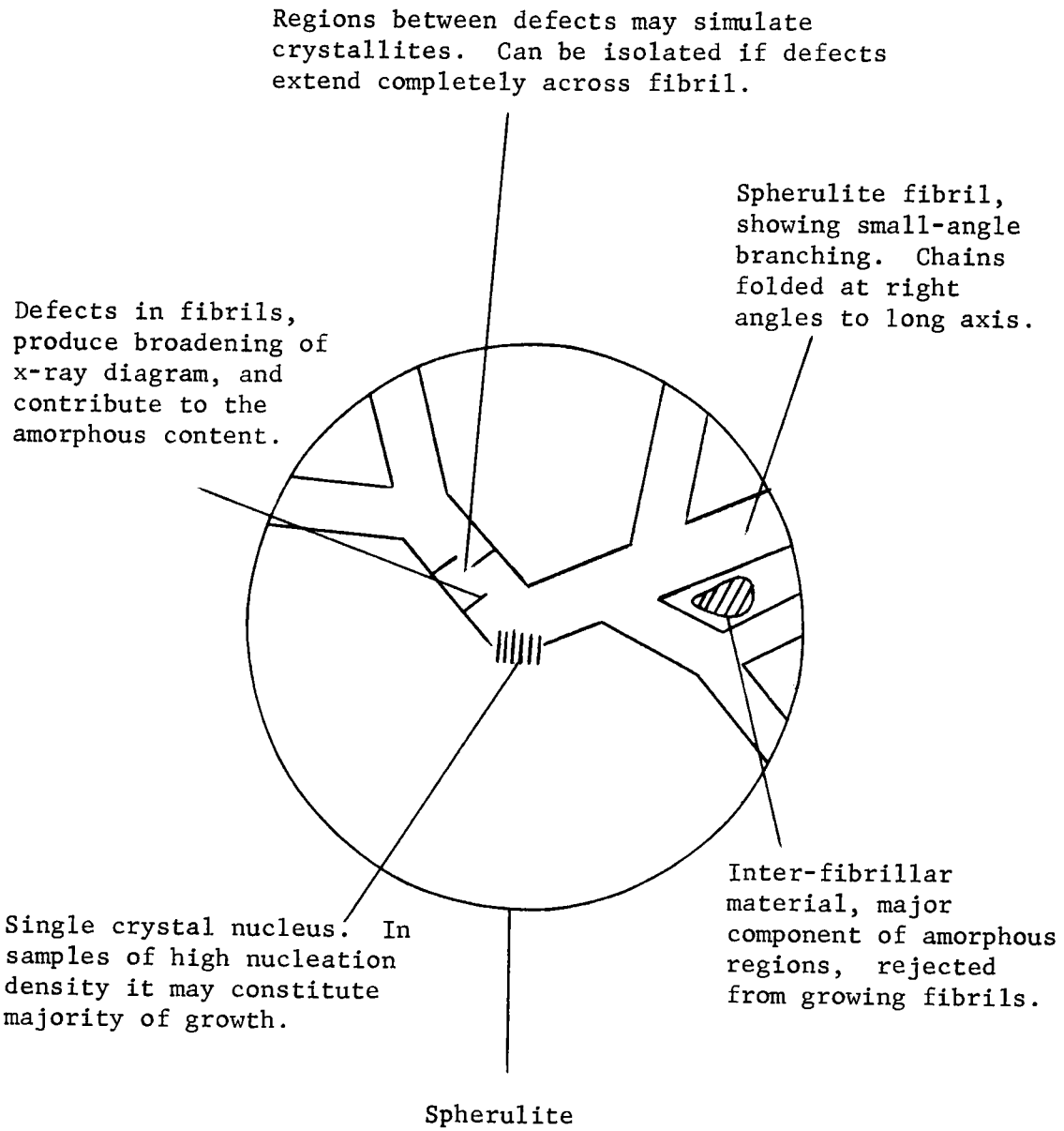

Figure 3. Proposed Overall Picture of Polymer Structure, for Melt-Crystallized Sample, Showing Interrelation of Various Morphological Units Within a Developing Spherulite. After Sharples (93).

Mandelkern (6, 65) subsequently modified Avrami's theory to describe the kinetics of polymer transformation from amorphous to partly crystalline composition. Modifications have also been made by Banks and Sharples (8, 9), and Lacko (62).

Numerous works on specific aspects of polymer crystallization can be found, and the literature is too extensive to review in its entirety. Additional information can be found in reviews by Mandelkern (67), Stuart (100), Keith (52), Baur (11), and Mark (71).

Nucleation in Polymer Crystallization

The crystallization of a substance includes two distinct processes, nucleation and growth. Investigations of the nucleation process in nonpolymers have been in progress for many years, and an extensive literature has resulted from these efforts. In this review emphasis will be placed on parts of the literature which apply to polymer systems. The reviews of Palermo and Bennett (83), Bradley (17), and the series of reviews beginning with Uhlman's article (107) may be consulted for nonpolymer nucleation theory.

Nucleation in polymer crystallization was first analyzed using theories developed for nonpolymeric materials (26). From that point until now there have been changes in the theory that make it more suitable to the actual phenomena seen in polymers. General discussions for nucleation in crystallization of polymers have been given by Price (88), Mandelkern (67), and Gornick and Hoffman (33). Classical homogeneous nucleation theory is based on the free energy change which results when converting one phase to another. Contributions to this free energy arise from a bulk free energy change per unit

volume and a surface free energy per unit area of growing phase. Using this concept one can assume a shape for a nucleus and calculate the dimensions for a critical size which must be achieved before growth can occur spontaneously with a decrease in free energy. A spherical nucleus is often assumed, and calculation of the critical nucleus radius is straightforward. In the case of polymers the nucleus is unlikely to be spherical. One approach assumes that the molecules form an elongated nucleus which can be approximately described as cylindrical. With proper assumptions the critical nucleus dimensions can be calculated for this case. A discussion of this calculation and its ramifications is given by Mandelkern (67).

Heterogeneous nucleation is defined as the nucleation caused by adventitious particles in the polymer. This phenomenon has become commercially useful in the polymer industry since it offers the manufacturer a means of changing the properties of his product by the addition of a small quantity of a nucleating agent. Several important papers have dealt with heterogeneous nucleation theory (106,24,68,69).

Early theoretical works in nonpolymers again formed the basis for initial explanations of heterogeneous nucleation in polymers. In 1950 Turnbull (106) published his theory of heterogeneous nucleation in phase changes in which he reviewed the experimental work of several investigators who studied the effect of added impurities upon the rate of phase change in solid-liquid nonpolymeric systems. Using theory developed for homogeneous nucleation on flat surfaces, Turnbull developed the kinetics of nucleation by solid phase material retained in conical and cylindrical pits in adventitious nuclei. He further

proposed an explanation of the effect of thermal history on nucleation rate based on the premise that stable embryos of the solid phase were retained in cavities of various types in the nucleating material at temperatures in excess of the melting temperature. He then showed how the size and number of such retained embryos decreased with increased temperature. This in turn changed the rate of nucleation upon cooling below the melting point.

Sharples (93), and Cormia et al. (23) performed some of the earlier nucleation experiments with polymers. Both of these investigators concluded that nucleation in most bulk polymers is entirely heterogeneous. Theoretical work in this field has been extensively pursued by Mandelkern and co-workers (24, 68, 69). Devoy and Mandelkern (24) specifically dealt with the theory of heterogeneous nucleation of long chain molecules. Their treatment of the process was an extension of Turnbull's (106) development to a system of long chain molecules which could not form spherical nucleus embryos because of the molecule geometry. They showed that the free energy barrier that must be overcome before spontaneous growth of a nucleus would be thermodynamically favored was lower for heterogeneous nucleation than for homogeneous nucleation. This condition, combined with a sufficiently large number of heterogeneities, would produce an increased nucleation rate.

Research directed toward identifying effective heterogeneous nucleating agents for various polymers has been quite active as may be seen, for example, in the case of polypropylene. Beck and Ledbetter (12) investigated the effectiveness of several nucleating agents using differential thermal analysis, and Binsbergen (15, 16) screened two

thousand substances for effective nucleating agents. Similar research has been carried out for polyethylene (84, 60), polyethylene terephthalate (115, 84), and other important polymers (60).

Strain Induced Crystallization

Although research in polymer crystallization has been extensive, it has dealt primarily with isothermal crystallization in stress free and unoriented polymers. It has been pointed out by many investigators that stress and molecular orientation play a very important part in polymer crystallization kinetics. Fiber spinning and injection molding are examples of industrial processes where crystallization under stress is an important factor in process dynamics and product quality. A summary of the literature dealing with this subject is given below.

In 1954 Gent (31) investigated stress relaxation caused by crystallization in stretched natural rubber vulcanizates. He found reasonable agreement between his data and the theories of Flory (27) and Avrami (5, 6, 7). In this case the effect of stress and orientation on crystallization was evident since these crosslinked materials would not crystallize at room temperature in a relaxed state. Yamamoto and White (114) recently refined the theory dealing with this type of strain induced crystallization in elastomeric network polymers. Evidence of the effect of orienting stress on structure was presented by Keller (54) in 1955. In his investigation of orientation phenomena in polyethylene and nylon 66 he obtained photos of unusual "row structure" crystal formations. The longitudinal axes of these formations were parallel to the deformation axes in the sample. Rabesiaka and Kovacs (89) observed a strong influence of sample

preparation method on the crystallization kinetics of polyethylene. They suggested the presence of "quasi-indestructible" nuclei which remained in the polymer above its melting point, and they also demonstrated a nucleating effect from pre-orientation in the sample. Maxwell (74) discussed stress induced nucleation and pressure induced crystallization in injection molding and how these phenomena could be used to alter the morphology of a material. In a discussion of deformation and crystallization Schuur (92) stated that a polymer subjected to shearing flow could crystallize far above its melting point. Binsbergen (13) investigated orientation induced nucleation in polypropylene. He observed crystalline structures oriented along lines of strain in deformed samples. Similarly Mitchell (76) observed a lowering of the Avrami exponent in synthetic rubber as a result of mechanically milling the rubber before crystallizing it. This was interpreted to be a change in kinetics caused by preorientation of the amorphous sample. McCord (78) measured crystallization rates in strained specimens of polyethylene terephthalate. He also observed that straining caused an increase in the number of nuclei and/or the rate of nucleation during subsequent isothermal annealing as evidenced by accelerated isothermal crystallization.

Symmetrical spherulites normally do not develop in polymers crystallized from the melt under an orienting stress. Lamellar crystals and fibrils form complex structures that are related to the deformation imposed during crystallization. A structure consisting of lamellae growing upon a central core of oriented long chain molecules has been frequently observed. This structure has been given the name "shish-kebab". Earlier mention of a similar morphology has been made under

the name "row structure" (109, 54).

Shish-kebabs have been produced by crystallizing polyethylene from hot xylene solution while stirring. Fibrous crystal growths appeared on the agitator during this type of experiment, and they possessed a highly oriented morphology. Krueger and Yeh (61) examined gold decorated shish-kebab structures and concluded that the lamellar crystalline overgrowths, known as the kebabs, were not separate surface growths but were interconnected with the shish by molecules passing through the structure. Keller and Wilhmouth (57, 58) examined stirring induced polyethylene crystals by several methods including electron microscopy and electron diffraction methods. They concluded that the shish-kebab contained a central core having a flat, ribbon shape which they named a micro-shish-kebab. This central ribbon core was more thermally stable and resistant to fuming nitric acid than conventionally crystallized material. They found from electron diffraction experiments that the crystallographic c-axis was parallel to the fiber direction and the a-axis was perpendicular to the ribbon plane.

Highly oriented polyethylene morphologies have been produced from the melt. Southern et al. (94) made filaments having a very high degree of crystalline orientation by extruding high density polyethylene near its melting point using high pressure in a capillary rheometer. They proposed a predominantly extended chain morphology to explain the high crystalline orientation and the unusual physical properties observed.

Orientation induced crystallization has been directly observed by Mackley and Keller (64) in a flowing stream of molten polyethylene. Their apparatus produced an elongating flow that was directly observable under polarized light. Long fibrous crystal structures were

seen to appear under certain flow conditions at temperatures above the equilibrium melting temperature. With the same apparatus similar crystal formations were observed in the flow field produced by passing molten polymer through a wire screen. Kobayashi and Nagasawa (59) investigated the crystallization of sheared polymer melts and presented a theoretical relationship between orientation and crystal volume growth rate.

B. FIBER MELT SPINNING

Rheology of Spinning

Ziabicki's treatment of the mechanical aspects of melt spinning included relationships for fiber diameter and velocity along the spin line (123), die swell at the spinneret exit (124), and tensile force and stress in the filament (117). The first and last of these articles are of interest in this section.

Ziabicki proposed the following criteria for a successful spinning process:

1. Continuity of flow,

$$A \times V \times \rho = \text{constant} = W \; ; \tag{1}$$

2. Limit for maximum stress,

$$\sigma_{max} \leq \bar{\sigma} \; , \tag{2}$$

where $\bar{\sigma}$ = tensile strength;

3. A strong increase in Trouton viscosity, η_e, along the spinline where Trouton viscosity is defined by

$$F/A = \eta_e \dot{\gamma} \; , \tag{3}$$

and F = tensile force in filament,

A = cross sectional area of filament,

$\dot{\gamma} = dV/dx$ = velocity gradient along the spin line. The relationships derived for spinning at constant tensile force were

$$\frac{V}{V_o} = \exp\left[\frac{\rho F}{W}\int_o^L \frac{1}{\eta_e}\,dx\right] , \tag{4}$$

$$\frac{d}{d_o} = \exp\left[-\frac{\rho F}{2W}\int_o^L \frac{1}{\eta_e}\,dx\right] , \tag{5}$$

where ρ = polymer density,

V_o = velocity at spinneret $(x = 0)$,

d_o = diameter at spinneret $(x = 0)$,

W = polymer mass flow rate.

In the last work of the three mentioned above Ziabicki discussed the components of tensile force F and summarized them as

$$F_{ext} = F_{rheo} + F_{drag} + F_{inert} , \tag{6}$$

with F_{ext} = external tensile force arising from winding apparatus,

F_{rheo} = rheological force,

F_{drag} = aerodynamic drag force,

F_{inert} = inertial force.

Small components due to gravity and surface tension were neglected.

Kase and Matsuo (46, 47, 48) made both transient and steady state analyses of melt spinning. In the steady state case their equations were of the same form as those resulting from Ziabicki's work with slight variations in the assumptions used during actual application to experiments. They derived equations (7) and (8).

$$V\left(\frac{\partial A}{\partial x}\right) + \left(\frac{\partial A}{\partial t}\right) = -A\left(\frac{\partial V}{\partial x}\right) \tag{7}$$

$$\frac{\partial V}{\partial x} = \frac{F}{\eta_e A} . \tag{8}$$

Non-Newtonian behavior in molten polymer has been considered in theoretical analyses of the spinning process by White (111), and Matovich and Pearson (72). An investigation of non-Newtonian melt behavior during isothermal spinning was presented by Acierno and coworkers (2). Hagler has investigated elongational viscosity of molten polyethylene in relation to melt spinning (35). Inclusion of a viscoelastic constitutive equation in the momentum balance of the spinning fiber would change equation (3) to

$$\sigma_{xx} = F_x/A \ , \tag{9}$$

and

$$\sigma_{ij} = -\rho\delta_{ij} + F_{ij}\left[e_m \underset{s=-\infty}{\overset{s=t}{}} (t-s)\right] \ . \tag{10}$$

In this respect theory is ahead of industrial practice. The mathematical complexities which arise from use of the above equation can be handled by modern computers. However there are few data available on the elongational viscosities of molten polymers, since a reliable method for obtaining such data has not been found. Thus a problem arises because the physical constants needed for a correct constitutive equation are not available. Kase and Matsuo (48) computed the apparent elongational viscosity from their data for polypropylene. Ishibashi et al. (43) made a similar calculation for nylon 6. Elongational viscosities calculated in this manner are useful approximations for predicting spinning processes only within a limited range of conditions.

Some research has been done on specialized aspects of melt spinning as illustrated by works such as that of Han (37) in which he deals with the rheology of fibers of noncircular cross sections. Such

studies are mentioned only as illustrations of the expansion of melt spinning research, and they will not be discussed in detail. Some reviews have summarized the results which were developed in recent years. Among these are the extensive reviews by Ziabicki (119, 120), and a short review by Perepelk (85) covering only the key aspects of melt spinning.

Heat Transfer

As the development of theory progressed for the mechanical aspects of spinning, it was also necessary to study heat transfer phenomena and their influence on the spinning process. Ziabicki (122) proposed a treatment based on the model of a hot cylinder suddenly immersed in an isothermal cooling medium. The resulting equations were quite complicated and required accurate knowledge of certain functions for exact calculations. Inclusion of simplifying assumptions improved the tractability of the equations slightly, but accuracy was not good in calculated answers.

Andrews (4) made a similar analysis of filament temperature versus length and also reached a solution which was difficult to apply to an actual spinning process. The complexity of this treatment, as well as Ziabicki's, was primarily due to the two dimensional approach to the problem in which radial temperature gradients were considered important. Wilhelm (112) applied Andrew's theory in evaluation of his extensive experimental work published in 1966 and obtained good agreement between theory and experiment in some cases.

Kase and Matsuo (46, 47, 48) presented heat transfer relationships in a form which was readily usable for calculations. Using a

simple heat balance on a differential element, they considered combined conduction-convection effects. In approximating an industrial spinning process the contributions of radiation and latent heat of crystallization were considered negligible to give:

$$V \frac{\partial T}{\partial x} + \frac{\partial T}{\partial t} = \frac{2\sqrt{\pi}\, h\, (T - Ta)}{C_p \sqrt{A}\, \rho} , \qquad (11)$$

where V = filament velocity,

T = temperature,

h = heat transfer coefficient,

A = cross sectional area,

ρ = filament density,

C_p = polymer specific heat,

T_a = ambient air temperature,

x = distance from spinneret,

t = time.

For steady state spinning conditions the $\frac{\partial T}{\partial t}$ term was set to zero. Kase and Matsuo provided correlations for h which included the effect of transverse quench air flow. Their treatment of the problem permitted easy calculation of fiber temperature as a function of distance from the spinnerette.

In their derivation, latent heat of crystallization was assumed negligible; and deviations from theory are often traceable to this assumption. Nakamura (79) and co-workers included heat of crystallization in an energy balance similar to that of Kase and Matsuo, and derived an expression relating fraction of crystallinity to polymer temperature. These equations are

$$\Delta H d\theta - R\,(T - T_a)\,dt = C_p dt\,, \tag{12}$$

$$\theta(t) = 1 - \exp\left[-\left\{\int_o^t K(T(\tau))\,d\tau\right\}^n\right]\,, \tag{13}$$

where ΔH = latent heat of crystallization,

θ = fraction of crystalline form,

C_p = specific heat,

T = polymer temperature,

T_a = environment temperature,

R = a "cooling parameter",

n = Avrami index,

$K(T) = k(T)^{1/n}$ where k is the isothermal crystallization rate constant in the Avrami equation,

t = time.

These two equations can be solved numerically by computer for a given set of conditions.

Several works have treated specific aspects of heat transfer in melt spinning. Acierno (2) et al. investigated boundary layer phenomena in spinning. Barnett (10) used computer techniques to calculate the temperature of filaments in forced and free convection, and with acceleration, radiation, and free stream turbulence effects considered. Copley (22) and co-workers investigated the effects of filament attenuation on axial temperature gradient of a fiber.

Morrison (77) made a numerical analysis of the cooling of a molten filament as it solidified from the melt. His analysis used a cylindrical coordinate system to describe the position of the solid-liquid interface and the effects of the heat of fusion, convective, and

radiative heat transfer on fiber temperature. Dimensionless variables were used to simplify the mathematics and calculate the temperature profile along the fiber radius and down the spinline.

A review of literature dealing with heat transfer in melt spinning has been made by Wanger and Fox (110).

Structure Development

The properties of melt spun, synthetic fibers are highly dependent on the spinning conditions used in their production. This behavior is presumably due to the effect of process variables on the structure of the spun filament. The formation of structure, i.e., crystallinity, orientation, and crystalline morphology, during the melt spinning of a partially crystalline polymer is complicated by the combined influences of rheological factors (stretching of the melt) and non-isothermal effects resulting from the heat transfer from the running filament. Because of these complications and in spite of a rapidly developing industry, early work was largely empirical, and fundamental study of the interaction of rheological behavior and structure formation did not begin until the late 1950's.

Experimental Studies of Structure Development. The crystalline structure of fibers was investigated in 1962 by Hearle (38) although he dealt only with fibers and not with spinning processes. Keller (55) qualitatively discussed orientation and crystallinity in melt spun synthetic fibers and gave supporting x-ray data from nylons, polyethylene, and polyethylene terephthalate.

Several investigators have examined the relationship between spinning conditions and the structure in the final fiber. In a series

of articles Ziabicki and Kedzierska (116, 121, 125) presented an extensive experimental and theoretical investigation of orientation and crystallization in melt spinning. Their work also extended into a discussion of the effect of polymer molecular structure upon the orientation observed in melt spun fibers (125). These authors found that the molecular orientation as measured by birefringence increased with spin line tension, the difference between the take-up and extrusion velocities, and the inverse of the filament diameter. Abbott and White (1) studied the melt spinning of high and low density polyethylene over a wide range of spinning conditions. They examined the variation of crystallinity and orientation in the final fiber with spinning speed, polymer flow rate, and melt temperature. They further examined the mechanical properties of the final fiber and found strong correlations with crystalline orientation. Ishikawa (44) studied the morphology of polyethylene fibers using special compression and stretching techniques combined with x-ray diffraction methods. He observed differences in morphology in fibers made under different spinning conditions.

Fung and Carr (29) studied the morphology of melt spun polyethylene fibers. From electron micrographs of the fiber surface they concluded that row nucleated structure occurs in a fiber and that it is caused by orientation of the melt during draw down to the final fiber diameter. They concluded that a stress-induced morphology was produced by a skin-core effect in the solidifying fiber which caused the skin layer to move faster than the molten core material. Birefringence measurements made across the diameter of the fiber showed

higher orientation at the fiber surface than at the center. This was interpreted as evidence of chain tilting with respect to the fiber axis at an angle which varied with radius.

Direct x-ray investigation of a spinning filament was first used by Chappel et al. (20) in their study of crystallization phenomena in rapidly quenched nylon 66. Their results were qualitative in nature and were limited to specific problems regarding only nylon 66 behavior. A more complete and significant investigation of the development of structure during the spinning process was made by Katayama, Amano, and Nakamura (49). They combined measurements of filament surface temperature, diameter, birefringence, and both wide angle (WAXS) and small angle x-ray scattering (SAXS) to study the formation of structure in polyethylene, polypropylene, and polybutene-1. In addition to demonstrating the increase in crystallization rate due to molecular orientation during melt spinning, their results showed a morphology consisting of lamellar and interlamellar regions stacked normal to the fiber axis and called attention to the interaction between the heat of crystallization and the rate of heat transfer from the running filament. Nakamura and co-workers (79, 80, 81) have subsequently treated the effect of heat of crystallization on fiber temperature in greater detail as was discussed in the previous section.

Theory of Structure Development. A theory of development of orientation during melt spinning was first developed by Ziabicki and Kedzierska (116, 121, 125). They derived differential equations of orientation for rigid ellipsoids and flexible coiled chain macromolecules flowing through a parallel velocity gradient field. To

quantitatively express orientation, a coefficient of fiber orientation was also derived. The equations were complicated and not analytically solvable. In a later article Ziabicki (118) simplified the orientation function equations and demonstrated their qualitative correctness by showing agreement with experimental data.

The above authors assumed the final orientation in the spun fiber to result from a balance between orientation produced by elongational flow in the melt and randomization caused by thermal motion of molecules. The rate of change of orientation down the spinline was thus assumed to follow the equation

$$\frac{df}{dt} = a\frac{dV}{dx} - \frac{f}{\tau} \quad , \tag{14}$$

where f = an orientation factor,

τ = a relaxation time characteristic of the polymer,

a = a constant characteristic of the polymer.

Solution of this equation, following various substitutions and assumptions, and evaluation at the takeup point produced an expression for final orientation in the fiber as a function of process variables.

$$f_L = a \exp\left\{3/k\sigma_L\right\}\left[E_i(-3S/k\sigma_L) - E_i(-3/k\sigma_L)\right] , \tag{15}$$

where $S = V_L/V_o$, the deformation ratio,

σ_L = takeup stress,

a, k = constants characteristic of the material,

and $E_i(x)$ is the integral exponential function.

Nishiumi (82) derived a similar equation relating birefringence in the fiber to process variables

$$\frac{d\Delta n}{dt} = A(\theta)\frac{dV}{dx} - \frac{\Delta n}{\tau(\theta)} \quad , \tag{16}$$

where Δn is birefringence, $A(\theta)$ is an optical constant, and $\tau(\theta)$ is a relaxation time.

Crystallization during melt spinning has also been treated theoretically by Ziabicki (118, 119, 120). He began with the Avrami equation as originally derived for isothermal crystallization and modified it for application to the nonisothermal conditions existing in melt spinning. The overall crystallization rate constant, although independent of time, depended on temperature which varied with time. He assumed that the rate of transformation $\frac{d\theta}{dt}$ could be described with the aid of a first order kinetics equation. Based on this assumption he derived the equation

$$\theta(t) = 1 - \exp\left\{-\int_o^t K[T(\tau)]d\tau\right\} \quad . \tag{17}$$

As a further simplification of this equation, Ziabicki defined the "kinetic crystallizability" as

$$G = \int_{T_g}^{T_m} K(T)dT \quad , \tag{18}$$

where $K(T)$ = isothermal crystallization rate constant,

T_m = polymer melting temperature,

T_g = glass transition temperature.

Using this parameter in conjunction with an assumed constant rate of cooling

$$\xi = dT/dt \quad , \tag{19}$$

he expressed the degree of crystallinity as

$$\theta = 1 - \exp\ (G/\xi) \quad . \tag{20}$$

Qualitative agreement was observed between this theory and part of the experimental data appearing in the literature.

Nakamura, Katayama, and Amano (80) also began with the Avrami equation and modified it to describe nonisothermal crystallization. The equation thus derived was

$$\theta = 1 - \exp\left[-\left\{ \int_o^t K[T(\tau)]d\tau \right\}^n \right] \quad , \tag{21}$$

where $K(T) = k(T)^{1/n}$ where $k(T)$ is the isothermal crystallization rate constant and n is the Avrami index determined from the data of isothermal crystallization. When combined with a suitable expression for calculating $k(T)$ and with the heat balance equation previously presented, this equation can be used to approximate the crystallinity and temperature changes in nonisothermal spinning. The investigators used numerical techniques to obtain solutions for melt spinning, and for crystallization in a quiescent melt under nonisothermal conditions (79, 80). In a more detailed extension of their theory, the calculation method was used for a numerical simulation of crystallization in a spinning fiber with radial variations in temperature included (81). A general theory of crystallization under nonisothermal and stressed or oriented conditions was given by Abbott and White (1) along with a discussion of two dimensional energy balance equations that apply to a crystal growth front moving through a solidifying fiber. They derived the equation

$$\theta = 1 - \exp\left[-\left(\Sigma_k \Sigma_j \int_o^t K_{kj}\ (\tau, T)d\tau \right) \right] \quad , \tag{22}$$

where

$$K_{kj} = \frac{N_{kj} C_j}{\rho_L} \beta^{j+\alpha} \xi^{j+\alpha} \quad . \tag{23}$$

Both homogeneous and heterogeneous nucleation are included in K_{kj}, and the nucleation rate N_{kj} is a function of temperature and deformation rate.

CHAPTER III

THEORY

A. CONTINUITY EQUATION AND MOMENTUM BALANCE ON THE FIBER

The governing differential equations for formation of a fiber by melt spinning have been derived by two different methods. Ziabicki (117, 123, 124) began with the general hydrodynamic equations of change and simplified them according to specific assumptions. Kase and Matsuo (47, 48) began with a carefully defined differential volume element of the filament and made mass, momentum, and energy balances on the element with appropriate assumptions. The governing differential equations derived by this method were very similar to those obtained by Ziabicki. Differences between the two treatments were caused by differences in the assumptions used.

A derivation based on a differential volume element will be presented here to more clearly illustrate the physical phenomena occurring in melt spinning. A differential segment of spinning filament is shown in Figure 4. The rectangular coordinate system shown has its origin on the fiber axis at the face of the spinneret with the x-axis increasing positively along the fiber axis toward the takeup device. The following assumptions are made: (1) the filament has circular symmetry about its axis; (2) the temperature, density, and viscosity are uniform across the filament diameter; (3) flow rate is constant at the spinneret.

Continuity Equation

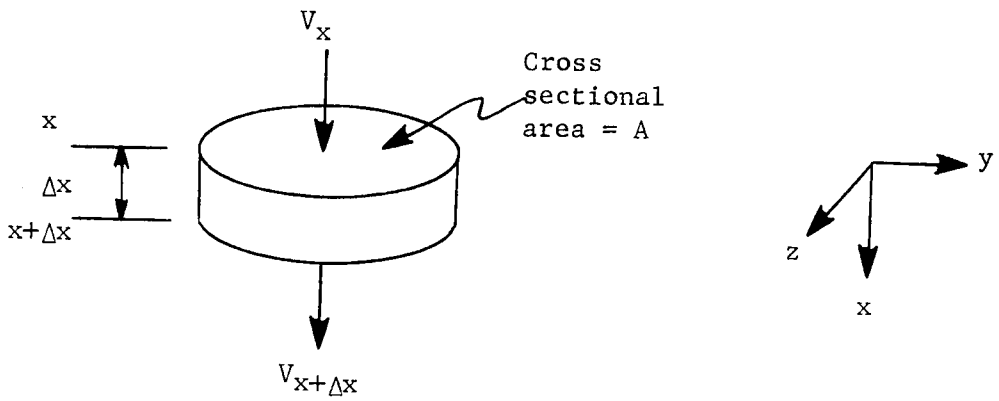

Figure 4. Incremental Volume Element in Fiber at Position x.

At time t the mass of fluid in the element is $(\rho A \Delta x)_t$, and at $t + \Delta t$ it is $(\rho A \Delta x)_{t+\Delta t}$. Mass accumulated in the element in time interval Δt is

$$(\rho A \Delta x)_{t+\Delta t} - (\rho A \Delta x)_t \ .$$

Mass enters the element through face x at the rate $(\rho VA)_x$, and the amount entering in time Δt is $(\rho VA)_x \Delta t$. In a similar manner the mass passing through the surface at $x + \Delta x$ in time Δt is $(\rho VA)_{x+\Delta x} \Delta t$. These components are now substituted into a mass balance

$$\text{Accumulation} = \Sigma \text{Inputs} - \Sigma \text{Outputs}.$$

Hence

$$(\rho A \Delta x)_{t+\Delta t} - (\rho A \Delta x)_t = (\rho VA)_x \Delta t - (\rho VA)_{x+\Delta x} \Delta t \ . \qquad (24)$$

Dividing by $\Delta x \Delta t$ gives

$$\frac{(\rho A)_{t+\Delta t} - (\rho A)_t}{\Delta t} = - \frac{(\rho AV)_{x+\Delta x} - (\rho VA)_x}{\Delta x} . \qquad (25)$$

Taking limits as Δx and Δt approach zero and applying a fundamental theorem of differential calculus yields the governing differential equation

$$\frac{\partial(\rho A)}{\partial t} = - \frac{\partial(\rho VA)}{\partial x} . \qquad (26)$$

For a constant density the equation reduces to

$$\frac{\partial A}{\partial t} = - \frac{\partial(VA)}{\partial x} . \qquad (27)$$

Although constant density is frequently assumed in the literature, sizeable errors can occur because of density changes with temperature. For steady state conditions the time transients are negligible and equation (26) reduces to

$$\frac{\partial(\rho VA)}{\partial x} = 0 . \qquad (28)$$

This implies a constant mass flow rate. Therefore,

$$\rho VA = W . \qquad (29)$$

Momentum Equation

Making a momentum balance on a differential volume of fiber we calculate the initial and final momentum values as follows: at time t the momentum in the element is $(\rho VA\Delta x)_t$, and at $t+\Delta t$ it is

$$(\rho VA\Delta x)_{t+\Delta t} .$$

The net change of momentum is

$$(\rho VA\Delta x)_{t+\Delta t} - (\rho VA\Delta x)_t \ .$$

Dividing by Δt and taking the limit as Δt approaches zero gives

$$\dot{M} = \frac{\partial(\rho VA)}{\partial t} \Delta_x \ . \tag{30}$$

The rate at which momentum enters the x face by convection is $(\rho VVA)_x$, and it leaves the $x+\Delta x$ face at the rate $(\rho VVA)_{x+\Delta x}$. Now there are tensile stresses normal to the x and $x+\Delta x$ faces; there is a shear stress on the surface because of aerodynamic drag and a force at the surface due to surface tension. Forces acting on the element transfer momentum into the element, and forces exerted by the element on its surroundings decrease its momentum. At x, a tensile stress is exerted by the element on the adjoining material; and the momentum transferred out of the element by this stress is

$$(\tau_{xx}A)_x \ .$$

At $x+\Delta x$, a tensile stress is exerted on the element by the adjoining material; and the momentum transferred into the element is

$$(\tau_{xx}A)_{x+\Delta x} \ .$$

Force exerted against air drag is

$$\pi\sigma_d d\Delta x \ .$$

The force exerted by the element against surface tension at x is

$$(\pi d\sigma_s)_x \ ,$$

and the surface tension force exerted on the element at $x+\Delta x$ is

$$(\pi d\sigma_s)_{x+\Delta x} .$$

The body force on the element is gravity which is expressed as

$$g\rho A\Delta x \ .$$

These terms are now substituted into equation (31) to give equation (32):

$$\begin{bmatrix}\text{Rate of}\\ \text{Change}\\ \text{of Momentum}\end{bmatrix} = \begin{bmatrix}\text{Rate of}\\ \text{Momentum}\\ \text{In}\end{bmatrix} - \begin{bmatrix}\text{Rate of}\\ \text{Momentum}\\ \text{Out}\end{bmatrix}$$

$$+ \begin{bmatrix}\text{Sum of Forces}\\ \text{Acting on}\\ \text{System}\end{bmatrix} \quad ; \qquad (31)$$

$$\frac{\partial(\rho VA)}{\partial t}\Delta x = (\rho V^2 A)_x - (\rho V^2 A)_{x+\Delta x}$$

$$- (\tau_{xx}A)_x + (\tau_{xx}A)_{x+\Delta x}$$

$$+ (\pi d\sigma_s)_{x+\Delta x} - (\pi d\sigma_s)_x - \sigma_d \pi d\Delta x + g\rho A\Delta x \ . \qquad (32)$$

Dividing by Δx and taking the limit as Δx approaches zero gives

$$\frac{\partial(\rho VA)}{\partial t} = - \frac{(\rho V^2 A)_{x+\Delta x} - (\rho V^2 A)_x}{\Delta x}$$

$$+ \frac{(\tau_{xx}A)_{x+\Delta x} - (\tau_{xx}A)_x}{\Delta x} + \frac{(\pi d\sigma_s)_{x+\Delta x} - (\pi d\sigma_s)_x}{\Delta x}$$

$$- \sigma_d \pi d + \rho gA \ , \qquad (33)$$

and

$$\frac{\partial(\rho VA)}{\partial t} = - \frac{\partial(\rho V^2 A)}{\partial x} + \frac{\partial(\tau_{xx}A)}{\partial x} + \frac{\partial(\pi d\sigma_s)}{\partial x}$$

$$- \sigma_d \pi d + \rho gA \ . \qquad (34)$$

This is the general momentum equation for the spinning fiber.

For steady state the time derivative is zero. Therefore

$$\frac{\partial(\rho V^2 A)}{\partial x} - \frac{\partial(\tau xxA)}{\partial x} + \frac{\partial(\pi d\sigma_s)}{\partial x} + \sigma_d \pi d - \rho gA = 0. \qquad (35)$$

By continuity $\rho VA = W$ at steady state, and

$$\frac{\partial(WV)}{\partial x} - \frac{\partial(\tau xxA)}{\partial x} + \frac{\partial(\pi d\sigma_s)}{\partial x} + \sigma_d \pi d - \rho gA = 0. \qquad (36)$$

Treating this as an ordinary differential equation in x and multiplying by dx gives

$$d(WV) - d(\tau xxA) + (\sigma_d \pi d)dx + d(\pi d\sigma_s) - \rho gAdx = 0. \qquad (37)$$

This can now be integrated with the following boundary conditions:

at $x = x$, $\tau_{xxA} = F_x$,

$V = V$,

$A = A$,

$d = d$;

at $x = L$, $\tau xxA = F_{ext}$,

$V = V_L$,

$A = A_L$,

$d = d_L$.

Therefore

$$W\int_V^{V_L} dV - \int_{F_x}^{F_{ext}} d(\tau xxA) + \int_x^L (\sigma_d \pi d)dx$$

$$+ \pi \int_d^{d_L} \sigma_s dd - \int_x^L \rho gAdx = 0, \qquad (38)$$

and

$$W(V_L - V) - \tau xxA\Big]_{F_x}^{F_{ext}} + \pi \int_x^L (\sigma_d d)dx$$

$$- g \int_x^L \rho Adx = 0, \qquad (39)$$

which yields

$$W(V_L-V) - (F_{ext}-F_x) + \pi \int_x^L (\sigma_d d)dx$$

$$+ \pi\sigma_s(d_L-d) - g \int_x^L \rho A dx = 0 \ . \qquad (40)$$

Equation (40) can be expressed as a force balance and rearranged to give

$$F_{ext} + F_{grav} = F_{rheo} + F_{inert} + F_{drag} + F_{surf}, \qquad (41)$$

where $F_{grav} = g\int_x^L \rho A dx,$ (42a)

$F_{rheo} = F_x,$ (42b)

$F_{inert} = W(V_L-V),$ (42c)

$F_{drag} = \pi\int_x^L \sigma_d d \, dx,$ (42d)

$F_{surf} = \pi\sigma_s(d_L-d).$ (42e)

At the high speeds used for commercial production aerodynamic drag is large enough to require consideration, but it is small at low spinning speeds such as those used in the present work. Surface tension is also a very small part of the overall force balance. Neglecting these contributions simplifies equation (41) to

$$F_{ext} + F_{grav} = F_{rheo} + F_{inert} \ . \qquad (43)$$

In the treatment of Kase and Matsuo (47) the gravity and inertia effects were considered negligible, and the equation reduced to

$$F_{ext} = F_{rheo} \qquad (44)$$

This simplified form of the equation must be used within the limitations of the assumptions. Inertia and gravity forces can be easily estimated in cases where the assumption is questionable. The stress at x may be written as

$$\tau_{xx} = F_{rheo}/A \quad . \tag{45}$$

Thus if F_{inert}, F_{ext}, F_{grav}, and A(x) can be obtained from experimental data, the force F_{rheo} and stress τ_{xx} can be calculated.

Assuming the deformation occurring in spinning to be only elongation the stress can be related to deformation rate by a proper constitutive equation. Assuming a Newtonian fluid gives

$$\tau_{xx} = \eta_e \frac{dV_x}{dx} \quad . \tag{46}$$

The Trouton viscosity, or apparent elongational viscosity η_e, can be calculated for each point in the filament if experimental data are available. Conversely, if the elongational viscosity of the polymer melt can be described by a suitable constitutive equation, the forces in the filament can be calculated approximately for a chosen set of spinning conditions. Solution of the mass, momentum, energy, and constitutive equations can be done numerically for the conditions normally encountered in melt spinning practice.

In this work the spinning speeds were in the low end of the commercial range, i.e., 556 meters/minute down to 50 meters/minute. Aerodynamic drag was a small part of the force at these spinning conditions and hence could be safely neglected in data analysis. Gravity force was taken into account in this work because of the large diameter filaments made. Inertia was included although it could be neglected without introducing serious errors.

B. HEAT BALANCE ON A SPINNING FIBER

The heat balance on an element of spinning filament will in general require a generation term to account for the heat of crystal-

lization. Axial conduction along the filament is assumed to be negligible. Heat transfer at the surface of the filament is assumed to be proportional to the difference between the filament temperature and ambient. Temperature across the filament diameter is also assumed to be uniform.

Heat accumulation in the fiber is the algebraic sum of inputs, outputs, and generations.

$$\begin{bmatrix}\text{Heat}\\ \text{Accumulation}\end{bmatrix} = \begin{bmatrix}\text{Heat}\\ \text{Input}\end{bmatrix} - \begin{bmatrix}\text{Heat}\\ \text{Output}\end{bmatrix} + \begin{bmatrix}\text{Heat}\\ \text{Generated}\end{bmatrix} \qquad (47)$$

The accumulation over time interval Δt is

$$(\rho C_p T_{t+\Delta t} - \rho C_p T_t) A \Delta x \ .$$

Heat flowing into the element through face x enters by convection with the polymer stream. In the time interval Δt the amount of heat entering is $(\rho C_p VT)_x A \Delta t$. Heat out at $x+\Delta x$ by convection is $(\rho C_p VT)_{x+\Delta x} A \Delta t$. Heat transferred from the filament surface to the surrounding cooling medium is $h\pi d\, \Delta x \Delta t (T-T_a)$. Heat generated by crystallization in the element is $\rho A \Delta x \Delta H \Delta t\ dX/dt$ where dX/dt is the rate of change of the crystalline fraction. Substituting into equation (47) gives

$$(\rho A C_p T_{t+\Delta t} - \rho A C_p T_t)\Delta x = (\rho C_p VT)_x A \Delta T - (\rho C_p VT)_{x+\Delta x} A \Delta t$$
$$- h\pi d \Delta x \Delta t (T-T_a) + \rho A \Delta x \Delta H \Delta t\ dX/dt \ . \qquad (48)$$

Dividing by $A\Delta x\Delta t$ and taking the limits as Δx and Δt approach zero yields

$$\frac{\rho C_p T_{t+\Delta t} - \rho C_p T_t}{\Delta t} = \frac{(\rho C_p VT)_x - (\rho C_p VT)_{x+\Delta x}}{\Delta x}$$
$$- \frac{hd\pi(T-T_a)}{A} + \rho\, \Delta H \frac{dX}{dt} \ , \qquad (49)$$

$$\frac{\partial}{\partial t}(\rho C_p T) = - \frac{\partial}{\partial x}(\rho C_p VT) - \frac{\pi dh(T-T_a)}{A}$$
$$+ \rho\, \Delta H \frac{dX}{dT} \ . \qquad (50)$$

For constant ρC_p and steady velocity V through the element we have

$$\rho C_p \frac{\partial T}{\partial t} = -\rho C_p V \frac{\partial T}{\partial x} - \frac{\pi dh(T-Ta)}{A} + \rho \Delta H \frac{dX}{dt} . \qquad (51)$$

Now

$$\pi d = 2\sqrt{\pi} \cdot \tfrac{1}{2} \sqrt{\pi} d ,$$

therefore,

$$\pi d = 2\sqrt{\pi} \sqrt{A} . \qquad (52)$$

Dividing by ρC_p, transposing terms, and making the substitution shown in equation (52) gives

$$\frac{\partial T}{\partial t} + V \frac{\partial T}{\partial x} = - \frac{2\sqrt{\pi} h (T-T_a)}{\rho C_p \sqrt{A}} + \frac{\Delta H}{C_p} \frac{dX}{dt} . \qquad (53)$$

This is the equation obtained by adding crystallization heat to the equation derived by Kase and Matsuo (47). By rearrangement the equation can be placed in a form similar to that given by Nakamura (79):

$$\frac{dX}{dt} = \frac{2\sqrt{\pi} h (T-T_a)}{\rho \sqrt{A} \Delta H} + \frac{C_p}{\Delta H} \left(\frac{\partial T}{\partial t} + V \frac{\partial T}{\partial x} \right) , \qquad (54)$$

and

$$\frac{dX}{dt} = \frac{R(T-T_a)}{\Delta H} + \frac{C_p}{\Delta H} \frac{dT}{dt} , \qquad (55)$$

where

$$R = 2\sqrt{\pi} h / (\sqrt{A} \rho) \qquad (56)$$

is the "cooling parameter" defined by Nakamura; and the substantial time derivative is used for temperature.

C. STRUCTURE DEVELOPMENT IN A SPINNING FIBER

Crystallization Kinetics

The transformation of one phase into another by a nucleation and growth process was treated by Johnson and Mehl (45), Avrami (5,

6, 7) and Evans (25). Their derivations included the effect of impingement of growth fronts on the kinetics of the transformation. The fraction of material transformed in time t is

$$X' = \int_o^t w(t,\tau)\, \dot{N}\, (\tau)\, d\tau \qquad (57)$$

if nuclei are allowed to appear throughout the entire system at the rate $\dot{N}$. This expression includes "ficticious" nuclei that appear in the transformed phase also. When impingement effects are included the actual fraction transformed is related to X' by

$$\frac{dX}{dX'} = 1 - X \quad . \qquad (58)$$

Integration of the above equation and substitution of X' from equation (57) yields

$$X = 1 - \exp(-X') \ , \qquad (59)$$

and

$$X = 1 - \exp\left[-\int_o^t w(t,\tau)\dot{N}(\tau)d\tau\right] . \qquad (60)$$

Equation (60) may also be written

$$X = 1 - \exp\left[-\frac{\rho_c}{\rho_L}\int_o^t v(t,\tau)\dot{N}(\tau)d\tau\right] . \qquad (61)$$

This is the general form of the Avrami equation. The integrals in equations (60) and (61) can be evaluated by specifying the growth function $v(t,\tau)$, or $w(t,\tau)$, and the nucleation function $\dot{N}$ that describe a specific transformation. For sporatic or instantaneous nucleation with a linear growth rate the integrated equation yields

$$\ell n \frac{1}{1-X} = kt^n \ , \qquad (62a)$$

or

$$X = 1 - \exp(-kt^n) \quad . \tag{62b}$$

The value of n is determined by the type of nucleation occurring and the mode of growth.

Implicit in the Avrami derivation was the assumption that the system was capable of transforming completely from one phase to another. This does not occur with polymers because amorphous material between crystalline regions is often sterically hindered from crystallizing. Mandelkern (65) modified the Avrami approach to include incomplete crystallization and thus derived the equations that describe crystallization kinetics in polymers. The transformed mass containing crystalline and amorphous material which would not crystallize further was the "effective fraction" of transformed material. The assumptions were made that this "effective fraction" was proportional to the actual mass fraction transformed and that the proportionality factor was $1/X_\infty$ where X_∞ is the mass fraction of polymer crystallized at the end of the transformation. The fraction $1/X_\infty$ was also assumed to be independent of time. The "effective fraction" was thus X/X_∞. Inserting this into equation (58) yields

$$\frac{dX}{dX'} = 1 - \frac{X}{X_\infty} \quad . \tag{63}$$

Integrating and substituting equation (57) for X' gives

$$\ell n \frac{1}{1-X/X_\infty} = \frac{1}{X_\infty} \frac{\rho_c}{\rho_L} \int_o^t v(t,\tau)\dot{N}\,(\tau)d\tau \quad . \tag{64}$$

If equation (64) is integrated under the mass assumptions used for equation (62a), the result is

$$\ell n \frac{1}{1-X/X_\infty} = \frac{1}{X_\infty} kt^n \quad . \tag{65}$$

This is often written in the form

$$\ln (1-\theta) = -Kt^n, \tag{66a}$$

or

$$\theta = 1 - e^{-Kt^n} \tag{66b}$$

where $\theta = X/X_\infty$, and $K = k/X_\infty$.

Crystallization in melt spinning proceeds nonisothermally over a wide range of temperature. Calculation of crystallinity under this condition requires additional modification of the theory as was done by Ziabicki (118). The overall crystallization rate constant, which contains contributions from nucleation and growth processes, depends on temperature.

$$K = K(T) .$$

Temperature in a spinline is a function of time, and the resulting time dependence of K can be written

$$K = K[T(t)] .$$

Ziabicki incorporated this relationship into the Avrami equation to yield

$$\theta(t) = 1-\exp\left[-\left\{\int_o^t K[T(\tau)]d\tau\right\}\right] , \tag{17}$$

where K(T) is the isothermal crystallization rate constant.

Nakamura and coworkers (79, 80, 81) similarly began with the original Avrami approach to crystallization and derived an expression for nonisothermal crystallization. The equation thus derived was

$$\theta = 1-\exp\left\{-\left(\int_o^t K[T(\tau)]d\tau\right)^n\right\} , \tag{21}$$

where $K(T) = k(T)^{1/n}$, and n and K(T) are the Avrami index and the isothermal crystallization rate constant respectively.

The most general form for nonisothermal crystallization in an oriented polymer was given by Abbott and White (1). Their equation was presented in Chapter II on page 26.

Equation (21) can be used to approximately describe the crystallization that occurs in a spinline if isothermal crystallization rate data are available. The method is an approximation since it does not include the effect of stress, or orientation, on the crystallization kinetics. The temperature dependence of the crystallization rate constant can be described by the following equation according to Takayanagi and Kusumato (102):

$$\ln k(T) = A - \frac{BT}{(T-Tg-51.6)^2} - \frac{CT_m}{T(T_m-T)}$$

A, B, and C are constants relevant to the polymer.

Orientation During Melt Spinning

Orientation of polymer molecules occurs during melt spinning of synthetic fiber. Long flexible molecules become elongated and oriented approximately parallel to the fiber axis by deformation processes in the spinneret capillary, in the molten portion of the threadline, and in the solidified section of the filament. Orientation originating from shearing flow of the melt through the capillary is rapidly lost as the polymer exits the capillary and enters the die swell region where radial flow and Brownian motion randomize the molecular configurations. Elongational deformation in the molten section of the filament produces molecular orientation which is partly retained in the fiber since thermal agitation of the molecules decreases as the filament temperature drops rapidly. Plastic stretching

of the solid section of the fiber that is above T_g produces orientation that is readily retained in the fiber; however, the amount of orientation produced by solid deformation is low because of the low deformation that actually occurs as the yield stress of the cooling filament continuously increases.

Total orientation is also increased by crystallization on oriented nuclei. Molecules elongated and oriented by deformation processes can become nuclei for further crystalline growth which will have the same orientation as the nuclei except for included amorphous material such as chain ends and folds at lamellar surfaces. In this way the amorphous region surrounding an oriented nucleus is transformed into a highly oriented semicrystalline material. The overall orientation in the material is higher than the level resulting from deformation processes alone.

The theoretical relationships between process variables and orientation in the spinline derived by Ziabicki (116) and Nishiumi (82) were presented in Chapter II. The increase of orientation by crystallization in the spinline was not included in their treatments. The expressions they derived also dealt only with an average value of orientation in the filament at the point of interest.

Fung and Carr (29) have experimentally measured changes in birefringence across the diameter of melt spun polyethylene fibers. Birefringence increased from a low value at the fiber center to its highest value at the surface. This condition is consistent with the theory proposed above for a balance between orienting processes and randomizing effects of thermal motion. The outer surface cooled faster

thus freezing the orientation developed there while the center of the fiber remained hot longer and lost orientation. The center was also under less stress because of its higher temperature and, hence, lower viscosity. Higher stress was carried by the cooler, more viscous outer layers of the filament.

CHAPTER IV

EXPERIMENTAL EQUIPMENT, MATERIALS, AND PROCEDURES

A. EQUIPMENT

The equipment used in this work consisted of a melt spinning apparatus for making synthetic fibers and a variety of test equipment used to make measurements both on the spinning filament and on the final fiber. Major items of equipment were the extruder-spinning machine, the winder, and the rotating anode x-ray generator. Several instruments were used to measure temperature, diameter, and tension on the spinline as well as a variety of properties of the final fiber. All of these equipment items and the procedures used for collecting data are discussed in this chapter. More detailed operating instructions for some items of equipment are given in Appendix C.

Melt Spinning Equipment

The complete spinning machine is shown schematically in Figure 5, and the extruder and x-ray machine are shown in Figure 6. Reference to these figures during the succeeding discussion will facilitate a better understanding of the equipment.

Filaments were spun from an extruder-spinning machine made by Fourne Associates of West Germany. The machine consisted of a thirteen millimeter diameter screw extruder which received polymer pellets by gravity feed from a seven liter, nitrogen purged hopper. The extruder supplied molten polymer at constant pressure to a gear pump which provided a constant polymer flow rate to the spinneret. The

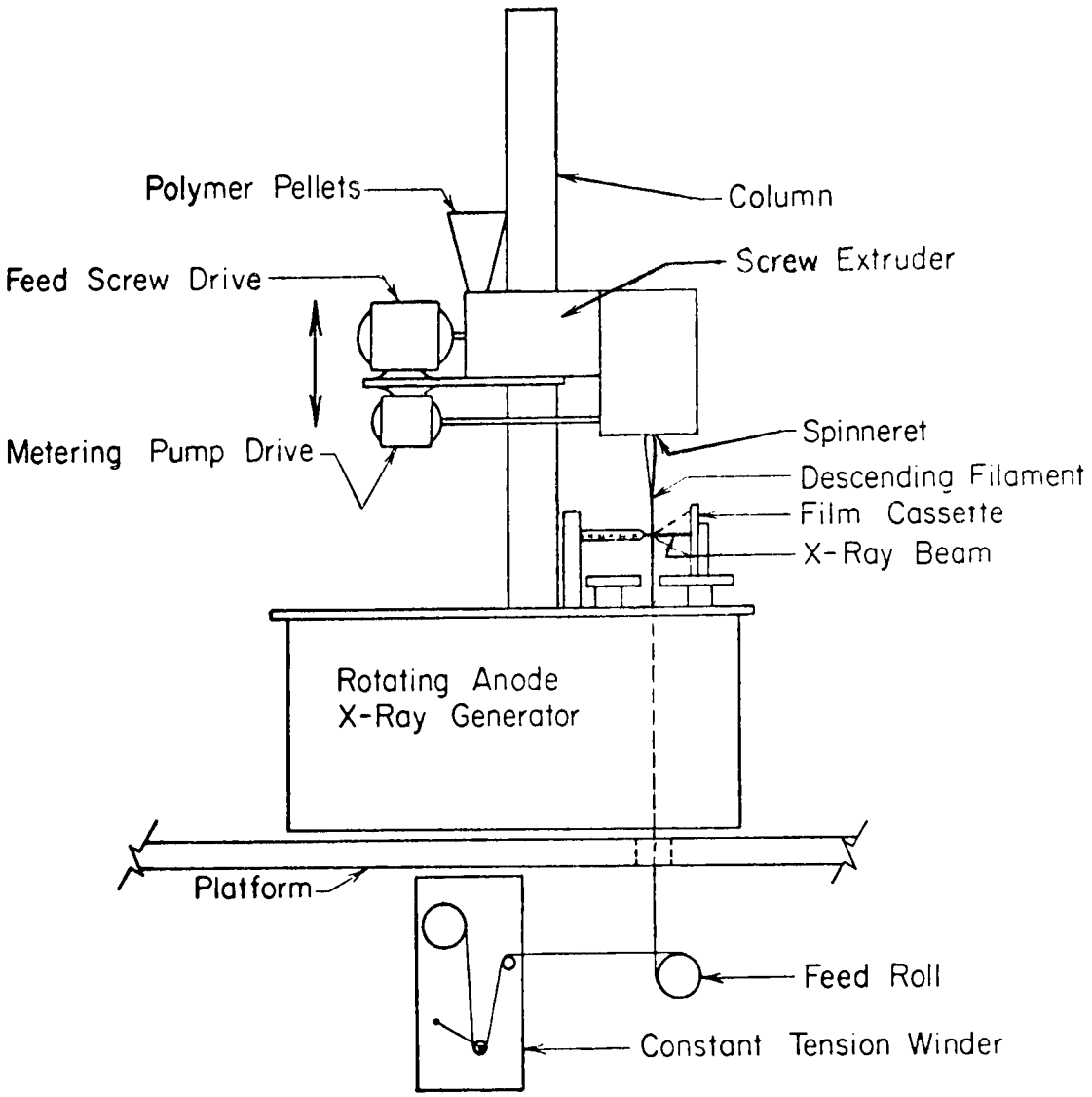

Figure 5. Schematic of Experimental Equipment.

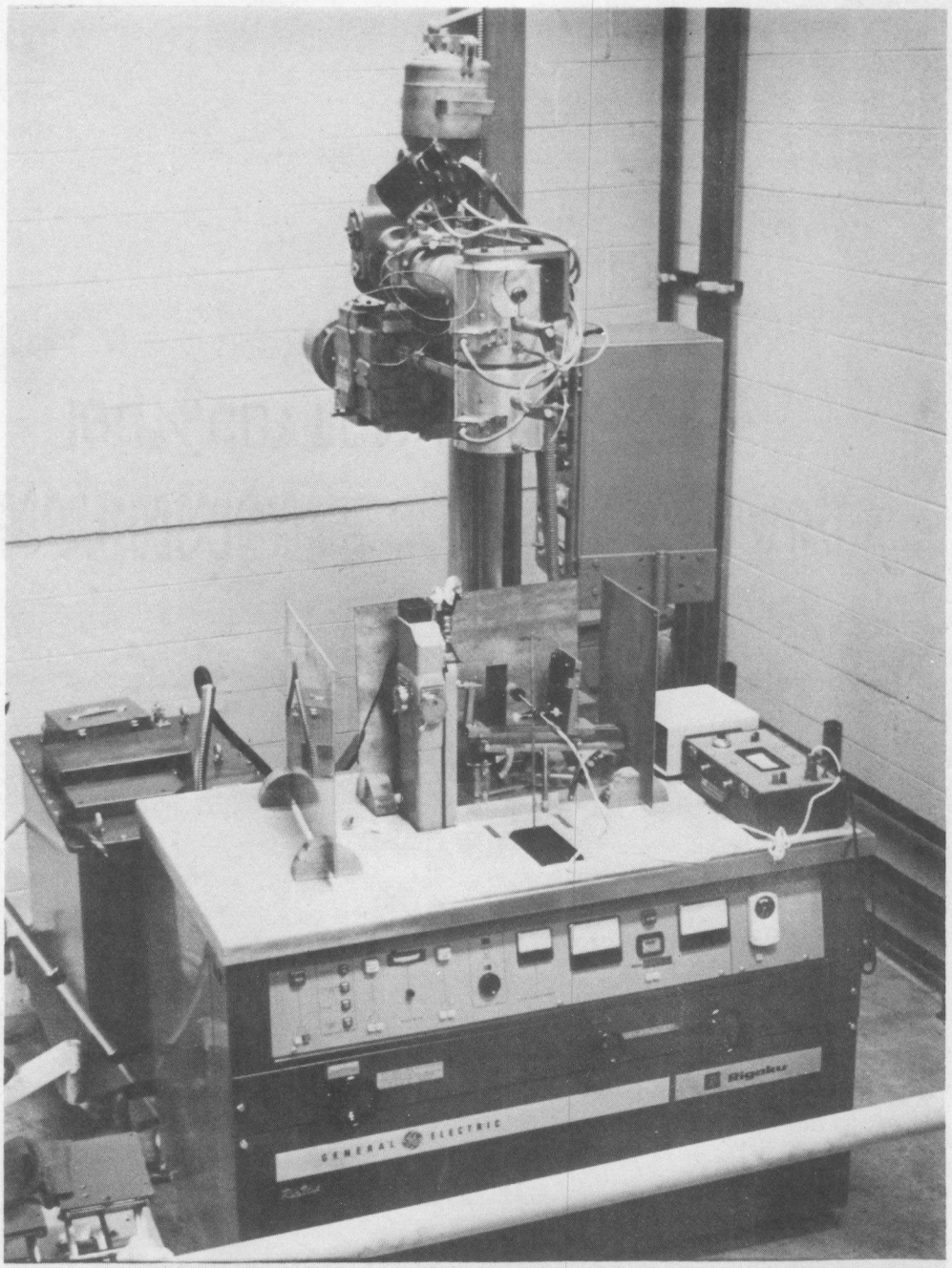

Figure 6. Photograph of Moveable Spinning Extruder and Rotating Anode X-Ray Generator

discharge stream from the meter pump passed through a 325 mesh filter screen and through a single capillary spinneret. Capillary dimensions of 0.762 mm diameter by 3.81 mm long were used for all samples. The extruder and spinning head assembly was wrapped with electrical band heaters arranged to provide four separate heating zones. Four controllers maintained the desired temperatures in these zones.

Polymer temperature was measured at two points by platinum-resistance thermometers inserted into the polymer stream. They were positioned in the extruder discharge stream and the meter pump discharge stream, and the temperatures were indicated by a meter on the control panel.

Polymer pressure between the extruder and the meter pump was sensed by a liquid filled bulb transducer and was indicated by a Bourdon tube type gauge. The gauge was also electrically coupled to the extruder speed controller to stop the extruder in case of high or low pressures beyond chosen limits. Feedback to the extruder speed controller also caused slight changes in screw speed to assist in maintaining constant extruder discharge pressure.

Meter pump speed was manually adjusted to the desired setting by means of a variable speed gear box between the pump and its motor. Once set, the pump speed remained constant.

During spinning, fiber was wound on cardboard bobbins at constant linear speed. The fiber speed was established by passing the fiber one full wrap around a feed roll rotating at the desired surface speed. The feed roll was a three inch outside diameter cardboard bobbin mounted on a direct current motor driven by a Heller controller.

Speeds from 30 to 556 meters per minute could be obtained with the feed roll. From the feed roll the filaments passed to a Leesona 955 constant tension winder where they were uniformly wound into a 3-9/16 inch outside diameter cardboard bobbin. The winder maintained a reasonably uniform tension between the feed roll and takeup roll by varying the takeup roll speed.

Rigaku-General Electric Rotating Anode X-Ray Generator

Wide angle x-ray patterns were obtained from the filaments, while they were being spun, by passing the fiber through an x-ray beam and obtaining a pattern on photographic film. The fiber passed through a Rigaku RU3V rotating anode x-ray generator which was positioned between the extruder and the windup system as shown in Figures 5 and 6. A 1½ inch diameter hole was drilled in the x-ray machine table top to allow undisturbed passage of the fiber through the x-ray beam and the generator. A clear area was provided through the interior of the x-ray machine cabinet and through a hole in the floor of the platform supporting the x-ray machine and the extruder.

A commercially available collimator, support track, and flat plate film cassette were used to make wide angle patterns. Holes and slots were machined in the track as needed to provide a passage for the fiber. A filament guide was made of two steel wires soldered in an "X" arrangement. This was placed beneath the x-ray film support track to stabilize the fiber during x-ray exposures.

The rotating anode x-ray generator provided a high intensity source of copper K_{α} radiation. The beam generated by the six kilovolt-ampere system was filtered through nickel foil to reduce K_{β} radiation

intensity.

GAF HR-3000 high resolution medical x-ray film and Dupont Cronex 2DC medical x-ray film was used for wide angle patterns. Film was developed using GAF developer and fixer for four minutes each followed by a thirty minute rinse in running water. All solutions and rinses were used at 20°C.

Rothschild Tensiometer

Fiber tension measurements were made using a Rothschild Tensiometer equipped with a ten gram measuring head. A switching system in the circuitry of the instrument permitted measurement on scales of zero to ten, zero to five, and zero to 2.5 grams. The zero to 2.5 gram scale was used for all measurements in this research. The instrument was calibrated and operated according to the manufacturer's instructions. All readings were corrected for changes in fiber diameter and stiffness as recommended in the instructions.

Hastings-Raydist Match-Temp Pyrometer

Temperature measurements on the running filament were taken with a Hastings-Raydist Match-Temp Pyrometer. This device measured fiber temperature over the range 25 to 250°C.using a heated thermocouple null point technique. The sensing head consisted of a hot wire in direct contact with a thermocouple. Upon touching a filament having a temperature different from the hot wire, heat would flow into or out of the wire, depending on the difference, and the thermocouple would sense a change in the temperature of the wire. If the filament and wire were at the same temperature, no heat would flow upon contacting

the filament and no temperature change would be detected. A temperature measurement was made by successively adjusting the hot wire temperature and touching the filament until no deflection in temperature was observed upon contact. At that point the fiber temperature was the same as the hot wire temperature. The sensitivity of the measuring technique was greatly improved by using a Leeds and Northrup Potentiometer to measure the thermocouple output. For this method the potentiometer was connected to the recorder terminals of the pyrometer, and the pyrometer was switched to the "RECORD" mode. Millivolt readings from the potentiometer were converted to temperatures using standard tables for chromel-alumel thermocouples. With this technique the accuracy of temperature measurements was limited by the variation of actual filament temperature, by the rise in temperature caused by friction between the fiber and the thermocouple, and by the variable cooling of the thermocouple by air moving with the fiber.

Photographic Equipment

Filament diameter measurements were made by photographing the filament, projecting the negative on a screen, and making a measurement of the projected image. Using the proper scale factor, the projected diameter was converted to actual fiber diameter.

A 35 mm single lens reflex camera equipped with a bellows and a 135 mm telephoto lens was used to photograph the fiber. The bellows was adjusted to its maximum length to give an image to object ratio slightly greater than 1.0 on the film. A precision centimeter scale was photographed using exactly the same equipment setup so a scale factor could be calculated. The filament was illuminated with a

photographic flood lamp which was carefully positioned to illuminate the full diameter of the fiber. A Kodak Carousel projector was used to project the negatives onto a screen where the diameter measurements were made.

Filament diameter photographs were made on twenty exposure rolls of Kodak Tri-X film. Processing was done according to the manufacturer's instructions using Microdol-X developer at full strength for eleven minutes followed by a thirty second rinse and four minutes in Kodak Rapid Fixer. After rinsing for thirty minutes in running water, the film was immersed thirty seconds in Photoflo solution and uncoiled from the developing tank reel and hung up to dry. After drying, the negatives were cut apart and placed in two by two inch slide holders for projection. Each slide was properly marked for easy identification.

Tech/Ops Microdensitometer

Wide angle x-ray patterns taken with the flat plate cassette were analyzed quantitatively using a scanning microdensitometer. The machine used was a Tech/Ops Scandig Model 25 high speed digital, x-y scanning microdensitometer. Optical densities were quantitatively measured up to 3.0D through 256 levels with a resolution of 0.012D, and the data were digitized at the rate of 20,000 data points per second. [$D = \log_{10} (I_o/I)$ where I_o = intensity of beam of light incident on the film and I = intensity of the transmitted beam.] The output of the microdensitometer was recorded on magnetic tape in binary form. Subsequent data processing with the tape was done on the IBM 360 Model 65 computer at the University of Tennessee Computer Center.

The x-ray pattern to be scanned was carefully mounted on a five inch by six inch card with the quadrant to be scanned placed over a 32 mm square cutout in the card. The geometric center of the pattern was carefully located and marked with a small pinhole. The pinhole caused a zero density reading at the pattern center which could be easily located during subsequent computer analysis of the scan. The card with its attached pattern was then mounted on the rotating drum of the scanning microdensitometer in a position that allowed scanning from the center of the pattern along the equator in the x direction. After a 31.0 mm scan along the x axis, the pattern was moved automatically to a new value on the y axis for the next scan. This was continued until a value of 31.0 mm was reached on the y axis. Optical densities were measured through a 100 micron aperture on a raster of 100 microns. Thus the x-ray pattern quadrant was converted from a 31.0 mm x 31.0 mm film pattern to a 310 x 310 x-y matrix of binary coded optical densities having values from 0 to 256. The 310 x 310 matrix was eventually read from magnetic tape into the computer's high speed core and processed by a program named PEXRAN to obtain percent crystallinity and orientation functions. Details of the PEXRAN program are given in Appendix B.

Loading the data into the computer core permitted rapid processing of a single pattern although a very large block of storage was required. The 310 x 310 matrix occupied 96,100 words of storage. Using words of two bytes in length required 192,200 bytes of storage, and the additional storage of the compiled program raised the core requirement to 204 K bytes. This approach was thus suitable only on a large computer.

A saving in storage requirements at the expense of computation time could be realized by using direct-access storage of data on magnetic disc. For smaller computers this would be a necessity, and an extensive revision of PEXRAN would be needed.

Small Angle X-Ray Scattering Equipment

Small angle x-ray scattering data were obtained by both pinhole patterns and Kratky goniometer techniques. Pinhole patterns were made on the Rigaku rotating anode x-ray machine using a custom made collimator mounted in a Kiessig camera. The camera was evacuated by a mechanical vacuum pump to reduce air scattered radiation. Exposure times were adjusted as required to obtain satisfactory patterns, and they usually were in the range of only one to four hours because of the high intensity of the x-ray beam used.

Quantitative SAXS data were obtained with a Kratky goniometer at the Oak Ridge National Laboratory using conventional counter techniques.

Pole Figure Equipment

Pole figure data were collected using a counter-diffractometer technique. For these measurements a bundle of filaments approximately 2.0 mm in diameter was prepared by embedding the semicrystalline fibers in a small amount of amorphous matrix. This sample was further shaped and mounted on a glass fiber for the pole figure scans.

Scanning Electron Microscope

Photographs of selected regions of the fiber surface were obtained with an AMR 900 scanning electron microscope. A Polaroid

film cassette was used to make photos from the electron microscope screen.

Instron Tensile Tester

Tensile properties of the fibers were measured at room temperature with an Instron tensile tester. A crosshead speed of one inch per minute was used with a fiber gauge length of one inch. Young's modulus, ultimate tensile strength, and elongation to break were measured.

Density Gradient Columns

Fiber density was measured using a density gradient column of the type discussed by Tung and Taylor (105). Density values were used to calculate percent crystallinity by applying the equation

$$X = \frac{1 - \rho_a/\rho}{1 - \rho_a/\rho_c} \tag{68}$$

where X is the weight fraction of crystalline polymer and ρ_a and ρ_c are the densities of the amorphous and crystalline phases and ρ is the density of the sample.

Birefringence Microscope

Birefringence was measured using a Leitz polarizing microscope with a Berek compensator.

Computers

Two computers were used in making the calculations required for data analysis. Numerical processing of the microdensitometer scans of x-ray patterns was done on the IBM 360 Model 65 at the University of

Tennessee Computer Center. Also part of the processing of diameter, temperature, and crystallinity data was done on the same computer. All other computations were made on an IBM 1800 computer located at the Monsanto Textiles Company's Technical Center in Pensacola, Florida.

B. MATERIALS

Two high density polyethylenes were used for these experiments. Both polymers had a melt index of 5.0. Spinning runs one through five were made using Texas Eastman 3310 Tenite, lot number 8819. Runs six through nine were made using Phillips high density polyethylene EMB-6050, lot number 01-2-1308. Both materials were in pellet form with dimensions of approximately three millimeters length by two millimeters diameter.

C. DATA COLLECTING PROCEDURES

To begin a spinning run the extruder hopper was filled with polymer pellets and the desired temperatures were set on the four extruder temperature controllers. After approximately three hours the extruder temperature had stabilized and polymer remaining in the spinning machine from previous operation had melted. The meter pump was then started, and the extruder was started and slowly speeded up until an extruder discharge pressure of 40 to 60 kg/cm^2 was obtained. The meter pump was then adjusted to the desired speed and the extruder again adjusted to deliver the correct pressure. After approximately one hour of continuous extrusion, the conditions were well stabilized, old polymer had been purged, and fiber collecting could begin.

Adjustments in extruder screw speed were made as required to keep the pressure in the 40 to 60 kg/cm^2 range.

The windup system was set to the desired speed, and the fiber was then passed through the x-ray machine to the winder. Stringup was achieved by starting the fiber on the windup bobbin using a fiber pickup device on the winder, and then placing one wrap around the feed roll. The winder tension arm, which had been held stationary to this point, was released and allowed to adjust to the proper level for feed roll speed being used.

At some time during the spinning run a sample bobbin was collected for approximately thirty minutes while the fiber was spun undisturbed by sampling or measuring techniques. Fiber from this bobbin was used for subsequent physical property measurements.

Before making direct measurements on the filament the extruder was lowered to place the spinneret 33.0 cm above the x-ray beam. While in this position diameter photographs and temperature measurements were obtained from the spinneret to the x-ray beam-filament intersection beginning 2.54 cm below the spinneret and moving down in 5.08 cm (2.0 inches) increments. The diameter and temperature instruments were then placed in fixed positions on the x-ray machine table and measurements were continued by elevating the spinning head in 5.08 cm increments until spinline length of 175 cm from the spinneret had been examined. The temperature profile down the filament was then complete, and photographs were on hand for subsequent determination of the diameter profile.

Wide angle x-ray diffraction patterns were then obtained at

15.24 cm (6.0 inch) intervals beginning at the 175 cm distance and moving the spinning head down until a region of completely amorphous polymer was reached. The location of this region was usually estimated beforehand from the filament temperature data. In making x-ray patterns the extruder was positioned to place the spinneret at the desired distance above the x-ray beam. The fiber was then placed in the guide and moved into the x-ray beam by adjusting the guide and checking the beam and fiber positions with a fluorescent screen. After properly positioning the fiber a film cassette was mounted on the track and carefully positioned 3.0 centimeters from the fiber x-ray beam intersection. The x-ray machine was then adjusted to 90 milliamps and 58 kilovolts and set to give the desired exposure time of fifteen to forty-five minutes. Successive exposures were made in this fashion until the fiber had been examined up to the amorphous region. After completing the spinning run, a fiber sample was taken from the sample bobbin and placed in a holder on the x-ray film track and used to make a wide angle pattern of the final product.

After the spinning run was completed, the x-ray and diameter films were developed. Diameter measurements were obtained from the film as previously described. X-ray patterns were mounted, scanned by the microdensitometer, and analyzed by computer to give percent crystallinity and Herman's orientation functions. The final fiber was subjected to previously described tests for physical properties, SAXS data, and electron microscopy.

CHAPTER V

DATA ANALYSIS

This chapter discusses the techniques used to analyze data collected from spinning tests. Numerous calculations were made using the diameter, temperature, and crystallinity profiles combined with mass flow rate, takeup velocity, and tension values. By suitable calculations these data produced profiles of velocity, velocity gradient, density, stress, and elongational viscosity. Travel time between any two points in the spinline was also computed. Actual calculations were done by computer using the programs contained in Appendix B. A discussion of the calculations used to analyze the x-ray patterns is also given.

A. CALCULATION OF CRYSTALLINITY AND ORIENTATION FROM X-RAY DIFFRACTION PATTERNS

Crystallinity

The method used to convert an x-ray film to a matrix of digitized data has been previously discussed, and the details of the crystallinity calculation are given in the program PEXRAN in Appendix B. The method used for computing crystallinity in polyethylene is discussed here.

The calculation of percent crystallinity was based on a modification of the method proposed by Matthews, Peiser, and Richards (73). The amorphous halo, 110, 200, and 020 Debye rings of a wide angle x-ray diffraction pattern are shown schematically in Figure 7.

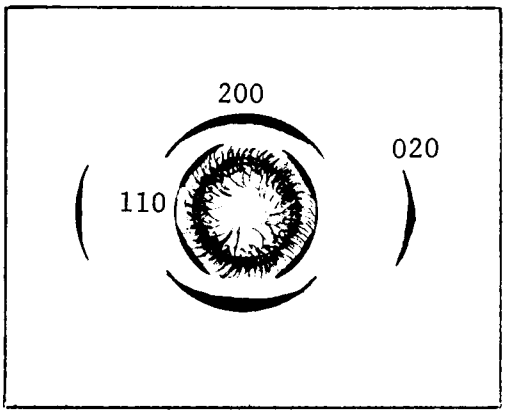

Figure 7. Schematic of Wide Angle X-Ray Diffraction Pattern of Polyethylene

The total intensity in the 110 and 200 rings was used to obtain an estimate of the crystalline fraction of the material. First a correction was made for background scattering from the amorphous halo to the 200 peak. The amorphous and 200 peaks were assumed to be symmetric, and the intensity of each was calculated by integrating the areas "a" and "c" shown in Figure 8 and doubling them. This gave

$$I_A = 2a \ ,$$

and

$$I_{200} = 2c \ .$$

The intensity of the 110 scatter was calculated by integrating the area "b" which extends from the maximum in the amorphous halo to the maximum in the 200 peak and subtracting the contributions of amorphous and 200 scatter. The calculation is

$$I_{110} = b - a - c \ . \qquad (69)$$

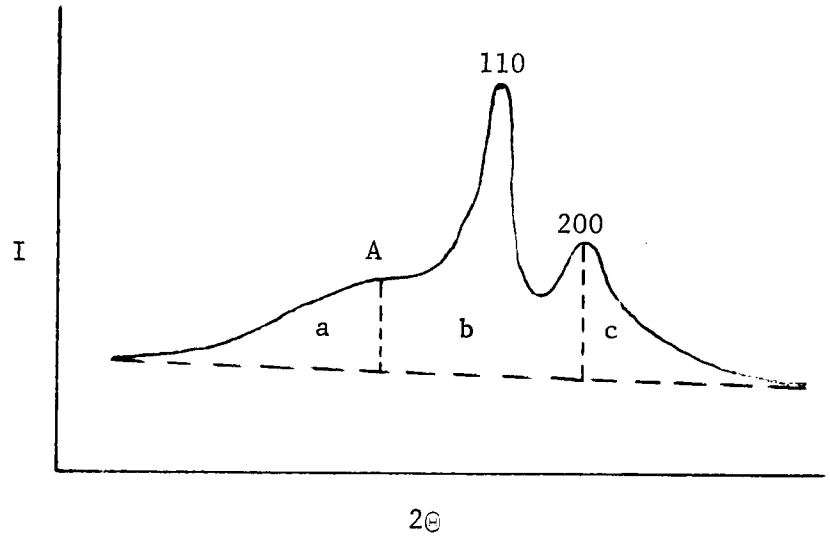

Figure 8. Diffracted Intensity Versus 2Θ Angle Along the Equator of a Polyethylene WAXS Pattern.

Total crystalline scatter is the sum of 110 and 200 contributions.

$$I_c = I_{110} + I_{200} \cdot \tag{70}$$

The ratio of crystalline to amorphous material is I_c/I_a, and the fraction of crystalline material is

$$X = \frac{I_c}{I_c + I_a} \cdot \tag{71}$$

Before applying these equations to the digitized data matrix several adjustments were made to the intensity values. First a linear background correction was subtracted from all points between the inner edge of the amorphous halo and the outer edge of the 200 peak throughout the complete quadrant. After subtracting background, the data were removed from the matrix as radial scans spaced at one degree intervals. Each radial scan contained data very similar to the plots of I vs 2Θ shown in Figure 8. Next the corrections that were functions of diffraction angle Θ were applied to each point along the radial

scan. The correction factor,

$$\frac{(1+\cos^2 2\Theta)\ (\tan 2\Theta)}{\sin^3\Theta\ \cos 2\ \Theta} \cdot f_c^2 \cdot e^{-2M},$$

included several geometric factors, a structure factor f_c^2 and a temperature factor e^{-2M}. After making the correction, points were collected into summations needed for a numerical integration of the areas in the quadrant.

The total power in a Debye ring is given by

$$P = \iint I_{corr}\ d2\Theta d\Psi\ , \tag{72}$$

where the angles are as shown in Figure 9, and I_{corr} is the average power per unit length of diffraction line obtained by making the corrections discussed above.

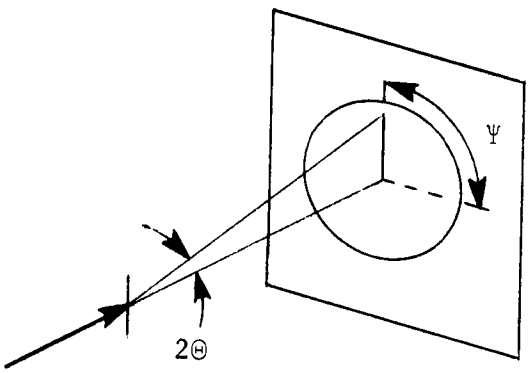

Figure 9. Schematic of Diffraction Patterns Showing Angles 2Θ and Ψ.

After completion of the integration, the total intensity for the 110 peak, for example, was then calculated as

$$I_{110} = \frac{P_{110}}{\left(\int_o^{\pi/2} I'_{110}\, d\Psi_{110} \Big/ \int_o^{\pi/2} I'_{110}\, \cos\Psi_{110}\, d\Psi_{110}\right)} , \qquad (73)$$

where the denominator is a correction for the non random distribution of crystals in the cylindrical fiber. The integrals were evaluated numerically. A similar equation was used for the 200 peak. For the amorphous halo the relation was simply

$$I_a = P_a .$$

Orientation Functions

Orientation was computed using the Hermans orientation function and the method of Stein (98). The equations used were

$$f_a = (3 \cos^2\Theta_{200}\, \overline{\sin^2\Psi_{200}} - 1)/2 , \qquad (74)$$

where

$$\overline{\sin^2\Psi_{200}} = \frac{\int_o^{\pi/2} I'(\Psi)_{200}\, \sin^2\Psi_{200}\, \cos\Psi_{200}\, d\Psi_{200}}{\int_o^{\pi/2} I'(\Psi)_{200}\, \cos\Psi_{200}\, d\Psi_{200}} \qquad (75)$$

Similar expressions were used to calculate f_b from the 020 Debye ring. The value of f_c was then computed from

$$f_a + f_b + f_c = 0 . \qquad (76)$$

Integrations were performed numerically using the trapezoid rule. Actual computation was done simultaneously with the crystallinity calculation.

B. EMPIRICAL EQUATION USED FOR DATA SMOOTHING

Point by point calculation of filament velocity, velocity gradient, and percent crystallinity from measured diameter and crystal-

linity data required some type of data smoothing or interpolation between measured points. In some cases this could be done numerically without causing undue errors in subsequent data analysis. However in the case of velocity gradient, crystallization rate, and travel time serious problems resulted when numerical methods were used to estimate these quantities directly from experimental data. For these reasons the data were first smoothed by fitting the following equation to diameter, velocity, and percent crystallinity data:

$$y = A \exp\left[B\left(\frac{x-C}{D}\right)^{E}\right] + F, \tag{77}$$

where A, B, C, D, E, and F are constants. This form of equation was adapted from the solution of the momentum equation given by Ziabicki for a constant tension spinning process. In that case

$$\frac{V}{V_o} = \exp\left[\frac{\rho F}{W}\int_o^L \frac{1}{\eta_e}\,dx\right], \tag{4}$$

and

$$\frac{d}{d_o} = \exp\left[-\frac{\rho F}{2W}\int_o^L \frac{1}{\eta_e}\,dx\right]. \tag{5}$$

Rearranging equation (77) produced

$$\frac{y-F}{A} = \left[B\left(\frac{x-C}{D}\right)^{E}\right].$$

This form of the equation is an approximation of (4) and (5) with the integral replaced by a power function of a dimensionless expression in x, and with the constant F included in a dimensionless y on the left hand side. This equation was suitable for fitting diameter,

velocity, and crystallinity profiles with the general shapes shown in Figure 10.

The equation was modified to adapt it to each data smoothing situation. For diameter profiles the constant C was given a value of zero to give equation (78).

$$d = A \exp (B'x^E) + F , \qquad (78)$$

where $B' = B/D^E$.

The same form was used for velocity profiles. For crystallinity profiles the constant C was fixed at the value of x at which crystallization was observed or estimated to have begun, and the values of A and F were -1.0 and 1.0 respectively for fractional crystallinity and -100.0 and 100.0 for percent crystallinity. After combining B and D the equation was

$$X = \left\{1 - \exp\left[B'(x-C)^E\right]\right\} . \qquad (79)$$

Fitting the equation to the data was done using a pattern search optimization program named PATRN. The fit was made to a minimum value of the root mean square difference between observed and calculated values. Standard errors for the equations were usually of the same order as the experimental error in the measuring technique used for data collection.

C. MECHANICAL ASPECTS OF THE SPINNING PROCESS

Velocity and Velocity Gradient

Velocity of the fiber at each point of a diameter measurement was calculated from the continuity equation:

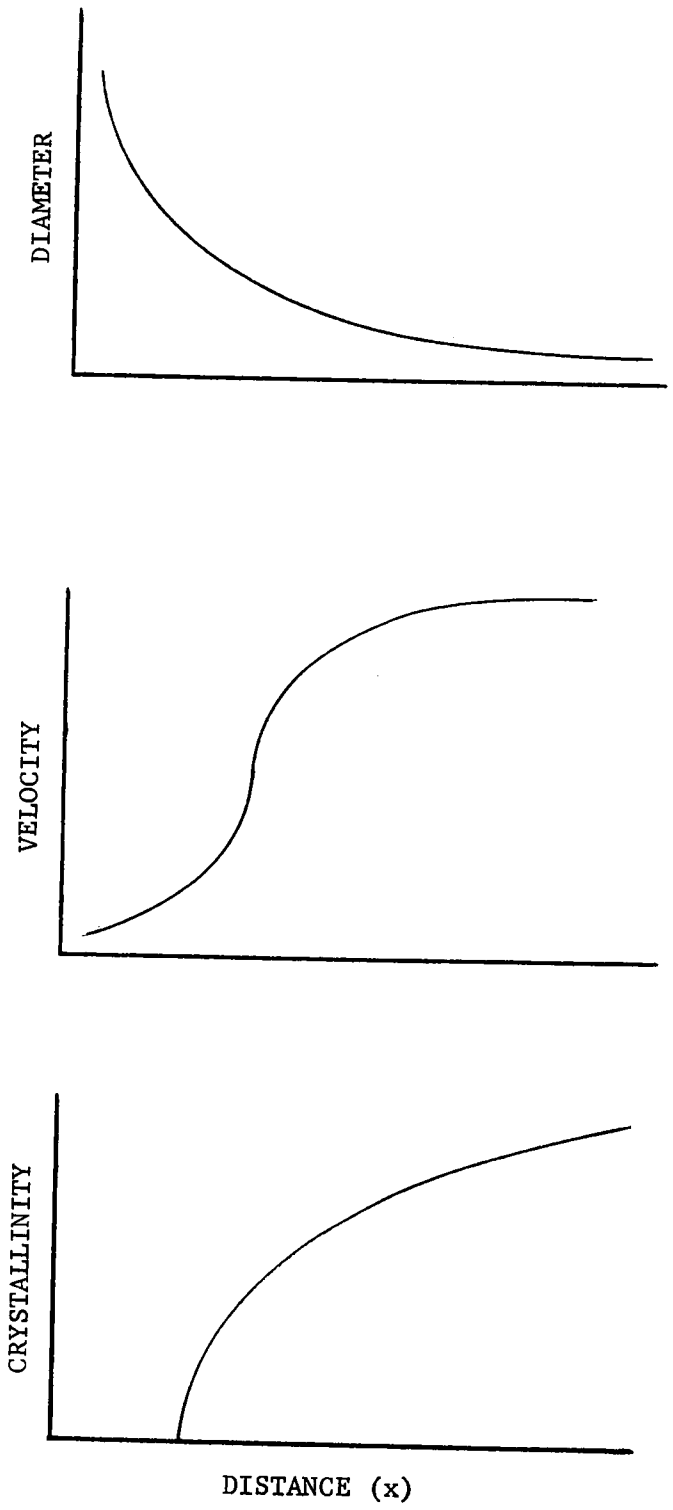

Figure 10. Types of Curves that are Described by the Function $y = A \exp\left(B\left(\frac{x-C}{D}\right)^{E}\right) + F$.

$$V_i = W/\rho_i A_i \ , \qquad (1)$$

where the A_i were calculated using

$$A_i = \frac{\pi}{4} d_i^2 \ ; \qquad (80)$$

and density was calculated at each point as a function of temperature and crystallinity. The densities of the amorphous, crystalline, and molten phases of linear polyethylene were given as functions of temperature by equations (81), (82), and (83) according to Swann (101).

$$\rho_a = 1.0/(1.1149 + .403 \times 10^{-3}T + .467 \times 10^{-5}T^2) \quad -20 \text{ to } +136.5^\circ C \qquad (81)$$

$$\rho_c = 1.0/(.9940 + .2614 \times 10^{-3}T + .443 \times 10^{-6}T^2) \quad -196 \text{ to } +130^\circ C \qquad (82)$$

$$\rho_L = 1.0/(1.1360 + 0.885 \times 10^{-3}T) \quad +136.5 \text{ to } +160^\circ C \qquad (83)$$

A two phase system was assumed for the density calculation. Experimentally measured temperature was used to calculate ρ_c and ρ_a. The fraction crystallinity at point "i" was calculated from the previously discussed empirical relationship for crystallinity versus distance. Combining these gave

$$\rho_i = \frac{\rho_c \rho_a}{\rho_c - X_i (\rho_c - \rho_a)} \ . \qquad (84)$$

Velocity was then calculated using equation (1) and equation (78) was fitted to the resultant data.

Velocities were calculated using experimentally observed values of d as well as values of d computed from the empirical equation previously fitted to experimental diameter data. When curve fits were made on these two velocity profiles, the results were quite

different. Velocities calculated directly from measured diameter values contained large errors because of the squared diameter value in the calculation. Also errors in temperature measurements appeared as scatter in the density values used in the velocity calculations. After curve fitting such data the calculated value for the takeup velocity deviated greatly from the known experimental value. Velocities calculated from fitted values of the diameter did not contain an inflated error from the squared diameter. Curve fits on these data produced takeup velocity predictions that were within five percent of the actual values. This technique was used for all velocity calculations unless otherwise stated.

After obtaining the fit for velocity data, the velocity gradient was calculated using a differentiated form of equation (78),

$$\frac{dV}{dx} = AB'Ex^{E-1} \exp (B'x^{E}) \ . \qquad (85)$$

Force Balance

To obtain a value for F_{rheo} at each position along the spinline a force balance was made using equation (43) rearranged to give

$$F_{rheo} = F_{ext} + F_{grav} - F_{inert} \ . \qquad (86)$$

Experimentally measured takeup tension provided the value of F_{ext}; F_{grav} was calculated using equation (42a).

$$F_{grav,x} = \int_{x}^{L} \rho g A dx \ . \qquad (42a)$$

Diameter and density change from x = 175 cm to the takeup bobbin was negligible, and F_{grav} at x = 175 was simply

$$F_{grav,175} = \rho_{175} A_{175} (L - 175)g \ .$$

A trapezoidal rule integration of equation (42a), moving up the filament was performed from the 175 cm point, to give a numerical value of F_{grav} at each point. For example, the next point up the fiber was at ~170 cm, and the calculation was as follows:

$$F_{grav,170} = F_{grav,175} + \tfrac{1}{2}(\rho_{175}+\rho_{170}) \times \tfrac{1}{2}(A_{175}+A_{170}) \times 5.0 \times g \ .$$

In finite difference form the calculation proceeded from the nth point to the (n-1)th using the expression

$$F_{n-1} = F_n + g(x_n - x_{n-1}) \left(\frac{\rho_n+\rho_{n-1}}{2}\right) \times \left(\frac{A_n+A_{n-1}}{2}\right). \qquad (87)$$

Inertia force was calculated at each point as shown in equation (42c):

$$F_{inert} = W(V_L - V_n) \ . \qquad (42c)$$

Finally F_{rheo} was calculated at each point by substitution of values into the right hand side of equation (86).

Rheological and Time Scale Calculations

Stress at each point was calculated using values of F_{rheo} and A;

$$\tau_n = F_{rheo,n}/A_n \ , \qquad (88)$$

and the apparent elongational viscosity was computed as

$$\eta_{e,n} = \tau_n/(dV/dx)_n \ . \qquad (89)$$

Position along the spinline was converted to a time scale using the fitted velocity profile and the equation

$$t = \int_{x_1}^{x_2} \frac{1}{V} \, dx \ . \qquad (90)$$

Travel time from the spinneret to the first point was hand calculated using an arithmetic average of the velocity at the spinneret and the velocity at the first point. The fitted velocity equation was accurate for estimating velocity along the spinline beginning at the first measured point. However, the die swell region immediately below the spinneret was not described by the equation and an arithmetic average velocity was used to calculate the travel time from the spinneret to the first point of measurement. Travel time between any other points x_1 and x_2 was calculated by computer using equation (90) and the trapezoidal rule with a 1.0 mm interval length.

D. ANALYSIS OF CRYSTALLINITY DATA

Crystallization Rate

Crystallization rate dX/dt was calculated from the fitted crystallinity versus distance function. The relationship between distance and time derivatives is

$$\frac{dX}{dt} = \frac{\partial X}{\partial t} + V_x \frac{\partial X}{\partial x} \quad . \tag{91}$$

For a steady state spinning process the assumption was made that the rate of crystallization was constant with respect to time at any fixed point along the spinline. For a stable spinning process this assumption is good, and the time derivative becomes

$$\frac{dX}{dt} = V_x \frac{\partial X}{\partial x} \quad . \tag{92}$$

The value of $\partial X/\partial x$ was obtained by differentiating equation (79) to give

$$\frac{\partial X}{\partial x} = -100B'E\ (x-C)^{E-1}\ \exp\left[B'\ (x-C)^{E}\right] . \qquad (93)$$

Calculations using the Avrami, Ziabicki, and Nakamura equations required an extent of transformation instead of a percent or fraction crystallinity since polymers do not crystallize completely. The value of crystallinity measured in the fiber collected on a bobbin was taken to be the maximum value of crystallinity reached by that specific polymer sample. This value was designated as X_∞. The extent of transformation, or extent of crystallinity, was then calculated as

$$\theta = \frac{X}{X_\infty} , \qquad (94)$$

therefore

$$\theta = \frac{100}{X_\infty}\ (1-\exp\left[B'(x-C)^{E}\right]), \qquad (95)$$

and

$$\frac{\partial \theta}{\partial x} = \frac{1}{X_\infty}\ \frac{\partial X}{\partial x} . \qquad (96)$$

Hence

$$\frac{\partial \theta}{\partial x} = -\frac{100B'E}{X_\infty}\ (x-C)^{E-1}\ \exp\left[B'(x-C)^{E}\right] . \qquad (97)$$

The rate of crystallization at any point along the fiber was obtained by substituting equation (97) into (92).

The rate of crystallization at one half of the conversion was also calculated for each run using the method of Nakamura (79). The crystallization rate at the half conversion is given by

$$\left(\frac{d\theta}{dt}\right)_{\theta=\frac{1}{2}} = \frac{R(T-T_a)}{\Delta H} , \qquad (98)$$

where T is the temperature at which a plateau appears in the temperature profile for the spinning test in question. The cooling parameter R was calculated from the expression

$$R = \frac{4h}{\rho d} \quad , \tag{99}$$

where h is given by equation (100) according to Kase and Matsuo (47).

$$h = 0.473 \times 10^{-4} A^{-0.334} \left[V_x^2 + (8V_y)^2\right]^{0.167} \quad . \tag{100}$$

V_y is the velocity of quench air flowing perpendicular to the fiber axis (47). ($V_y = 0$ in this work.) The heat of fusion, ΔH, used in this case was based on a unit mass of partially crystallized polymer (79). Its relation to the heat of fusion per unit mass of crystalline material is

$$\Delta H = X_\infty \Delta H_c \quad . \tag{101}$$

Half time values of $d\theta/dt$ were also calculated from fitted data using the expression

$$\left(\frac{d\theta}{dt}\right)_{\theta=\frac{1}{2}} = \left(V_x \frac{d\theta}{dx}\right)_{\theta=\frac{1}{2}} \quad . \tag{102}$$

Crystallization Rate Constants and Avrami Index

Analysis of crystallization data to obtain rate constants and Avrami indices is difficult because of combined effects of time, stress, and temperature on the kinetics. With certain assumptions it is possible to analyze the data within the framework of existing nonisothermal crystallization theory. However, the results obtained in this case must be interpreted carefully.

Beginning with the equation of Nakamura (79),

$$\theta = 1 - \exp\left[-\left\{\int_o^t K[T(\tau)]d\tau\right\}^n\right] , \qquad (103)$$

we transpose terms and take the natural logarithm of both sides to obtain

$$\left(\int_o^t K[T(\tau)]d\tau\right)^n = -\ell n\ (1-\theta) \ . \qquad (104)$$

The right hand side of equation (104) can be calculated directly from experimental data. However, the relationship of such calculated values to the terms on the left hand side is not obvious since the function being integrated has an unspecified form. Also the value of n is not known from any separate analysis of the data. To proceed further one may assume or estimate a value for n and make further simplifications of equation (104); or, as an alternate approach, one may assume a form for the left hand side of the equation and proceed to apply it to the data.

If one assumes or otherwise obtains a value of n, values of $K[T(t)]$ can be calculated from a differentiated form of equation (104):

$$\frac{d}{dt}\int_o^t K[T(\tau)]d\tau = \frac{d}{dt}\left[-\ell n\ (1-\theta)\right]^{1/n} \ . \qquad (105)$$

Now

$$\frac{d}{dt}\int_o^t K[T(\tau)]d\tau = K[T(t)] \ , \qquad (106)$$

therefore,

$$K[T(t)] = \frac{d}{dt}\left[-\ell n\ (1-\theta)\right]^{1/n} \ , \qquad (107)$$

and

$$K[T(t)] = \frac{1}{n}\left[-\ell n\,(1-\theta)\right]^{\frac{1-n}{n}} \frac{1}{1-\theta}\frac{d\theta}{dt} \quad . \tag{108}$$

Values of K were calculated using equation (108) and integer values of one to four for n. For the case of n=1 equation (103) is the same as that derived by Ziabicki, and equation (108) readily simplifies to

$$K[T(t)] = \frac{1}{1-\theta}\frac{d\theta}{dt} \quad . \tag{109}$$

This expression was used with values of θ available directly from experimental data with values of $d\theta/dt$ calculated from fitted functions using equations (94) and (97) substituted into (92).

For the second method the assumption was made that the left hand side of equation (104) was an unknown function in t, and information about the form of the relationship could be obtained by the application of commonly used plotting techniques beginning with a plot of $-\ell n\,(1-\theta)$ versus t. Because of the dependence of K upon temperature, which itself varied with time, the interpretation of relationships obtained by this method must be done carefully.

CHAPTER VI

RESULTS AND DISCUSSION

The objective of this research was an experimental investigation of the development of structure in a semicrystalline synthetic fiber during the fiber forming, or spinning, process. To achieve this goal a spinning apparatus was constructed that would provide a controlled and reproducible spinning process while also permitting direct examination of the spinline by x-ray, photograph, and temperature measuring techniques. Tests were made at a variety of spinning conditions to determine the effect of process variables on structure formation in the fiber. Sample designations and spinning conditions for eight spinning tests are given in Table I. Future references to the runs or samples will be made using the sample designations shown in the table.

TABLE I. SPINNING CONDITIONS FOR LINEAR POLYETHYLENE SAMPLES

Sample Designation	Mass Flow Rate (g/min)	Take-up Velocity (m/min)	Extrusion[a] Temperature (°C)
PE03	1.93 ± 0.03	50	205
PE01		100	205
PE02		200	205
PE06		400	209
PE07		556	210
PE04		50	180
PE09	0.71 ± 0.02	200	207
PE05	4.00 ± 0.03	100	182

[a]Temperature of polymer measured within extruder.

The ensuing discussion contains numerous plots of typical data selected to clearly illustrate the principles under consideration. In such cases only a partial presentation of the data available from all spinning tests is made in order to avoid confusion in the plots. A complete tabulation of all experimental and calculated values is contained in Appendix A.

A. FILAMENT DIAMETER, VELOCITY, AND TEMPERATURE PROFILES

Filament diameter versus distance from the spinneret is shown for runs PE02, PE03, and PE07 in Figure 11. These runs cover the lowest to the highest spinning speeds used, and the shapes of the diameter profiles are typical of those obtained in all of the runs. As the polymer emerged from the spinneret it passed into a die swell region where the stream diameter increased from the the capillary diameter to a value slightly larger than the first measured data points shown in Figure 11. As polymer passes out of the die swell region its velocity increases and filament diameter decreases. Draw-down continues until the fiber has reached its final diameter and velocity and has solidified. Measured deniers of the final fibers are given in Table II.

Velocity profiles obtained by curve fitting the velocities calculated using the continuity equation are shown in Figure 12.

The transition from a low initial velocity to the final takeup velocity is clearly shown. The calculated velocity gradient dv/dx is shown in Figure 13 for the region below the die swell. As velocity changes the gradient increases to a peak value and then decreases

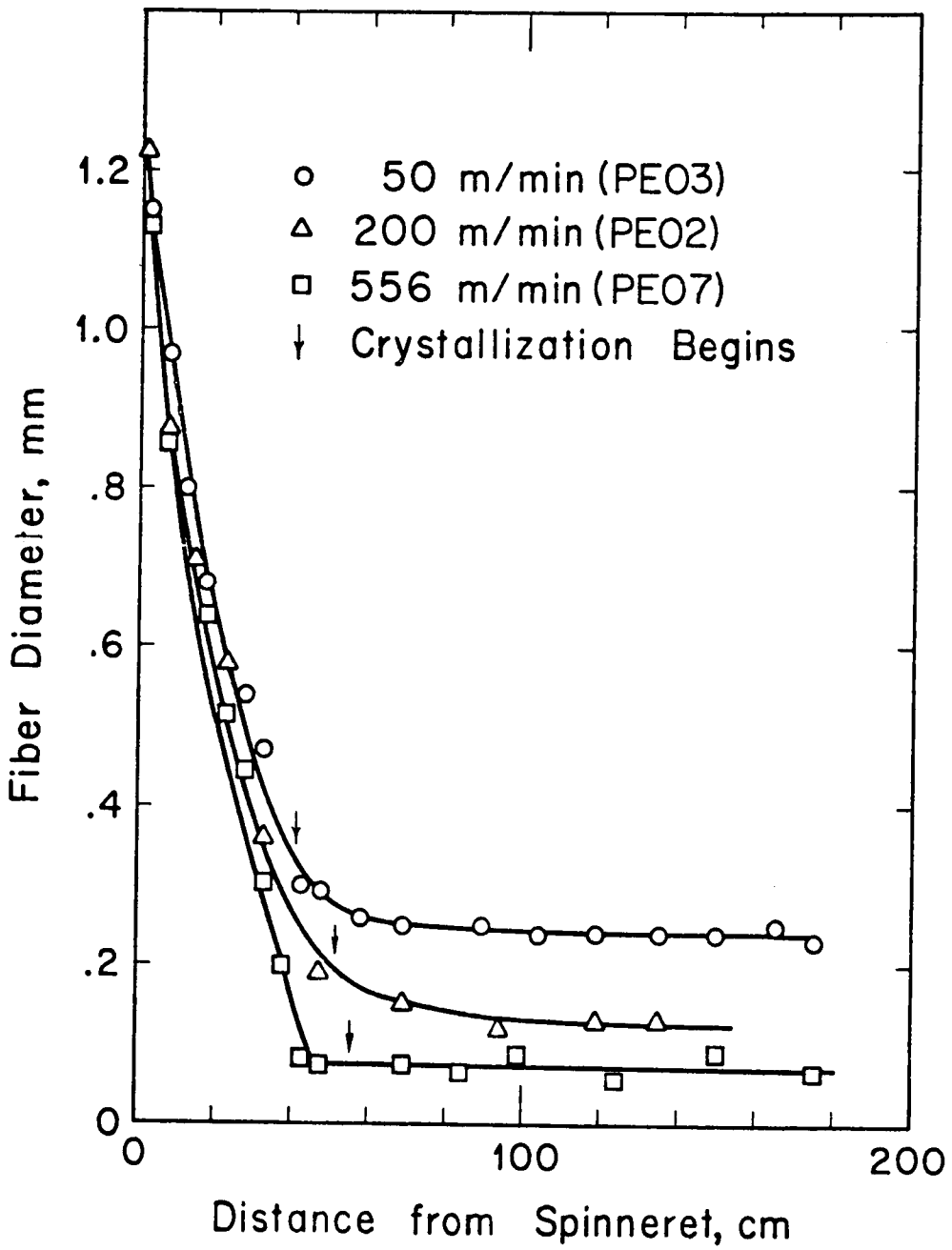

Figure 11. Filament Diameter Versus Distance From Spinneret.

TABLE II. FINAL FIBER DENIER

Run	Denier
PE01	190
PE02	104
PE03	328
PE04	319
PE05	335
PE06	42
PE07	25
PE09	33

to zero as takeup velocity is reached.

The peak in the velocity gradient also becomes narrower with decrease in mass flow rate showing that the draw-down zone becomes shorter. The elongation of the molten filament from the die swell diameter to its final diameter is described by the mass, momentum, energy and constitutive equations. Specific features of diameter, velocity, and velocity gradient profiles, such as the shape and location of the maximum velocity gradient, are complicated functions of several variables; consequently, simple statements of the effects of individual variables on these specific features are not always possible. This is the case with the maximum velocity gradient calculated for the spinning tests reported here. At constant mass flow rate an increase in take-up velocity causes the location of the maximum velocity gradient to move further down the spinline initially. With increasing take-up velocity a point is reached where the point of maximum velocity gradient begins to move back toward the spinneret. This behavior is possibly a result of a balance between heat transfer phenomena and the forces

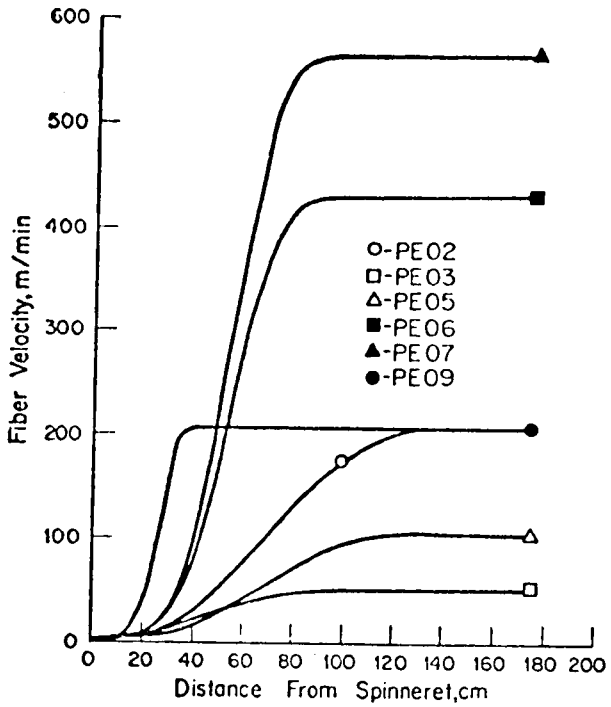

Figure 12. Velocity as a Function of Distance From the Spinneret.

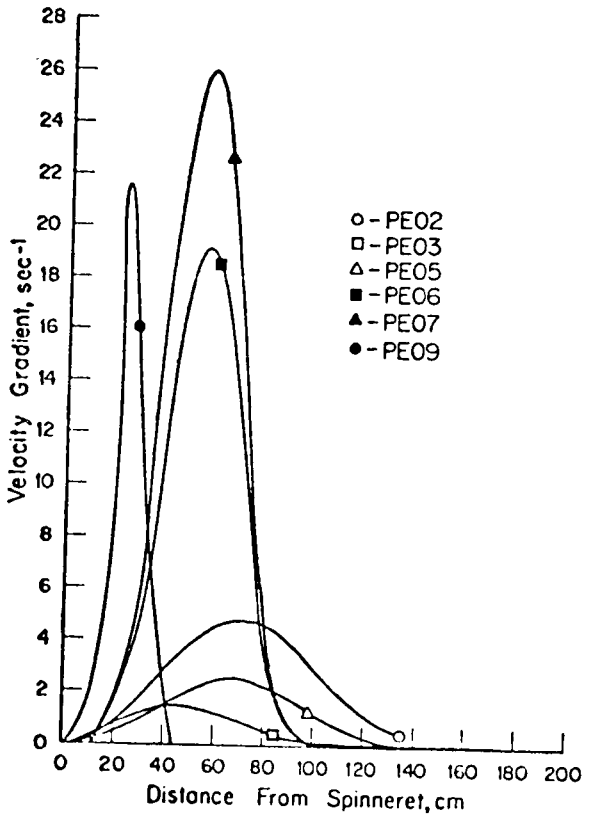

Figure 13. Velocity Gradient as a Function of Distance From Spinneret.

acting on the filament. At low speeds the momentum effects predominate and the maximum velocity gradient moves further down the filament as takeup velocity increases. As higher speeds are reached cooling of the filament increases dramatically because of smaller fiber diameter and higher velocity. This rapid cooling produces rapid changes in viscosity and the velocity gradient peak moves back toward the spinneret to maintain the proper momentum balance in the filament.

The increase in elongational velocity gradient (and stress) presumably increases the molecular orientation in the molten polymer and this in turn enhances crystallization kinetics as will be discussed in more detail in a later section. Crystallization is observed to begin at a point near the peak in the curves of velocity gradient versus distance from the spinneret where the melt stresses are highest. Once crystallization sets in the velocity gradient rapidly decreases to zero and the diameter becomes essentially constant.

The fiber surface temperature versus distance from the spinneret is shown in Figure 14. The fiber cools rapidly from the spinneret exit temperature until crystallization begins. The liberation of the enthalpy of crystallization causes a decrease in cooling rate which, in most cases examined, leads to an actual hold, or plateau, in the temperature (in one case an increase in temperature was observed). After a significant fraction of the crystallization has been completed, the fiber continues to cool, but the cooling rate decreases as the temperature approaches ambient. It should be noted that the point at which crystalline x-ray peaks were first observed occurred just ahead of the onset of the plateau in the temperature profile as would be

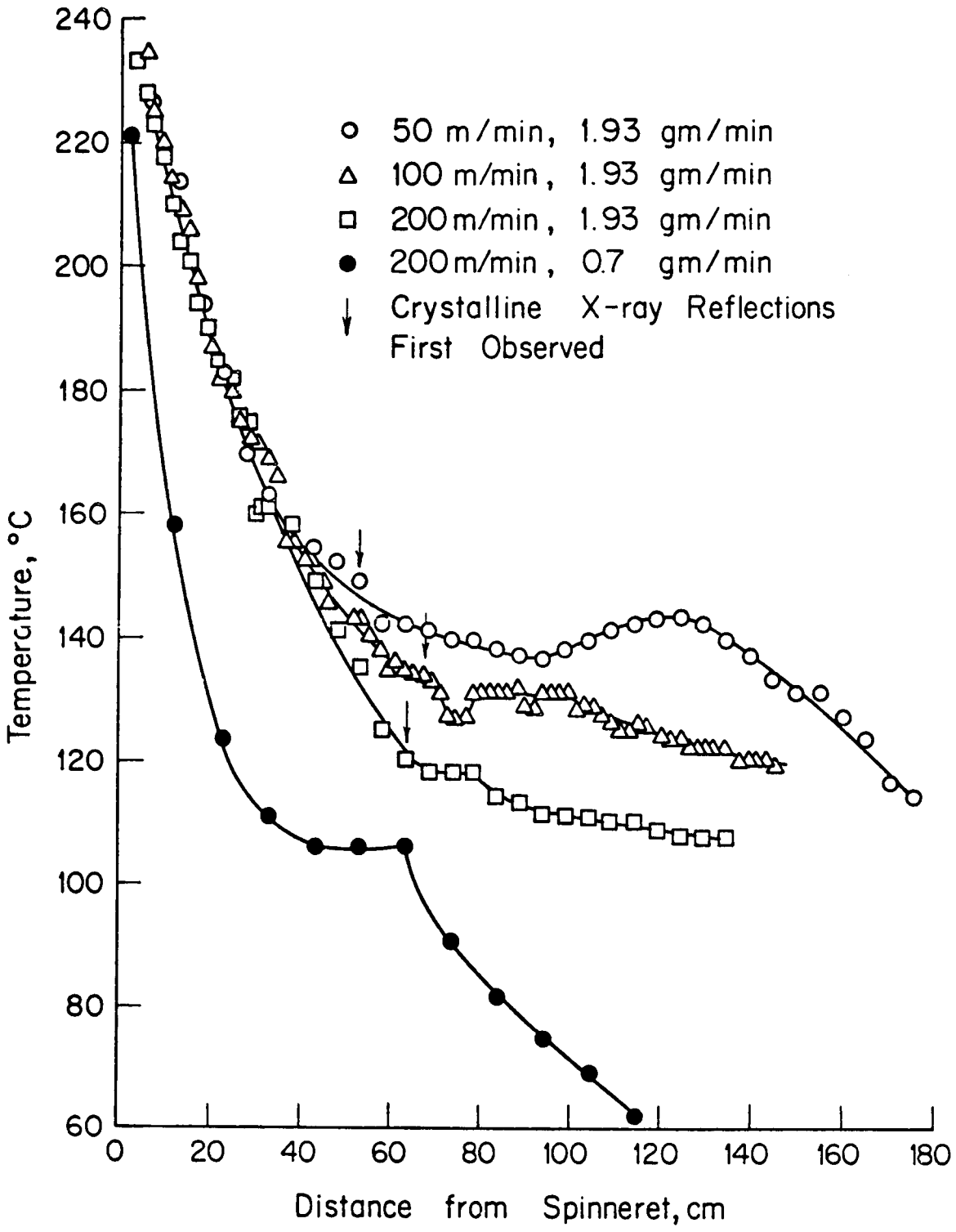

Figure 14. Fiber Surface Temperature Versus Distance from Spinneret.

expected. The diameter and velocity have almost reached their final values before the temperature plateau begins, and the velocity gradient has decreased significantly from its peak value. These observations are qualitatively consistent with those of Katayama, et. al., (49).

At constant mass flow rate the temperature profiles for various take-up velocities were quite similar in the portion of the spinline above the draw-down zone. Upon passing through the draw-down zone the cooling rate increases with takeup velocity because of the increased surface to volume ratio caused by the diameter change and also because of higher linear velocity through the cooling medium. The increased cooling rate at higher takeup velocities results in a more rapid decrease in fiber temperature with distance from the spinneret and in lower crystallization plateau temperatures. An increase in cooling rate is also obtained by decreasing the mass flow rate at constant takeup velocity thus reducing fiber diameter. The plateau temperature is plotted versus takeup velocity for several runs in Figure 15.

Crystallization temperatures for the Tenite polymer crystallized under quiescent conditions in a differential scanning calorimeter (DSC) are shown in Table III. The crystallization temperatures for samples cooled at rather modest cooling rates in the DSC are much lower than the plateau temperatures of several of the melt spinning runs. The cooling rates during melt spinning at temperatures near the plateau lie in the range 50 °C/sec to 2100 °C/sec for takeup velocities between 50 and 556 m /min at a mass flow rate of 1.93 g/min. The relatively high crystallization temperatures associated with rapid cooling conditions existing during melt spinning indicate that molecular

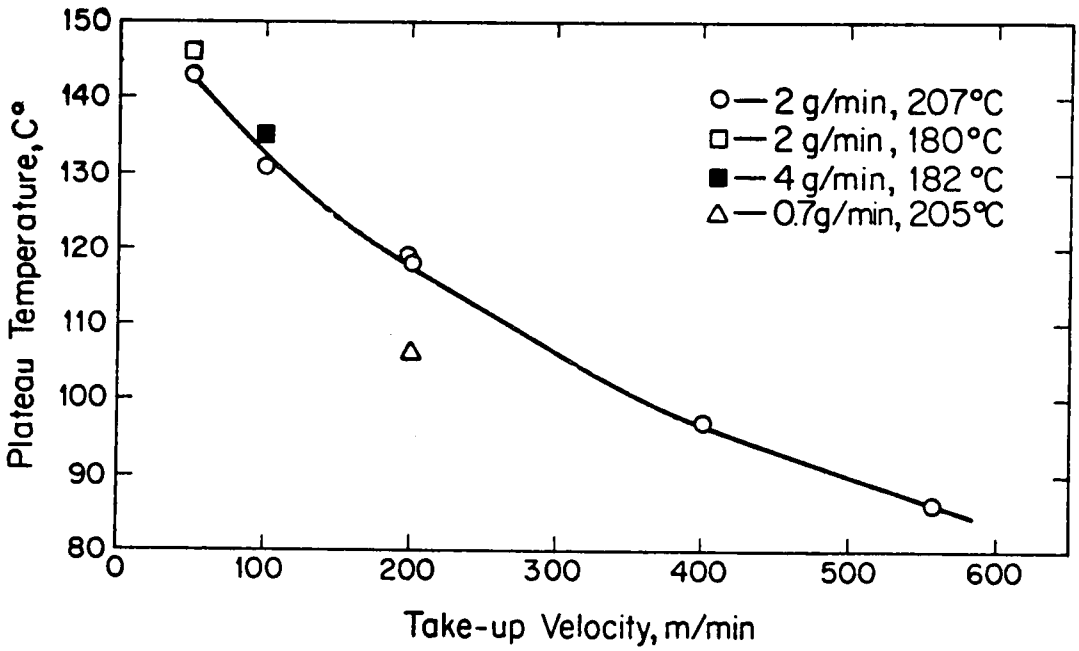

Figure 15. Temperature of Plateau in the Temperature Profile Versus Take-up Velocity.

TABLE III. CRYSTALLIZATION OF TENITE LINEAR POLYETHYLENE IN DIFFERENTIAL SCANNING CALORIMETER

DSC Cooling Rate[a] °C/min	Start of Crystallization[b] °C	Peak of Exotherm[b] °C
5	119	116
10	118	114
20	115	111

[a]All samples held 15 min at 205°C prior to cooling.

[b]Average of two runs at each cooling rate.

orientation resulting from the elongational flow and draw-down forces in the filament greatly increase crystallization rate. Although this idea has been proposed by previous investigators (1, 49) it is clear from the present data that in the case of linear polyethylene only relatively modest spinning conditions are required to provide a sizeable effect. It is also interesting that at low takeup velocities (ca. 50 m/min) crystallization proceeds at temperatures near or slightly above the melting point of the polymer crystallized under quiescent conditions.

At any takeup velocity and mass flow rate the temperature at which crystallization begins is the result of a balance between the supercooling effect provided by the high cooling rate and the increased crystallization rate caused by the molecular orientation in the filament. Since the crystallization temperature decreases with increasing takeup velocity in the range above 50 m/min, it would appear that in this range the increased cooling rates override any increase in crystallization kinetics resulting from increased molecular orientation. The

reverse must of course be true in some very low takeup velocity range.

B. SPINLINE STRESS AND ELONGATIONAL VISCOSITY

Stress in the filament is shown as a function of distance from the spinneret for several runs in Figure 16. Although the tension in the fiber varies only several percent from the spinneret to the takeup (see tabulated data in Appendix A), the stress increases as much as two orders of magnitude in some cases. This is caused by the decrease in cross sectional area of the fiber as it moves away from the spinneret.

Elongational viscosities for each run are tabulated in Appendix A. The values given were calculated using components for gravity and inertia in the force balance as well as a temperature and crystallinity dependent density. The data show a slight decrease in elongational viscosity in the first few centimeters below the spinneret followed by increasing viscosity. Several variations in calculation technique were tried to determine whether the initial viscosity decrease was introduced by the data analysis method or whether it actually occurred in the tests. These calculation methods included, as the simplest case, a calculation of spinline stress using a constant density and no gravity or inertia corrections; and experimental values of diameter were used without smoothing. Velocity gradient was calculated from the curve fitted velocity data using the expression discussed in the previous chapter. These measures reduced the size of the calculated viscosity decrease to a value within the limits of accuracy of the data. Other methods of data analysis evidently inflated the error and produced the

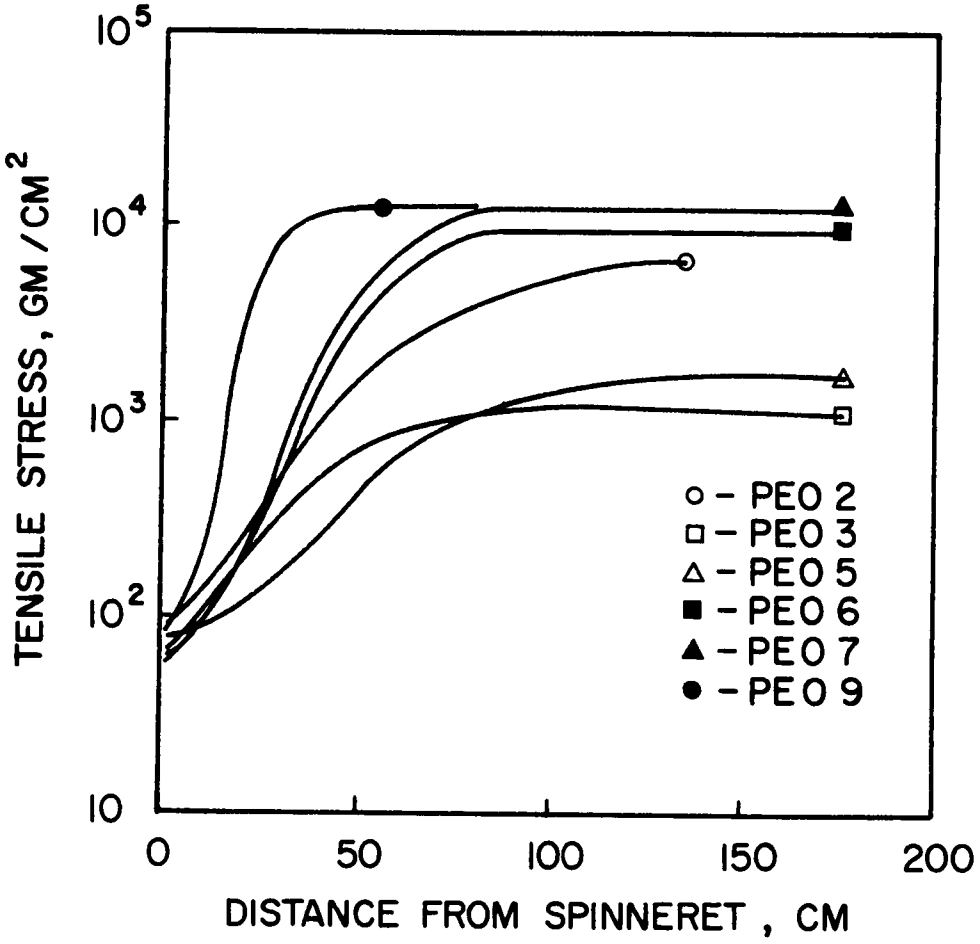

Figure 16. Tensile Stress in Spinning Filament as a Function of Distance from the Spinneret.

unexpected values. Future research requiring calculation of elongational viscosity in the molten part of the spinline should incorporate more data points, replication and averaging of measurements, and careful analysis of the data for the upper spinline.

The calculation used for elongational viscosity involves several assumptions. First, it assumes the fluid exhibits negligible elastic behavior and shows a very small response time in reacting to applied stresses. Also the calculated values are functions of temperature as well as deformation rate, and the filament temperature changes rapidly down the spinline. Thus the values calculated for apparent elongational viscosity are not fully representative of what would be obtained in isothermal steady state measurements. The deformation occurring during melt spinning never reaches a steady rate as can be seen in the rapid rise and fall of the velocity gradient as shown in Figure 13, page 79. Polymers that exhibit elastic behavior have stress-strain responses that include time related phenomena when subjected to such rapid deformation. These responses require more complex formulation than the simple Trouton viscosity. Also the deformation occurs over a range of rapidly changing temperature. Some form of temperature dependence must be assumed for the elongational viscosity for a complete data analysis.

A further complication in interpretation of the apparent elongational viscosity is the phase change that occurs during spinning. As the melt cools it begins to crystallize thus creating a two phase system. The elongational behavior of this system can no longer be described by the same constitutive equation as the melt phase alone.

C. DEVELOPMENT OF CRYSTALLINITY

Plots of percent crystallinity versus distance from the spinneret derived from the x-ray patterns taken along the spinline during operation are presented in Figures 17 and 18. Figure 17 is an example showing the x-ray patterns and typical data scatter. Figure 18 shows a comparison between the results for several runs. It should be realized that the crystalline orientation developed and hence the appearance of the x-ray patterns varies considerably from run to run; this will be discussed in detail below after discussion of the crystallization rates.

Crystallization begins at a point in the filament near the maximum in the velocity gradient and continues as the filament moves to the takeup bobbin. A large fraction of the final crystallinity, of the order of 60 percent, is developed prior to the end of the temperature plateau; but some increase in crystallinity continues further down the spinline. This behavior agrees with that expected for a material that remains above its glass transition temperature throughout the entire spinning process. Except for a reversal at the highest takeup speed, the polymer starts crystallizing slightly further down the spinline and progresses to a lower ultimate crystallinity as spinning speed increases as shown in Table IV. This latter behavior was also observed by Abbott and White (1) and attributed to the increased cooling rate at the higher takeup velocity as previously mentioned (compare samples PE03, PE02, PE06 and PE07).

One effect of mass flow rate clearly evident in Figure 18 is

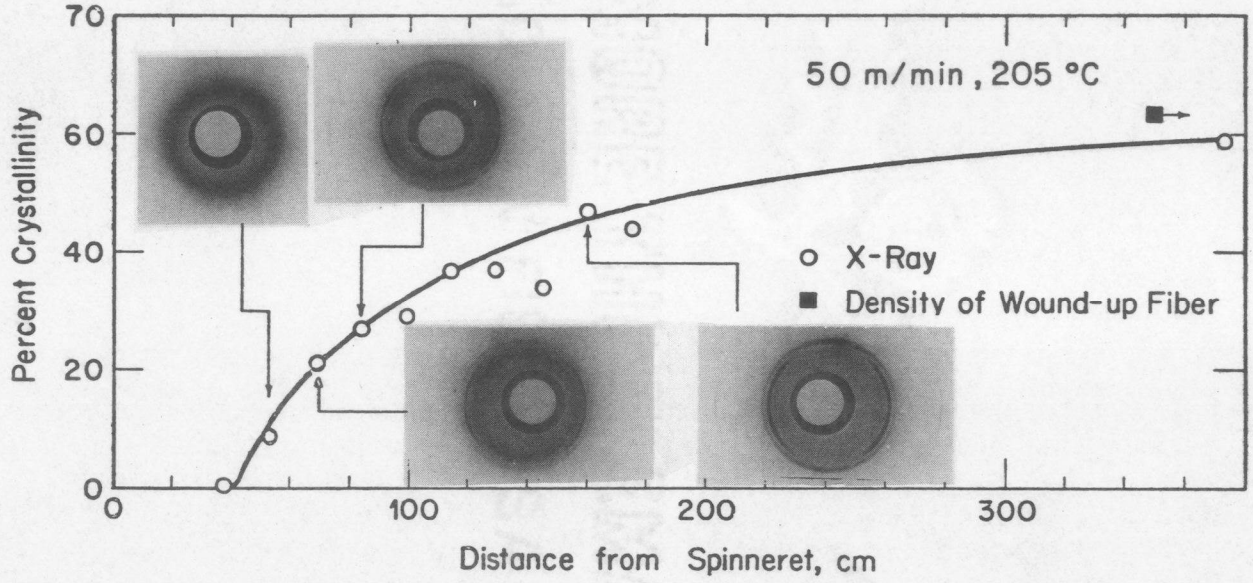

Figure 17. Typical Plot of Crystallinity Versus Distance from Spinneret.

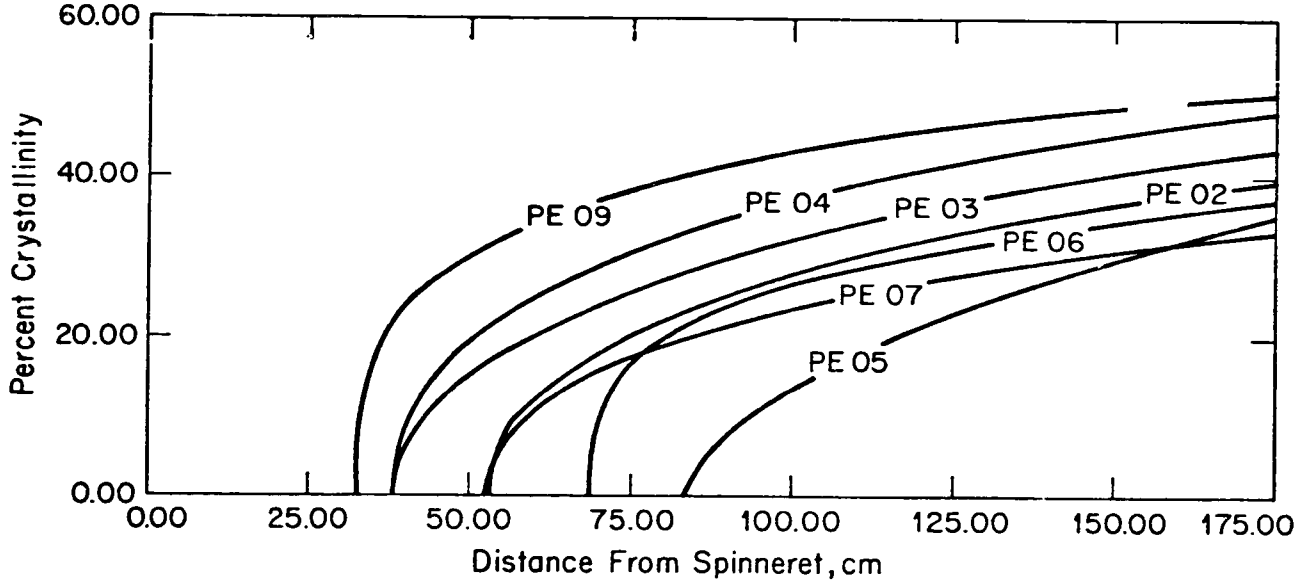

Figure 18. Crystallinity Versus Distance from Spinneret. Comparison of Results for Several Runs.

TABLE IV. ULTIMATE CRYSTALLINITY DEVELOPED DURING SPINNING

Run Number	Takeup Velocity (m/min)	Ultimate Crystallinity (%)
PE03	50	63.4
PE01	100	62.3
PE02	200	61.7
PE06	400	57.2
PE07	556	57.7
PE04	50	66.0
PE09	200	59.4
PE05	100	64.0

to move the point at which crystallization begins further from the spinneret with increasing flow rate (compare PE05, PE02 and PE09). Decreasing the mass flow rate at a given take-up velocity increases the cooling rate (Figure 14), increases the maximum velocity gradient and stress (Figures 13 and 16), and thereby would be expected to increase crystallization rates.

Conditions that increase the stress in the filament cause the curves in Figure 18 to rise abruptly as crystallization begins (sample PE06, PE09), while low spinline stresses lead to a more gradual rise in crystallinity with distance (PE03 and PE05).

Figures 19 and 20 show the percent crystallinity for a volume element in the filament versus a time scale calculated from the velocity profiles. Figure 19 shows the effect of increasing takeup velocity at constant mass flow rate and extrusion temperature. The time plotted in Figure 19 is measured from the point of extrusion. Figure 20 shows

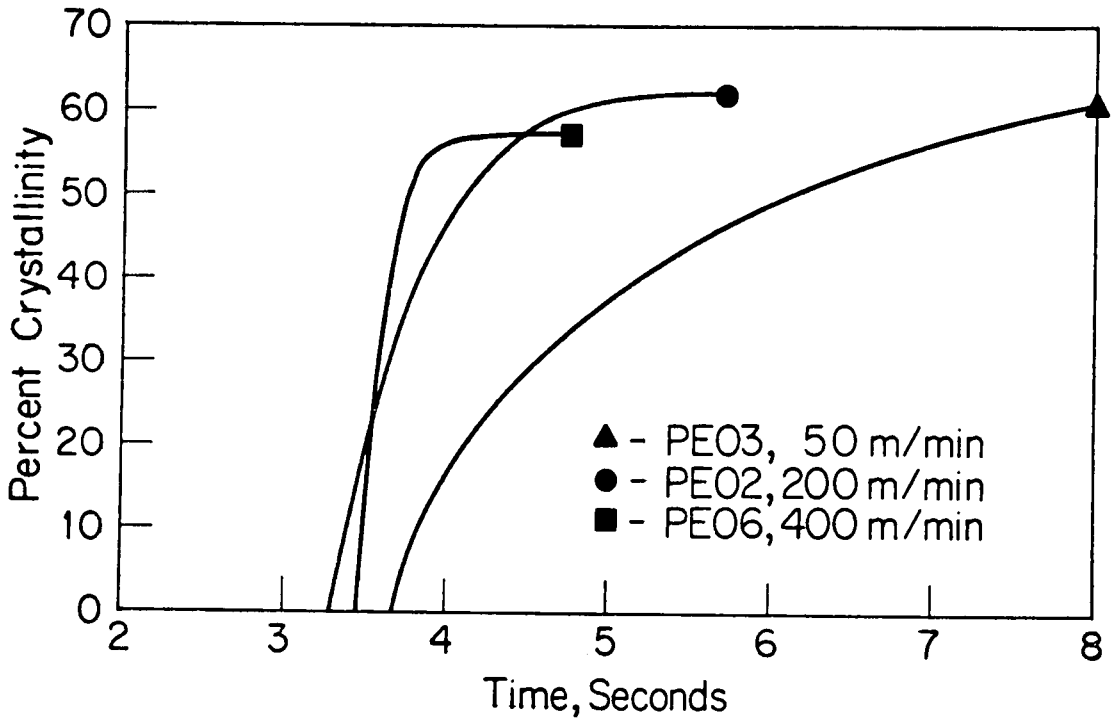

Figure 19. Crystallinity Versus Time After Leaving Spinneret Showing the Effect of Increasing Take-up Velocity at Constant Mass Flow Rate.

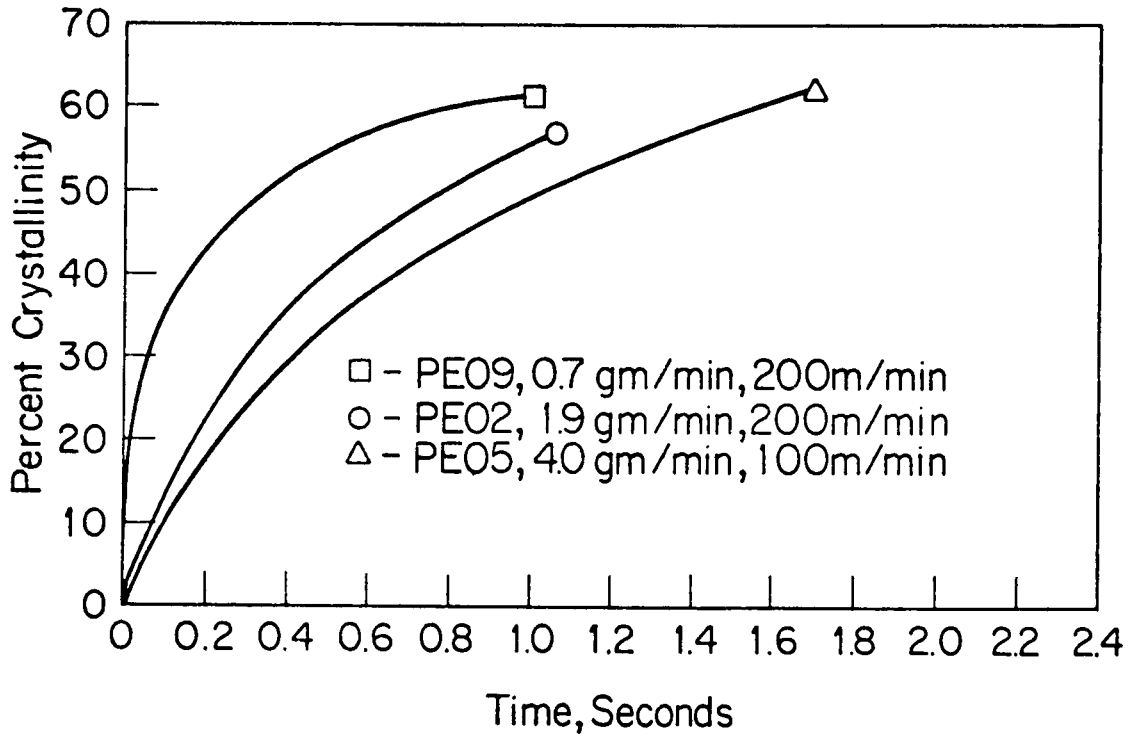

Figure 20. Crystallinity Versus Time from Start of Crystallization Showing the Effect of Changing the Mass Flow Rate.

the effect of changing the mass flow rate, and the time is measured from the start of crystallization. Because changing the mass flow rate has a marked effect upon the time the polymer spends in the molten zone, it is more meaningful for intercomparison to measure crystallization time from the start of crystallization rather than from extrusion in this case.

The effect of changing either the takeup velocity or mass flow rate may be interpreted in terms of the effect these changes have on the stress and the cooling rate of the filament. At constant mass flow rate an increase in takeup velocity will result in an increase in both stress and cooling rate in the filament leading to increased crystallization rates as shown in Figure 21. At a fixed spinning speed an increase in mass flow rate will cause an increase in filament cross sectional area and a slight change in tension with the net result being a decrease in stress. The larger diameter also results in a decrease in cooling rate. These factors thus lead to a decrease in crystallization rates (compare PE09 and PE02 in Figure 21).

The time required to reach one-half the final crystallinity measured from a point at which the fiber temperature was 150 °C is given together with the spinline stress (based on final diameter) in Table V. The choice of 150 °C as the temperature from which to measure crystallization times was arbitrary but based on the idea that above this temperature the filament would not be expected to have any tendency toward crystallization even with molecular orientation. Since more than half the crystallization occurred at the plateau temperature, this temperature is also given in Table V. For comparison the time to reach

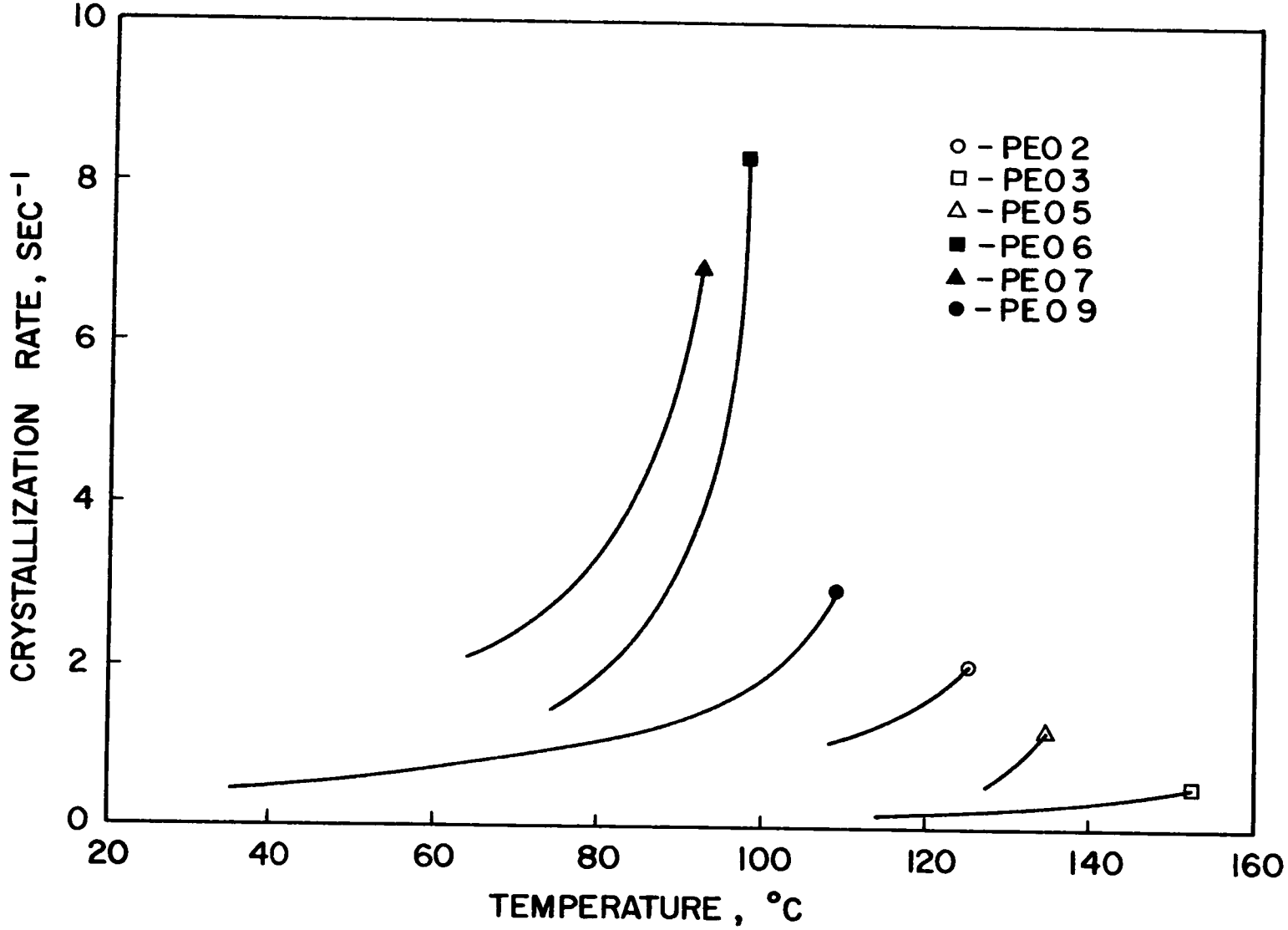

Figure 21. Crystallization Rate Versus Temperature as Calculated from Fitted Crystallinity Versus Distance Functions.

TABLE V. CRYSTALLIZATION HALF TIMES
DURING MELT SPINNING

Mass Flow Rate (g/min)	Takeup Velocity (m/min)	Extrusion Temperature[a] (°C)	Spinning Stress (dynes/cm^2 x 10^{-6})	Plateau Crystallization Temperature[b] (°C)	Crystallization Rate at Half Time[c] (sec^{-1})	Spinning Half Time[d] (sec)	Isothermal Half Time[e] (sec)
1.93 ± 0.03	50	205	1.0	143	1.6	0.65	---
	100	205	2.8	131	2.5	0.61	2.3 x 10^7 (66)
	200	205	5.5	118	4.9	0.51	306 (66)
	400	209	10.0	97	12.1	0.17	2.2 x 10^5 (66)
	556	210	17.1	86	16.0	0.08	3.8 x 10^8 (66)
	50	180	2.1	146	1.5	0.46	---
0.71 ± 0.02	200	207	12.1	106	12.2	0.44	3.5 x 10^3 (66)
4.00 ± 0.03	100	182	1.8	136	1.7	0.90	>10^{12} (66)

[a]Temperature of polymer measured within extruder.

[b]Temperature of plateau in surface temperature versus distance from spinneret curve.

[c]Calculated using equation (98) according to Nakamura (79).

[d]Time to reach 50% of the ultimate crystallinity starting from the point at which the surface temperature is 150 °C.

[e]Crystallization half times for quiescent, isothermal conditions. Numbers in parentheses refer to list of references.

one-half the ultimate crystallinity under quiescent isothermal conditions at a temperature corresponding to the plateau temperature is also given. The first values presented [Reference (66)] were obtained by fitting the data given by Mandelkern (66) to the equation given by Takayanagi and Kusumoto (102) for the temperature dependence of the crystallization rate constant, and then computing from this equation the values of crystallization half-time at the appropriate temperatures. Although differences in polymers and small errors in temperature can make large changes in the comparisons, it is clear that a conservative estimate of at least a several hundred fold increase in crystallization rate occurs during melt spinning as compared to quiescent conditions. Increases in crystallization rate of about the same order observed here have been observed by Haas and Maxwell (34) in linear polyethylene crystallized under shear stress.

The crystallization rate at the time of one-half transformation was calculated by the method of Nakamura using equation (98). The values obtained are presented in Table V. Similarly the half-time calculation made using equation (102) is given in Figure 22. In both cases the rates increased with increasing spinline stress although the values were quantitatively different in the two cases. The differences probably arise from experimental error as well as the assumptions used in the Nakamura method. As shown in Figure 21, crystallization began at initially high rates in all runs and decreased to lower rates as the filament cooled. More than half of the crystallization occurred over a temperature range of ten degrees or less, and it developed at high rates. The low temperature parts of the curves in Figure 21 represent crystallization that occurs after the half-time and in the presence of a large enough fraction

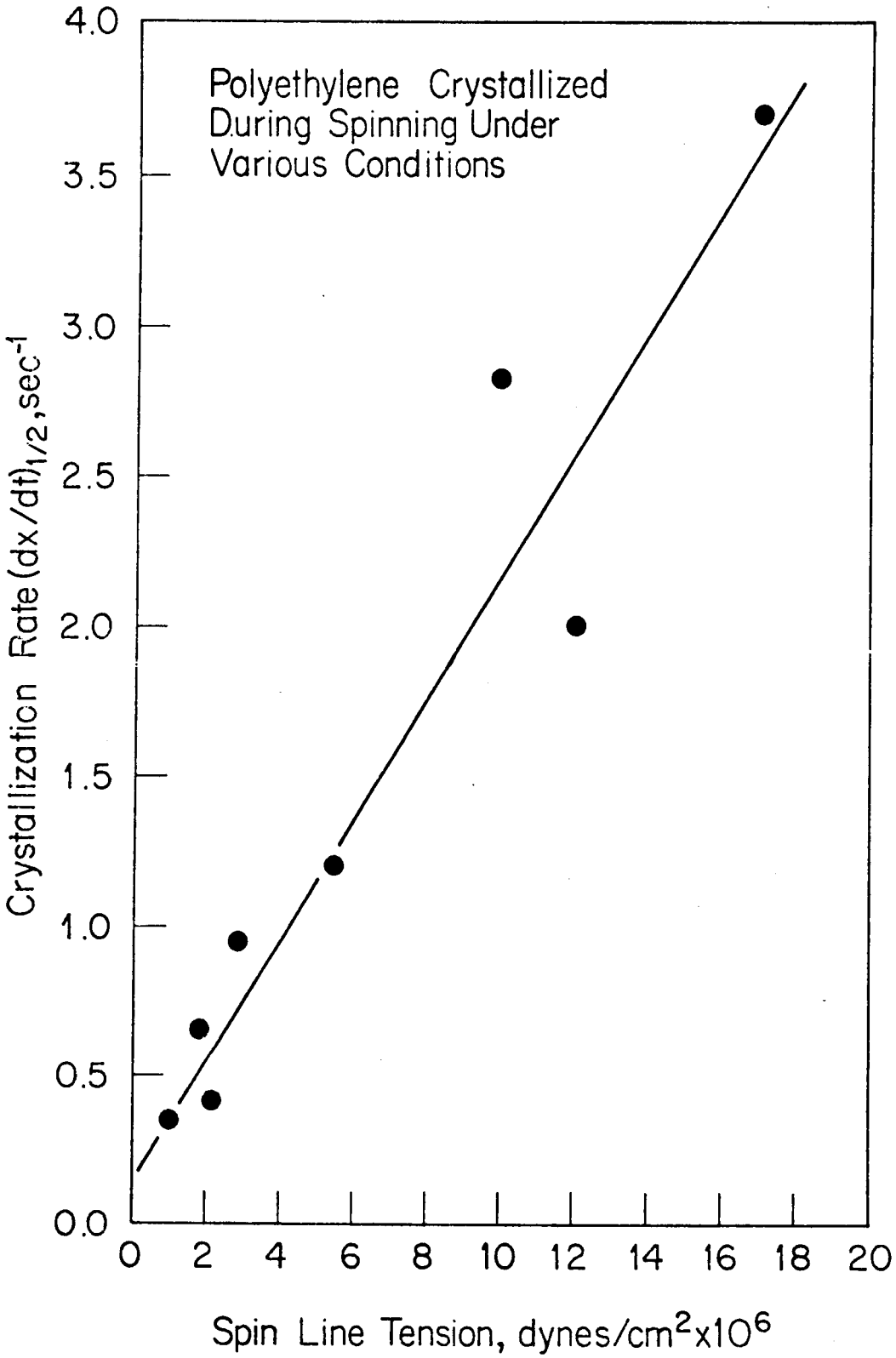

Figure 22. Plot of Crystallization Rate at the Half Time Versus Spinline Tension.

of crystalline material to cause significant impingement effects in further crystal growth.

Values of the crystallization rate constant were calculated using Avrami exponents of one through four in equation (108). $K[T(t)]$ is plotted against temperature for an Avrami exponent of one in Figure 23. As with crystallization rate, the values of $K[T(t)]$ are higher at the high stress spinning conditions and show an increase with increasing spinning speeds. (Compare PE03, PE02, PE06, and PE07.)

Graphical analysis of the $-\ell n\,(1-\theta)$ data produced a linear relationship between this quantity and time in all of the runs. Typical cases are shown plotted in Figure 24. It was not obvious from theory that linear behavior would occur, and this result is not readily explainable in terms of existing nonisothermal crystallization theory. A better understanding of the mechanisms involved in crystallization in a spinning filament is needed to resolve this problem. The slopes of the linear plots of $-\ell n\,(1-\theta)$ versus t provide another measure of the rate of crystallization. A plot of these slopes versus spinline stress is shown in Figure 25. The increase in crystallization rate is directly related to the increase in the slopes of the $-\ell n\,(1-\theta)$ versus t plots as shown by comparison with Figure 22 and with the data in Table V.

D. DEVELOPMENT OF CRYSTALLINE ORIENTATION

Crystalline orientation was observed in all samples investigated. At a takeup velocity of 50 m/min and above, the 020 reflection was

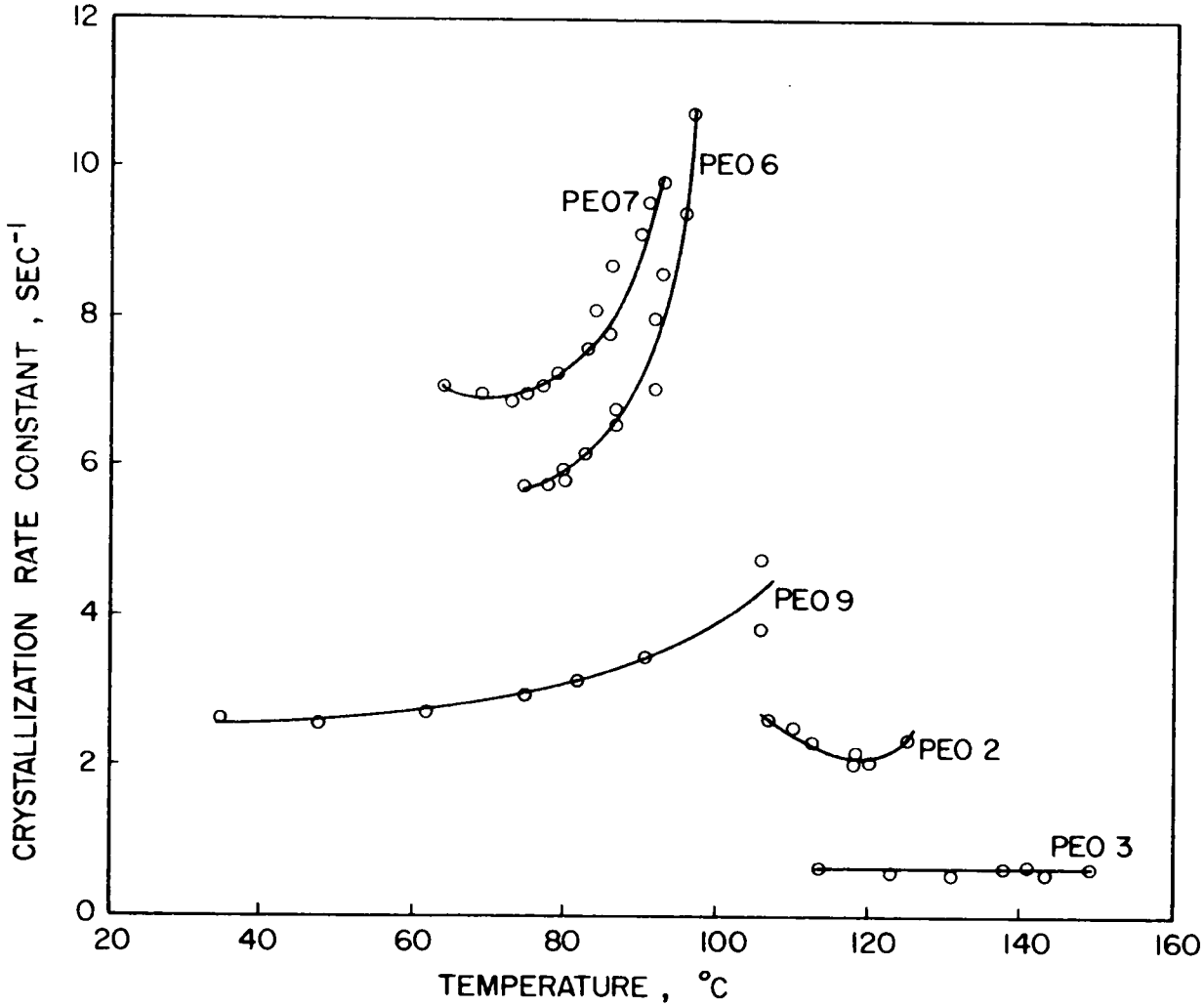

Figure 23. Crystallization Rate Constants Calculated from Equation (108) with an Exponent of One and Plotted Against Temperature.

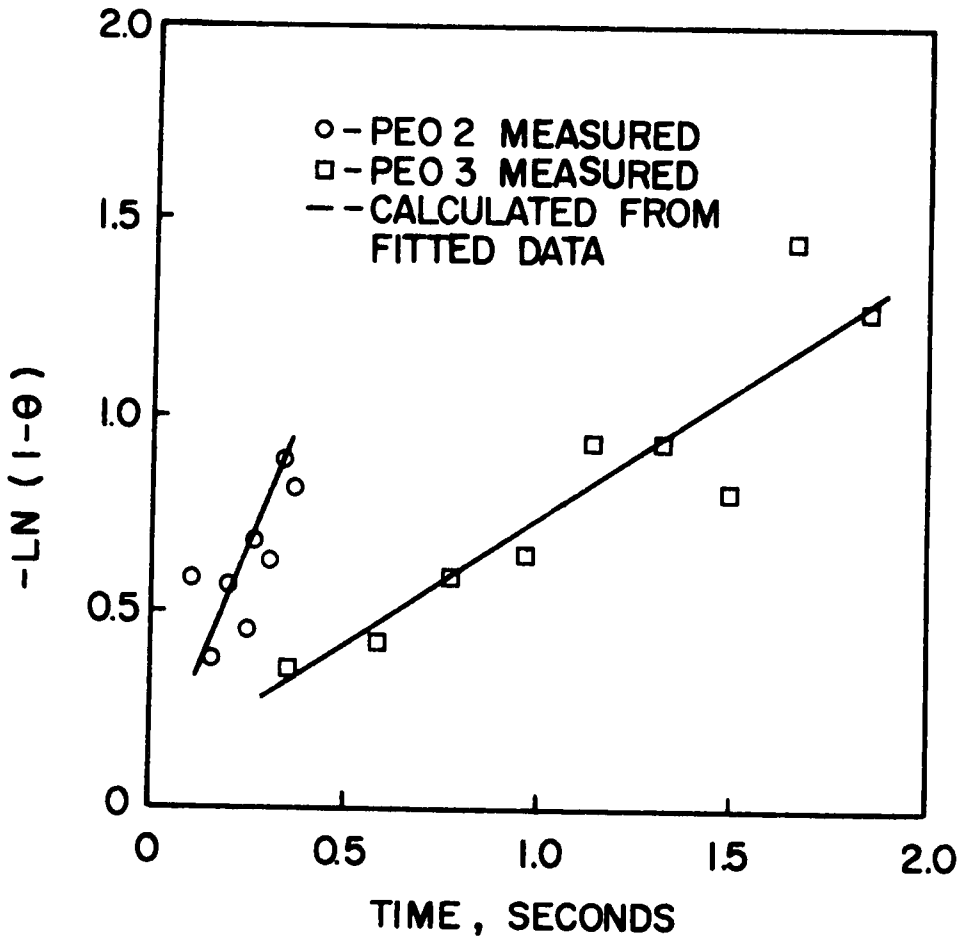

Figure 24. Plot of Phase Transformation data as $-\ell n\,(1-\theta)$ Versus Time.

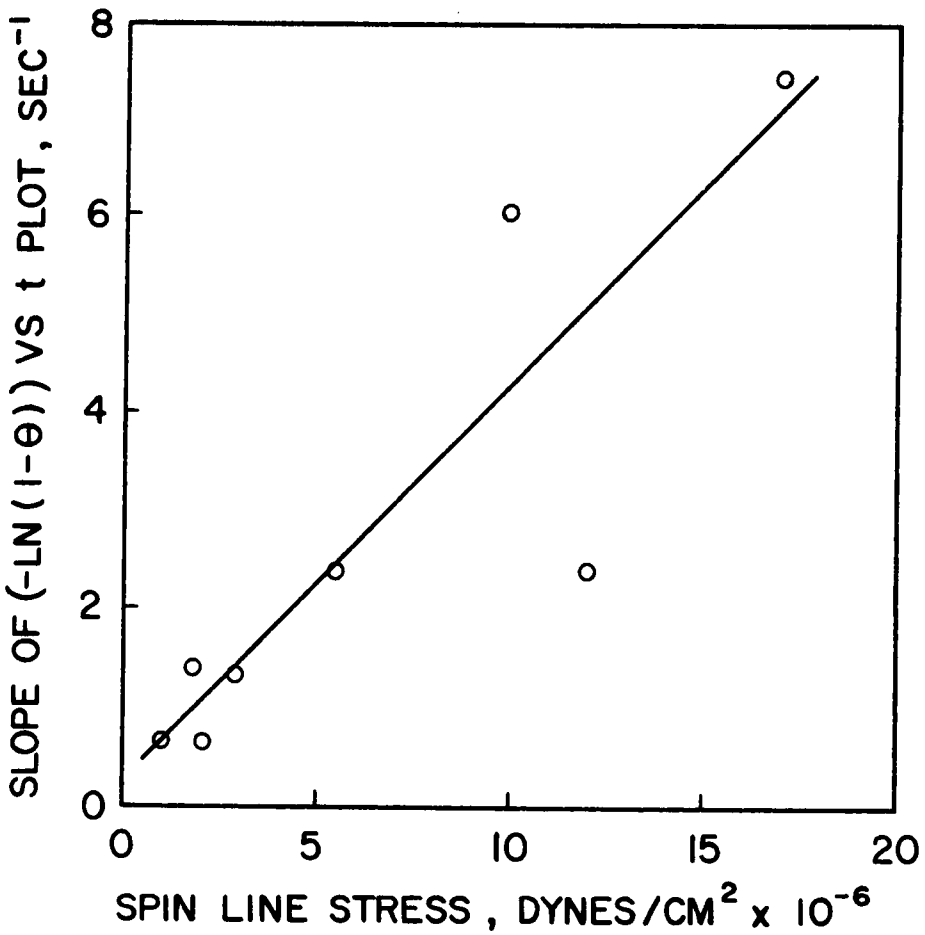

Figure 25. Slope of the $-\ell n\,(1-\theta)$ Versus Time Plots Shown Plotted Against Take-up Stress in the Spinline.

concentrated near the equator, thus indicating a tendency for the b-axes of the orthorhombic polyethylene unit cells to lie perpendicular to the fiber axis. The intensity distribution around the 200 reflection varied markedly with takeup velocity. It exhibited a maximum on the meridian at low takeup velocities but this changed to a maximum on the equator at higher takeup velocities. This effect may be observed clearly and quantitatively in the pole figures presented in Figure 26.

The values of the orientation functions f_a, f_b, and f_c computed from the diffractometer data are shown plotted as a function of takeup velocity in Figure 27. According to Equation (110) the values of the orientation functions should be zero for a random sample. If an axis is parallel to the fiber axis, the orientation for that axis is 1.0; and if an axis is perpendicular to the fiber axis, the respective orientation function is -0.5. With increasing takeup velocity f_c increased indicating a tendency for the c-axes to align with the fiber axis. The value of f_b rapidly decreased to values near -0.4 indicating that the b-axes were nearly perpendicular to the fiber axis. The behavior of f_a, first increasing and then decreasing, is more complex and will be considered in detail later. Similar trends in the variation of the orientation functions with takeup velocity were observed by Abbott and White (1) at mass flow rates both higher (5 g/min) and lower (0.5 g/min) than those used in the present investigation. As mass flow rate decreased the takeup velocity at which f_c rises rapidly and f_a goes negative decreases.

Figure 28 shows the variation of f_a, f_b, and f_c as a function of position along the spinline for three different takeup velocities.

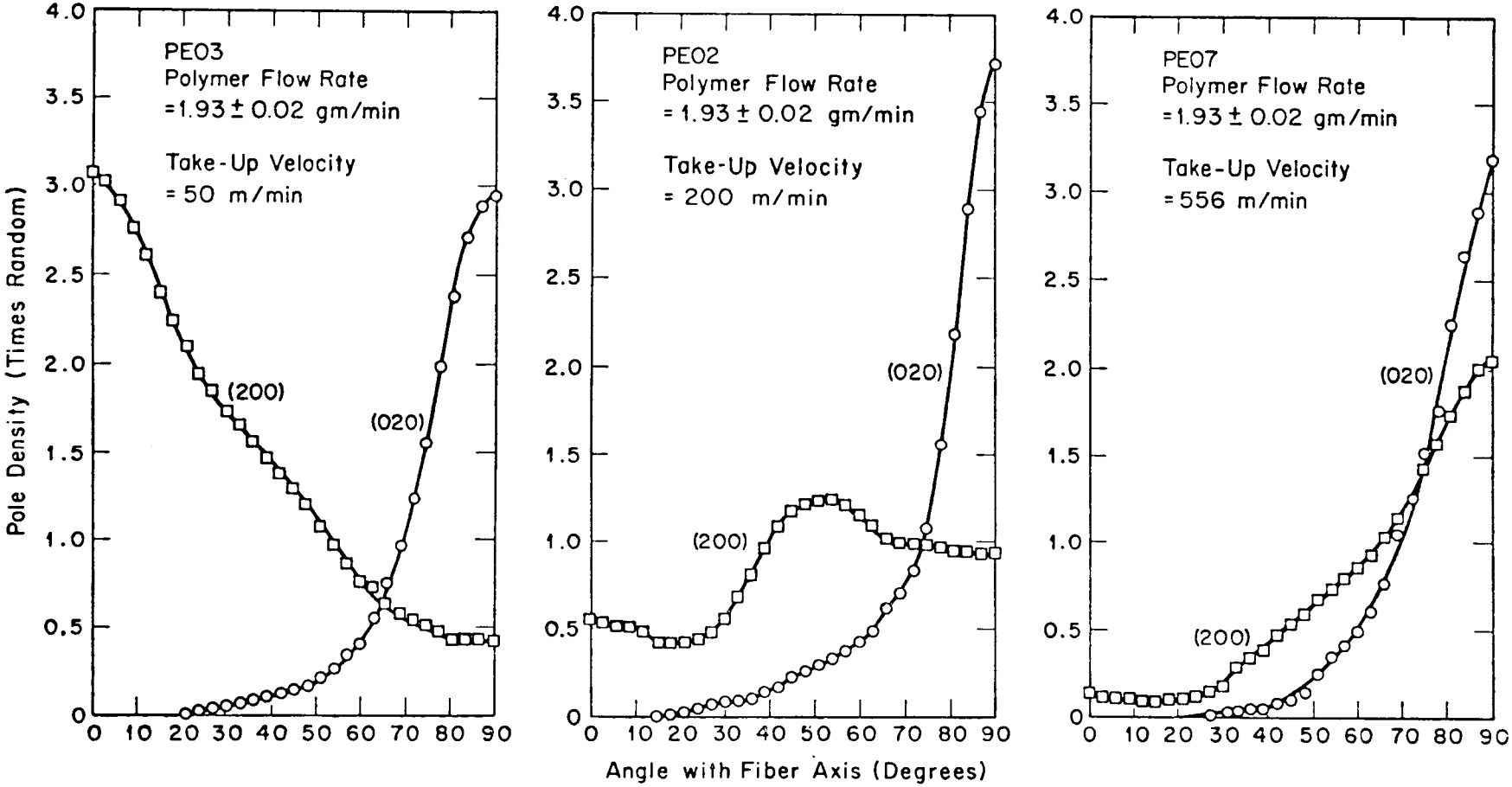

Figure 26. Pole Density Distributions for the (200) and (020) Reflections at Take-up Velocities of 50 m/min, 200 m/min, and 556 m/min.

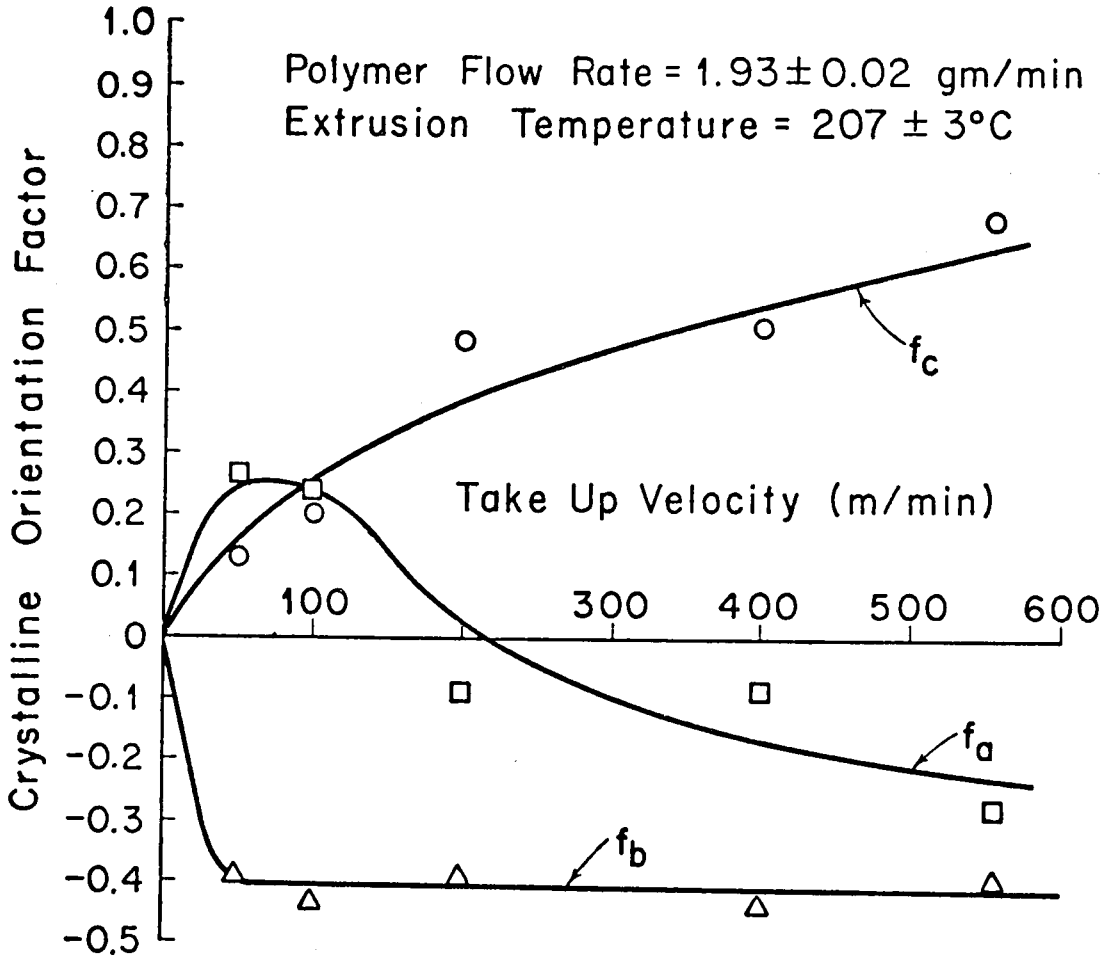

Figure 27. Crystalline Orientation Functions Versus Take-up Velocity.

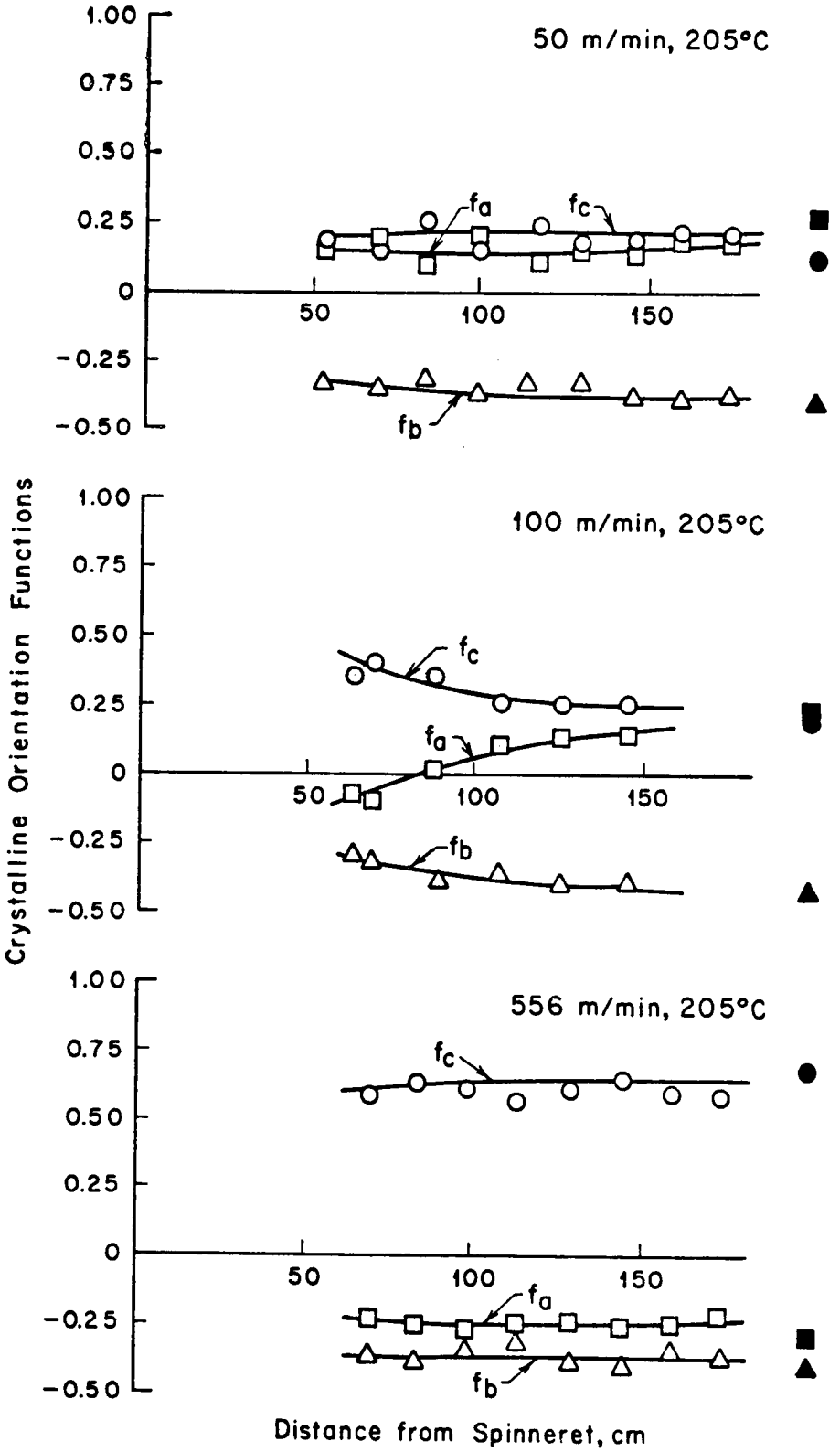

Figure 28. Variation of Crystalline Orientation Functions Along Spinline for Take-up Velocities of 50 m/min, 100 m/min, and 556 m/min.

These values were computed from the microdensitometer scans of the WAXS patterns made during spinning. The trends observed in the three examples shown are typical of the observed behavior. At both low and high takeup velocities (50 m/min and 556 m/min) the orientation is very similar to that observed in the final fiber from the point at which the crystalline reflections could first be observed onward. In the intermediate takeup velocity range (100-200 m/min) the a- and c-axis orientation functions were observed to change along the spinning way as shown in Figure 28. The a-axis orientation function increases from a negative to a positive value while the c-axis orientation function decreases. During the early stages of crystallization the observed patterns are similar to those developed at higher takeup velocities (and therefore high stress). Further down the spinline the patterns change toward those observed for lower takeup velocities. A similar change in c-axis orientation along the spinning way was observed by Katayama et. al., (49), but their spinning conditions were evidently not sufficiently diversified to observe the other extreme conditions shown in Figures 19 and 20. They attributed the decrease in c-axis orientation to a sudden tilting of the polyethylene chains within lamellar crystals. Our interpretation differs from this, it will be presented in the discussion of fiber morphology.

E. SMALL ANGLE X-RAY SCATTERING

The SAXS results are presented in Figure 29 and Table VI. The patterns in Figure 29 show that there is a strong intensity maximum on the meridian for a takeup velocity as low as 50 m/min. It should

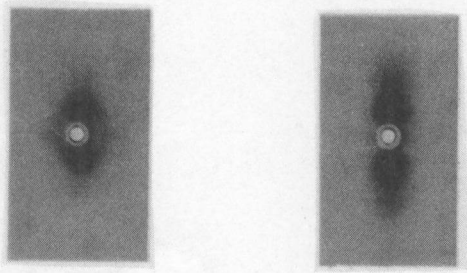

50 m/min
PE03

400 m/min
PE06

Figure 29. Pinhole SAXS Patterns for a Low Take-up Velocity (50 m/min, PE03) and a Relatively High Take-up Velocity (400 m/min, PE 06)

TABLE VI. LONG PERIODS OF SPUN FIBERS

Mass Flow Rate (g/min)	Takeup Velocity (m/min)	Long Period (Å)
1.93 ± 0.03	50	247
	100	239
	200	226
	400	227
	556	229
0.71 ± 0.02	50	248
4.00 ± 0.03	200	220
	100	248

be noted, however, that the intensity spreads around the incident beam at low takeup velocities and that this effect disappears as takeup velocity increases. If we assume the usual interpretation that the meridional maxima are caused by alternating lamellar crystalline and amorphous (or disordered regions) along the fiber axis directions, the intensity spread can be associated with a spread in the orientations of the lamellar crystals. This is also consistent with the increase in c-axis orientation parallel to the fiber axis with increasing takeup velocity as shown in Figure 27.

A weak second order peak was observed on the meridian in the original patterns; and, if highly overexposed, a third order maximum could be observed on samples spun at the highest takeup velocities. This is further evidence for a fairly regular stacking of lamellar and interlamellar regions parallel to the fiber axis. Patterns for as-spun fibers similar to our high takeup velocity cases showing second and third order maxima have previously been published by Statton (97).

The values of long period spacing shown in Table VI were computed by applying Bragg's law to the centroids of the first order maxima in the scattering curves. Although the changes are not large there seems to be a trend toward smaller long periods with increasing takeup velocity and decreasing mass flow rate. Recalling that the temperature at which much of the crystallization occurred decreased and the stress in the draw-down region increased with increasing takeup velocity and decreasing mass flow rate, the observed trend seems reasonable.

The values of the long period spacings in our spun fibers are much smaller at similar crystallization temperatures than those observed by Kavesh and Schultz (50) for quiescent melts, and our values do not vary as much with crystallization temperature. Our results are consistent with Statton's values for melt spun fibers, however (97). The differences between the long period spacings for quiescent melts and melt spun fibers is undoubtedly associated with the more rapid crystallization kinetics caused by molecular orientation.

F. SCANNING ELECTRON MICROSCOPY

The surfaces of the spun fibers were examined in a scanning electron microscope. A lamellar texture perpendicular to the fiber axis was observed. Since the resolution of this instrument is insufficient to clearly resolve lamellae of approximately 200 Å dimensions, the observed texture probably consisted of "bundles" of lamellar crystals. The appearance of the texture varied somewhat with spinning conditions as shown in Figure 30. With increasing takeup velocity the surface texture became finer and somewhat more uniform.

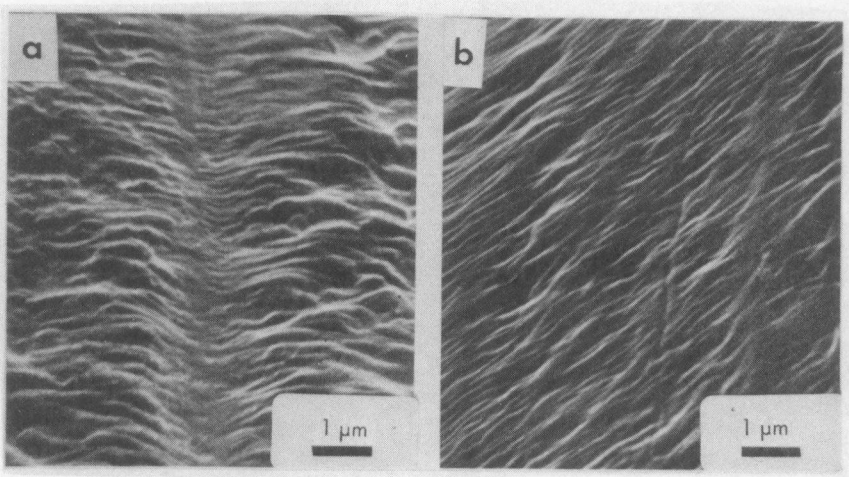

50 m/min 556 m/min

Figure 30. Scanning Electron Micrographs of the Surface Texture of Polyethylene Fibers Spun With Take-up Velocities of 50 m/min and 556 m/min.

Lamellae perpendicular to the fiber axis in melt spun polyethylene have also been observed using transmission electron microscopy (replica technique) by Fung and Carr (29).

G. BIREFRINGENCE, TENSILE PROPERTIES, AND THE ROLE OF SPIN LINE STRESS

At a mass flow rate of 1.93 g/min and an extrusion temperature of 205°C the spinline stress increased by a factor of about seventeen with an increase in takeup velocity from 50 to 556 m/min (see Table V, page 96). Spinline stress also increased with decreasing mass flow rate of decreasing extrusion temperature. Thus the important effect of such variables as takeup velocity and mass flow rate on the orientation developed in the fiber can be traced largely to the effect of these variables on the spinline stress.

Figure 31 shows experimental values of as-spun fiber birefringence plotted as a function of spinline stress. As the stress increases, the c-axis orientation and, hence, the birefringence increases steadily. This figure also shows values of crystalline birefringence calculated from the equation (99, 103)

$$x_c \Delta_c = x_c \frac{2}{9} \pi \frac{(\eta^2 + 2)^2}{\eta} (\alpha_{||} - \alpha_{\perp}) f_c \qquad (110)$$

using our orientation functions and density crystallinity values together with the values of the other parameters given by Stein and Norris (99). In Equation (110) η is the average refractive index and $\alpha_{||}$ and $\alpha_{\perp}$ are the average polarizabilities per unit volume of the crystal parallel to and perpendicular to the c-axis. Within the experimental accuracy

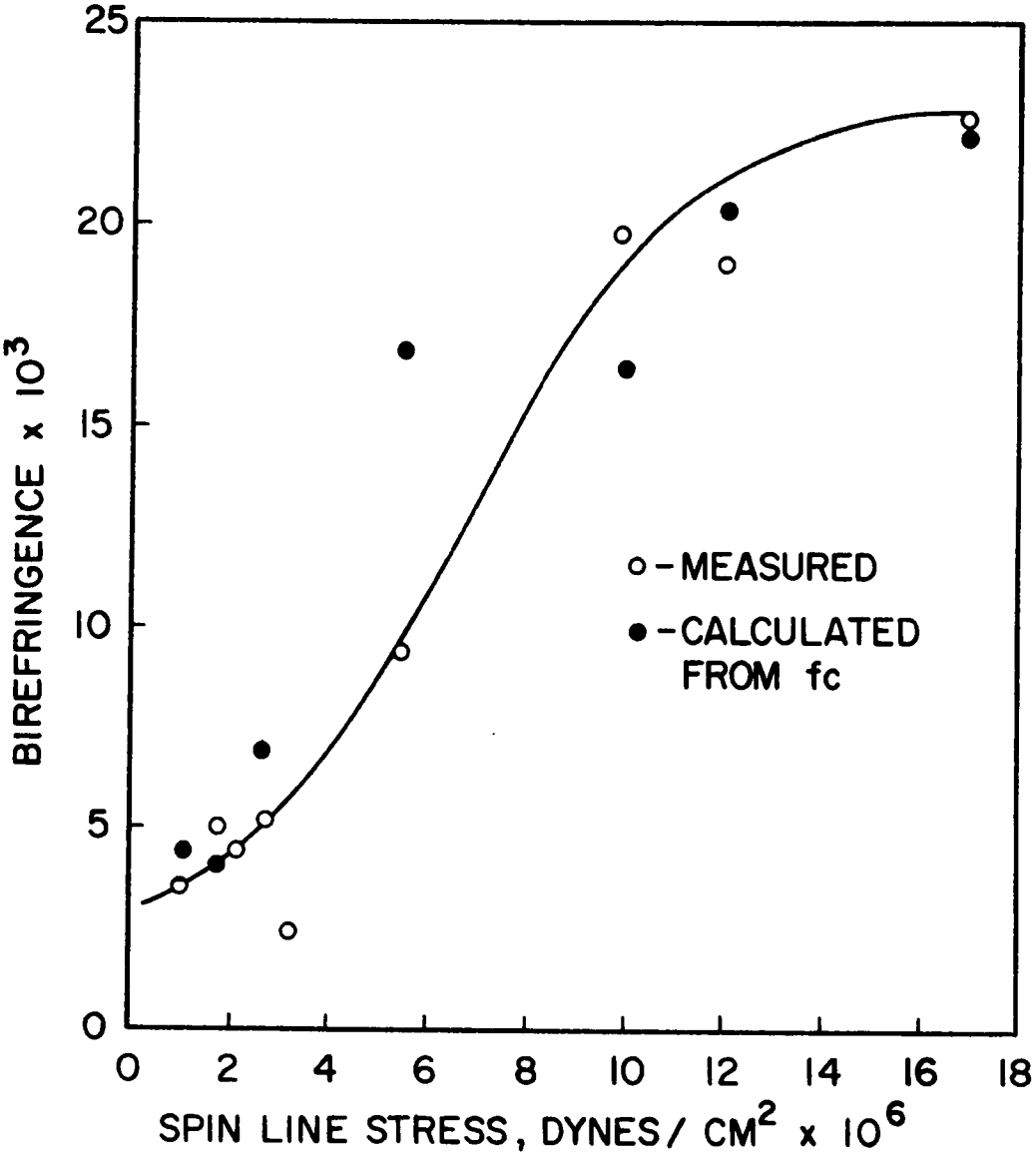

Figure 31. Birefringence of Fiber Versus Stress During Spinning.

of our birefringence, orientation function and crystallinity results it would appear that the total birefringence of these as-spun fibers is given by the crystalline contribution (a small negative contribution by the amorphous fraction may be indicated over part of the range). This result is perhaps not surprising in view of the high crystallinities of these linear polyethylene filaments and the likelihood that the "amorphous" portions probably consist of loose chain folds between the lamellar crystals together with various structural defects.

The tensile strength, elongation to break and Young's modulus of as-spun linear polyethylene fibers is shown in Figures 32 and 33 plotted versus the c-axis, crystalline orientation function f_c. A strong correlation is observed between the c-axis orientation and each of the measured properties. Since the crystallinity (density) of the fibers only varies from 57-66 percent, (see Table IV, page 91), the effect of such variation per se on the properties should be small. The large differences in properties therefore appear to be a consequence of the molecular orientation and/or changes in morphology with spinning conditions.

Investigators studying drawn fibers (75, 90, 91) prepared from low orientation starting materials have argued that the amorphous orientation and particularly the number of tie molecules is of overriding importance in determining the mechanical properties. As spinline stress increases we might expect the greater molecular orientation developed in the molten zone to create larger numbers of tie molecules in the spun fiber and thereby lead to the observed increases in modulus and tensile strength. In as-spun polyethylene fiber our data indicate

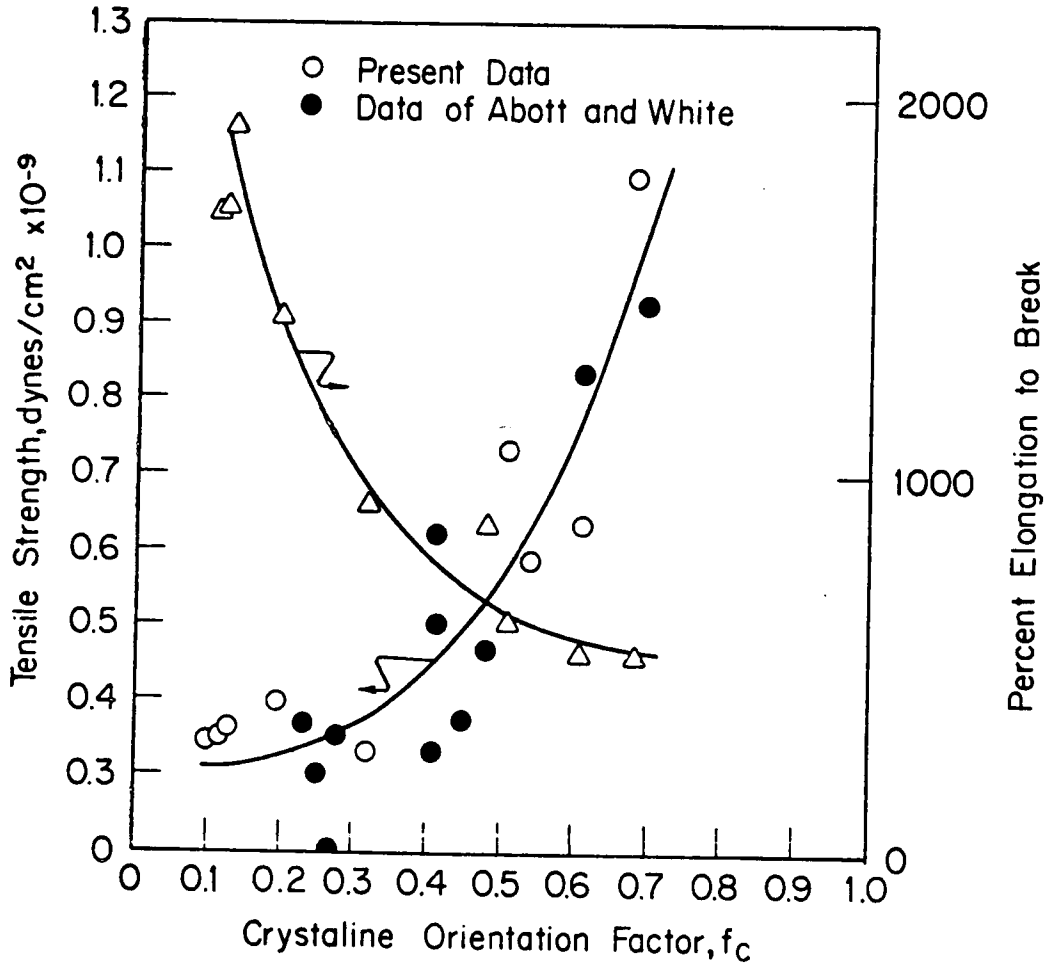

Figure 32. Tensile Strength and Elongation to Break Versus c-Axis Crystalline Orientation Function.

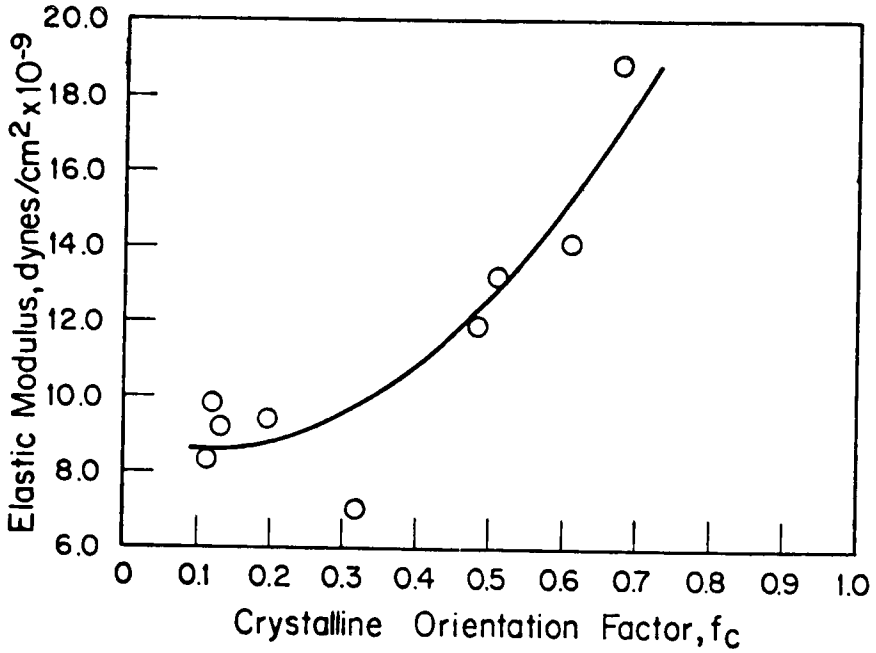

Figure 33. Young's Modulus Versus c-Axis Crystalline Orientation Function.

that the amorphous contribution to birefringence is small over the entire range of spinning conditions investigated. Hence, this parameter is clearly not a useful measure of the number of tie molecules or other factors which control the mechanical properties in such samples.

The strong correlation of the properties with c-axis crystalline orientation function may arise due to two factors. In the first case the factors which lead to increased c-axis orientation may also lead to increased numbers of tie molecules as already mentioned. The mechanical properties correlate at least as well with spinline stress as they do with the c-axis crystalline orientation function. This fact may be quite useful from a technological point of view since spinline stress is relatively easy to measure. The second factor relates to the ease of deformation (both elastic and plastic) of the crystals themselves as a function of orientation and the details of their interconnection by tie molecules.

H. MORPHOLOGICAL MODEL FOR MELT SPUN LINEAR POLYETHYLENE FIBER

Our data together with that of previous investigators allow a rather detailed interpretation of the morphology of the spun fubers and how this varies with spinning conditions. The evidence cited for strain induced nucleation, the two-point SAXS patterns, and the scanning electron microscope suggest a "row nucleated" structure. These data taken together with the WAXS data suggest the morphological development presented schematically in Figure 34. The model is based upon the interpretation first given by Keller and coworkers (40, 56) to results

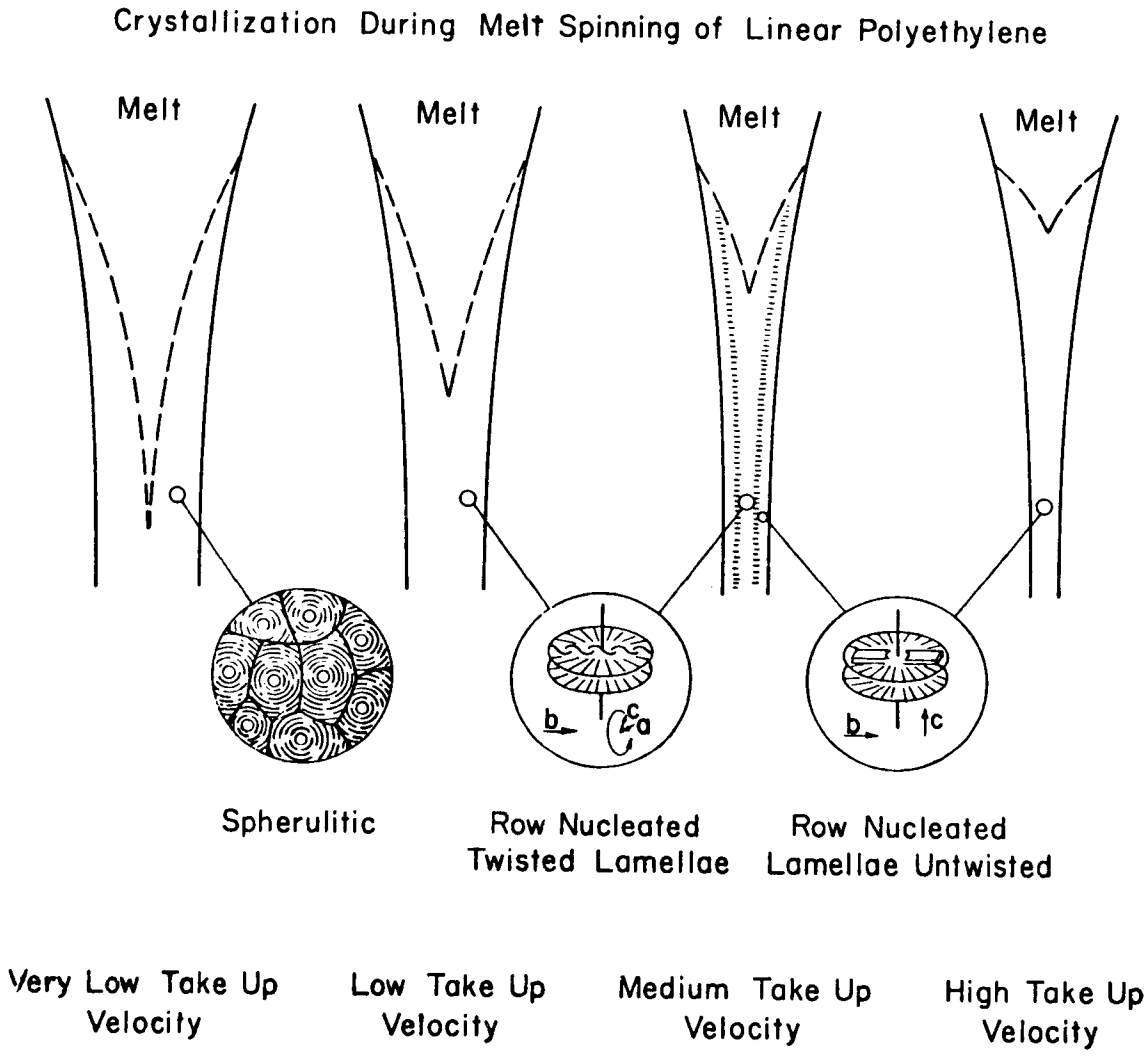

Figure 34. Morphological Model of Structures Developed in As-Spun Linear Polyethylene.

from samples crystallized during stretching of the melt. Ribbon-like, lamellar polyethylene crystals are nucleated by and grow epitaxially on fibril nuclei generated by the elongational straining and orientation of the melt. The lamellar crystals may twist as they grow outward from the fibril nucleus if the stress is low just as they apparently do during the growth of polyethylene spherulites in quiescent melts (30). During crystallization at higher levels of stress, the ribbon-like crystals do not exhibit as much twist. A model similar to that discussed here has been developed by Clark and Garber (21) to explain the morphology of blown film and injection molded polyoxymethylene. These authors also suggested that such an approach might be applicable to fiber spinning.

In applying this model to our data for melt spun fibers it should be kept in mind that the direction of growth of the polyethylene crystals is along the b-axis of the polyethylene unit cell. Assuming that the c-axis, the chain direction, is perpendicular to the flat face of the ribbon-like crystals while the a-axis lies in the plane of the ribbon, regular twisting of the lamellae causes a rotation of the a- and c-axes about the growth direction of the lamellar crystal. Thus, if we calculate the Hermans' orientation functions for the extreme, idealized case corresponding to all lamellar crystals growing perpendicular to the fiber axis, but regularly twisting, we obtain $f_a = f_c = + 0.25$ and $f_b = -0.5$. For the case that the lamellae do not twist $f_a = f_b = -0.5$ and $f_c = 1.0$. Comparing these values to the experimental results shown in Figure 27, we observe that the peak in the value of f_a corresponds to regular twisting of the lamellae while the

decreasing values at higher takeup velocities may be interpreted as a tendency for the lamellae to be less twisted, on the average. The spreading of the SAXS maximum about the incident beam occurs for samples with considerable lamellar twisting.

The orientation data taken as a function of position along the spinline (Figure 28) may be interpreted as indicating that at low takeup velocity (50 m/min) ribbon-like lamellar crystals twist as they grow outward from the fibril nuclei from the beginning of crystallization as well as on the average, throughout the final filament. Similarly, at high takeup velocities (556 m/min) the lamellae are relatively untwisted throughout the crystallization process. In the intermediate range of takeup velocities (≈100 - 200 m/min) crystallization begins near the outer surface of the filament due to the lower temperature at this point resulting from the radial heat transfer from the filament. This slightly lower temperature results in higher viscosity and stress in this region which then leads at these takeup velocities to growth of relatively untwisted lamellar crystals in this "skin" layer. Once this layer is formed it supports most of the load; crystallization continues throughout the inner portion of the filament at lower stress and therefore greater helicoidal twisting of the lamellae. The net effect is an overall decrease in c-axis orientation function with distance down the spinline. Further evidence of a "skin effect" in melt spun filaments ic contained in the birefringence measurements of Katayama et al., (49), Fung and Carr (29), and in the scanning electron microscopy studies of Van Veld, et al. (108).

For linear polyethylene the transition from spherulitic

crystallization to a row nucleated morphology apparently occurs at very low levels of spinline stress. We interpret the data shown in Figure 27 to indicate that at a mass flow rate of 1.93 g/min this transition occurs in the range of takeup velocities between 0 and 50 m/min. This is also consistent with the trends observed in the crystallization kinetics including the large increases in crystallization rates at relatively low levels of spinline stress.

The model proposed by Katayama et al., (49) involving row nucleated lamellar crystals stacked normal to the fiber axis with the chains tilted at an angle within each crystal is a possible interpretation consistent with the data from fibers spun under conditions which produce textures similar to our intermediate takeup velocity range. This model has several shortcomings, however, when considered in the light of all the available experimental results. For example, the reason given for the "sudden tilting" of the c-axis direction away from the fiber axis is that stress on crystals formed previously causes the chain tilting. This would imply that fiber spun at higher stress levels should exhibit greater chain tilting rather than less in contradiction to the observed behavior. The model of Katayama et al. thus does not provide an integrated picture of how the crystalline texture changes from the spherulitic condition which exists in gravitationally spun fiber to the texture observed in the filaments spun under high spin line stresses.

CHAPTER VII

CONCLUSIONS AND RECOMMENDATIONS

A unique synthetic fiber spinning machine was assembled for this research. It was capable of continuous, steady state melt spinning; and it was instrumented for measuring filament diameter, temperature, percent crystallinity and crystalline orientation from the spinneret to a point 175 cm down the spinline. These properties were measured for eight different sets of operating conditions. From the analysis of these data several important points were learned about melt spinning of linear polyethylene fiber. The conclusions and recommendations that can be drawn from this work are presented here. Although linear polyethylene was used in this research, the fundamental principles underlying its behavior during melt spinning should have a general application to most semicrystalline polymers that can be melt spun into fibers.

A. CONCLUSIONS

Diameter, Velocity, and Temperature

Diameter decreases rapidly in the molten zone of a spinline until crystallization begins. At that point the diameter is near its final takeup value, and it changes only slightly along the remainder of the spinline.

The velocity of the fiber increases rapidly until crystallization begins. At that point the rate of velocity change, the velocity

gradient, is near its peak value. From that point the velocity gradient decreases to near zero values as the takeup velocity is reached. At constant mass flow rate the maximum value of the velocity gradient increases with increasing spinning speed. The location of the maximum value of the velocity gradient changes as process conditions are changed.

The fiber cooling rate increases with increasing spinning speed and with decreasing filament diameter. Crystallization causes a change in the cooling rate leading to a plateau in the temperature profile or under slow cooling conditions, an increase in temperature.

Elongational Viscosity and Stress

Spinline stress increases with increasing takeup velocity at constant mass flow rate. In any given spinning process it increases from a low value near the spinneret to a much higher value at the take-up. This latter change results primarily from large changes in fiber cross sectional area. A strong correlation exists between spinline stress and orientation and crystallization rate in the fiber. Spin-line stress is thus an important factor in determining the process dynamics and the final morphology of the fiber.

Elongational viscosity increases slowly in the molten zone of the spinline until crystallization begins. At that point the viscosity increases rapidly because of the two phase nature of the fiber. A constitutive equation usable for the molten polymer is not suitable for describing the behavior of the two phase zone of the fiber.

Crystallization

Crystallization begins at an initially high rate at a point near the peak in the velocity gradient profile. The rates occurring in the temperature plateau regions are several orders of magnitude higher than those occurring in a quiescent melt at the same temperature. Crystallization rate increases with increasing takeup stress in the filament. The level of crystallinity in the final fiber decreases with increasing cooling rate over the range of spinning speeds used in this work.

The expression $(\int_0^t K[T(\tau)]d\tau)^n$ in the Nakamura equation is a linear function in time. Values of K calculated with n=1 increase with increasing takeup stress in the spinning filament.

Orientation, Morphology, and Mechanical Properties

Both total and crystalline orientation in the final fiber increase with takeup stress. The orientation as measured by birefringence of the final fiber consists largely of crystalline orientation with a small contribution from amorphous orientation.

At both low and high spinning speeds the crystalline orientation along the spinline is essentially the same as that observed in the final fiber. At an intermediate speed range the orientation decreases slightly down the spinline. This behavior is qualitatively similar to the mechanism proposed by Keller for orientation in samples molded under stress.

Lamellar thickness, as indicated by long period spacing from SAXS patterns, decreases with increasing spinning speed.

Final fiber Young's modulus and tensile strength increase with

crystalline c-axis orientation while elongation at break decreases. The good correlations obtained indicate the usefulness of crystalline orientation as a predictor of final fiber properties.

The phenomena occurring in the deformation zone in a spinning filament are primarily responsible for the changes observed in final fiber morphology and properties. Careful control of the processes in this zone is essential for the production of uniform, high quality filaments.

B. RECOMMENDATIONS

Although this research provided insight into some of the fundamental physical processes occurring in melt spinning, there are still many questions remaining to be answered. Given below are several recommendations concerning important aspects of melt spinning that require more investigation. Suggestions for improvement of the techniques used in this work are made in Appendix C since they will be of real value only to those who attempt to duplicate the techniques.

Equipment should be installed for measuring birefringence on the filament during spinning. This will provide a measure of the total orientation in the developing filament. When combined with crystalline orientation functions from WAXS patterns, the orientation of the amorphous phase can be calculated. Such data would permit a clearer understanding of the effect of orientation in the melt on crystallization kinetics as well as the effect of crystal growth on the change in orientation as the fiber is made.

Additional information on structure development could also be obtained by making small angle x-ray patterns on the spinning fiber. This would be especially valuable for spinning conditions where large differences in morphology were produced.

The crystallization rate data obtained in this work were generated under dynamic conditions in which stress, deformation rate, and temperature were changing simultaneously. For this reason it was difficult to see the effect of each independent variable on crystalline growth. It is recommended that crystallization rates be measured under conditions where temperature and deformation rate can be independently controlled. Such data would eventually permit a quantitative description of the crystallization kinetics during melt spinning.

The step from describing a spinning process in terms of its independent variables to predicting the physical properties of the resulting fiber requires a more extensive knowledge of the relationship between fiber morphology and physical properties. A continuing investigation is recommended on the fundamental relationships between polymer structure and properties.

A complete quantitative description of melt spinning will require a correct constitutive equation, or equations, for partly crystalline polymer. The two phase nature of the crystallizing fiber cannot be adequately described by the same equation used for the single phase molten region. Consideration must be given to the relative amounts of each phase and their rheological behavior under conditions of changing temperature and stress.

This research dealt only with polyethylene. Other research projects should examine other materials to establish the generality of the phenomena observed with polyethylene and also to investigate other phenomena such as crystal-crystal transitions and alteration of crystallization kinetics by plasticizers and nucleating agents. Several other polymers such as nylon 6, nylon 66, polyethylene terephthalate and polyurethane are spun into fibers in commercial quantities. Investigations of these materials could be of value to the synthetic fiber industry.

It is recommended that a wider range of spinning conditions be investigated, especially higher spinning speeds. Commercial processes are being pushed to speeds of several thousand meters per minute which produce marked changes in fiber properties. Coverage of a wider range of conditions would bring research closer to the processes actually used in industry.

LIST OF REFERENCES

LIST OF REFERENCES

1. Abbott, L. E. and J. L. White, Appl. Polymer Symp., 20, (1973).

2. Acierno, Domenico, J. Nelson Dalton, Jorge M. Rodriguez, and James L. White, J. Appl. Polymer Sci., 15, 2395 (1971).

3. Alfrey, T. and H. Mark, J. Phys. Chem., 46, 112 (1942).

4. Andrews, E. H., Brit. J. Appl. Phys., 10, 39 (1959).

5. Avrami, M., J. Chem. Phys., 7, 1103 (1939).

6. Avrami, M., J. Chem. Phys., 8, 212 (1940).

7. Avrami, M., J. Chem. Phys., 9, 177 (1941).

8. Banks, W. and A. Sharples, Makromol. Chem., 59, 233 (1963).

9. Banks, W., A. Sharples, and J. N. Hay, J. Polymer Sci., A2, 9, 4059 (1964).

10. Barnett, T. R., Amer. Chem. Soc., Div. Poly. Chem. Preprints, 7, 691 (1966).

11. Baur, H., Kolloid Z., 203, 97 (1965).

12. Beck, H. N. and H. D. Ledbetter, J. Appl. Polymer Sci., 9, 2131 (1965).

13. Binsbergen, F. L., Nature, 211, 516 (1966).

14. Binsbergen, F. L., Kolloid Z.-Z. Polym., 238, 389 (1970).

15. Binsbergen, F. L., Polymer, 11, 253 (1970).

16. Binsbergen, F. L. and B. G. M. DeLange, Polymer, 11, 309 (1970).

17. Bradley, R. S., Quart. Rev. (London), 5, 315 (1951).

18. Barnett, B. B. and W. H. McDevit, J. Appl. Phys., 28, 1101 (1957).

19. Carothers, W. H. and J. W. Hill, J. Amer. Chem. Soc., 54, 1579 (1932).

20. Chappel, F. P., M. F. Culpin, R. G. Gasden, and T. C. Tranten, J. Appl. Chem. (London), 14, 12 (1964).

21. Clark, E. S. and C. A. Garber, Intern. J. Polymeric Mater., 1, 31 (1971).

22. Copley, M., N. H. Chamberlain and K. W. Hillier, Am. Chem. Soc., Div. Poly. Chem., Preprints 7, 679 (1966).

23. Cormia, R. L., F. P. Price and D. J. Turnbull, J. Chem. Phys., 37, 1333 (1962).

24. Devoy, C. and L. Mandelkern, J. Chem. Phys., 52, 3827 (1970).

25. Evans, R. U., Trans. Faraday Soc., 41, 365 (1945).

26. Fisher, J. C., J. H. Hollomon, and D. Turnbull, J. Appl. Phys., 19, 775 (1948).

27. Flory, Paul J., Principles of Polymer Chemistry, pp. 451-453, Cornell University Press, 1953.

28. Frank, F. C. and M. Tosi, Proc. Roy. Soc., A263, 323 (1961).

29. Fung, P. Y. F. and S. H. Carr, J. Macromol. Sci., B, 6, 621 (1972).

30. Geil, P. H., Polymer Single Crystals, Wiley-Interscience, New York, 1963.

31. Gent, A. N., Trans. Faraday Soc., 50, 521 (1954).

32. Gornick, F., J. Appl. Phys., 36, 3012 (1965).

33. Gornick, F. and John D. Hoffman, Ind. Eng. Chem., 58, 41 (1966).

34. Haas, T. W. and B. Maxwell, Polym. Eng. Sci., 9, 225 (1969).

35. Hagler, Gerald E., Ph.D. Dissertation in Chem. Eng., University of Tennessee, 1972.

36. Han, C. D., Rheol. Acta., 9, 355 (1970).

37. Han, Chang Dae, J. Appl. Polymer Sci., 15, 1091 (1971).

38. Hearle, J. W. S., J. Textile Inst., 53, P449 (1962).

39. Hermans, J. J., P. H. Hermans, D. Vermeas, and A. Weidinger, Rec. Chim. Trav., 65, 427 (1946).

40. Hill, M. J. and A. Keller, J. Macromol. Sci., B, 3, 153 (1969).

41. Hoffman, John D. and John S. Lauritzen, J. Res. Natl. Bur. Standards, 65A, 297 (1961).

42. Hoffman, John D. and James J. Weeks, J. Chem. Phys, 37, 1723 (1962).

43. Ishibashi, T., K. Aoki and T. Ishii, J. Appl. Polymer Sci., 14, 1597 (1970).

44. Ishikawa, K., J. Polymer Sci., A2, 7, 1259 (1969).

45. Johnson, W. A. and R. F. Mehl, Trans. Am. Inst. Mining Met. Engrs., 135, 416 (1939).

46. Kase, S. and T. Matsuo, J. Text. Mach. Soc. of Japan, 18, 188 (1965).

47. Kase, S. and T. Matsuo, J. Polymer Sci., A, 3, 2541 (1965).

48. Kase, S. and T. Matsuo, J. Appl. Polymer Sci., 11, 251 (1967).

49. Katayama, K., T. Amano, and K. Nakamura, Kolloid Z.-Z. Poly., 226, 125 (1967).

50. Kavesh, S. and J. M. Schultz, J. Polymer Sci., A, 9, 85 (1971).

51. Keith, H. D., Am. Chem. Soc., Div. Polymer Chem., Preprints 3, 17 (1962).

52. Keith, H. D., "Physics and Chemistry of the Organic Solid State," Editor David Fox, Interscience, New York, 1963, p. 873.

53. Keith, H. D. and F. J. Padden, J. Appl. Phys., 34, 2409 (1963).

54. Keller, A., J. Polymer Sci., 15, 31 (1955).

55. Keller, A., J. Polymer Sci., 21, 363 (1956).

56. Keller, A. and M. J. Machin, J. Macromol. Sci., B, 1, 41 (1967).

57. Keller, A. and F. M. Willmouth, J. Macromol. Sci., B, 6, 493 (1972).

58. Keller, A. and F. M. Willmouth, J. Macromol. Sci., B, 6, 539 (1972).

59. Kobayashi, Keinosuke and Toshio Nagasawa, J. Macromol. Sci., B, 4, 331 (1970).

60. Koutsky, J. A., A. G. Walton, and Eric Baer, J. Appl. Phys., 38, 1832 (1967).

61. Krueger, D. and G. S. Y. Yeh, J. Macromol. Sci., B, 6, 431 (1972).

62. Lacko, Vladimin, Faserforsch, Textiltech, 14, 337 (1963).

63. Limbert, Frank J. and Eric Baer, J. Polymer Sci., A, 1, 3317 (1963).

64. Mackley, M. R. and A. Keller, Polymer, 14, 16 (1973).

65. Mandelkern, L., J. Appl. Phys., 26, 443 (1955).

66. Mandelkern, L., "Growth and Perfection of Crystals," John Wiley & Sons, Inc., New York, 1958, p. 478.

67. Mandelkern, L., "Crystallization of Polymers," McGraw-Hill, New York, 1964.

68. Mandelkern, L., J. G. Fatou, and C. Howard, J. Phys. Chem., 68, 3386 (1964).

69. Mandelkern, L., J. G. Fatou, and C. Howard, J. Phys. Chem., 69, 956 (1965).

70. Mandelkern, L., Fred A. Quinn, Jr., and Paul J. Flory, J. Appl. Phys., 25, 830 (1954).

71. Mark, H. F., S. M. Atlas, and E. Cernia, Eds., "Man-Made Fibers, Science and Technology," Volume 1, Interscience Publishers, New York, 1967, p. 283-340.

72. Matovich, M. A. and J. R. A. Pearson, Ind. Eng. Chem., Fundam., 8, 512 (1969).

73. Matthews, J. L., H. S. Peiser, and R. B. Richards, Acta Cryst., 21, 85 (1949).

74. Maxwell, B., J. Polymer Sci., C, 9, 43 (1965).

75. Meinel, G., M. Morosoff and A. Peterlin, J. Polymer Sci., A, 8, 1723 (1970).

76. Mitchell, J. C., Polymer, 8, 369 (1967).

77. Morrison, Milton E., A.I.Ch.E. Journal, 16, 57 (1970).

78. McCord, Don Edward, M. S. Thesis, University of Tennessee, August 1970.

79. Nakamura, K., T. Watanabe, K. Katayama, and T. Amano, J. Appl. Polymer Sci., 16, 1077 (1972).

80. Nakamura, K., K. Katayama, and T. Amano, J. Appl. Polymer Sci., 17, 1031 (1973).

81. Nakamura, K., T. Watanabe, T. Amano, and K. Katayama, J. Appl. Polymer Sci., 18, 615 (1974).

82. Nishiumi, S., J. Text. Mach. Soc., Japan, 18, 174 (1965).

83. Palermo, Joseph A. and Gary F. Bennett, Ind. Eng. Chem., 57, 68 (1965).

84. Parrini, Paolo and Guglielmo Corrieri, Makromol. Chem., 86, 271 (1965).

85. Perepelk, K. E., Int. Chem. Eng., 9, 323 (1969).

86. Price, F. P., J. Polymer Sci., 54, S40 (1961).

87. Price, F. P., J. Chem. Phys., 35, 1884 (1961).

88. Price, F. P., Am. Chem. Soc., Div. Polymer Chem., Preprints 3, 28 (1962).

89. Rabesiaka, J. and A. J. Kovacs, J. Appl. Phys., 32, 2314 (1961).

90. Samuels, R. J., J. Macromol. Sci., B4, 701 (1970).

91. Samuels, R. J., J. Polymer Sci., A-2, 10, 781 (1972).

92. Schuur, G., Kolloid Z.-Z. Poly., 208, 123 (1966).

93. Sharples, A., "Introduction to Polymer Crystallization," St. Martin's Press, New York, 1966.

94. Southern, John H., Norman Weeks, Roger S. Porter, and Richard G. Crystal, Die Molekularie Chemie, 162, 19 (1972).

95. Spearot, J. A. and A. B. Metznev, Trans. Soc. Rheol., 16, 495 (1972).

96. Sprague, B. S., Bull. Amer. Phys. Soc. II, 18, 345 (1973).

97. Statton, W. O., J. Polymer Sci., 28, 423 (1958).

98. Stein, R. S., J. Polymer Sci., 31, 327 (1958).

99. Stein, R. S. and F. N. Norris, J. Polymer Sci., 21, 381 (1956).

100. Stuart, H. A., Pure Appl. Chem., 5, 743 (1962).

101. Swann, P. R., J. Polymer Sci., 42, 525 (1960).

102. Takayanagi, M. and T. Kusumato, Kogyo Kagaku Zasshi, 62, 587 (1959).

103. Taylor, G. R. and S. R. Darin, J. Appl. Phys., 26, 1075 (1955).

104. Thompson, A. B., in "Fibre Structure," edited by J. W. S. Hearle and R. H. Peters, Textile Inst.-Butterworth, Manchester, 1963.

105. Tung, L. H. and W. C. Taylor, J. Polymer Sci., 21, 144 (1956).

106. Turnbull, D., J. Chem. Phys., 18, 198 (1950).

107. Uhlmann, D. R. and B. Chalmers, Ind. Eng., Chem., 57, 19 (1965).

108. Van Veld, R. D., G. Morris and H. R. Billica, J. Appl. Polymer Sci., 12, 2709 (1968).

109. Vonk, C. G., Kolloid Z., 206, 121 (1965).

110. Wanger, W. H. and V. G. Fox, Man-Made Fiber Technology, Part 1, Symposium at Seventh Nat'l Metting of A.I.Ch.E., Atlantic City, New Jersey, August 29, September 1, 1971.

111. White, J. L., J. Appl. Polymer Sci., 8, 2339 (1964).

112. Wilhelm, Von Gerhard, Kolloid Z. and Z. Poly., 208, 97 (1966).

113. Wilson, Otto, Ind. Eng. Chem., 18, 829 (1926).

114. Yamamoto, M. and J. L. White, J. Polymer Sci., A-2, 9, 399 (1971).

115. Yoshida, Mikio and Hiroshi Sato, Reports on Prog. in Poly. Phys. in Japan, 13, 173 (1970).

116. Ziabicki, Andrzej, J. Appl. Polymer Sci., 2, 24 (1959).

117. Ziabicki, A., Kolloid Z., 175, 14 (1960).

118. Ziabicki, A., Applied Polymer Symposia, 6, 1 (1967).

119. Ziabicki, A., in "Man-Made Fibers," H. T. Mark, S. M. Atlas, and E. Cernia, Eds., Interscience, New York, (1967), p. 13.

120. Ziabicki, A., ibid., p. 169.

121. Ziabicki, A. and Krystyna Kedzierska, J. Appl. Polymer Sci., 2, 14 (1959).

122. Ziabicki, A. and K. Kedzierska, Chemie Stosowana, 4, 151 (1960).

123. Ziabicki, A. and K. Kedzierska, Kolloid Z., 171, 51 (1960).

124. Ziabicki, A. and K. Kedzierska, Kolloid, 171, 111 (1960).

125. Ziabicki, A. and K. Kedzierska, J. Appl. Polymer Sci., 6, 111 (1962).

126. Ziabicki, A. and K. Kedzierska, J. Appl. Polymer Sci., 6, 361 (1962).

APPENDICES

APPENDIX A

EXPERIMENTAL DATA

TABLE VII. SPINNING RUN CONDITIONS

Run Number	Polymer Rate (g/min)	Takeup Velocity (m/min)	Melt Temperature (°C)	Takeup Tension (g)	Ambient Temperature (°C)
PE01	1.930	100	205	0.60	28.0
PE02	1.930	200	205	0.68	30.0
PE03	1.940	50	205	0.41	28.0
PE04	1.954	50	180	0.77	28.0
PE05	3.988	100	182	0.70	28.0
PE06	1.911	400	209	0.50	29.0
PE07	1.911	556	210	0.50	28.5
PE08	1.911	200	204	0.48	30.0
PE09	0.705	200	207	0.47	30.0

TABLE VIII. CONSTANTS FOR EMPIRICAL DIAMETER VERSUS DISTANCE EQUATION*

Run Number	A (cm)	B	C (cm)	D (cm)	E	F (cm)
PE01	.106598	-8.11306	0	142.752	1.20152	.0173645
PE02	.109175	-5.54422	0	126.409	1.05893	.0113273
PE03	.0961991	-10.9627	0	172.446	1.20022	.0235906
PE04	.0978076	-31.7240	0	173.121	1.68991	.0244968
PE05	.122162	-8.88885	0	174.996	1.37884	.0238824
PE06	.108192	-18.4099	0	174.382	1.46300	.00799049
PE07	.112999	-10.5505	0	172.355	1.10494	.00619396
PE08	.102499	-12.0531	0	165.362	1.00000	.0114342
PE09	.0963121	-38.0885	0	83.1676	1.87914	.00877254

*These constants apply to the equation

$$\text{diameter} = A \exp\left(B\left(\frac{\text{distance}-C}{D}\right)^{E}\right) + F.$$

TABLE IX. CONSTANTS FOR EMPIRICAL VELOCITY VERSUS DISTANCE EQUATION*

Run Number	A (m/min)	B	C	D (cm)	E	F (m/min)
PE01	-90.2882	-3.74478	0	103.027	2.74407	93.6124
PE02	-204.518	-3.80013	0	129.219	2.88107	209.225
PE03	-48.3408	-11.6794	0	147.393	2.43733	51.7104
PE04	-45.5162	-38.0328	0	112.341	3.48278	48.4283
PE05	-99.7056	-8.53089	0	156.663	3.05325	104.344
PE06	-425.538	-4.13814	0	83.1477	4.25487	429.418
PE07	-560.398	-34.2191	0	133.021	4.37879	563.841
PE08	-208.447	-24.2630	0	159.812	2.55548	212.762
PE09	-206.047	-99.5096	0	67.2219	5.0000	206.941

*These constants apply to the equation

$$\text{velocity} = A \exp\left(B\left(\frac{\text{distance}-C}{D}\right)^{E}\right) + F.$$

TABLE X. CONSTANTS FOR EMPIRICAL CRYSTALLINITY VERSUS DISTANCE EQUATION*

Run Number	A (Percent)	B	C (cm)	D (cm)	E	F (Percent)
PE01	-100.0	-.958799	56.50	316.88	.499499	100.0
PE02	-100.0	-.802097	53.34	320.039	.476998	100.0
PE03	-100.0	-.941397	38.10	335.28	.539498	100.0
PE04	-100.0	-1.00359	38.10	335.28	.468149	100.0
PE05	-100.0	-.939196	83.82	289.56	.662899	100.0
PE06	-100.0	-.668393	68.58	304.80	.352594	100.0
PE07	-100.0	-.665193	53.34	320.039	.475496	100.0
PE08	-100.0	-.766796	53.34	320.039	.409746	100.0
PE09	-100.0	-.963395	33.02	340.359	.335247	100.0

*These constants apply to the equation

$$\text{percent crystallinity} = A \exp\left(B\left(\frac{\text{distance}-C}{D}\right)^{E}\right) + F.$$

TABLE XI. RUN PE01 EXPERIMENTAL DISTANCE, DIAMETER, AND TEMPERATURE DATA

DISTANCE FROM SPINNERETTE CM	FIBER DIAMETER CM	FIBER TEMPERATURE DEG C
0.1900E 01	0.1200E 00	0.2580E 03
0.3810E 01	0.1190E 00	0.2490E 03
0.5710E 01	0.1050E 00	0.2345E 03
0.7620E 01	0.9900E-01	0.2250E 03
0.9520E 01	0.9500E-01	0.2200E 03
0.1143E 02	0.8500E-01	0.2140E 03
0.1333E 02	0.8500E-01	0.2090E 03
0.1524E 02	0.7500E-01	0.2060E 03
0.1714E 02	0.7700E-01	0.1982E 03
0.1905E 02	0.7000E-01	0.1900E 03
0.2095E 02	0.6100E-01	0.1870E 03
0.2286E 02	0.5800E-01	0.1820E 03
0.2476E 02	0.5400E-01	0.1802E 03
0.2667E 02	0.5500E-01	0.1752E 03
0.2857E 02	0.5200E-01	0.1720E 03
0.3048E 02	0.5000E-01	0.1710E 03
0.3238E 02	0.4300E-01	0.1687E 03
0.3302E 02	0.4600E-01	0.1675E 03
0.3492E 02	0.4500E-01	0.1660E 03
0.3683E 02	0.4400E-01	0.1555E 03
0.3873E 02	0.4600E-01	0.1555E 03
0.4064E 02	0.4000E-01	0.1525E 03
0.4254E 02	0.3700E-01	0.1520E 03
0.4445E 02	0.3600E-01	0.1485E 03
0.4635E 02	0.2400E-01	0.1455E 03
0.4826E 02	0.2600E-01	0.1475E 03
0.5016E 02	0.2600E-01	0.1455E 03
0.5207E 02	0.2400E-01	0.1430E 03
0.5397E 02	0.2800E-01	0.1430E 03
0.5588E 02	0.2200E-01	0.1402E 03
0.5778E 02	0.2200E-01	0.1380E 03
0.5969E 02	0.2000E-01	0.1345E 03
0.6159E 02	0.1800E-01	0.1360E 03
0.6350E 02	0.1900E-01	0.1352E 03
0.6540E 02	0.1800E-01	0.1345E 03
0.6731E 02	0.2200E-01	0.1337E 03
0.6921E 02	0.2000E-01	0.1325E 03
0.7112E 02	0.2000E-01	0.1305E 03
0.7302E 02	0.1900E-01	0.1270E 03
0.7493E 02	0.1900E-01	0.1265E 03
0.7683E 02	0.1900E-01	0.1270E 03
0.7874E 02	0.1800E-01	0.1310E 03
0.8064E 02	0.1600E-01	0.1315E 03
0.8255E 02	0.1700E-01	0.1310E 03
0.8445E 02	0.1800E-01	0.1310E 03
0.8636E 02	0.1800E-01	0.1310E 03
0.8826E 02	0.1800E-01	0.1315E 03
0.9017E 02	0.1800E-01	0.1292E 03
0.9207E 02	0.1800E-01	0.1285E 03
0.9398E 02	0.1700E-01	0.1310E 03
0.9588E 02	0.1800E-01	0.1310E 03
0.9779E 02	0.1800E-01	0.1310E 03
0.9969E 02	0.1800E-01	0.1310E 03
0.1016E 03	0.1800E-01	0.1277E 03
0.1035E 03	0.2000E-01	0.1292E 03
0.1054E 03	0.1700E-01	0.1285E 03
0.1073E 03	0.2000E-01	0.1270E 03
0.1092E 03	0.1700E-01	0.1260E 03
0.1111E 03	0.1800E-01	0.1250E 03
0.1130E 03	0.1700E-01	0.1250E 03
0.1149E 03	0.2000E-01	0.1260E 03
0.1168E 03	0.1800E-01	0.1255E 03
0.1187E 03	0.1800E-01	0.1242E 03
0.1206E 03	0.1800E-01	0.1242E 03
0.1225E 03	0.1800E-01	0.1235E 03
0.1244E 03	0.1800E-01	0.1235E 03
0.1263E 03	0.1900E-01	0.1220E 03
0.1282E 03	0.1700E-01	0.1220E 03
0.1301E 03	0.2200E-01	0.1220E 03
0.1320E 03	0.1800E-01	0.1220E 03
0.1339E 03	0.1700E-01	0.1220E 03
0.1358E 03	0.1700E-01	0.1210E 03
0.1377E 03	0.1700E-01	0.1200E 03
0.1397E 03	0.2000E-01	0.1200E 03
0.1416E 03	0.2000E-01	0.1200E 03
0.1435E 03	0.1900E-01	0.1200E 03
0.1454E 03	0.1900E-01	0.1190E 03

TABLE XII. RUN PE02 EXPERIMENTAL DISTANCE, DIAMETER, AND TEMPERATURE DATA

DISTANCE FROM SPINNERETTE CM	FIBER DIAMETER CM	FIBER TEMPERATURE DEC C
0.1900E 01	0.1230E 00	0.2450E 03
0.3810E 01	0.1020E 00	0.2330E 03
0.5710E 01	0.9800E-01	0.2280E 03
0.7620E 01	0.8700E-01	0.2225E 03
0.9520E 01	0.8100E-01	0.2175E 03
0.1143E 02	0.8300E-01	0.2100E 03
0.1333E 02	0.7700E-01	0.2040E 03
0.1524E 02	0.7200E-01	0.2005E 03
0.1714E 02	0.6900E-01	0.1940E 03
0.1905E 02	0.6400E-01	0.1900E 03
0.2095E 02	0.6700E-01	0.1850E 03
0.2286E 02	0.5800E-01	0.1830E 03
0.2476E 02	0.5400E-01	0.1820E 03
0.2667E 02	0.4700E-01	0.1760E 03
0.2857E 02	0.4800E-01	0.1745E 03
0.3048E 02	0.4200E-01	0.1595E 03
0.3238E 02	0.4300E-01	0.1605E 03
0.3302E 02	0.3600E-01	0.1605E 03
0.3810E 02	0.3700E-01	0.1580E 03
0.4318E 02	0.3500E-01	0.1490E 03
0.4826E 02	0.1900E-01	0.1410E 03
0.5334E 02	0.2600E-01	0.1345E 03
0.5842E 02	0.1300E-01	0.1250E 03
0.6350E 02	0.1400E-01	0.1200E 03
0.6858E 02	0.1500E-01	0.1180E 03
0.7366E 02	0.1600E-01	0.1180E 03
0.7874E 02	0.1700E-01	0.1180E 03
0.8382E 02	0.1200E-01	0.1140E 03
0.8890E 02	0.1300E-01	0.1130E 03
0.9398E 02	0.1200E-01	0.1115E 03
0.9906E 02	0.1400E-01	0.1110E 03
0.1041E 03	0.1200E-01	0.1105E 03
0.1092E 03	0.1400E-01	0.1100E 03
0.1143E 03	0.1600E-01	0.1100E 03
0.1193E 03	0.1300E-01	0.1092E 03
0.1244E 03	0.1200E-01	0.1077E 03
0.1295E 03	0.1300E-01	0.1077E 03
0.1346E 03	0.1300E-01	0.1077E 03

TABLE XIII. RUN PE03 EXPERIMENTAL DISTANCE, DIAMETER, AND TEMPERATURE DATA

DISTANCE FROM SPINNERETTE CM	FIBER DIAMETER CM	FIBER TEMPERATURE DEC C
0.2540E 01	0.1150E 00	0.2500E 03
0.7620E 01	0.9700E-01	0.2265E 03
0.1270E 02	0.8000E-01	0.2140E 03
0.1778E 02	0.6800E-01	0.1940E 03
0.2286E 02	0.6300E-01	0.1830E 03
0.2794E 02	0.5400E-01	0.1695E 03
0.3302E 02	0.4700E-01	0.1630E 03
0.3810E 02	0.4800E-01	0.1580E 03
0.4318E 02	0.3000E-01	0.1545E 03
0.4826E 02	0.2900E-01	0.1520E 03
0.5334E 02	0.2800E-01	0.1490E 03
0.5842E 02	0.2600E-01	0.1420E 03
0.6350E 02	0.2500E-01	0.1420E 03
0.6858E 02	0.2500E-01	0.1410E 03
0.7366E 02	0.2600E-01	0.1395E 03
0.7874E 02	0.2500E-01	0.1395E 03
0.8382E 02	0.2500E-01	0.1380E 03
0.8890E 02	0.2500E-01	0.1370E 03
0.9398E 02	0.2500E-01	0.1365E 03
0.9906E 02	0.2400E-01	0.1380E 03
0.1041E 03	0.2400E-01	0.1395E 03
0.1092E 03	0.2300E-01	0.1410E 03
0.1143E 03	0.2400E-01	0.1420E 03
0.1193E 03	0.2400E-01	0.1430E 03
0.1244E 03	0.2300E-01	0.1430E 03
0.1295E 03	0.2300E-01	0.1420E 03
0.1346E 03	0.2400E-01	0.1395E 03
0.1397E 03	0.2300E-01	0.1370E 03
0.1447E 03	0.2300E-01	0.1330E 03
0.1498E 03	0.2400E-01	0.1310E 03
0.1549E 03	0.2500E-01	0.1310E 03
0.1600E 03	0.2500E-01	0.1270E 03
0.1651E 03	0.2500E-01	0.1235E 03
0.1701E 03	0.2500E-01	0.1165E 03
0.1752E 03	0.2300E-01	0.1140E 03

TABLE XIV. RUN PE04 EXPERIMENTAL DISTANCE, DIAMETER AND TEMPERATURE DATA

DISTANCE FROM SPINNERETTE CM	FIBER DIAMETER CM	FIBER TEMPERATURE DEC C
0.2540E 01	0.1220E 00	0.2120E 03
0.7620E 01	0.1070E 00	0.1925E 03
0.1270E 02	0.8600E-01	0.1850E 03
0.1778E 02	0.7500E-01	0.1770E 03
0.2286E 02	0.6200E-01	0.1720E 03
0.2794E 02	0.5000E-01	0.1645E 03
0.3302E 02	0.4300E-01	0.1595E 03
0.3810E 02	0.3000E-01	0.1570E 03
0.4318E 02	0.2300E-01	0.1530E 03
0.4826E 02	0.2300E-01	0.1470E 03
0.5334E 02	0.2400E-01	0.1440E 03
0.5842E 02	0.2400E-01	0.1430E 03
0.6350E 02	0.2300E-01	0.1455E 03
0.6858E 02	0.2400E-01	0.1470E 03
0.7366E 02	0.2500E-01	0.1440E 03
0.7874E 02	0.2600E-01	0.1440E 03
0.8382E 02	0.2500E-01	0.1430E 03
0.8890E 02	0.2500E-01	0.1430E 03
0.9398E 02	0.2700E-01	0.1420E 03
0.9906E 02	0.2500E-01	0.1395E 03
0.1041E 03	0.2500E-01	0.1395E 03
0.1092E 03	0.2400E-01	0.1395E 03
0.1143E 03	0.2500E-01	0.1395E 03
0.1193E 03	0.2200E-01	0.1370E 03
0.1244E 03	0.2300E-01	0.1360E 03
0.1295E 03	0.2500E-01	0.1345E 03
0.1346E 03	0.2900E-01	0.1320E 03
0.1397E 03	0.2500E-01	0.1300E 03
0.1447E 03	0.2500E-01	0.1285E 03
0.1498E 03	0.2200E-01	0.1270E 03
0.1549E 03	0.2500E-01	0.1270E 03
0.1600E 03	0.2400E-01	0.1260E 03
0.1651E 03	0.2800E-01	0.1200E 03
0.1701E 03	0.2700E-01	0.1150E 03
0.1752E 03	0.2400E-01	0.1130E 03

TABLE XV. RUN PE05 EXPERIMENTAL DISTANCE, DIAMETER, AND TEMPERATURE DATA

DISTANCE FROM SPINNERETTE CM	FIBER DIAMETER CM	FIBER TEMPERATURE DEC C
0.2540E 01	0.1440E 00	0.2305E 03
0.7620E 01	0.1330E 00	0.2225E 03
0.1270E 02	0.1180E 00	0.2100E 03
0.1778E 02	0.1070E 00	0.2040E 03
0.2286E 02	0.9900E-01	0.1950E 03
0.2794E 02	0.7500E-01	0.1850E 03
0.3302E 02	0.7800E-01	0.1720E 03
0.3810E 02	0.6400E-01	0.1630E 03
0.4318E 02	0.6000E-01	0.1580E 03
0.4826E 02	0.5300E-01	0.1545E 03
0.5334E 02	0.4500E-01	0.1490E 03
0.5842E 02	0.4300E-01	0.1470E 03
0.6350E 02	0.4700E-01	0.1440E 03
0.6858E 02	0.3200E-01	0.1420E 03
0.7366E 02	0.3200E-01	0.1395E 03
0.7874E 02	0.2600E-01	0.1370E 03
0.8382E 02	0.2000E-01	0.1345E 03
0.8890E 02	0.2600E-01	0.1320E 03
0.9398E 02	0.2000E-01	0.1310E 03
0.9906E 02	0.2800E-01	0.1310E 03
0.1041E 03	0.2600E-01	0.1345E 03
0.1092E 03	0.2500E-01	0.1345E 03
0.1143E 03	0.2400E-01	0.1330E 03
0.1193E 03	0.2500E-01	0.1330E 03
0.1244E 03	0.2400E-01	0.1320E 03
0.1295E 03	0.2400E-01	0.1320E 03
0.1346E 03	0.2500E-01	0.1320E 03
0.1397E 03	0.2600E-01	0.1310E 03
0.1447E 03	0.2500E-01	0.1310E 03
0.1498E 03	0.2500E-01	0.1300E 03
0.1549E 03	0.2500E-01	0.1300E 03
0.1600E 03	0.2500E-01	0.1285E 03
0.1651E 03	0.2500E-01	0.1270E 03
0.1701E 03	0.2500E-01	0.1270E 03
0.1752E 03	0.2500E-01	0.1285E 03

TABLE XVI. RUN PE06 EXPERIMENTAL DISTANCE, DIAMETER, AND TEMPERATURE DATA

DISTANCE FROM SPINNERETTE CM	FIBER DIAMETER CM	FIBER TEMPERATURE DEC C
0.2540E 01	0.1173E 00	0.2570E 03
0.7620E 01	0.9150E-01	0.2345E 03
0.1270E 02	0.7500E-01	0.2090E 03
0.1778E 02	0.6700E-01	0.1885E 03
0.2286E 02	0.5380E-01	0.1770E 03
0.2794E 02	0.4390E-01	0.1670E 03
0.3302E 02	0.3590E-01	0.1555E 03
0.3810E 02	0.1540E-01	0.1520E 03
0.4318E 02	0.1466E-01	0.1470E 03
0.4826E 02	0.1100E-01	0.1370E 03
0.5334E 02	0.8780E-02	0.1270E 03
0.5842E 02	0.8060E-02	0.1085E 03
0.6350E 02	0.9520E-02	0.1040E 03
0.6858E 02	0.9520E-02	0.1015E 03
0.7366E 02	0.8060E-02	0.9700E 02
0.7874E 02	0.9160E-02	0.9250E 02
0.8382E 02	0.9890E-02	0.9700E 02
0.8890E 02	0.9890E-02	0.9600E 02
0.9398E 02	0.9890E-02	0.9250E 02
0.9906E 02	0.9160E-02	0.9150E 02
0.1041E 03	0.8780E-02	0.9150E 02
0.1092E 03	0.8420E-02	0.9150E 02
0.1143E 03	0.7330E-02	0.8700E 02
0.1193E 03	0.8790E-02	0.8700E 02
0.1244E 03	0.8790E-02	0.8600E 02
0.1295E 03	0.9520E-02	0.8300E 02
0.1346E 03	0.7330E-02	0.8150E 02
0.1397E 03	0.8420E-02	0.8000E 02
0.1447E 03	0.7690E-02	0.8000E 02
0.1498E 03	0.7690E-02	0.8000E 02
0.1549E 03	0.8420E-02	0.7900E 02
0.1600E 03	0.7330E-02	0.7900E 02
0.1651E 03	0.7330E-02	0.7800E 02
0.1701E 03	0.8060E-02	0.7600E 02
0.1752E 03	0.7330E-02	0.7500E 02

TABLE XVII. RUN PE07 EXPERIMENTAL DISTANCE, DIAMETER, AND TEMPERATURE DATA

DISTANCE FROM SPINNERETTE CM	FIBER DIAMETER CM	FIBER TEMPERATURE DEC C
0.2540E 01	0.1130E 00	0.2570E 03
0.7620E 01	0.8600E-01	0.2370E 03
0.1270E 02	0.7500E-01	0.2160E 03
0.1778E 02	0.6390E-01	0.2050E 03
0.2286E 02	0.5140E-01	0.1965E 03
0.2794E 02	0.4440E-01	0.1870E 03
0.3302E 02	0.3010E-01	0.1780E 03
0.3810E 02	0.1985E-01	0.1720E 03
0.4318E 02	0.8080E-02	0.1645E 03
0.4826E 02	0.7350E-02	0.1570E 03
0.5334E 02	0.5880E-02	0.1345E 03
0.5842E 02	0.1212E-01	0.1150E 03
0.6350E 02	0.1103E-01	0.9800E 02
0.6858E 02	0.7350E-02	0.9250E 02
0.7366E 02	0.8450E-02	0.9050E 02
0.7874E 02	0.6250E-02	0.8950E 02
0.8382E 02	0.6620E-02	0.8600E 02
0.8890E 02	0.7350E-02	0.8600E 02
0.9398E 02	0.6250E-02	0.8400E 02
0.9906E 02	0.8820E-02	0.8600E 02
0.1041E 03	0.6620E-02	0.8300E 02
0.1092E 03	0.5880E-02	0.8150E 02
0.1143E 03	0.7350E-02	0.7900E 02
0.1193E 03	0.8080E-02	0.7700E 02
0.1244E 03	0.5520E-02	0.7700E 02
0.1295E 03	0.7720E-02	0.7500E 02
0.1346E 03	0.5520E-02	0.7500E 02
0.1397E 03	0.6620E-02	0.7400E 02
0.1447E 03	0.6250E-02	0.7300E 02
0.1498E 03	0.8820E-02	0.7300E 02
0.1549E 03	0.6620E-02	0.7300E 02
0.1600E 03	0.7350E-02	0.6900E 02
0.1651E 03	0.6620E-02	0.6500E 02
0.1701E 03	0.5520E-02	0.6500E 02
0.1752E 03	0.6620E-02	0.6400E 02

TABLE XVIII. RUN PE08 EXPERIMENTAL DISTANCE, DIAMETER, AND TEMPERATURE DATA

DISTANCE FROM SPINNERETTE CM	FIBER DIAMETER CM	FIBER TEMPERATURE DEC C
0.2540E 01	0.1025E 00	0.2660E 03
0.7620E 01	0.6220E-01	0.2500E 03
0.1270E 02	0.5120E-01	0.2370E 03
0.1778E 02	0.4060E-01	0.2100E 03
0.2286E 02	0.3300E-01	0.2005E 03
0.2794E 02	0.2860E-01	0.1900E 03
0.3302E 02	0.2200E-01	0.1795E 03
0.3810E 02	0.1580E-01	0.1670E 03
0.4318E 02	0.1540E-01	0.1570E 03
0.4826E 02	0.1580E-01	0.1480E 03
0.5334E 02	0.1100E-01	0.1395E 03
0.5842E 02	0.1470E-01	0.1320E 03
0.6350E 02	0.1100E-01	0.1270E 03
0.6858E 02	0.1026E-01	0.1220E 03
0.7366E 02	0.1320E-01	0.1180E 03
0.7874E 02	0.9880E-02	0.1180E 03
0.8382E 02	0.1470E-01	0.1190E 03
0.8890E 02	0.1530E-01	0.1190E 03
0.9398E 02	0.1135E-01	0.1190E 03
0.9906E 02	0.1100E-01	0.1150E 03
0.1041E 03	0.1210E-01	0.1130E 03
0.1092E 03	0.1210E-01	0.1130E 03
0.1143E 03	0.1100E-01	0.1085E 03
0.1193E 03	0.9880E-02	0.1085E 03
0.1244E 03	0.1170E-01	0.1085E 03
0.1295E 03	0.1170E-01	0.1070E 03
0.1346E 03	0.1465E-01	0.1070E 03
0.1397E 03	0.1245E-01	0.1070E 03
0.1447E 03	0.1100E-01	0.1070E 03
0.1498E 03	0.1100E-01	0.1050E 03
0.1549E 03	0.9880E-02	0.1040E 03
0.1600E 03	0.1100E-01	0.1040E 03
0.1651E 03	0.7320E-02	0.1025E 03
0.1701E 03	0.1025E-01	0.1025E 03
0.1752E 03	0.9880E-02	0.1005E 03

TABLE XIX. RUN PE09 EXPERIMENTAL DISTANCE, DIAMETER, AND TEMPERATURE DATA

DISTANCE FROM SPINNERETTE CM	FIBER DIAMETER CM	FIBER TEMPERATURE DEC C
0.2540E 01	0.1000E 00	0.2210E 03
0.1270E 02	0.4038E-01	0.1580E 03
0.2286E 02	0.1202E-01	0.1235E 03
0.3302E 02	0.9620E-02	0.1110E 03
0.4318E 02	0.1010E-01	0.1060E 03
0.5334E 02	0.1154E-01	0.1060E 03
0.6350E 02	0.1930E-02	0.1060E 03
0.7366E 02	0.1298E-01	0.9050E 02
0.8382E 02	0.9620E-02	0.8150E 02
0.9398E 02	0.7690E-02	0.7500E 02
0.1041E 03	0.7690E-02	0.6900E 02
0.1143E 03	0.8650E-02	0.6200E 02
0.1244E 03	0.9620E-02	0.5800E 02
0.1346E 03	0.7210E-02	0.5200E 02
0.1447E 03	0.8650E-02	0.4750E 02
0.1549E 03	0.8650E-02	0.4100E 02
0.1651E 03	0.9620E-02	0.3700E 02
0.1752E 03	0.8170E-02	0.3500E 02

TABLE XX. PE01 CALCULATED SPINLINE DATA

DISTANCE FROM SPINNERET CM	CALCULATED FIBER VELOCITY M/MIN	CALCULATED VELOCITY GRADIENT 1/SEC	LOCAL TENSILE STRESS GM/SQ CM	LOCAL ELONGATIONAL VISCOSITY POISE	LOCAL FIBER DENSITY GM/CC
0.1900E 01	0.2357E 01	0.1418E-01	0.7179E 02	0.4964E 07	0.7329E 00
0.3810E 01	0.2591E 01	0.4770E-01	0.7784E 02	0.1600E 07	0.7372E 00
0.5710E 01	0.2965E 01	0.9653E-01	0.8534E 02	0.8669E 06	0.7443E 00
0.7620E 01	0.3202E 01	0.1594E 00	0.9435E 02	0.5804E 06	0.7489E 00
0.9520E 01	0.3602E 01	0.2344E 00	0.1049E 03	0.4387E 06	0.7514E 00
0.1143E 02	0.4066E 01	0.3213E 00	0.1172E 03	0.3577E 06	0.7544E 00
0.1333E 02	0.4600E 01	0.4182E 00	0.1314E 03	0.3082E 06	0.7570E 00
0.1524E 02	0.5223E 01	0.5251E 00	0.1479E 03	0.2762E 06	0.7585E 00
0.1714E 02	0.5912E 01	0.6396E 00	0.1667E 03	0.2555E 06	0.7625E 00
0.1905E 02	0.6697E 01	0.7621E 00	0.1882E 03	0.2422E 06	0.7667E 00
0.2095E 02	0.7606E 01	0.8898E 00	0.2126E 03	0.2343E 06	0.7683E 00
0.2286E 02	0.8627E 01	0.1022E 01	0.2403E 03	0.2303E 06	0.7709E 00
0.2476E 02	0.9788E 01	0.1158E 01	0.2713E 03	0.2296E 06	0.7718E 00
0.2667E 02	0.1107E 02	0.1296E 01	0.3063E 03	0.2316E 06	0.7745E 00
0.2857E 02	0.1250E 02	0.1434E 01	0.3451E 03	0.2359E 06	0.7762E 00
0.3048E 02	0.1412E 02	0.1571E 01	0.3884E 03	0.2423E 06	0.7767E 00
0.3238E 02	0.1588E 02	0.1705E 01	0.4358E 03	0.2506E 06	0.7780E 00
0.3302E 02	0.1650E 02	0.1749E 01	0.4528E 03	0.2539E 06	0.7786E 00
0.3492E 02	0.1849E 02	0.1876E 01	0.5064E 03	0.2646E 06	0.7794E 00
0.3683E 02	0.2053E 02	0.1997E 01	0.5649E 03	0.2773E 06	0.7851E 00
0.3873E 02	0.2287E 02	0.2110E 01	0.6276E 03	0.2916E 06	0.7851E 00
0.4064E 02	0.2533E 02	0.2213E 01	0.6951E 03	0.3079E 06	0.7868E 00
0.4254E 02	0.2798E 02	0.2305E 01	0.7665E 03	0.3260E 06	0.7870E 00
0.4445E 02	0.3073E 02	0.2385E 01	0.8423E 03	0.3461E 06	0.7890E 00
0.4635E 02	0.3358E 02	0.2452E 01	0.9211E 03	0.3682E 06	0.7906E 00
0.4826E 02	0.3669E 02	0.2505E 01	0.1003E 04	0.3926E 06	0.7895E 00
0.5016E 02	0.3976E 02	0.2543E 01	0.1087E 04	0.4193E 06	0.7906E 00
0.5207E 02	0.4290E 02	0.2567E 01	0.1174E 04	0.4485E 06	0.7920E 00
0.5397E 02	0.4614E 02	0.2574E 01	0.1261E 04	0.4804E 06	0.7920E 00
0.5588E 02	0.4932E 02	0.2567E 01	0.1349E 04	0.5156E 06	0.7935E 00
0.5778E 02	0.5199E 02	0.2544E 01	0.1437E 04	0.5539E 06	0.8023E 00
0.5969E 02	0.5463E 02	0.2507E 01	0.1524E 04	0.5962E 06	0.8105E 00
0.6159E 02	0.5760E 02	0.2456E 01	0.1609E 04	0.6426E 06	0.8123E 00
0.6350E 02	0.6038E 02	0.2392E 01	0.1693E 04	0.6941E 06	0.8157E 00
0.6540E 02	0.6306E 02	0.2316E 01	0.1773E 04	0.7509E 06	0.8187E 00
0.6731E 02	0.6565E 02	0.2229E 01	0.1851E 04	0.8144E 06	0.8214E 00
0.6921E 02	0.6807E 02	0.2133E 01	0.1925E 04	0.8850E 06	0.8244E 00
0.7112E 02	0.7031E 02	0.2029E 01	0.1995E 04	0.9645E 06	0.8280E 00
0.7302E 02	0.7227E 02	0.1919E 01	0.2062E 04	0.1053E 07	0.8324E 00
0.7493E 02	0.7435E 02	0.1804E 01	0.2125E 04	0.1155E 07	0.8347E 00
0.7683E 02	0.7636E 02	0.1686E 01	0.2183E 04	0.1269E 07	0.8356E 00
0.7874E 02	0.7854E 02	0.1566E 01	0.2238E 04	0.1401E 07	0.8331E 00
0.8064E 02	0.8028E 02	0.1447E 01	0.2288E 04	0.1551E 07	0.8339E 00
0.8255E 02	0.8180E 02	0.1327E 01	0.2335E 04	0.1724E 07	0.8355E 00
0.8445E 02	0.8323E 02	0.1211E 01	0.2377E 04	0.1924E 07	0.8365E 00
0.8636E 02	0.8453E 02	0.1097E 01	0.2416E 04	0.2158E 07	0.8377E 00
0.8826E 02	0.8576E 02	0.9894E 00	0.2452E 04	0.2430E 07	0.8382E 00
0.9017E 02	0.8663E 02	0.8856E 00	0.2484E 04	0.2751E 07	0.8413E 00
0.9207E 02	0.8752E 02	0.7881E 00	0.2513E 04	0.3127E 07	0.8429E 00
0.9398E 02	0.8863E 02	0.6965E 00	0.2539E 04	0.3576E 07	0.8415E 00
0.9588E 02	0.8940E 02	0.6119E 00	0.2563E 04	0.4107E 07	0.8424E 00
0.9779E 02	0.9010E 02	0.5338E 00	0.2584E 04	0.4747E 07	0.8433E 00
0.9969E 02	0.9072E 02	0.4629E 00	0.2603E 04	0.5514E 07	0.8441E 00
0.1016E 03	0.9096E 02	0.3985E 00	0.2620E 04	0.6446E 07	0.8473E 00
0.1035E 03	0.9158E 02	0.3411E 00	0.2635E 04	0.7575E 07	0.8473E 00
0.1054E 03	0.9194E 02	0.2897E 00	0.2649E 04	0.8963E 07	0.8487E 00
0.1073E 03	0.9217E 02	0.2446E 00	0.2659E 04	0.1066E 08	0.8509E 00
0.1092E 03	0.9241E 02	0.2049E 00	0.2669E 04	0.1277E 08	0.8524E 00
0.1111E 03	0.9260E 02	0.1707E 00	0.2678E 04	0.1538E 08	0.8539E 00
0.1130E 03	0.9285E 02	0.1410E 00	0.2686E 04	0.1868E 08	0.8546E 00
0.1149E 03	0.9316E 02	0.1158E 00	0.2693E 04	0.2280E 08	0.8544E 00
0.1168E 03	0.9329E 02	0.9434E-01	0.2699E 04	0.2805E 08	0.8555E 00
0.1187E 03	0.9333E 02	0.7638E-01	0.2704E 04	0.3471E 08	0.8572E 00
0.1206E 03	0.9347E 02	0.6131E-01	0.2708E 04	0.4331E 08	0.8579E 00
0.1225E 03	0.9351E 02	0.4892E-01	0.2711E 04	0.5435E 08	0.8591E 00
0.1244E 03	0.9360E 02	0.3870E-01	0.2714E 04	0.6878E 08	0.8587E 00
0.1263E 03	0.9354E 02	0.3042E-01	0.2717E 04	0.8757E 08	0.8615E 00
0.1282E 03	0.9360E 02	0.2371E-01	0.2719E 04	0.1124E 09	0.8621E 00
0.1301E 03	0.9365E 02	0.1836E-01	0.2720E 04	0.1452E 09	0.8627E 00
0.1320E 03	0.9368E 02	0.1409E-01	0.2721E 04	0.1894E 09	0.8633E 00
0.1339E 03	0.9371E 02	0.1074E-01	0.2722E 04	0.2484E 09	0.8634E 00
0.1358E 03	0.9364E 02	0.8119E-02	0.2723E 04	0.3289E 09	0.8652E 00
0.1377E 03	0.9356E 02	0.6095E-02	0.2723E 04	0.4381E 09	0.8655E 00
0.1397E 03	0.9356E 02	0.4533E-02	0.2723E 04	0.5891E 09	0.8670E 00
0.1416E 03	0.9356E 02	0.3349E-02	0.2723E 04	0.7973E 09	0.8675E 00
0.1435E 03	0.9355E 02	0.2451E-02	0.2723E 04	0.1089E 10	0.8680E 00
0.1454E 03	0.9345E 02	0.1782E-02	0.2722E 04	0.1498E 10	0.8693E 00

TABLE XXI. PE02 CALCULATED SPINLINE DATA

DISTANCE FROM SPINNERET CM	CALCULATED FIBER VELOCITY M/MIN	CALCULATED VELOCITY GRADIENT 1/SEC	LOCAL TENSILE STRESS GM/SQ CM	LOCAL ELONGATIONAL VISCOSITY POISE	LOCAL FIBER DENSITY GM/CC
0.1900E 01	0.2574E 01	0.1031E-01	0.8112E 02	0.7713E 07	0.7391E 00
0.3810E 01	0.2901E 01	0.3817E-01	0.9052E 02	0.2325E 07	0.7450E 00
0.5710E 01	0.3291E 01	0.8168E-01	0.1014E 03	0.1217E 07	0.7475E 00
0.7620E 01	0.3740E 01	0.1404E 00	0.1140E 03	0.7963E 06	0.7502E 00
0.9520E 01	0.4253E 01	0.2133E 00	0.1285E 03	0.5907E 06	0.7527E 00
0.1143E 02	0.4832E 01	0.3004E 00	0.1451E 03	0.4736E 06	0.7565E 00
0.1333E 02	0.5491E 01	0.4004E 00	0.1639E 03	0.4014E 06	0.7595E 00
0.1524E 02	0.6253E 01	0.5138E 00	0.1854E 03	0.3539E 06	0.7613E 00
0.1714E 02	0.7096E 01	0.6388E 00	0.2097E 03	0.3220E 06	0.7647E 00
0.1905E 02	0.8065E 01	0.7762E 00	0.2374E 03	0.2999E 06	0.7667E 00
0.2095E 02	0.9144E 01	0.9237E 00	0.2684E 03	0.2849E 06	0.7693E 00
0.2286E 02	0.1038E 02	0.1082E 01	0.3035E 03	0.2750E 06	0.7704E 00
0.2476E 02	0.1177E 02	0.1249E 01	0.3427E 03	0.2690E 06	0.7709E 00
0.2667E 02	0.1328E 02	0.1425E 01	0.3868E 03	0.2661E 06	0.7741E 00
0.2857E 02	0.1500E 02	0.1608E 01	0.4358E 03	0.2657E 06	0.7749E 00
0.3048E 02	0.1677E 02	0.1798E 01	0.4904E 03	0.2674E 06	0.7829E 00
0.3238E 02	0.1889E 02	0.1992E 01	0.5507E 03	0.2710E 06	0.7824E 00
0.3302E 02	0.1965E 02	0.2058E 01	0.5724E 03	0.2726E 06	0.7824E 00
0.3810E 02	0.2659E 02	0.2593E 01	0.7706E 03	0.2913E 06	0.7838E 00
0.4318E 02	0.3512E 02	0.3125E 01	0.1019E 04	0.3199E 06	0.7887E 00
0.4826E 02	0.4546E 02	0.3625E 01	0.1323E 04	0.3579E 06	0.7931E 00
0.5334E 02	0.5751E 02	0.4062E 01	0.1679E 04	0.4055E 06	0.7977E 00
0.5842E 02	0.6934E 02	0.4410E 01	0.2083E 04	0.4633E 06	0.8218E 00
0.6350E 02	0.8308E 02	0.4645E 01	0.2524E 04	0.5329E 06	0.8319E 00
0.6858E 02	0.9772E 02	0.4753E 01	0.2988E 04	0.6164E 06	0.8376E 00
0.7366E 02	0.1127E 03	0.4727E 01	0.3458E 04	0.7175E 06	0.8407E 00
0.7874E 02	0.1273E 03	0.4569E 01	0.3919E 04	0.8412E 06	0.8434E 00
0.8382E 02	0.1405E 03	0.4292E 01	0.4357E 04	0.9953E 06	0.8493E 00
0.8890E 02	0.1530E 03	0.3919E 01	0.4761E 04	0.1191E 07	0.8523E 00
0.9398E 02	0.1641E 03	0.3475E 01	0.5124E 04	0.1445E 07	0.8555E 00
0.9906E 02	0.1739E 03	0.2992E 01	0.5442E 04	0.1783E 07	0.8577E 00
0.1041E 03	0.1823E 03	0.2500E 01	0.5717E 04	0.2242E 07	0.8597E 00
0.1092E 03	0.1893E 03	0.2025E 01	0.5950E 04	0.2880E 07	0.8617E 00
0.1143E 03	0.1952E 03	0.1589E 01	0.6144E 04	0.3790E 07	0.8631E 00
0.1193E 03	0.1999E 03	0.1208E 01	0.6305E 04	0.5116E 07	0.8651E 00
0.1244E 03	0.2035E 03	0.8885E 00	0.6434E 04	0.7100E 07	0.8676E 00
0.1295E 03	0.2067E 03	0.6315E 00	0.6538E 04	0.1015E 08	0.8688E 00
0.1346E 03	0.2092E 03	0.4335E 00	0.6621E 04	0.1497E 08	0.8700E 00

TABLE XXII. CALCULATED SPINLINE DATA

DISTANCE FROM SPINNERET CM	CALCULATED FIBER VELOCITY M/MIN	CALCULATED VELOCITY GRADIENT 1/SEC	LOCAL TENSILE STRESS GM/SQ CM	LOCAL ELONGATIONAL VISCOSITY POISE	LOCAL FIBER DENSITY GM/CC
0.2540E 01	0.2609E 01	0.4537E-01	0.6667E 02	0.1441E 07	0.7367E 00
0.7620E 01	0.3450E 01	0.2183E 00	0.8451E 02	0.3795E 06	0.7482E 00
0.1270E 02	0.4731E 01	0.4454E 00	0.1116E 03	0.2456E 06	0.7544E 00
0.1778E 02	0.6490E 01	0.6958E 00	0.1498E 03	0.2112E 06	0.7647E 00
0.2286E 02	0.8885E 01	0.9432E 00	0.2013E 03	0.2093E 06	0.7704E 00
0.2794E 02	0.1192E 02	0.1163E 01	0.2676E 03	0.2255E 06	0.7776E 00
0.3302E 02	0.1569E 02	0.1336E 01	0.3486E 03	0.2558E 06	0.7810E 00
0.3810E 02	0.2004E 02	0.1445E 01	0.4420E 03	0.2999E 06	0.7838E 00
0.4318E 02	0.2466E 02	0.1483E 01	0.5434E 03	0.3593E 06	0.7899E 00
0.4826E 02	0.2925E 02	0.1449E 01	0.6470E 03	0.4376E 06	0.7986E 00
0.5334E 02	0.3363E 02	0.1354E 01	0.7467E 03	0.5408E 06	0.8062E 00
0.5842E 02	0.3741E 02	0.1209E 01	0.8373E 03	0.6787E 06	0.8170E 00
0.6350E 02	0.4093E 02	0.1035E 01	0.9157E 03	0.8676E 06	0.8202E 00
0.6858E 02	0.4381E 02	0.8483E 00	0.9804E 03	0.1133E 07	0.8241E 00
0.7366E 02	0.4606E 02	0.6663E 00	0.1031E 04	0.1518E 07	0.8281E 00
0.7874E 02	0.4787E 02	0.5014E 00	0.1071E 04	0.2094E 07	0.8305E 00
0.8382E 02	0.4914E 02	0.3615E 00	0.1100E 04	0.2984E 07	0.8342E 00
0.8890E 02	0.5007E 02	0.2495E 00	0.1120E 04	0.4404E 07	0.8372E 00
0.9398E 02	0.5075E 02	0.1649E 00	0.1135E 04	0.6747E 07	0.8396E 00
0.9906E 02	0.5132E 02	0.1043E 00	0.1144E 04	0.1075E 08	0.8401E 00
0.1041E 03	0.5173E 02	0.6308E-01	0.1149E 04	0.1787E 08	0.8405E 00
0.1092E 03	0.5203E 02	0.3646E-01	0.1152E 04	0.3098E 08	0.8408E 00
0.1143E 03	0.5220E 02	0.2013E-01	0.1152E 04	0.5614E 08	0.8415E 00
0.1193E 03	0.5232E 02	0.1061E-01	0.1152E 04	0.1064E 09	0.8422E 00
0.1244E 03	0.5234E 02	0.5340E-02	0.1150E 04	0.2112E 09	0.8437E 00
0.1295E 03	0.5227E 02	0.2561E-02	0.1147E 04	0.4393E 09	0.8461E 00
0.1346E 03	0.5211E 02	0.1171E-02	0.1144E 04	0.9584E 09	0.8496E 00
0.1397E 03	0.5193E 02	0.5099E-03	0.1141E 04	0.2194E 10	0.8531E 00
0.1447E 03	0.5169E 02	0.2113E-03	0.1137E 04	0.5278E 10	0.8578E 00
0.1498E 03	0.5152E 02	0.8330E-04	0.1133E 04	0.1334E 11	0.8607E 00
0.1549E 03	0.5146E 02	0.3121E-04	0.1129E 04	0.3547E 11	0.8618E 00
0.1600E 03	0.5121E 02	0.1111E-04	0.1125E 04	0.9927E 11	0.8662E 00
0.1651E 03	0.5099E 02	0.3757E-05	0.1120E 04	0.2925E 12	0.8701E 00
0.1701E 03	0.5061E 02	0.1205E-05	0.1116E 04	0.9084E 12	0.8766E 00
0.1752E 03	0.5045E 02	0.3666E-06	0.1112E 04	0.2974E 13	0.8795E 00

TABLE XXIII. PE04 CALCULATED SPINLINE DATA

DISTANCE FROM SPINNERET CM	CALCULATED FIBER VELOCITY M/MIN	CALCULATED VELOCITY GRADIENT 1/SEC	LOCAL TENSILE STRESS GM/SQ CM	LOCAL ELONGATIONAL VISCOSITY POISE	LOCAL FIBER DENSITY GM/CC
0.2540E 01	0.2292E 01	0.7338E-02	0.9364E 02	0.1251E 08	0.7555E 00
0.7620E 01	0.2803E 01	0.1118E 00	0.1112E 03	0.9750E 06	0.7654E 00
0.1270E 02	0.3894E 01	0.3914E 00	0.1499E 03	0.3756E 06	0.7693E 00
0.1778E 02	0.5848E 01	0.8648E 00	0.2205E 03	0.2500E 06	0.7736E 00
0.2286E 02	0.9148E 01	0.1480E 01	0.3400E 03	0.2253E 06	0.7762E 00
0.2794E 02	0.1423E 02	0.2096E 01	0.5258E 03	0.2460E 06	0.7802E 00
0.3302E 02	0.2121E 02	0.2506E 01	0.7807E 03	0.3054E 06	0.7829E 00
0.3810E 02	0.2935E 02	0.2531E 01	0.1077E 04	0.4172E 06	0.7843E 00
0.4318E 02	0.3661E 02	0.2135E 01	0.1361E 04	0.6253E 06	0.7973E 00
0.4826E 02	0.4209E 02	0.1477E 01	0.1587E 04	0.1053E 07	0.8105E 00
0.5334E 02	0.4576E 02	0.8211E 00	0.1738E 04	0.2075E 07	0.8185E 00
0.5842E 02	0.4789E 02	0.3568E 00	0.1826E 04	0.5017E 07	0.8236E 00
0.6350E 02	0.4911E 02	0.1179E 00	0.1871E 04	0.1556E 08	0.8247E 00
0.6858E 02	0.4965E 02	0.2873E-01	0.1891E 04	0.6455E 08	0.8263E 00
0.7366E 02	0.4962E 02	0.4996E-02	0.1898E 04	0.3725E 09	0.8319E 00
0.7874E 02	0.4960E 02	0.5993E-03	0.1899E 04	0.3107E 10	0.8344E 00
0.8382E 02	0.4946E 02	0.4782E-04	0.1897E 04	0.3890E 11	0.8376E 00
0.8890E 02	0.4936E 02	0.2445E-05	0.1893E 04	0.7593E 12	0.8398E 00
0.9398E 02	0.4920E 02	0.7713E-07	0.1889E 04	0.2402E 14	0.8426E 00
0.9906E 02	0.4897E 02	0.1441E-08	0.1885E 04	0.1283E 16	0.8467E 00
0.1041E 03	0.4887E 02	0.1530E-10	0.1881E 04	0.1205E 18	0.8485E 00
0.1092E 03	0.4877E 02	0.8862E-13	0.1877E 04	0.2076E 20	0.8501E 00
0.1143E 03	0.4868E 02	0.2677E-15	0.1872E 04	0.6859E 22	0.8517E 00
0.1193E 03	0.4848E 02	0.4037E-18	0.1868E 04	0.4538E 25	0.8553E 00
0.1244E 03	0.4835E 02	0.2903E-21	0.1864E 04	0.6296E 28	0.8576E 00
0.1295E 03	0.4820E 02	0.9502E-25	0.1859E 04	0.1919E 32	0.8602E 00
0.1346E 03	0.4802E 02	0.1350E-28	0.1855E 04	0.1347E 36	0.8635E 00
0.1397E 03	0.4786E 02	0.7934E-33	0.1850E 04	0.1701E 39	0.8664E 00
0.1447E 03	0.4773E 02	0.0000E 00	0.1846E 04	0.9999E 04	0.8687E 00
0.1498E 03	0.4760E 02	0.0000E 00	0.1841E 04	0.9999E 04	0.8711E 00
0.1549E 03	0.4754E 02	0.0000E 00	0.1837E 04	0.9999E 04	0.8721E 00
0.1600E 03	0.4744E 02	0.0000E 00	0.1833E 04	0.9999E 04	0.8740E 00
0.1651E 03	0.4714E 02	0.0000E 00	0.1828E 04	0.9999E 04	0.8796E 00
0.1701E 03	0.4689E 02	0.0000E 00	0.1824E 04	0.9999E 04	0.8843E 00
0.1752E 03	0.4676E 02	0.0000E 00	0.1819E 04	0.9999E 04	0.8866E 00

TABLE XXIV. PE05 CALCULATED SPINLINE DATA

DISTANCE FROM SPINNERET CM	CALCULATED FIBER VELOCITY M/MIN	CALCULATED VELOCITY GRADIENT 1/SEC	LOCAL TENSILE STRESS GM/SQ CM	LOCAL ELONGATIONAL VISCOSITY POISE	LOCAL FIBER DENSITY GM/CC
0.2540E 01	0.3331E 01	0.5831E-02	0.6971E 02	0.1172E 08	0.7462E 00
0.7620E 01	0.3858E 01	0.5559E-01	0.7677E 02	0.1354E 07	0.7502E 00
0.1270E 02	0.4653E 01	0.1581E 00	0.8874E 02	0.5501E 06	0.7565E 00
0.1778E 02	0.5790E 01	0.3134E 00	0.1060E 03	0.3319E 06	0.7595E 00
0.2286E 02	0.7318E 01	0.5184E 00	0.1300E 03	0.2459E 06	0.7641E 00
0.2794E 02	0.9342E 01	0.7670E 00	0.1621E 03	0.2072E 06	0.7693E 00
0.3302E 02	0.1195E 02	0.1049E 01	0.2043E 03	0.1909E 06	0.7762E 00
0.3810E 02	0.1533E 02	0.1352E 01	0.2587E 03	0.1876E 06	0.7810E 00
0.4318E 02	0.1960E 02	0.1658E 01	0.3271E 03	0.1933E 06	0.7838E 00
0.4826E 02	0.2483E 02	0.1948E 01	0.4105E 03	0.2066E 06	0.7857E 00
0.5334E 02	0.3096E 02	0.2200E 01	0.5093E 03	0.2269E 06	0.7887E 00
0.5842E 02	0.3802E 02	0.2395E 01	0.6219E 03	0.2545E 06	0.7898E 00
0.6350E 02	0.4571E 02	0.2517E 01	0.7453E 03	0.2903E 06	0.7914E 00
0.6858E 02	0.5382E 02	0.2554E 01	0.8749E 03	0.3359E 06	0.7926E 00
0.7366E 02	0.6195E 02	0.2503E 01	0.1005E 04	0.3939E 06	0.7939E 00
0.7874E 02	0.6980E 02	0.2368E 01	0.1131E 04	0.4685E 06	0.7953E 00
0.8382E 02	0.7697E 02	0.2161E 01	0.1248E 04	0.5662E 06	0.7977E 00
0.8890E 02	0.8243E 02	0.1902E 01	0.1352E 04	0.6970E 06	0.8089E 00
0.9398E 02	0.8746E 02	0.1611E 01	0.1441E 04	0.8770E 06	0.8148E 00
0.9906E 02	0.9175E 02	0.1313E 01	0.1516E 04	0.1131E 07	0.8187E 00
0.1041E 03	0.9562E 02	0.1028E 01	0.1576E 04	0.1502E 07	0.8187E 00
0.1092E 03	0.9835E 02	0.7729E 00	0.1624E 04	0.2060E 07	0.8219E 00
0.1143E 03	0.1002E 03	0.5563E 00	0.1660E 04	0.2927E 07	0.8262E 00
0.1193E 03	0.1018E 03	0.3830E 00	0.1687E 04	0.4321E 07	0.8289E 00
0.1244E 03	0.1028E 03	0.2518E 00	0.1707E 04	0.6649E 07	0.8323E 00
0.1295E 03	0.1036E 03	0.1579E 00	0.1721E 04	0.1069E 08	0.8347E 00
0.1346E 03	0.1041E 03	0.9425E-01	0.1730E 04	0.1800E 08	0.8369E 00
0.1397E 03	0.1043E 03	0.5346E-01	0.1736E 04	0.3184E 08	0.8400E 00
0.1447E 03	0.1045E 03	0.2877E-01	0.1739E 04	0.5926E 08	0.8420E 00
0.1498E 03	0.1045E 03	0.1467E-01	0.1740E 04	0.1163E 09	0.8448E 00
0.1549E 03	0.1045E 03	0.7072E-02	0.1739E 04	0.2412E 09	0.8467E 00
0.1600E 03	0.1043E 03	0.3217E-02	0.1738E 04	0.5297E 09	0.8498E 00
0.1651E 03	0.1040E 03	0.1379E-02	0.1736E 04	0.1234E 10	0.8528E 00
0.1701E 03	0.1039E 03	0.5561E-03	0.1733E 04	0.3056E 10	0.8545E 00
0.1752E 03	0.1039E 03	0.2104E-03	0.1729E 04	0.8060E 10	0.8548E 00

TABLE XXV. PE06 CALCULATED SPINLINE DATA

DISTANCE FROM SPINNERET CM	CALCULATED FIBER VELOCITY M/MIN	CALCULATED VELOCITY GRADIENT 1/SEC	LOCAL TENSILE STRESS GM/SQ CM	LOCAL ELONGATIONAL VISCOSITY POISE	LOCAL FIBER DENSITY GM/CC
0.2540E 01	0.2637E 01	0.1759E-02	0.6165E 02	0.3435E 08	0.7334E 00
0.7620E 01	0.3434E 01	0.6285E-01	0.7656E 02	0.1194E 07	0.7443E 00
0.1270E 02	0.4947E 01	0.3310E 00	0.1066E 03	0.3158E 06	0.7570E 00
0.1778E 02	0.7657E 01	0.9853E 00	0.1613E 03	0.1606E 06	0.7675E 00
0.2286E 02	0.1249E 02	0.2207E 01	0.2591E 03	0.1151E 06	0.7736E 00
0.2794E 02	0.2099E 02	0.4146E 01	0.4321E 03	0.1022E 06	0.7789E 00
0.3302E 02	0.3550E 02	0.6852E 01	0.7310E 03	0.1046E 06	0.7851E 00
0.3810E 02	0.5950E 02	0.1019E 02	0.1224E 04	0.1177E 06	0.7870E 00
0.4318E 02	0.9597E 02	0.1379E 02	0.1983E 04	0.1409E 06	0.7898E 00
0.4826E 02	0.1455E 03	0.1698E 02	0.3039E 04	0.1754E 06	0.7953E 00
0.5334E 02	0.2040E 03	0.1893E 02	0.4335E 04	0.2245E 06	0.8055E 00
0.5842E 02	0.2618E 03	0.1894E 02	0.5723E 04	0.2963E 06	0.8239E 00
0.6350E 02	0.3179E 03	0.1678E 02	0.7020E 04	0.4102E 06	0.8282E 00
0.6858E 02	0.3637E 03	0.1295E 02	0.8090E 04	0.6123E 06	0.8306E 00
0.7366E 02	0.3878E 03	0.8552E 01	0.8876E 04	0.1017E 07	0.8528E 00
0.7874E 02	0.4068E 03	0.4723E 01	0.9408E 04	0.1953E 07	0.8612E 00
0.8382E 02	0.4216E 03	0.2129E 01	0.9741E 04	0.4486E 07	0.8607E 00
0.8890E 02	0.4289E 03	0.7625E 00	0.9943E 04	0.1278E 08	0.8640E 00
0.9398E 02	0.4318E 03	0.2106E 00	0.1006E 05	0.4683E 08	0.8689E 00
0.9906E 02	0.4335E 03	0.4348E-01	0.1012E 05	0.2284E 09	0.8715E 00
0.1041E 03	0.4345E 03	0.6475E-02	0.1016E 05	0.1539E 10	0.8731E 00
0.1092E 03	0.4347E 03	0.6706E-03	0.1018E 05	0.1488E 11	0.8745E 00
0.1143E 03	0.4329E 03	0.4641E-04	0.1018E 05	0.2152E 12	0.8791E 00
0.1193E 03	0.4326E 03	0.2058E-05	0.1019E 05	0.4854E 13	0.8803E 00
0.1244E 03	0.4319E 03	0.5595E-07	0.1019E 05	0.1785E 15	0.8821E 00
0.1295E 03	0.4304E 03	0.8891E-09	0.1018E 05	0.1123E 17	0.8853E 00
0.1346E 03	0.4295E 03	0.7858E-11	0.1018E 05	0.1270E 19	0.8873E 00
0.1397E 03	0.4286E 03	0.3666E-13	0.1017E 05	0.2722E 21	0.8892E 00
0.1447E 03	0.4282E 03	0.8547E-16	0.1017E 05	0.1167E 24	0.8901E 00
0.1498E 03	0.4278E 03	0.9401E-19	0.1017E 05	0.1060E 27	0.8908E 00
0.1549E 03	0.4271E 03	0.4593E-22	0.1016E 05	0.2170E 30	0.8923E 00
0.1600E 03	0.4268E 03	0.9361E-26	0.1016E 05	0.1064E 34	0.8930E 00
0.1651E 03	0.4261E 03	0.7456E-30	0.1015E 05	0.1335E 38	0.8944E 00
0.1701E 03	0.4252E 03	0.2167E-34	0.1015E 05	0.1701E 39	0.8964E 00
0.1752E 03	0.4246E 03	0.0000E 00	0.1014E 05	0.9999E 04	0.8976E 00

TABLE XXVI. PE07 CALCULATED SPINLINE DATA

DISTANCE FROM SPINNERET CM	CALCULATED FIBER VELOCITY M/MIN	CALCULATED VELOCITY GRADIENT 1/SEC	LOCAL TENSILE STRESS GM/SQ CM	LOCAL ELONGATIONAL VISCOSITY POISE	LOCAL FIBER DENSITY GM/CC
0.2540E 01	0.2899E 01	0.1635E-02	0.6540E 02	0.3922E 08	0.7334E 00
0.7620E 01	0.3696E 01	0.6693E-01	0.7967E 02	0.1167E 07	0.7430E 00
0.1270E 02	0.5271E 01	0.3756E 00	0.1097E 03	0.2865E 06	0.7534E 00
0.1778E 02	0.8201E 01	0.1166E 01	0.1660E 03	0.1396E 06	0.7590E 00
0.2286E 02	0.1355E 02	0.2698E 01	0.2698E 03	0.9807E 05	0.7634E 00
0.2794E 02	0.2329E 02	0.5202E 01	0.4604E 03	0.8678E 05	0.7683E 00
0.3302E 02	0.4073E 02	0.8792E 01	0.8048E 03	0.8976E 05	0.7730E 00
0.3810E 02	0.7085E 02	0.1333E 02	0.1403E 04	0.1032E 06	0.7762E 00
0.4318E 02	0.1189E 03	0.1833E 02	0.2374E 04	0.1269E 06	0.7802E 00
0.4826E 02	0.1877E 03	0.2285E 02	0.3789E 04	0.1626E 06	0.7843E 00
0.5334E 02	0.2700E 03	0.2566E 02	0.5587E 04	0.2135E 06	0.7977E 00
0.5842E 02	0.3475E 03	0.2569E 02	0.7535E 04	0.2876E 06	0.8292E 00
0.6350E 02	0.4178E 03	0.2258E 02	0.9337E 04	0.4055E 06	0.8488E 00
0.6858E 02	0.4755E 03	0.1709E 02	0.1078E 05	0.6185E 06	0.8565E 00
0.7366E 02	0.5165E 03	0.1090E 02	0.1181E 05	0.1062E 07	0.8605E 00
0.7874E 02	0.5426E 03	0.5711E 01	0.1248E 05	0.2142E 07	0.8634E 00
0.8382E 02	0.5564E 03	0.2384E 01	0.1288E 05	0.5299E 07	0.8680E 00
0.8890E 02	0.5650E 03	0.7686E 00	0.1310E 05	0.1672E 08	0.8697E 00
0.9398E 02	0.5684E 03	0.1845E 00	0.1322E 05	0.7027E 08	0.8727E 00
0.9906E 02	0.5713E 03	0.3175E-01	0.1328E 05	0.4103E 09	0.8725E 00
0.1041E 03	0.5705E 03	0.3754E-02	0.1331E 05	0.3478E 10	0.8761E 00
0.1092E 03	0.5698E 03	0.2913E-03	0.1333E 05	0.4486E 11	0.8784E 00
0.1143E 03	0.5683E 03	0.1414E-04	0.1333E 05	0.9248E 12	0.8814E 00
0.1193E 03	0.5668E 03	0.4073E-06	0.1333E 05	0.3210E 14	0.8839E 00
0.1244E 03	0.5663E 03	0.6587E-08	0.1333E 05	0.1985E 16	0.8849E 00
0.1295E 03	0.5648E 03	0.5638E-10	0.1333E 05	0.2318E 18	0.8872E 00
0.1346E 03	0.5643E 03	0.2399E-12	0.1332E 05	0.5445E 20	0.8881E 00
0.1397E 03	0.5633E 03	0.4753E-15	0.1332E 05	0.2748E 23	0.8897E 00
0.1447E 03	0.5623E 03	0.4088E-18	0.1331E 05	0.3194E 26	0.8912E 00
0.1498E 03	0.5618E 03	0.1418E-21	0.1331E 05	0.9202E 29	0.8920E 00
0.1549E 03	0.5613E 03	0.1838E-25	0.1330E 05	0.7097E 32	0.8928E 00
0.1600E 03	0.5592E 03	0.8214E-30	0.1330E 05	0.1588E 38	0.8962E 00
0.1651E 03	0.5572E 03	0.1162E-34	0.1329E 05	0.1701E 39	0.8995E 00
0.1701E 03	0.5568E 03	0.0000E 00	0.1329E 05	0.9999E 04	0.9001E 00
0.1752E 03	0.5560E 03	0.0000E 00	0.1329E 05	0.9999E 04	0.9014E 00

TABLE XXVII. PE08 CALCULATED SPINLINE DATA

DISTANCE FROM SPINNERET CM	CALCULATED FIBER VELOCITY M/MIN	CALCULATED VELOCITY GRADIENT 1/SEC	LOCAL TENSILE STRESS GM/SQ CM	LOCAL ELONGATIONAL VISCOSITY POISE	LOCAL FIBER DENSITY GM/CC
0.2540E 01	0.3575E 01	0.2144E 00	0.7660E 02	0.3502E 06	0.7291E 00
0.7620E 01	0.6692E 01	0.1173E 01	0.1379E 03	0.1152E 06	0.7367E 00
0.1270E 02	0.1208E 02	0.2527E 01	0.2445E 03	0.9489E 05	0.7430E 00
0.1778E 02	0.2062E 02	0.4052E 01	0.4188E 03	0.1013E 06	0.7565E 00
0.2286E 02	0.3369E 02	0.5530E 01	0.6827E 03	0.1210E 06	0.7613E 00
0.2794E 02	0.5156E 02	0.6750E 01	0.1048E 04	0.1523E 06	0.7667E 00
0.3302E 02	0.7375E 02	0.7534E 01	0.1508E 04	0.1963E 06	0.7722E 00
0.3810E 02	0.9847E 02	0.7780E 01	0.2031E 04	0.2560E 06	0.7789E 00
0.4318E 02	0.1236E 03	0.7477E 01	0.2571E 04	0.3372E 06	0.7843E 00
0.4826E 02	0.1471E 03	0.6709E 01	0.3081E 04	0.4503E 06	0.7892E 00
0.5334E 02	0.1673E 03	0.5626E 01	0.3527E 04	0.6148E 06	0.7939E 00
0.5842E 02	0.1790E 03	0.4412E 01	0.3892E 04	0.8651E 06	0.8186E 00
0.6350E 02	0.1898E 03	0.3234E 01	0.4179E 04	0.1267E 07	0.8290E 00
0.6858E 02	0.1975E 03	0.2214E 01	0.4394E 04	0.1946E 07	0.8376E 00
0.7366E 02	0.2031E 03	0.1414E 01	0.4550E 04	0.3155E 07	0.8443E 00
0.7874E 02	0.2076E 03	0.8415E 00	0.4661E 04	0.5431E 07	0.8469E 00
0.8382E 02	0.2109E 03	0.4658E 00	0.4739E 04	0.9976E 07	0.8482E 00
0.8890E 02	0.2130E 03	0.2395E 00	0.4792E 04	0.1962E 08	0.8502E 00
0.9398E 02	0.2143E 03	0.1142E 00	0.4828E 04	0.4146E 08	0.8521E 00
0.9906E 02	0.2149E 03	0.5041E-01	0.4852E 04	0.9439E 08	0.8571E 00
0.1041E 03	0.2144E 03	0.2056E-01	0.4867E 04	0.2321E 09	0.8603E 00
0.1092E 03	0.2146E 03	0.7740E-02	0.4876E 04	0.6178E 09	0.8617E 00
0.1143E 03	0.2138E 03	0.2683E-02	0.4882E 04	0.1783E 10	0.8667E 00
0.1193E 03	0.2138E 03	0.8554E-03	0.4884E 04	0.5599E 10	0.8680E 00
0.1244E 03	0.2137E 03	0.2502E-03	0.4884E 04	0.1913E 11	0.8691E 00
0.1295E 03	0.2133E 03	0.6710E-04	0.4882E 04	0.7136E 11	0.8714E 00
0.1346E 03	0.2131E 03	0.1645E-04	0.4880E 04	0.2908E 12	0.8724E 00
0.1397E 03	0.2129E 03	0.3685E-05	0.4877E 04	0.1297E 13	0.8734E 00
0.1447E 03	0.2127E 03	0.7524E-06	0.4874E 04	0.6352E 13	0.8744E 00
0.1498E 03	0.2122E 03	0.1398E-06	0.4870E 04	0.3416E 14	0.8768E 00
0.1549E 03	0.2118E 03	0.2360E-07	0.4866E 04	0.2021E 15	0.8785E 00
0.1600E 03	0.2116E 03	0.3615E-08	0.4862E 04	0.1318E 16	0.8793E 00
0.1651E 03	0.2111E 03	0.5015E-09	0.4858E 04	0.9499E 16	0.8812E 00
0.1701E 03	0.2110E 03	0.6290E-10	0.4853E 04	0.7567E 17	0.8820E 00
0.1752E 03	0.2104E 03	0.7122E-11	0.4849E 04	0.6677E 18	0.8842E 00

TABLE XXVIII. PE09 CALCULATED SPINLINE DATA

DISTANCE FROM SPINNERET CM	CALCULATED FIBER VELOCITY M/MIN	CALCULATED VELOCITY GRADIENT 1/SEC	LOCAL TENSILE STRESS GM/SQ CM	LOCAL ELONGATIONAL VISCOSITY POISE	LOCAL FIBER DENSITY GM/CC
0.2540E 01	0.1201E 01	0.5181E-02	0.7023E 02	0.1329E 08	0.7509E 00
0.1270E 02	0.6999E 01	0.3161E 01	0.3807E 03	0.1180E 06	0.7838E 00
0.2286E 02	0.7270E 02	0.2161E 02	0.4007E 04	0.1817E 06	0.8091E 00
0.3302E 02	0.2003E 03	0.8596E 01	0.1125E 05	0.1283E 07	0.8215E 00
0.4318E 02	0.2163E 03	0.8129E-02	0.1270E 05	0.1532E 10	0.8598E 00
0.5334E 02	0.2158E 03	0.2563E-10	0.1277E 05	0.4886E 18	0.8674E 00
0.6350E 02	0.2145E 03	0.6311E-29	0.1277E 05	0.1984E 37	0.8725E 00
0.7366E 02	0.2108E 03	0.0000E 00	0.1276E 05	0.9999E 04	0.8879E 00
0.8382E 02	0.2087E 03	0.0000E 00	0.1275E 05	0.9999E 04	0.8970E 00
0.9398E 02	0.2071E 03	0.0000E 00	0.1274E 05	0.9999E 04	0.9037E 00
0.1041E 03	0.2058E 03	0.0000E 00	0.1273E 05	0.9999E 04	0.9095E 00
0.1143E 03	0.2045E 03	0.0000E 00	0.1272E 05	0.9999E 04	0.9154E 00
0.1244E 03	0.2036E 03	0.0000E 00	0.1271E 05	0.9999E 04	0.9193E 00
0.1346E 03	0.2026E 03	0.0000E 00	0.1270E 05	0.9999E 04	0.9239E 00
0.1447E 03	0.2018E 03	0.0000E 00	0.1269E 05	0.9999E 04	0.9275E 00
0.1549E 03	0.2009E 03	0.0000E 00	0.1268E 05	0.9999E 04	0.9319E 00
0.1651E 03	0.2002E 03	0.0000E 00	0.1267E 05	0.9999E 04	0.9348E 00
0.1752E 03	0.1998E 03	0.0000E 00	0.1266E 05	0.9999E 04	0.9367E 00

TABLE XXIX. DISTANCE VERSUS TIME OF TRAVEL
FROM THE SPINNERET

DISTANCE CM	PE01 TIME SEC	PE02 TIME SEC	PE03 TIME SEC	PE04 TIME SEC	PE05 TIME SEC	PE06 TIME SEC	PE07 TIME SEC	PE08 TIME SEC	PE09 TIME SEC
0.254000E 01	0.311000E 00	0.277000E 00	0.310000E 00	0.340000E 00	0.175[illegible]E 00	0.296000E 00	0.310000E 00	0.278000E 00	0.277000E 00
0.508000E 01	0.761820E 00	0.597241E 00	0.749987E 00	0.858563E 00	0.[illegible]E 00	0.686785E 00	0.750345E 00	0.601412E 00	0.264469E 01
0.762000E 01	0.119682E 01	0.910682E 00	0.116726E 01	0.136556E 01	0.[illegible]E 00	0.107464E 01	0.118687E 01	0.870239E 00	0.407665E 01
0.101600E 02	0.160340E 01	0.121073E 01	0.154964E 01	0.184463E 01	0.114325E 01	0.145268E 01	0.161018E 01	0.107494E 01	0.496489E 01
0.127000E 02	0.197069E 01	0.149043E 01	0.188949E 01	0.227620F 01	0.145128E 01	0.180847E 01	0.200307E 01	0.122438E 01	0.537761E 01
0.152400E 02	0.229302E 01	0.174456E 01	0.218520E 01	0.264590E 01	0.174647E 01	0.212683E 01	0.234540E 01	0.133811E 01	0.559810E 01
0.177800E 02	0.256823E 01	0.196892E 01	0.243789E 01	0.294757E 01	0.202049E 01	0.239358E 01	0.262131E 01	0.141315E 01	0.564266E 01
0.203200E 02	0.280046E 01	0.216377E 01	0.265316E 01	0.318729E 01	0.227410E 01	0.260509E 01	0.283037E 01	0.147367E 01	0.568677E 01
0.228600E 02	0.299422E 01	0.232998E 01	0.283576E 01	0.337458E 01	0.250337E 01	0.276507E 01	0.298156E 01	0.152047E 01	0.571233E 01
0.254000E 02	0.315614E 01	0.247107E 01	0.299177E 01	0.352148E 01	0.270862E 01	0.288349E 01	0.308913E 01	0.155769E 01	0.572885E 01
0.279400E 02	0.329165E 01	0.259018E 01	0.312567E 01	0.363770E 01	0.289010E 01	0.297028E 01	0.316542E 01	0.158794E 01	0.574069E 01
0.304800E 02	0.340568E 01	0.269076E 01	0.324151E 01	0.373118E 01	0.304940E 01	0.303411E 01	0.322004E 01	0.161306E 01	0.575008E 01
0.330200E 02	0.350220E 01	0.277577E 01	0.334242E 01	0.380774E 01	0.318837E 01	0.308150E 01	0.325970E 01	0.163428E 01	0.575822E 01
0.355600E 02	0.358490E 01	0.284822E 01	0.343148E 01	0.387208E 01	0.330983E 01	0.311731E 01	0.328915E 01	0.165260E 01	0.576583E 01
0.381000E 02	0.365626E 01	0.291022E 01	0.351066E 01	0.392728E 01	0.341584F 01	0.314480E 01	0.331141E 01	0.166865E 01	0.577324E 01
0.406400E 02	0.371842E 01	0.296362E 01	0.358170E 01	0.397570E 01	0.350854E 01	0.316626E 01	0.332858E 01	0.168292E 01	0.578060E 01
0.431800E 02	0.377295E 01	0.300985E 01	0.364587E 01	0.401904E 01	0.358973E 01	0.318330E 01	0.334205E 01	0.169574E 01	0.578793E 01
0.457200E 02	0.382139E 01	0.305030E 01	0.370456E 01	0.405876E 01	0.366138E 01	0.319712E 01	0.335286E 01	0.170747E 01	0.579528E 01
0.482600E 02	0.386472E 01	0.308587E 01	0.375857E 01	0.409580E 01	0.372482E 01	0.320849E 01	0.336170E 01	0.171828E 01	0.580263E 01
0.508000E 02	0.390380F 01	0.311738E 01	0.380865E 01	0.413090E 01	0.378127E 01	0.321803E 01	0.336905E 01	0.172836E 01	0.580998E 01
0.533400E 02	0.393933E 01	0.314547E 01	0.385542E 01	0.416465E 01	0.383178E 01	0.322615E 01	0.337528E 01	0.173785E 01	0.581733E 01
0.558800E 02	0.397188E 01	0.317068E 01	0.389940E 01	0.419748E 01	0.387723E 01	0.323319E 01	0.338064E 01	0.174685E 01	0.582468F 01
0.584200E 02	0.400192E 01	0.319345E 01	0.394102E 01	0.422972E 01	0.391836E 01	0.323939E 01	0.338535E 01	0.175547E 01	0.583203E 01
0.609600E 02	0.402982E 01	0.321413E 01	0.398064E 01	0.426158E 01	0.395580E 01	0.324494E 01	0.338955E 01	0.176377E 01	0.583938E 01
0.635000E 02	0.405587E 01	0.323301E 01	0.401849E 01	0.429316E 01	0.399000E 01	0.324997E 01	0.339335E 01	0.177179E 01	0.584671E 01
0.660400E 02	0.408044E 01	0.325038E 01	0.405498E 01	0.432468E 01	0.402154E 01	0.325462E 01	0.339686E 01	0.177963E 01	0.585406E 01
0.685800E 02	0.410364E 01	0.326641E 01	0.409019E 01	0.435607E 01	0.405068E 01	0.325896E 01	0.340013E 01	0.178729E 01	0.586140E 01
0.711200E 02	0.412578E 01	0.328133E 01	0.412443E 01	0.438750E 01	0.407785E 01	0.326307E 01	0.340323E 01	0.179484E 01	0.586875E 01
0.736600E 02	0.414692E 01	0.329523E 01	0.415775E 01	0.441885E 01	0.410320F 01	0.326700E 01	0.340619E 01	0.180227E 01	0.587608E 01
0.762000E 02	0.416729E 01	0.330830E 01	0.419040E 01	0.445026E 01	0.412709E 01	0.327080E 01	0.340907E 01	0.180963E 01	0.588343E 01
0.787400E 02	0.418693E 01	0.332059E 01	0.422238E 01	0.448161E 01	0.414961E 01	0.327451E 01	0.341187E 01	0.181693E 01	0.589076E 01
0.812800E 02	0.420601E 01	0.333224E 01	0.425391E 01	0.451301E 01	0.417103E 01	0.327816E 01	0.341464E 01	0.182419E 01	0.589811E 01
0.838200E 02	0.422456E 01	0.334330E 01	0.428496E 01	0.454436E 01	0.419141E 01	0.328176E 01	0.341737E 01	0.183140E 01	0.590545E 01
0.863600E 02	0.424268E 01	0.335386E 01	0.431566E 01	0.457570E 01	0.421093E 01	0.328533E 01	0.342009E 01	0.183859E 01	0.591278E 01
0.889000E 02	0.426049E 01	0.336400E 01	0.434614E 01	0.460711E 01	0.422974E 01	0.328890E 01	0.342279E 01	0.184578E 01	0.592013E 01
0.914400E 02	0.427796E 01	0.337372E 01	0.437633E 01	0.463845E 01	0.424786E 01	0.329244E 01	0.342549E 01	0.185294E 01	0.592747E 01
0.939800E 02	0.429522E 01	0.338313E 01	0.440639E 01	0.466986E 01	0.426545E 01	0.329599E 01	0.342819E 01	0.186011E 01	0.593481E 01
0.965200E 02	0.431224E 01	0.339222E 01	0.443624E 01	0.470120E 01	0.428252E 01	0.329953E 01	0.343088E 01	0.186725E 01	0.594215E 01
0.990600E 02	0.432912E 01	0.340107E 01	0.446603E 01	0.473261E 01	0.429921E 01	0.330307E 01	0.343358E 01	0.187441E 01	0.594950E 01
0.101600E 03	0.434583E 01	0.340967E 01	0.449567E 01	0.476395E 01	0.431550E 01	0.330662E 01	0.343627E 01	0.188155E 01	0.595683E 01
0.104140E 03	0.436243E 01	0.341807E 01	0.452524E 01	0.479530E 01	0.433149E 01	0.331014E 01	0.343897E 01	0.188869E 01	0.596417E 01
0.106680E 03	0.437898E 01	0.342631E 01	0.455482E 01	0.482671E 01	0.434726E 01	0.331368E 01	0.344166E 01	0.189584E 01	0.597152E 01
0.109220E 03	0.439542E 01	0.343439E 01	0.458429E 01	0.485805E 01	0.436276E 01	0.331722E 01	0.344436E 01	0.190297E 01	0.597885E 01
0.111760E 03	0.441184E 01	0.344235E 01	0.461379E 01	0.488946E 01	0.437812E 01	0.332076E 01	0.344705E 01	0.191012E 01	0.598620E 01
0.114300E 03	0.442818E 01	0.345019E 01	0.464320E 01	0.492080E 01	0.439329E 01	0.332429E 01	0.344975E 01	0.191725E 01	0.599353E 01
0.116840E 03	0.444452E 01	0.345794E 01	0.467266E 01	0.495221E 01	0.440836E 01	0.332783E 01	0.345244E 01	0.192440E 01	0.600088E 01
0.119380E 03	0.446080E 01	0.346559E 01	0.470204E 01	0.498355E 01	0.442330E 01	0.333137E 01	0.345514E 01	0.193154E 01	0.600822E 01
0.121920E 03	0.447710E 01	0.347319E 01	0.473148E 01	0.501496E 01	0.443814E 01	0.333491E 01	0.345783E 01	0.193869E 01	0.601557E 01
0.124460E 03	0.449335E 01	0.348071E 01	0.476085E 01	0.504630E 01	0.445297E 01	0.333845E 01	0.346052E 01	0.194582E 01	0.602292E 01
0.127000E 03	0.450959E 01	0.348819E 01	0.479021E 01	0.507765E 01	0.446779E 01	0.334198E 01	0.346322E 01	0.195296E 01	0.603024E 01
0.129540E 03	0.452582E 01	0.349562E 01	0.481957E 01	0.510899E 01	0.448238E 01	0.334552E 01	0.346591E 01	0.196009E 01	0.603757E 01
0.132080E 03	0.454208E 01	0.350303E 01	0.484899E 01	0.514040E 01	0.449706E 01	0.334906E 01	0.346861E 01	0.196724E 01	0.604492E 01
0.134620E 03	0.455833E 01	0.351041E 01	0.487841E 01	0.517180E 01	0.451171E 01	0.335260E 01	0.347130E 01	0.197439E 01	0.605227E 01
0.137160E 03	0.457459E 01	0.351776E 01	0.490776E 01	0.520315E 01	0.452632E 01	0.335613E 01	0.347400E 01	0.198152E 01	0.605960E 01
0.139700E 03	0.459084E 01	0.352510E 01	0.493718E 01	0.523455E 01	0.454093E 01	0.335969E 01	0.347669E 01	0.198867E 01	0.606695E 01
0.142240E 03	0.460716E 01	0.353242E 01	0.496659E 01	0.526596E 01	0.455554E 01	0.336322E 01	0.347939E 01	0.199582E 01	0.607430E 01
0.144780E 03	0.462327E 01	0.353972E 01	0.499595E 01	0.529731E 01	0.457011E 01	0.336675E 01	0.348208E 01	0.200296E 01	0.608164E 01
0.147320E 03	0.463952E 01	0.354702E 01	0.502536E 01	0.532871E 01	0.458470E 01	0.337035E 01	0.348478E 01	0.201012E 01	0.608899E 01
0.149860E 03	0.465576E 01	0.355431E 01	0.505477E 01	0.536012E 01	0.459925E 01	0.337384E 01	0.348748E 01	0.201725E 01	0.609634E 01

TABLE XXX. PE01 SPINLINE FORCES

Distance (cm)	Inertia (g)	Gravity (g)	Rheological (g)
0.190000E 01	-0.533792E-02	0.207225E 00	0.801887E 00
0.381000E 01	-0.532512E-02	0.191590E 00	0.786254E 00
0.571000E 01	-0.531013E-02	0.177441E 00	0.772131E 00
0.762000E 01	-0.529176E-02	0.164579E 00	0.759287E 00
0.952000E 01	-0.526987E-02	0.153127E 00	0.747857E 00
0.114300E 02	-0.524452E-02	0.142894E 00	0.737650E 00
0.133300E 02	-0.521532E-02	0.133876E 00	0.728661E 00
0.152400E 02	-0.518127E-02	0.125863E 00	0.720682E 00
0.171400E 02	-0.514358E-02	0.118842E 00	0.713699E 00
0.190500E 02	-0.510067E-02	0.112608E 00	0.707507E 00
0.209500E 02	-0.505097E-02	0.107132E 00	0.702081E 00
0.228600E 02	-0.499517E-02	0.102286E 00	0.697291E 00
0.247600E 02	-0.493167E-02	0.980362E-01	0.693104E 00
0.266700E 02	-0.486152E-02	0.942703E-01	0.689408E 00
0.285700E 02	-0.478315E-02	0.909584E-01	0.686175E 00
0.304800E 02	-0.469476E-02	0.880107E-01	0.683315E 00
0.323800E 02	-0.459857E-02	0.854141E-01	0.680815E 00
0.330200E 02	-0.456445E-02	0.846364E-01	0.680071E 00
0.349200E 02	-0.445567E-02	0.824148E-01	0.677959E 00
0.368300E 02	-0.434399E-02	0.804218E-01	0.676077E 00
0.387300E 02	-0.421623E-02	0.786364E-01	0.674420E 00
0.406400E 02	-0.408152E-02	0.770249E-01	0.672943E 00
0.425400E 02	-0.393679E-02	0.755778E-01	0.671641E 00
0.444500E 02	-0.378684E-02	0.742607E-01	0.670473E 00
0.463500E 02	-0.363052E-02	0.730674E-01	0.669436E 00
0.482600E 02	-0.346101E-02	0.719699E-01	0.668508E 00
0.501600E 02	-0.329281E-02	0.709705E-01	0.667677E 00
0.520700E 02	-0.312120E-02	0.700435E-01	0.666922E 00
0.539700E 02	-0.294424E-02	0.691889E-01	0.666244E 00
0.558800E 02	-0.277045E-02	0.683900E-01	0.665619E 00
0.577800E 02	-0.262442E-02	0.676465E-01	0.665022E 00
0.596900E 02	-0.248028E-02	0.669376E-01	0.664457E 00
0.615900E 02	-0.231775E-02	0.662662E-01	0.663948E 00
0.635000E 02	-0.216578E-02	0.656254E-01	0.663460E 00
0.654000E 02	-0.201917E-02	0.650191E-01	0.662999E 00
0.673100E 02	-0.187749E-02	0.644346E-01	0.662557E 00
0.692100E 02	-0.174523E-02	0.638761E-01	0.662130E 00
0.711200E 02	-0.162279E-02	0.633346E-01	0.661711E 00
0.730200E 02	-0.151540E-02	0.628131E-01	0.661297E 00
0.749300E 02	-0.140189E-02	0.623031E-01	0.660901E 00
0.768300E 02	-0.129214E-02	0.618099E-01	0.660517E 00
0.787400E 02	-0.117275E-02	0.613272E-01	0.660154E 00
0.806400E 02	-0.107778E-02	0.608604E-01	0.659782E 00
0.825500E 02	-0.994697E-03	0.604012E-01	0.659406E 00
0.844500E 02	-0.916748E-03	0.599529E-01	0.659036E 00
0.863600E 02	-0.845284E-03	0.595101E-01	0.658664E 00
0.882600E 02	-0.778141E-03	0.590763E-01	0.658298E 00
0.901700E 02	-0.730890E-03	0.586465E-01	0.657915E 00
0.920700E 02	-0.682035E-03	0.582232E-01	0.657541E 00
0.939800E 02	-0.621535E-03	0.578020E-01	0.657190E 00
0.958800E 02	-0.579069E-03	0.573883E-01	0.656809E 00
0.977900E 02	-0.540950E-03	0.569760E-01	0.656435E 00
0.996900E 02	-0.507205E-03	0.565690E-01	0.656061E 00
0.101600E 03	-0.494053E-03	0.561627E-01	0.655668E 00
0.103500E 03	-0.459821E-03	0.557596E-01	0.655299E 00
0.105410E 03	-0.440296E-03	0.553571E-01	0.654916E 00
0.107310E 03	-0.427595E-03	0.549583E-01	0.654530E 00
0.109220E 03	-0.414740E-03	0.545584E-01	0.654143E 00
0.111120E 03	-0.404249E-03	0.541616E-01	0.653757E 00
0.113030E 03	-0.390649E-03	0.537635E-01	0.653372E 00
0.114930E 03	-0.373890E-03	0.533686E-01	0.652994E 00
0.116840E 03	-0.366373E-03	0.529729E-01	0.652606E 00
0.118740E 03	-0.364154E-03	0.525799E-01	0.652215E 00
0.120650E 03	-0.356891E-03	0.521849E-01	0.651828E 00
0.122550E 03	-0.354586E-03	0.517926E-01	0.651438E 00
0.124460E 03	-0.349535E-03	0.513984E-01	0.651048E 00
0.126360E 03	-0.352844E-03	0.510067E-01	0.650653E 00
0.128270E 03	-0.349517E-03	0.506126E-01	0.650263E 00
0.130170E 03	-0.346926E-03	0.502209E-01	0.649873E 00
0.132080E 03	-0.344958E-03	0.498273E-01	0.649482E 00
0.133980E 03	-0.343556E-03	0.494359E-01	0.649092E 00
0.135890E 03	-0.347479E-03	0.490425E-01	0.648695E 00
0.137790E 03	-0.351780E-03	0.486509E-01	0.648299E 00
0.139700E 03	-0.351645E-03	0.482570E-01	0.647905E 00
0.141600E 03	-0.351840E-03	0.478651E-01	0.647513E 00
0.143510E 03	-0.352322E-03	0.474711E-01	0.647118E 00
0.145410E 03	-0.357750E-03	0.470791E-01	0.646721E 00

TABLE XXXI. PE02 SPINLINE FORCES

Distance (cm)	Inertia (g)	Gravity (g)	Rheological (g)
0.190000E 01	-0.107928E-01	0.153373E 00	0.822580E 00
0.381000E 01	-0.107750E-01	0.139057E 00	0.808282E 00
0.571000E 01	-0.107537E-01	0.126417E 00	0.795663E 00
0.762000E 01	-0.107291E-01	0.115216E 00	0.784487E 00
0.952000E 01	-0.107011E-01	0.105413E 00	0.774712E 00
0.114300E 02	-0.106694E-01	0.967469E-01	0.766077E 00
0.133300E 02	-0.106333E-01	0.891590E-01	0.758525E 00
0.152400E 02	-0.105917E-01	0.824468E-01	0.751855E 00
0.171400E 02	-0.105456E-01	0.765829E-01	0.746037E 00
0.190500E 02	-0.104926E-01	0.713885E-01	0.740895E 00
0.209500E 02	-0.104337E-01	0.668420E-01	0.736408E 00
0.228600E 02	-0.103660E-01	0.628108E-01	0.732444E 00
0.247600E 02	-0.102901E-01	0.592787E-01	0.728988E 00
0.266700E 02	-0.102072E-01	0.561470E-01	0.725939E 00
0.285700E 02	-0.101132E-01	0.533870E-01	0.723273E 00
0.304800E 02	-0.100168E-01	0.509306E-01	0.720913E 00
0.323800E 02	-0.990051E-02	0.487441E-01	0.718843E 00
0.330200E 02	-0.985890E-02	0.480905E-01	0.718231E 00
0.381000E 02	-0.947998E-02	0.431033E-01	0.713623E 00
0.431800E 02	-0.901321E-02	0.394161E-01	0.710402E 00
0.482600E 02	-0.844808E-02	0.366250E-01	0.708176E 00
0.533400E 02	-0.778953E-02	0.344686E-01	0.706679E 00
0.584200E 02	-0.714256E-02	0.327639E-01	0.705621E 00
0.635000E 02	-0.639160E-02	0.313501E-01	0.704958E 00
0.685800E 02	-0.559099E-02	0.301700E-01	0.704579E 00
0.736600E 02	-0.477137E-02	0.291668E-01	0.704395E 00
0.787400E 02	-0.397147E-02	0.282970E-01	0.704325E 00
0.838200E 02	-0.324761E-02	0.275271E-01	0.704279E 00
0.889000E 02	-0.256471E-02	0.268298E-01	0.704265E 00
0.939800E 02	-0.196020E-02	0.261893E-01	0.704229E 00
0.990600E 02	-0.142519E-02	0.255920E-01	0.704166E 00
0.104140E 03	-0.967573E-03	0.250283E-01	0.704060E 00
0.109220E 03	-0.583007E-03	0.244905E-01	0.703907E 00
0.114300E 03	-0.259743E-03	0.239727E-01	0.703713E 00
0.119380E 03	-0.259927E-05	0.234705E-01	0.703468E 00
0.124460E 03	0.000000E 00	0.229802E-01	0.702980E 00
0.129540E 03	0.000000E 00	0.224986E-01	0.702498E 00
0.134620E 03	0.000000E 00	0.220244E-01	0.702024E 00

TABLE XXXII. PE03 SPINLINE FORCES

Distance (cm)	Inertia (g)	Gravity (g)	Rheological (g)
0.254000E 01	-0.260415E-02	0.265346E 00	0.672741E 00
0.762000E 01	-0.255794E-02	0.227583E 00	0.635025E 00
0.127000E 02	-0.248757E-02	0.199023E 00	0.606535E 00
0.177800E 02	-0.239092E-02	0.178194E 00	0.585803E 00
0.228600E 02	-0.225931E-02	0.163009E 00	0.570750E 00
0.279400E 02	-0.209206E-02	0.151917E 00	0.559825E 00
0.330200E 02	-0.188526E-02	0.143656E 00	0.551770E 00
0.381000E 02	-0.164598E-02	0.137375E 00	0.545729E 00
0.431800E 02	-0.139217E-02	0.132459E 00	0.541067E 00
0.482600E 02	-0.114014E-02	0.128463E 00	0.537323E 00
0.533400E 02	-0.899357E-03	0.125094E 00	0.534195E 00
0.584200E 02	-0.691812E-03	0.122164E 00	0.531472E 00
0.635000E 02	-0.497952E-03	0.119530E 00	0.529032E 00
0.685800E 02	-0.339946E-03	0.117123E 00	0.526783E 00
0.736600E 02	-0.215988E-03	0.114873E 00	0.524657E 00
0.787400E 02	-0.116928E-03	0.112734E 00	0.522617E 00
0.838200E 02	-0.470561E-04	0.110675E 00	0.520628E 00
0.889000E 02	0.000000E 00	0.108670E 00	0.518670E 00
0.939800E 02	0.000000E 00	0.106702E 00	0.516702E 00
0.990600E 02	0.000000E 00	0.104760E 00	0.514760E 00
0.104140E 03	0.000000E 00	0.102840E 00	0.512840E 00
0.109220E 03	0.000000E 00	0.100936E 00	0.510936E 00
0.114300E 03	0.000000E 00	0.990418E-01	0.509041E 00
0.119380E 03	0.000000E 00	0.971542E-01	0.507154E 00
0.124460E 03	0.000000E 00	0.952708E-01	0.505270E 00
0.129540E 03	0.000000E 00	0.933880E-01	0.503388E 00
0.134620E 03	0.000000E 00	0.915029E-01	0.501502E 00
0.139700E 03	0.000000E 00	0.896117E-01	0.499611E 00
0.144780E 03	0.000000E 00	0.877143E-01	0.497714E 00
0.149860E 03	0.000000E 00	0.858074E-01	0.495807E 00
0.154940E 03	0.000000E 00	0.838948E-01	0.493894E 00
0.160020E 03	0.000000E 00	0.819800E-01	0.491980E 00
0.165100E 03	0.000000E 00	0.800558E-01	0.490055E 00
0.170180E 03	0.000000E 00	0.781232E-01	0.488123E 00
0.175260E 03	0.000000E 00	0.761763E-01	0.486176E 00

TABLE XXXIII. PE04 SPINLINE FORCES

Distance (cm)	Inertia (g)	Gravity (g)	Rheological (g)
0.254000E 01	-0.264117E-02	0.284255E 00	0.105661E 01
0.762000E 01	-0.261290E-02	0.240949E 00	0.101333E 01
0.127000E 02	-0.255248E-02	0.205532E 00	0.977980E 00
0.177800E 02	-0.244429E-02	0.180039E 00	0.952594E 00
0.228600E 02	-0.226160E-02	0.163063E 00	0.935802E 00
0.279400E 02	-0.197998E-02	0.152211E 00	0.925231E 00
0.330200E 02	-0.159355E-02	0.145236E 00	0.918643E 00
0.381000E 02	-0.114319E-02	0.140556E 00	0.914413E 00
0.431800E 02	-0.741126E-03	0.137173E 00	0.911432E 00
0.482600E 02	-0.437422E-03	0.134461E 00	0.909024E 00
0.533400E 02	-0.234497E-03	0.132103E 00	0.906869E 00
0.584200E 02	-0.116747E-03	0.129933E 00	0.904817E 00
0.635000E 02	-0.487873E-04	0.127860E 00	0.902812E 00
0.685800E 02	-0.188246E-04	0.125839E 00	0.900820E 00
0.736600E 02	-0.208676E-04	0.123840E 00	0.898819E 00
0.787400E 02	-0.218695E-04	0.121839E 00	0.896817E 00
0.838200E 02	-0.293743E-04	0.119837E 00	0.894808E 00
0.889000E 02	-0.351031E-04	0.117830E 00	0.892795E 00
0.939800E 02	-0.439920E-04	0.115819E 00	0.890775E 00
0.990600E 02	-0.569122E-04	0.113801E 00	0.888744E 00
0.104140E 03	-0.624213E-04	0.111773E 00	0.886711E 00
0.109220E 03	-0.676575E-04	0.109742E 00	0.884674E 00
0.114300E 03	-0.726302E-04	0.107706E 00	0.882634E 00
0.119380E 03	-0.840488E-04	0.105667E 00	0.880583E 00
0.124460E 03	-0.911152E-04	0.103619E 00	0.878528E 00
0.129540E 03	-0.992080E-04	0.101566E 00	0.876467E 00
0.134620E 03	-0.109543E-03	0.995067E-01	0.874397E 00
0.139700E 03	-0.118288E-03	0.974391E-01	0.872320E 00
0.144780E 03	-0.125535E-03	0.953647E-01	0.870239E 00
0.149860E 03	-0.132558E-03	0.932846E-01	0.868152E 00
0.154940E 03	-0.135829E-03	0.911990E-01	0.866063E 00
0.160020E 03	-0.141332E-03	0.891107E-01	0.863969E 00
0.165100E 03	-0.158072E-03	0.870181E-01	0.861860E 00
0.170180E 03	-0.171909E-03	0.849121E-01	0.859740E 00
0.175260E 03	-0.178860E-03	0.827948E-01	0.857616E 00

TABLE XXXIV. PE05 SPINLINE FORCES

Distance (cm)	Inertia (g)	Gravity (g)	Rheological (g)
0.254000E 01	-0.109198E-01	0.429319E 00	0.111840E 01
0.762000E 01	-0.108603E-01	0.368506E 00	0.105764E 01
0.127000E 02	-0.107704E-01	0.316002E 00	0.100523E 01
0.177800E 02	-0.106420E-01	0.272470E 00	0.961828E 00
0.228600E 02	-0.104694E-01	0.237485E 00	0.927016E 00
0.279400E 02	-0.102408E-01	0.209804E 00	0.899564E 00
0.330200E 02	-0.994552E-02	0.188119E 00	0.878174E 00
0.381000E 02	-0.956407E-02	0.171176E 00	0.861612E 00
0.431800E 02	-0.908150E-02	0.157964E 00	0.848882E 00
0.482600E 02	-0.849072E-02	0.147631E 00	0.839140E 00
0.533400E 02	-0.779817E-02	0.139473E 00	0.831675E 00
0.584200E 02	-0.700117E-02	0.132931E 00	0.825930E 00
0.635000E 02	-0.613203E-02	0.127603E 00	0.821471E 00
0.685800E 02	-0.521624E-02	0.123171E 00	0.817955E 00
0.736600E 02	-0.429721E-02	0.119407E 00	0.815110E 00
0.787400E 02	-0.341119E-02	0.116137E 00	0.812726E 00
0.838200E 02	-0.260077E-02	0.113235E 00	0.810634E 00
0.889000E 02	-0.198447E-02	0.110603E 00	0.808619E 00
0.939800E 02	-0.141632E-02	0.108146E 00	0.806729E 00
0.990600E 02	-0.931453E-03	0.105829E 00	0.804898E 00
0.104140E 03	-0.494287E-03	0.103621E 00	0.803127E 00
0.109220E 03	-0.185447E-03	0.101503E 00	0.801317E 00
0.114300E 03	0.000000E 00	0.994435E-01	0.799443E 00
0.119380E 03	0.000000E 00	0.974232E-01	0.797423E 00
0.124460E 03	0.000000E 00	0.954337E-01	0.795433E 00
0.129540E 03	0.000000E 00	0.934639E-01	0.793463E 00
0.134620E 03	0.000000E 00	0.915091E-01	0.791509E 00
0.139700E 03	0.000000E 00	0.895644E-01	0.789564E 00
0.144780E 03	0.000000E 00	0.876237E-01	0.787623E 00
0.149860E 03	0.000000E 00	0.856866E-01	0.785686E 00
0.154940E 03	0.000000E 00	0.837489E-01	0.783748E 00
0.160020E 03	0.000000E 00	0.818112E-01	0.781811E 00
0.165100E 03	0.000000E 00	0.798696E-01	0.779869E 00
0.170180E 03	0.000000E 00	0.779233E-01	0.777923E 00
0.175260E 03	0.000000E 00	0.759748E-01	0.775974E 00

TABLE XXXV. PE06 SPINLINE FORCES

Distance (cm)	Inertia (g)	Gravity (g)	Rheological (g)
0.254000E 01	-0.215137E-01	0.130724E 00	0.609210E 00
0.762000E 01	-0.214705E-01	0.939092E-01	0.572438E 00
0.127000E 02	-0.213886E-01	0.656401E-01	0.544251E 00
0.177800E 02	-0.212419E-01	0.460131E-01	0.524771E 00
0.228600E 02	-0.209797E-01	0.333328E-01	0.512353E 00
0.279400E 02	-0.205196E-01	0.255646E-01	0.505045E 00
0.330200E 02	-0.197342E-01	0.209404E-01	0.501206E 00
0.381000E 02	-0.184347E-01	0.182056E-01	0.499770E 00
0.431800E 02	-0.164601E-01	0.165739E-01	0.500113E 00
0.482600E 02	-0.137766E-01	0.155622E-01	0.501785E 00
0.533400E 02	-0.106107E-01	0.148951E-01	0.504284E 00
0.584200E 02	-0.747793E-02	0.144191E-01	0.506941E 00
0.635000E 02	-0.444479E-02	0.140484E-01	0.509603E 00
0.685800E 02	-0.196152E-02	0.137429E-01	0.511781E 00
0.736600E 02	-0.655220E-03	0.134760E-01	0.512820E 00
0.787400E 02	0.000000E 00	0.132257E-01	0.513225E 00
0.838200E 02	0.000000E 00	0.129870E-01	0.512987E 00
0.889000E 02	0.000000E 00	0.127567E-01	0.512756E 00
0.939800E 02	0.000000E 00	0.125304E-01	0.512530E 00
0.990600E 02	0.000000E 00	0.123055E-01	0.512305E 00
0.104140E 03	0.000000E 00	0.120816E-01	0.512081E 00
0.109220E 03	0.000000E 00	0.118581E-01	0.511858E 00
0.114300E 03	0.000000E 00	0.116348E-01	0.511635E 00
0.119380E 03	0.000000E 00	0.114105E-01	0.511410E 00
0.124460E 03	0.000000E 00	0.111861E-01	0.511186E 00
0.129540E 03	0.000000E 00	0.109613E-01	0.510961E 00
0.134620E 03	0.000000E 00	0.107357E-01	0.510735E 00
0.139700E 03	0.000000E 00	0.105097E-01	0.510509E 00
0.144780E 03	0.000000E 00	0.102831E-01	0.510283E 00
0.149860E 03	0.000000E 00	0.100564E-01	0.510056E 00
0.154940E 03	0.000000E 00	0.982947E-02	0.509829E 00
0.160020E 03	0.000000E 00	0.960215E-02	0.509602E 00
0.165100E 03	0.000000E 00	0.937465E-02	0.509374E 00
0.170180E 03	0.000000E 00	0.914681E-02	0.509146E 00
0.175260E 03	0.000000E 00	0.891846E-02	0.508918E 00

TABLE XXXVI. PE07 SPINLINE FORCES

Distance (cm)	Inertia (g)	Gravity (g)	Rheological (g)
0.254000E 01	-0.299455E-01	0.117778E 00	0.587833E 00
0.762000E 01	-0.299024E-01	0.842936E-01	0.554391E 00
0.127000E 02	-0.298171E-01	0.580277E-01	0.528210E 00
0.177800E 02	-0.296585E-01	0.396089E-01	0.509950E 00
0.228600E 02	-0.293684E-01	0.277698E-01	0.498401E 00
0.279400E 02	-0.288415E-01	0.206081E-01	0.491766E 00
0.330200E 02	-0.278972E-01	0.164393E-01	0.488542E 00
0.381000E 02	-0.262662E-01	0.140555E-01	0.487789E 00
0.431800E 02	-0.236637E-01	0.126852E-01	0.489021E 00
0.482600E 02	-0.199389E-01	0.118687E-01	0.491929E 00
0.533400E 02	-0.154834E-01	0.113514E-01	0.495868E 00
0.584200E 02	-0.112849E-01	0.109918E-01	0.499706E 00
0.635000E 02	-0.748184E-02	0.107125E-01	0.503230E 00
0.685800E 02	-0.435566E-02	0.104801E-01	0.506124E 00
0.736600E 02	-0.213828E-02	0.102759E-01	0.508137E 00
0.787400E 02	-0.725071E-03	0.100879E-01	0.509363E 00
0.838200E 02	0.000000E 00	0.990900E-02	0.509909E 00
0.889000E 02	0.000000E 00	0.973451E-02	0.509734E 00
0.939800E 02	0.000000E 00	0.956268E-02	0.509562E 00
0.990600E 02	0.000000E 00	0.939186E-02	0.509391E 00
0.104140E 03	0.000000E 00	0.922192E-02	0.509222E 00
0.109220E 03	0.000000E 00	0.905175E-02	0.509051E 00
0.114300E 03	0.000000E 00	0.888135E-02	0.508881E 00
0.119380E 03	0.000000E 00	0.871049E-02	0.508710E 00
0.124460E 03	0.000000E 00	0.853921E-02	0.508539E 00
0.129540E 03	0.000000E 00	0.836776E-02	0.508367E 00
0.134620E 03	0.000000E 00	0.819587E-02	0.508195E 00
0.139700E 03	0.000000E 00	0.802381E-02	0.508023E 00
0.144780E 03	0.000000E 00	0.785145E-02	0.507851E 00
0.149860E 03	0.000000E 00	0.767880E-02	0.507678E 00
0.154940E 03	0.000000E 00	0.750599E-02	0.507506E 00
0.160020E 03	0.000000E 00	0.733303E-02	0.507333E 00
0.165100E 03	0.000000E 00	0.715941E-02	0.507159E 00
0.170180E 03	0.000000E 00	0.698516E-02	0.506985E 00
0.175260E 03	0.000000E 00	0.681078E-02	0.506810E 00

TABLE XXXVII. PE08 SPINLINE FORCES

Distance (cm)	Inertia (g)	Gravity (g)	Rheological (g)
0.254000E 01	-0.106346E-01	0.921802E-01	0.561545E 00
0.762000E 01	-0.104658E-01	0.650265E-01	0.534560E 00
0.127000E 02	-0.101737E-01	0.505185E-01	0.520244E 00
0.177800E 02	-0.971090E-02	0.424863E-01	0.512775E 00
0.228600E 02	-0.900416E-02	0.377814E-01	0.508777E 00
0.279400E 02	-0.803623E-02	0.348993E-01	0.506863E 00
0.330200E 02	-0.683484E-02	0.330164E-01	0.506181E 00
0.381000E 02	-0.549644E-02	0.317000E-01	0.506203E 00
0.431800E 02	-0.413137E-02	0.307140E-01	0.506582E 00
0.482600E 02	-0.286109E-02	0.299290E-01	0.507068E 00
0.533400E 02	-0.176870E-02	0.292692E-01	0.507500E 00
0.584200E 02	-0.113278E-02	0.286889E-01	0.507556E 00
0.635000E 02	-0.551306E-03	0.281467E-01	0.507595E 00
0.685800E 02	-0.129942E-03	0.276351E-01	0.507505E 00
0.736600E 02	0.000000E 00	0.271438E-01	0.507143E 00
0.787400E 02	0.000000E 00	0.266658E-01	0.506665E 00
0.838200E 02	0.000000E 00	0.261981E-01	0.506198E 00
0.889000E 02	0.000000E 00	0.257379E-01	0.505737E 00
0.939800E 02	0.000000E 00	0.252820E-01	0.505282E 00
0.990600E 02	0.000000E 00	0.248291E-01	0.504829E 00
0.104140E 03	0.000000E 00	0.243760E-01	0.504376E 00
0.109220E 03	0.000000E 00	0.239232E-01	0.503923E 00
0.114300E 03	0.000000E 00	0.234708E-01	0.503470E 00
0.119380E 03	0.000000E 00	0.230167E-01	0.503016E 00
0.124460E 03	0.000000E 00	0.225626E-01	0.502562E 00
0.129540E 03	0.000000E 00	0.221083E-01	0.502108E 00
0.134620E 03	0.000000E 00	0.216531E-01	0.501653E 00
0.139700E 03	0.000000E 00	0.211975E-01	0.501197E 00
0.144780E 03	0.000000E 00	0.207415E-01	0.500741E 00
0.149860E 03	0.000000E 00	0.202852E-01	0.500285E 00
0.154940E 03	0.000000E 00	0.198276E-01	0.499827E 00
0.160020E 03	0.000000E 00	0.193693E-01	0.499369E 00
0.165100E 03	0.000000E 00	0.189105E-01	0.498910E 00
0.170180E 03	0.000000E 00	0.184507E-01	0.498450E 00
0.175260E 03	0.000000E 00	0.179906E-01	0.497990E 00

TABLE XXXVIII. PE09 SPINLINE FORCES

Distance (cm)	Inertia (g)	Gravity (g)	Rheological (g)
0.254000E 01	-0.396989E-02	0.826734E-01	0.548703E 00
0.127000E 02	-0.385411E-02	0.230611E-01	0.489207E 00
0.228600E 02	-0.254207E-02	0.128280E-01	0.480285E 00
0.330200E 02	0.000000E 00	0.118428E-01	0.481842E 00
0.431800E 02	0.000000E 00	0.114853E-01	0.481485E 00
0.533400E 02	0.000000E 00	0.111542E-01	0.481154E 00
0.635000E 02	0.000000E 00	0.108223E-01	0.480822E 00
0.736600E 02	0.000000E 00	0.104885E-01	0.480488E 00
0.838200E 02	0.000000E 00	0.101489E-01	0.480148E 00
0.939800E 02	0.000000E 00	0.980575E-02	0.479805E 00
0.104140E 03	0.000000E 00	0.946002E-02	0.479460E 00
0.114300E 03	0.000000E 00	0.911207E-02	0.479112E 00
0.124460E 03	0.000000E 00	0.876185E-02	0.478761E 00
0.134620E 03	0.000000E 00	0.841017E-02	0.478410E 00
0.144780E 03	0.000000E 00	0.805671E-02	0.478056E 00
0.154940E 03	0.000000E 00	0.770187E-02	0.477701E 00
0.165100E 03	0.000000E 00	0.734537E-02	0.477345E 00
0.175260E 03	-0.229812E-05	0.698775E-02	0.476985E 00

TABLE XXXIX. PE01 DISTANCE VERSUS MEASURED CRYSTALLINITY

Distance (cm)	Crystallinity (%)
0.565000E 02	0.000000E 00
0.628600E 02	0.154200E 02
0.692200E 02	0.248900E 02
0.882600E 02	0.219300E 02
0.107320E 03	0.242000E 02
0.126360E 03	0.354200E 02
0.145420E 03	0.430400E 02
0.373380E 03	0.630700E 02
0.373380E 03	0.623100E 02

TABLE XXXX. PE02 DISTANCE VERSUS MEASURED CRYSTALLINITY

Distance (cm)	Crystallinity (%)
0.533400E 02	0.000000E 00
0.635000E 02	0.248900E 02
0.736600E 02	0.181500E 02
0.838200E 02	0.246100E 02
0.939800E 02	0.207600E 02
0.104140E 03	0.271100E 02
0.114300E 03	0.265500E 02
0.124460E 03	0.335500E 02
0.134620E 03	0.317100E 02
0.373380E 03	0.521800E 02
0.373380E 03	0.617000E 02

TABLE XXXXI. PE03 DISTANCE VERSUS MEASURED CRYSTALLINITY

Distance (cm)	Crystallinity (%)
0.381000E 02	0.000000E 00
0.533400E 02	0.187500E 02
0.685800E 02	0.214700E 02
0.838200E 02	0.272200E 02
0.990600E 02	0.293300E 02
0.114300E 03	0.371100E 02
0.129540E 03	0.371000E 02
0.144780E 03	0.337700E 02
0.160020E 03	0.466400E 02
0.175260E 03	0.444800E 02
0.373380E 03	0.588000E 02
0.373380E 03	0.633500E 02

TABLE XXXXII. PE04 DISTANCE VERSUS MEASURED CRYSTALLINITY

Distance (cm)	Crystallinity (%)
0.381000E 02	0.000000E 00
0.533400E 02	0.197700E 02
0.685800E 02	0.282900E 02
0.838200E 02	0.293100E 02
0.990600E 02	0.360700E 02
0.114300E 03	0.426500E 02
0.129540E 03	0.400300E 02
0.144780E 03	0.453900E 02
0.160020E 03	0.477400E 02
0.175260E 03	0.515800E 02
0.373380E 03	0.577400E 02
0.373380E 03	0.660300E 02

TABLE XXXXIII. PE05 DISTANCE VERSUS MEASURED CRYSTALLINITY

Distance (cm)	Crystallinity (%)
0.838200E 02	0.000000E 00
0.990600E 02	0.169900E 02
0.114300E 03	0.223400E 02
0.129540E 03	0.222800E 02
0.144780E 03	0.269600E 02
0.160020E 03	0.302900E 02
0.175260E 03	0.326300E 02
0.373380E 03	0.603800E 02
0.373380E 03	0.639500E 02

TABLE XXXXIV. PE06 DISTANCE VERSUS MEASURED CRYSTALLINITY

Distance (cm)	Crystallinity (%)
0.685800E 02	0.000000E 00
0.838200E 02	0.364700E 02
0.990600E 02	0.229100E 02
0.114300E 03	0.336900E 02
0.129540E 03	0.274500E 02
0.144780E 03	0.271900E 02
0.160020E 03	0.241400E 02
0.175260E 03	0.321400E 02
0.373380E 03	0.519400E 02
0.373380E 03	0.571500E 02

TABLE XXXXV. PE07 DISTANCE VERSUS MEASURED CRYSTALLINITY

Distance (cm)	Crystallinity (%)
0.533400E 02	0.000000E 00
0.685800E 02	0.230700E 02
0.838200E 02	0.146400E 02
0.990600E 02	0.155500E 02
0.114300E 03	0.328900E 02
0.129540E 03	0.223800E 02
0.144780E 03	0.273100E 02
0.160020E 03	0.416700E 02
0.175260E 03	0.326900E 02
0.373380E 03	0.398100E 02
0.373380E 03	0.576800E 02

TABLE XXXXVI. PE08 DISTANCE VERSUS MEASURED CRYSTALLINITY

Distance (cm)	Crystallinity (%)
0.533400E 02	0.000000E 00
0.685800E 02	0.139000E 02
0.838200E 02	0.214300E 02
0.990600E 02	0.345700E 02
0.114300E 03	0.314400E 02
0.129540E 03	0.363400E 02
0.144780E 03	0.424600E 02
0.154940E 03	0.417300E 02
0.165100E 03	0.372800E 02
0.175260E 03	0.390800E 02
0.373380E 03	0.475700E 02
0.373380E 03	0.542900E 02
0.373380E 03	0.471800E 02
0.373380E 03	0.611700E 02

TABLE XXXXVII. PE09 DISTANCE VERSUS MEASURED CRYSTALLINITY

Distance (cm)	Crystallinity (%)
0.330200E 02	0.000000E 00
0.431800E 02	0.263900E 02
0.533400E 02	0.317200E 02
0.939800E 02	0.432000E 02
0.134620E 03	0.433400E 02
0.373380E 03	0.660200E 02
0.373380E 03	0.594300E 02

APPENDIX B

COMPUTER PROGRAMS

A. POLYETHYLENE X-RAY ANALYSIS PROGRAM PEXRAN

The purpose of this program is to calculate percent crystallinity and crystalline orientation functions from polyethylene x-ray diffraction patterns that have been reduced to a digital format by the Tech/Ops Scanning Microdensitometer. The method of Pieser, Matthews and Richards is used in making calculations. The program is divided into the following sections:

1. Data input,
2. Location of the pattern center,
3. Calculation of specimen to film distance,
4. Background correction,
5. Location of important maxima and minima in the pattern,
6. Calculation of summations for orientation function calculations,
7. Summations for crystallinity calculations,
8. Final orientation and crystallinity calculations,
9. Output of results.

The subprograms used by PEXRAN and their functions are given below.

Function STRUT. This function subprogram is used to calculate the structure factor to be used in correcting the x-ray intensity calculation.

Function IFOX. This function subprogram locates important maxima in the pattern.

Function ISET. This function subprogram locates important minima in the pattern.

Subroutine PUTOUT. This subroutine subprogram outputs the calculated results of the program.

Subroutine FILL. This subroutine enters the digitized pattern matrix with a specific angle and radius and locates the intensity values that are to be used for calculations.

Description of the Program

Data are read into the program by two methods. The digitized x-ray pattern data are read from magnetic tape and stored directly into the computer's core. The approximate locations of critical arcs on the pattern are read from cards along with identifying information for that particular pattern. After completion of data input, the program searches a 60 x 60 corner of the matrix to locate the center of the pattern. Since only a quadrant of the original pattern was scanned, the center of the pattern is located near a corner of the digitized matrix. The center is located by finding the minimum intensity value in the corner being searched. Once located, the coordinates of the center are stored for repeated use in subsequent calculating. Next the specimen to film distance is computed. This is done by locating the 110 arc exactly, and using its distance from the center along with its known Bragg angle to determine the actual specimen to

film distance. This value is also stored for repeated subsequent use.

The background correction section of the program searches throughout the limits of the area to be used for the crystallinity calculation, and locates the minimum density readings that appear on the boundaries. These values are then used to calculate the level of background under the peaks used for crystallinity calculation, and that level is subtracted uniformly around the ninety degree segment of the pattern. The same value of background is used at a constant radius from center for the entire ninety degree swing. The actual background correction is made at the time the summations for orientation and crystallinity are made.

The remainder of the program does the actual computation. The calculating scheme used is as follows. Beginning along the equator, the program enters the pattern data matrix and removes the intensity values from the center out to a previously specified radial limit. The intensity values in this radial scan are searched for the critical arcs, and the minima between these arcs are also located. Background corrections are then made for the arcs used in orientation function calculation, and the summations for the orientation functions are made. Next the background corrections are made for crystallinity, and the summations for it are performed. The calculation then loops back to increment the angle between the equator and meridian and repeats the entire process. This continues until the meridional scan has been completed. At that point the crystallinity calculations are made using the summations made previously, and orientation functions are computed using their summations and the orthogonality relationship.

All pertinent calculated values along with proper identifying information are printed by subroutine PUTOUT.

B. MELT SPINNING DATA ANALYSIS PROGRAM SPINLINE

This program is used to process the diameter, temperature, and crystallinity data obtained from direct measurements on a spinning filament. Using the input data it produces empirical curve fits for diameter data. It computes a velocity profile and makes an empirical curve fit of these data. Calculations are also made for the velocity gradient, the elongational viscosity, the forces acting on the filament, and the filament density. These results are then printed. The subprograms used are as follows:

Subroutine EXFIT. This subroutine subprogram calculates the starting values and incremental values of the constants used in the empirical equations for diameter and velocity. It calls PATERN to make the nonlinear curve fit of the experimental data, and it prints the computed constants as well as the input values, the corresponding calculated values using the empirical equation, and the derivative of the function calculated at the same points.

Subroutine PATERN. This subroutine makes a curve fit of experimental data to the specified model. It uses the method of a pattern search to optimize the sum of squares at a minimum value. PATERN calls two subroutines, PROC and BOUNDS.

Subroutine PROC. This subroutine uses the chosen model, the input data, and the constans computed by PATERN to calculate the

optimizing criterion. In this case the root mean square is used.

Subroutine BOUND. This subroutine specifies and checks the limits imposed upon the constants used in the model. If they exceed the limits a sentinel value is returned to PATERN.

Subroutine FGRAV. This subroutine calculates the effect of gravity on the spinline.

Subroutine FINIT. This subroutine calculates the values of inertia force on the spinline.

Description of the Program

The program reads input data from cards. This includes the experimentally measured values of filament diameter, temperature, crystallinity, and distance from the spinneret for each reading. Proper identifying information is also read in with the data. The diameter data are curve fitted by subroutine EXFIT and the smoothed values are used to calculate the velocity of the fiber at each experimental point. A local density is calculated at each measurement point using the temperature, the crystallinity, and the appropriate equations. With this density and the filament diameter the fiber velocity is calculated. The velocity values are next curve fitted by the subroutine EXFIT, and the velocity gradient is calculated from the differentiated empirical function. Next a force balance is made on the filament. Using the rheological force and the velocity gradient, an elongational viscosity is next calculated. The calculated data along with the experimental data are then printed.

The program as written was intended only for linear polyethylene. However, it can be used for other polymers by replacing the density calculation with the expression that suitably relates the desired polymer's temperature to its density. A two phase system may be assumed for this type of calculation, and percent crystallinity may be included in the calculation. Certain format statements must also be changed.

C. CALCULATION OF CRYSTALLIZATION RATE CONSTANTS PROGRAM FINAL

This program computes the crystallization rate constants for a polymer during the spinning of a fiber. The required input is a function of crystallinity versus distance from the spinneret. The nonisothermal crystallization equation of Nakamura is used for calculation. In its differentiated form it yields an explicit expression for the rate constant. A value for the Avrami index must be assumed for the calculation, and the program is set up to make calculations for Avrami indices of 1, 2, 3, and 4. At the completion of the calculation the rate constant values are printed along with the position, crystallinity, and temperature data that were read in with the initial data input.

Function Time

This subprogram calculates the time required for an infinitesimal layer of polymer to travel between two points on the threadline. It requires a common statement to specify the constants used in the velocity equation. The calculation is performed by summing the travel time numerically for many infinitesimal slices of the fiber.

D. LISTING OF COMPUTER PROGRAMS

Computer printed listings of the programs are arranged in the same order in which they were discussed. Subroutines and function subprograms are positioned immediately after the main programs that employ them.

```
C  PEXRAN  POLYETHYLENE X-RAY PATTERN ANALYSIS PROGRAM
C
C
      INTEGER*2 INT
      LOGICAL*1 LINT(640,320)
      INTEGER RPK
      INTEGER RMIN,RA,RAY,RB,R200,R020,RF,RC,RAD,RX,RY,RG,
     1RH,R110
      DIMENSION POS(2)
      COMMON/AA/INT(320,320)
      COMMON/BB/RAY(320)
      COMMON /CC/PC,FA,FB,FC
      COMMON/DD/IRUN,INO,POS,IO,JO
      COMMON/EE/RX(320),RY(320)
      COMMON/FF/RAD,RA,RB,RC,RF,RG,RH
      EQUIVALENCE (LINT(1,1),INT(1,1))
C  INITIALIZE INT ARRAY TO ZEROS
      DO 1 J=1,320
      DO 1 I=1,320
    1 INT(I,J)=0
C  READ NUMBER OF SAMPLES TO BE PROCESSED ON THIS RUN
C  BEGIN SAMPLE PROCESSING
      IABC=0
      FTN110=0.0
      FTD110=0.0
      FTN200=0.0
      FTD200=0.0
      A = 0.
      B = 0.
      C = 0.0
      CSQ200 = .9566
      CSQ020= .9022
      XN200 = 0.0
      D200 = 0.0
      XN020 = 0.0
      D020 = 0.0
C  READ SAMPLE DATA FROM CARDS
      READ(5,2002)IRUN,INO,POS,TFIB
      IF(TFIB.EQ.9999.)GO TO 501
      READ(5,2003)RAD,RA,RB,RC,RF,RG,RH,RPK,LSIDE
      READ(5,2003)R110,R200,R020
 2002 FORMAT(2(5X,A4),5X,2A4,5X,F7.0)
 2003 FORMAT (9(2X,I3))
C  READ SAMPLE DATA FROM MAGNETIC TAPE
      READ(8,2004,END=300,ERR=502)((LINT(I,J),I=2,600,2),
     1 J=1,320)
 2004 FORMAT(150A1,150A1)
  300 CONTINUE
      WRITE(6,3000)J
 3000 FORMAT(1H0,10X,'NO. RECORDS PER FILE = ',I4)
C  LOCATE THE CENTER OF THE MATRIX
      LSIDE=60
      NXY = LSIDE
```

```
      IHOLD=256
      DO 2 I=1,NXY
      DO 2 J=1,NXY
      IF(INT(I,J).LT.IHOLD)IHOLD=INT(I,J)
      IF(INT(I,J).EQ.IHOLD)IO=I
      IF(INT(I,J).EQ.IHOLD)JO=J
    2 CONTINUE
      WRITE(6,1001) IO,JO
 1001 FORMAT(1H0,10X,'MATRIX CENTER IS AT ',I4,I4)
      IS200=R200
      IS110=R110
      IS020=R020
      ISRH = RH
      ISRF = RF
      ISRA = RA
C  ROUTINE TO COMPUTE SFD
      CALL FILL(0.0,RAD,IO,JO)
      R110=IFOX(R110-5,R110+5)
      SFD=FLOAT(R110)*2.5517
      SSFD=SFD*SFD
      WRITE (6,1004) SFD
 1004 FORMAT(1H0,10X,'CALCULATED SFD = ',F7.2)
C  ROUTINE FOR LOCATING VALUES TO BE USED FOR ABSOLUTE
C  BACKGROUND CORRECTIONS.
      JJSV=256
      IISV=256
      ILINE=SFD*.256
      JLINE=SFD*.50953
      DANG=3.1416/180.
      BANG=-DANG
      DO 20 JJ=1,91
      BANG=BANG+DANG
      IIX=FLOAT(ILINE)*SIN(BANG)
      IIX=IIX+IO
      IIY=FLOAT(ILINE)*COS(BANG)
      IIY=IIY+JO
      IF(INT(IIX,IIY).LT.IISV)IISV=INT(IIX,IIY)
      JJX=FLOAT(JLINE)*SIN(BANG)
      JJX=JJX+IO
      JJY=FLOAT(JLINE)*COS(BANG)
      JJY=JJY+JO
   20 IF(INT(JJX,JJY).LT.JJSV)JJSV=INT(JJX,JJY)
C  WRITE MINIMUM VALUES LOCATED
      WRITE(6,1002)IISV,JJSV
 1002 FORMAT(1H0,10X,'BACKGROUND VALUE IN AMORPHOUS REGION',
     1 ' = ',I4,/1H0,10X,'BACKGROUCD LEVEL IN CRYSTALLINE ',
     2  'REGION = ',I4)
C  CALCULATE CONSTANTS FOR BACKGROUND EQUATION
C  NORMAL BACKGROUND CORRECTION
      S=FLOAT(JJSV-IISV)/FLOAT(JLINE-ILINE)
      Q=FLOAT(IISV)-S*FLOAT(ILINE)
      DELPHI = 3.1416/180.
      PHI = -DELPHI
```

```
      DO 100 IT = 1,91
      PHI = PHI + DELPHI
      R110=IS110
      R200=IS200
      R020=IS020
      RH = ISRH
      RF = ISRF
      RA = ISRA
      CALL FILL (PHI,RAD,IO,JO)
C  LOCATE RMIN
      RMIN=ISET(10,RA)
C  LOCATE RA
      RA = IFOX(RMIN,RB)
C  LOCATE R200
      R200=IFOX(R200-5,R200+5)
C  LOCATE R020
      R020=IFOX(R020-5,R020+5)
C  LOCATE RF
      RF=ISET(R200,RPK)
C  LOCATE R110
      R110=IFOX(R110-5,R110+5)
C  LOCATE RG
      RG=ISET(RPK,R020)
C  LOCATE RH
      RH=ISET(R020,RAD)
C  LOCATE RC
      RC = ISET(R110,R200)
C  ORIENTATION FUNCTION CALCULATIONS
C  REMOVE BACKGROUND LOCALLY FROM R200 AND R020
      DDA=R200-RC
      DDB=RF-RC
      DDC=RAY(RF)-RAY(RC)
      DDD=RAY(R200)-RAY(RC)
      X200=DDD-DDC*DDA/DDB
      DDE=R020-RG
      DDF=RH-RG
      DDG=RAY(RH)-RAY(RG)
      DDH=RAY(R020)-RAY(RG)
      X020=DDH-DDG*DDE/DDF-3.0
      IF(IT.EQ.1.OR.IT.EQ.91)X200=X200/2.0
      IF(IT.EQ.1.OR.IT.EQ.91)X020=X020/2.0
C  CALCULATE AND SUM VALUES FOR FINAL COMPUTATION OF
C  AVERAGE SINES.
      CP=COS(PHI)
      SSP=SIN(PHI)**2
      XN200=XN200+(DELPHI*SSP*CP*X200)
      XN020=XN020+(DELPHI*SSP*CP*X020)
      D200=D200+(DELPHI*CP*X200)
      D020=D020+(DELPHI*CP*X020)
C  MAKE BACKGROUND CORRECTION
      RMIN=SFD*.256
      RA = 0.9+SFD*.35895
      RF=SFD*.50953
```

```
      DO 50 K=RMIN,RF
      RAY(K) = RAY(K)-IFIX(Q+S*FLOAT(K))+4
      IF(RAY(K).LT.IABC)IABC=RAY(K)
      XR=FLOAT(RX(K)-IO)
      YR=FLOAT(RY(K)-JO)
      RSQ=XR*XR+YR*YR
      R = SQRT(RSQ)
      DCS2T=RSQ+SSFD
      CS2T=SSFD/DCS2T
      C2T=SQRT(CS2T)
      T2T=R/SFD
      CST=.5*(1.+C2T)
      SST=.5*(1.-C2T)
      SCT=SST**1.5
      IF(SCT.EQ.0.0) GO TO 50
      XLPF=(1.+CS2T)*T2T/(SCT*CST)
      SFAC=SST/2.3778
      FAC=SQRT(SFAC)
      TFB=5.
      TF=EXP(-2.0*TFB*SFAC)
      SF=STRUT(FAC)
      SF=SF*SF
      XCF=XLPF*SF*TF
   99 CONTINUE
      XRAY=FLOAT(RAY(K))/XCF
C  MAKE CRYSTALLINITY SUMMATIONS
      IF(XRAY.LT.0.0)XRAY=0.0
      ZNEW=XRAY
      TTH=ATAN(T2T)
      DELTH=TTH-SVTH
      D=.25*DELPHI*DELTH*(ZOLD+ZNEW)
      IF(K.GT.RMIN.AND.K.LE.RA)A=A+D
      IF(K.GT.RA.AND.K.LE.R200)C=C+D
      IF(K.GT.R200.AND.K.LE.RF)B=B+D
      SVTH=TTH
      ZOLD=ZNEW
   50 CONTINUE
      IF(IT.EQ.1.OR.IT.EQ.91)RAY(R110)=RAY(R110)/2
      IF(IT.EQ.1.OR.IT.EQ.91)RAY(R200)=RAY(R200)/2
      FTN110=DELPHI*FLOAT(RAY(R110))+FTN110
      FTD110=DELPHI*CP*FLOAT(RAY(R110))+FTD110
      FTN200=DELPHI*FLOAT(RAY(R200))+FTN200
      FTD200=DELPHI*CP*FLOAT(RAY(R200))  +FTD200
  100 CONTINUE
C  CRYSTALLINITY CALCULATION
      XIA = 2*A
      XI200=2*B
      XI110=C-A-B
      FT110=FTN110/FTD110
      FT200=FTN200/FTD200
      XI110=XI110/FT110
      XI200=XI200/FT200
      WR=XIA/(XI110+XI200)
```

```
      PC=100./(WR+1.)
C  ORIENTATION CALCULATION
      ASS200=XN200/D200
      ASS020=XN020/D020
      FA=(3.*(CSQ200      )*ASS200-1.)/2.
      FB=(3.*(CSQ020      )*ASS020-1.)/2.
      FC=-(FA+FB)
      CALL PUTOUT
      GO TO 500
  502 WRITE(6,1006) IRUN,INO
 1006 FORMAT(1H1,5X,'INPUT ERROR OCCURRED IN READING SAMPLE'
     1 ,1X,A4,2X,A4,2X,'FROM TAPE.  SUBSEQUENT CALCULATION',
     2 'S DELETED.')
  500 CONTINUE
  501 CONTINUE
      CALL EXIT
      END
```

```
      FUNCTION STRUT(XRATIO)
C
C
      DIMENSION RATIO(12),F(12)
      DATA RATIO/0.,.1,.2,.3,.4,.5,.6,.7,.8,.9,1.,1.1/
      DATA F/6.,4.6,3.,2.2,1.9,1.7,1.6,1.4,1.3,1.16,1.,.9/
      N= 0
      M=0
      DO1 K=1,11
      IF(XRATIO.GT.RATIO(K).AND.XRATIO.LT.RATIO(K+1))N=K
      IF(XRATIO.EQ.RATIO(K))M=K
    1 CONTINUE
      IF(XRATIO.EQ.RATIO(12))M=12
      IF(M.NE.0) GO TO 2
      GO TO 3
    2 STRUT=F(M)
      RETURN
    3 STRUT=F(N)+(F(N+1)-F(N))*(XRATIO-RATIO(N))/(RATIO(N+1)
     1 -RATIO(N))
      RETURN
      END
```

```
      FUNCTION IFOX(IA,IB)
C
C
      COMMON/BB/M(320)
      MX = 0
      DO 10 K = IA,IB
      MX = MAX0(MX,M(K))
   10 IF(MX.EQ.M(K)) IFOX = K
      RETURN
      END
```

```
      FUNCTION ISET(IA,IB)
C
C
      COMMON/BB/N(320)
      MN = 256
      DO 10 K = IA,IB
      MN = MIN0(MN,N(K))
   10 IF(MN.EQ.N(K)) ISET = K
      RETURN
      END
```

```
      SUBROUTINE PUTOUT
C
C
      DIMENSION POS(2)
      COMMON /CC/PC,FA,FB,FC
      COMMON /DD/IRUN,INO,POS,IO,JO
      WRITE (6,1004)
      WRITE (6,1001)IRUN,INO,POS
      WRITE (6,1002) PC
      WRITE (6,1003)FA,FB,FC
 1004 FORMAT(1H1,13X,'X-RAY DIFFRACTION PATTERN ANALYSIS'/
     11H0,29X,'FOR'/1H0,21X,'POLYETHYLENE FIBER'///)
 1001 FORMAT(1H0,10X,'SPINNING RUN NUMBER = ',A4,/1H0,10X,
     1 'X-RAY FILM NUMBER = ',A4,/1H0,10X,'DISTANCE FROM',
     2' SPINNERET = ',2A4,' CM.'//)
 1002 FORMAT(1H0,10X,'PERCENT CRYSTALLINITY = ',F6.2//)
 1003 FORMAT(1H0,10X,'HERMANS ORIENTATION FUNCTIONS',/
     1 1H0,15X,16H'A' AXIS   FA = ,F6.3/
     2 1H0,15X,16H'B' AXIS   FB = ,F6.3/
     3 1H0,15X,16H'C' AXIS   FC = ,F6.3)
      RETURN
      END
```

```
      SUBROUTINE FILL(ANG,IRAD,IO,JO)
C
C
      INTEGER*2 INT
      COMMON/AA/INT(320,320)
      COMMON/BB/IRAY(320)
      COMMON/EE/IR(320),JR(320)
      R = 0
      DO 1 K = 1,IRAD
      R = R + 1.0
      IR(K) = R*COS(ANG)
      JR(K) = R*SIN(ANG)
      I = IR(K) + IO
      J = JR(K) + JO
      IR(K) = I
      JR(K) = J
      IRAY(K) = INT(I,J)
    1 CONTINUE
      RETURN
      END
```

```
C  SPINLINE   MELT SPINNING DATA ANALYSIS PROGRAM
C
C
      DIMENSION P(6)
      COMMON NNN,AA(77),BB(77),XAA,XBB,XCC,XDD,
     1DIST(77),TFIB(77),DIAM(77),CRYST(77),VEL(77),GRAD(77),
     2 PSI(77),TVIS(77),CCRX(77),DIFF(77),RHO(77),SDIA(77),
     3           TAVG(77),VAVG(77),TIME(77),CON(77),RCON(77),
     4              XRUN, IPOLY, FLOW,SPEED,TAMB,TMEL,FORCE
  100 READ (2,101) XRUN, IPOLY, FLOW,SPEED,TAMB,TMEL,FORCE
  101 FORMAT(2X,A4,I3,5F6.0)
      IF(IPOLY-999)105,998,105
  105 LIM = 0
  102 READ (2,103) NUM, DIST(NUM), DIAM(NUM), TFIB(NUM),
     1 CRYST(NUM), COUNT
  103 FORMAT(I4,F6.0,F7.0,F6.0,F6.0,F3.0)
      LIM = LIM + 1
  106 IF(NUM)104,990,104
  104 IF(COUNT)710,102,710
  710  DO 2000 K=1,LIM,1
      AA(K)=0.0
      TVIS(K) = 0
      RHO(K) = 0
      DIFF(K) = 0
      VEL(K) = 0
      GRAD(K) = 0
      PSI(K) = 0
      VAVG(K) = 0
      TAVG(K) = 0
       RCON(K) = 0
      CON(K) = 0
      TIME(K) = 0
 2000  CCRX(K)=0
      NNN=LIM
      READ(2,3001)P
 3001 FORMAT(6E13.6)
      PTM=141.0
      PTG=-125.0
C
C     CALCULATION OF KINEMATICS OF THE SPINNING PROCESS
C
C  CALCULATE CRYSTALLINITY
C
      DO 420 K=1,LIM
  420 CRYST(K)=P(1)*EXP(P(2)*((DIST(K)-P(3))/P(4))**P(5))+
     1P(6)
C
C  CALCULATE FILAMENT DENSITY
C
      DO 201 K=1,LIM
      IF(DIST(K)-P(3))202,202,203
  202 IF(TFIB(K)-136.5)400,410,410
  410 RHO(K)=1.0/(1.136+0.885E-3*TFIB(K))
```

```
      GO TO 201
  400 RHO(K)=1.0/(1.1149+0.403E-3*TFIB(K)+0.467E-5*TFIB(K)
     1 **2)
      GO TO 201
  203 ROA=1.0/(1.1149+0.403E-3*TFIB(K)+0.467E-5*TFIB(K)**2)
      ROC=1.0/(0.994+0.2614E-3*TFIB(K)+0.443E-6*TFIB(K)**2)
      RHO(K)= 100.0*ROC*ROA/(100.*ROC-CRYST(K)*(ROC-ROA))
  201 CONTINUE
C
C  CURVE FIT EXPERIMENTAL DIAMETER DATA
      CALL EXFIT(LIM,DIST,DIAM,SDIA,GRAD)
      DO 220 K=1,LIM
  220 DIAM(K)=SDIA(K)
C  CALCULATE LOCAL VELOCITY
C
      DO 210 K=1,LIM
  210 VEL(K)=(4.0*FLOW)/(314.16*RHO(K)*DIAM(K)**2)
C
C  FIT VELOCITY DATA AND OBTAIN GRADIENT
       CALL EXFIT(LIM,DIST,VEL,SDIA,GRAD)
C
C  CALCULATE FORCE ON FILAMENT
      CALL FINIT
      CALL FGRAV
      DO 4000 K=1,LIM
      GRAD(K)=5.0*GRAD(K)/3.0
 4000 PSI(K)=FORCE+       BB(K)+TAVG(K)
C
C  WRITE SUMMARY OF FORCES
      WRITE(3,4001)XRUN
      WRITE (3,4002)(DIST(K),TAVG(K),BB(K),PSI(K),K=1,LIM)
 4001 FORMAT(1H1,45X,A4,2X,'FORCE SUMMARY',///1H ,10X,'DIS',
     1'TANCE',12X,'INERTIA',13X,'WEIGHT',14X,'RHEOL.'//)
 4002 FORMAT(1H ,10X,E13.6,7X,E13.6,7X,E13.6,7X,E13.6)
C
C  CALCULATE STRESS IN FILAMENT
      DO 5000 K=1,LIM
      PSI(K)=(4.0*PSI(K))/(3.1416*DIAM(K)**2)
 5000 CONTINUE
C
C  CALCULATE ELONGATIONAL VISCOSITY
  131 DO 140 K    =1,LIM,1
      IF(GRAD(K))133,132,133
  133 TVIS(K)=980.665*PSI(K)/ABS(GRAD(K))
      GO TO 140
  132  TVIS(K) = 9999.
  140  CONTINUE
C
C      ALL OUTPUT STATEMENTS FOLLOW
C
      LIM=NNN
  163 JPAGE = 1
C
```

```
C      CALCULATE NUMBER OF PAGES TO BE PRINTED.
  225 IF(LIM-38)226,226,227
  226 IPAGE=2
      GO TO 210
  227 IF(LIM-45)228,228,229
  228 IPAGE=3
      GO TO 210
  229 IPAGE=(((LIM-39)/45)+  ((LIM-1)/45)+3)
  210 WRITE (3,211) XRUN,JPAGE,IPAGE,FLOW,SPEED,TMEL,TAMB,
     1   FORCE
  211 FORMAT(1H1,15X,'MELT SPINNING RUN NUMBER ',A4,12X,
     1'HIGH DENSITY POLYETHYLENE',10X,'PAGE ',I2,' OF',I2///
     21H ,5X,'POLYMER MASS FLOW RATE = ',F6.3,' GRAMS/MIN',
     320X,'FIBER TAKEUP VELOCITY = ',F6.1,' METERS/MIN',//
     41H ,5X,'POLYMER MELT TEMPERATURE = ',F6.1,' DEGREES ',
     5'C',18X,'AMBIENT TEMPERATURE    = ',F6.1,' DEGREES C',
     6//1H ,5X,'TENSION AT TAKEUP = ',F6.2,' GRAMS',///)
C
C      REMAINING LINE COUNT AT THIS POINT IS 45
C     1FOR THE FIRST PAGE.  ALL REMAINING PAGE HEADINGS
C     2WILL REQUIRE 10 LINES LEAVING 45 FOR DATA.  THIS
C     3PAGE WILL TAKE 38 LINES OF DATA.  PAGES WILL EJECT
C     4AT 55 LINES OF PRINT.
C
C      THE FOLLOWING WRITE STATEMENT PROVIDES HEADINGS FOR
C     1 EXPERIMENTAL DATA PRINTOUT.
  230 WRITE (3,231)
  231 FORMAT (1H ,51X,17HEXPERIMENTAL DATA,//
     1    1H ,8X,4HDATA,14X,8HDISTANCE,13X,5HFIBER,15X,
     25HFIBER,14X,8HMEASURED/1H ,7X,5HPOINT,16X,4HFROM,14X,
     38HDIAMETER,10X,11HTEMPERATURE,12X,5HFIBER/1H , 7X,
     46HNUMBER,11X,11HSPINNERETTE,48X,13HCRYSTALLINITY/1H ,
     529X,2HCM,18X,2HCM,16X,6HDEC C.,13X,7HPERCENT//)
C      BEGIN WRITING EXPERIMENTAL DATA CHECKING FOR FULL
C     1  PAGES.
  300 NX=38
  301 DO 350 K=1,LIM,1
      IF(K-NX-1)309,310,309
309   GO TO 232
  310 JPAGE = JPAGE + 1
C
C      THESE TWO STATEMENTS MAKE A HEADING ON EACH PAGE.
  240 WRITE (3,241) XRUN, JPAGE,IPAGE
  241 FORMAT (1H1, 14X, 25HMELT SPINNING RUN NUMBER , A6,
     1 14H     CONTINUED,  31X, 5HPAGE , I2,4H OF ,I2///)
      NX = NX + 45
      WRITE (3,231)
  232 WRITE(3,233)K,DIST(K),DIAM(K),TFIB(K),CRYST(K)
C      FORMAT FOR EXPERIMENTAL DATA
  233 FORMAT(1H ,8X,I4,12X,E11.4,3( 9X,E11.4))
  350 CONTINUE
C
C      BEGIN NEW PAGE FOR KINEMATEC DATA.
```

```
  360 JPAGE = JPAGE + 1
      WRITE (3,241) XRUN, JPAGE, IPAGE
C
C     THE FOLLOWING WRITE AND FORMAT GIVE HEADINGS FOR
C    1  THE COLUMNS OF THE KINEMATIC DATA
  250 WRITE (3,251)
  251 FORMAT(1H ,46X,'CALCULATED KINEMATIC DATA'//1H ,6X,
     1'DISTANCE',11X,'CALCULATED',10X,'CALCULATED',12X,
     2'LOCAL',15X,'LOCAL',15X,'LOCAL'/1H ,8X,'FROM',15X,
     3'FIBER',14X,'VELOCITY',12X,'TENSILE',11X,'ELONGATION',
     4'AL',11X,'FIBER'/1H ,4X,'SPINNERET',11X,'VELOCITY',
     512X,'GRADIENT',13X,'STRESS',12X,'VISCOSITY',12X,'DEN',
     6'SITY'/1H ,9X,'CM',16X,'M/MIN',15X,'1/SEC',14X,
     7'GM/SQ CM',13X,'POISE',15X,'GM/CC'//)
      NX = 45
C     WRITE KINEMATIC DATA CHECKING FOR FULL PAGES
  365 DO 400 K=1,LIM,1
C     FORMAT FOR CALCULATED KINEMATIC DATA
  252 WRITE (3,253) DIST(K), VEL(K), GRAD(K), PSI(K),
     1   TVIS(K), RHO(K)
  253 FORMAT(1H ,4X,E11.4,5( 9X,E11.4))
      IF(K-NX)254,370,254
  254 GO TO 400
  370 JPAGE = JPAGE + 1
      WRITE (3,241) XRUN, JPAGE, IPAGE
      WRITE (3,251)
      NX= NX + 45
  400 CONTINUE
C
C  EJECT TO NEW PAGE BEFORE RETURNING TO CALCULATIONS
      WRITE(3,410)
  410 FORMAT(1H1)
      GO TO 100
C
C     ERROR STATEMENT FOR BLANK CARD STOP BY STATEMENT 106
  990 WRITE (3,991)
  991 FORMAT ( 39H0  PROGRAM TERMINATED BY STATEMENT 106.,
     1         33H  CHECK DATA DECK FOR BLANK CARD.)
C
 1000   CONTINUE
  998 CALL EXIT
      END
```

```
      SUBROUTINE EXFIT(N,X,Y,YC,DY)
C
C
      DIMENSION P(6),X(77),Y(77),YC(77),DY(77),STEP(6),
     1 XS(77),YS(77)
      COMMON MO,XS,YS,XMIN,XMAX,YMIN,YMAX,DIST(77),TFIB(77),
     1DIAM(77),CRYST(77),VEL(77),GRAD(77),PSI(77),TVIS(77),
     2CCRX(77),DIFF(77),RHO(77),SDIA(77),TAVG(77),VAVG(77),
     3TIME(77),CON(77),RCON(77),XRUN,IPOLY,FLOW,SPEED,TAMB,
     4TMEL,FORCE
      MO = N
      COUNT = FLOAT(N)
      XMAX = X(1)
      XMIN = X(1)
      YMAX = Y(1)
      YMIN = Y(1)
      DO 10  K = 2,N
      IF(XMAX-X(K))1,2,2
    1 XMAX=X(K)
    2 CONTINUE
      IF(XMIN-X(K))4,4,3
    3 XMIN=X(K)
    4 CONTINUE
      IF(YMAX-Y(K))5,6,6
    5 YMAX=Y(K)
    6 CONTINUE
      IF(YMIN-Y(K))8,8,7
    7 YMIN=Y(K)
    8 CONTINUE
   10 CONTINUE
      TESTY = Y(N)
      IF(TESTY-3.0)11,11,20
   11 A = YMAX-YMIN
      G = YMIN
      GO TO 30
   20 A = YMIN-YMAX
      G = YMAX
   30 C = XMIN
      D = XMAX-XMIN
      E = 2.0
      SUM = 0.
      NOCT = 0
      DO 40 K = 1,N
      XS(K) = X(K)
      YS(K) = Y(K)
      DIF = (X(K)-C)
      IF(DIF)61,60,61
   61 DENOM = (DIF/D)**E
      ARG = (Y(K)-G)/A
      IF(ARG)60,60,62
   62 SUM = SUM+ALOG((Y(K)-G)/A)/DENOM
      GO TO 40
   60 NOCT = NOCT+1
```

```
 40 CONTINUE
    NO = N-NOCT
    R = FLOAT(NO)
    B = SUM/R
    C = 0.
    P(1) = A
    P(2)=B/D
    P(3) = C
    P(4)=1.0
    P(5) = E
    P(6) = G
    STEP(1)=0.2*YMAX
    STEP(2)=20.0
    STEP(3)=1.0
    STEP(4)=0.0
    STEP(5)=0.4
    STEP(6)=0.1*YMAX
     CALL PATRN(6,P,STEP,3,1,COST)
    DO 70 K = 1,N
 70 YC(K)= P(1)*EXP(P(2)*((X(K)-P(3))/P(4))**P(5))+P(6)
    YSUM = 0.
    DO 80 K = 1,N
 80 YSUM = YSUM+Y(K)
    YAV = YSUM/COUNT
    SDIF = 0.0
    AERR = 0.
    CERR = 0.
    DO 90 K = 1,N
    DY(K) = (P(1)*P(2)*P(5)/P(4))*(((X(K)-P(3))/P(4))**
   1 (P(5)-1.))
   1 *EXP(P(2)*((X(K)-P(3))/P(4))**P(5))
    SDIF = SDIF+(Y(K)-YC(K))**2
    AERR = AERR+(Y(K)-YAV)**2
 90 CERR = CERR+(YC(K)-YAV)**2
    CORR = SQRT(CERR/AERR)
    STDER=SQRT(SDIF/COUNT)
    WRITE (3,1001)
    WRITE (3,1002) P
    WRITE (3,1003) STDER,CORR
    WRITE (3,1004)
    DO 100 J=1,N
100 WRITE (3,1005) J,X(J),Y(J),YC(J),DY(J)
    RETURN
1001 FORMAT (1H1,40X,29HY = A*EXP(B*((X-C)/D)**E) + G  )
1002 FORMAT (1H0,20X,4HA = ,E13.6,10X,4HB = ,E13.6,10X,
   1 4HC = ,E13.6//21X,4HD = ,E13.6,10X,4HE = ,E13.6,10X,
   2 4HG = ,E13.6)
1003 FORMAT (1H0,20X,17HSTANDARD ERROR = ,E13.6,10X,
   1 26HCORRELATION COEFFICIENT = ,E13.6)
1004 FORMAT (1H0,9X,12H   NUMBER   ,10X,12H     X      ,
   1 10X,5X,'X',6X,10X,5X,'Y',21X,'YC',20X,'DY',5X,//)
1005 FORMAT(1H ,14X,I2,5X,4(10X,E13.6))
    END
```

```
      SUBROUTINE  PATRN(NP,P,STEP,NRD,IO,COST)
C
C
C-----THE SIZE OF B1,B2,T,AND S NEED ONLY BE EQUAL TO THE
C     NUMBER OF PARAMETERS IN THE FUNCTION.
      DIMENSION P(6),STEP(6),B1(6),B2(6),T(6),S(6)
C-----STARTING POINT
      L=1
      ICK=2
      ITTER=0
      DO5 I=1,NP
      B1(I)=P(I)
      B2(I)=P(I)
      T(I)=P(I)
  5   S(I)=STEP(I)*10.
C-----INITIAL BOUNDARY CHECK AND COST EVALUATION
      CALL BOUND (P,IOUT)
      IF(IOUT)10,10,110
  110 IF(IO)6,6,106
  106               WRITE(3,1005)
                    WRITE(3,1000)(J,P(J),J=1,NP)
  6   RETURN
 10   CALL PROC(P,C1)
      IF(IO)11,11,111
  111               WRITE(3,1001)ITTER,C1
                    WRITE(3,1000)(J,P(J),J=1,NP)
C-------BEGINNING OF PATTERN SEARCH STRATEGY
 11   DO99 INRD=1,NRD
      DO12 I=1,NP
 12   S(I)=S(I)/10.
      IF(IO)20,20,120
  120               WRITE(3,1003)
                    WRITE(3,1000)(J,S(J),J=1,NP)
 20   IFAIL=0.0
C-----PRETURBATION ABOUT T
      DO30 I=1,NP
      IC=0
 21   P(I)=T(I)+S(I)
      IC=IC+1
      CALL BOUND (P,IOUT)
      IF(IOUT)123,123,23
  123 CALL PROC(P,C2)
                    L=L+1
      IF(IO-3)22,122,122
  122               WRITE(3,1002)L,C2
                    WRITE(3,1000)(J,P(J),J=1,NP)
   22 IF(ABS(C1-C2)-(C2*1.0E-4))23,223,223
  223 IF(C1-C2)23,23,25
   23 IF(IC-2)124,24,24
  124 S(I)=-S(I)
      GOTO21
 24   IFAIL=IFAIL+1
      P(I)=T(I)
```

```
      GOTO30
 25   T(I)=P(I)
      C1=C2
 30   CONTINUE
      IF(NP-IFAIL)135,135,35
  135 IF(ICK-2)190,90,190
  190 IF(ICK-1)191,35,191
  191 CALL PROC(T,C2)
                    L=L+1
      IF(3-IO)131,131,31
  131               WRITE(3,1002)L,C2
                    WRITE(3,1000)(J,T(J),J=1,NP)
 31   IF(C1-C2)32,34,34
 32   ICK=1
      DO33 I=1,NP
      B1(I)=B2(I)
      P(I)=B2(I)
 33   T(I)=B2(I)
      GOTO20
 34   C1=C2
 35   IB1=0
      DO39 I=1,NP
      B2(I)=T(I)
      IF(ABS(B1(I)-B2(I))-(.01*ABS(S(I))))201,39,39
  201  IB1=IB1+1
 39   CONTINUE
      IF(IB1-NP)290,90,290
  290 ICK=0
                    ITTER=ITTER+1
      IF(IO-2)40,140,140
  140               WRITE(3,1001)ITTER,C1
                    WRITE(3,1000)(J,T(J),J=1,NP)
C-----ACCELERATION STEP
   40 CONTINUE
      DO45 II=1,11
      SJ=11-II
      SJ=SJ/10.
      DO42 I=1,NP
      T(I)=B2(I)+SJ*(B2(I)-B1(I))
 42   P(I)=T(I)
      SJ=SJ-.1
      CALL BOUND (T,IOUT)
      IF(IOUT-1)46,146,146
  146 IF(II-11)45,101,45
  101 ICK=1
 45   CONTINUE
 46   DO47 I=1,NP
 47   B1(I)=B2(I)
      GOTO20
 90   DO91 I=1,NP
 91   T(I)=B2(I)
 99   CONTINUE
      DO100 I=1,NP
```

```
100    P(I)=T(I)
       COST=C1
       IF(IO)999,999,998
  998              WRITE(3,1004)L,C1
                   WRITE(3,1000)(J,P(J),J=1,NP)
  999 RETURN
1000   FORMAT(10X,5(I7,E13.6)/)
1001   FORMAT(//1X14HITERATION NO.    ,I5/5X,5HCOST= ,E15.6,
     1 20X,10HPARAMETERS)
     1    10HPARAMETERS)
1002   FORMAT(10X3HNO.,I4, 8X5HCOST=,E15.6)
1003   FORMAT(/1X28HSTEP SIZE FOR EACH PARAMETER    )
1004   FORMAT(1H113HANSWERS AFTER ,I3,2X,'FUNCTIONAL ',
     1'EVALUATIONS    '//5X,'COST=',E15.6,20X,'OPTIMAL ',
     2 'PARAMETERS  ')
1005   FORMAT(1H135HINITIAL PARAMETERS OUT OF BOUNDS          )
       END
```

```
       SUBROUTINE PROC(P,COST)
C
C
       DIMENSION P(6),X(77),Y(77)
       COMMON N,X,,A,B,C,D,                    DIST(77),TFIB(77),
      1DIAM(77),CRYST(77),VEL(77),GRAD(77),PSI(77),TVIS(77),
      2CCRX(77),DIFF(77),RHO(77),SDIA(77),TAVG(77),VAVG(77),
      3TIME(77),CON(77),RCON(77),XRUN,IPOLY,FLOW,SPEED,TAMB,
      4TMEL,FORCE
       COST = 0.
       DO 10 K = 1,N
   10   COST = COST+(Y(K)-P(1)*EXP(P(2)*((X(K)-P(3))/P(4))**
     1 P(5))-P(6))**2
       COST = COST/FLOAT(N)
       COST = SQRT(COST)
       RETURN
       END
```

```
      SUBROUTINE BOUND (P,IOUT)
C
C
      DIMENSION P(6),X(77),Y(77)
      COMMON N,X,Y,XMIN,XMAX,YMIN,YMAX,DIST(77),TFIB(77),
     1DIAM(77),CRYST(77),VEL(77),GRAD(77),PSI(77),TVIS(77),
     2CCRX(77),DIFF(77),RHO(77),SDIA(77),TAVG(77),VAVG(77),
     3TIME(77),CON(77),RCON(77),XRUN,IPOLY,FLOW,SPEED,TAMB,
     4TMEL,FORCE
      IOUT = 0
      IF(P(1)+YMAX)100,5,5
    5 IF(P(1)-YMAX)10,10,100
   10 IF(P(1))15,100,15
   15 IF(P(2)+1.E02)100,20,20
   20 IF(P(2)-1.E02)30,30,100
   30 IF(P(2))40,100,40
   40 IF(P(3))100,50,100
   50 IF(P(4)-1.0)100,60,100
   60 GO TO 70
   70 IF(P(5)-5.0)80,80,100
   80 IF(P(5)-1.0)100,90,90
   90 IF(P(6)-YMAX)91,91,100
   91 IF(P(6))100,100,92
   92 IF((XMIN-P(3))/P(4))100,200,200
  100 IOUT=1
  200 CONTINUE
      RETURN
      END
```

```
      SUBROUTINE FGRAV
C
C
C  THIS ROUTINE CALCULATES GRAVITY FORCES ON THE THREADLINE
      COMMON NNN,AA(77),BB(77),XAA,XBB,XCC,XDD,
     1DIST(77),TFIB(77),DIAM(77),CRYST(77),VEL(77),GRAD(77),
     2 PSI(77),TVIS(77),CCRX(77),DIFF(77),RHO(77),SDIA(77),
     3 TAVG(77),VAVG(77),TIME(77),CON(77),RCON(77) ,
     4              XRUN, IPOLY, FLOW,SPEED,TAMB,TMEL,FORCE
      J=NNN
      BB(NNN)=RHO(J)*3.1416*DIAM(J)**2*(147.*2.54-DIST(J))
     1 /4.0
      DO 100 K=2,NNN
      J=NNN+1-K
  100 BB(J)=BB(J+1)+RHO(J)*3.1416*DIAM(J)**2*(DIST(J+1)-
     1 DIST(J))/4.0
      RETURN
      END
```

```
      SUBROUTINE FINIT
C
C
C  THIS ROUTINE CALCULATES INERTIA FORCES ON THE THREADLINE
      COMMON NNN,AA(77),BB(77),XAA,XBB,XCC,XDD,
     1DIST(77),TFIB(77),DIAM(77),CRYST(77),VEL(77),GRAD(77),
     2 PSI(77),TVIS(77),CCRX(77),DIFF(77),RHO(77),SDIA(77),
     3TAVG(77),VAVG(77),TIME(77),CON(77),RCON(77) ,
     4              XRUN, IPOLY, FLOW,SPEED,TAMB,TMEL,FORCE
      DO 100 K=1,NNN
      TAVG(K)=-FLOW*(SPEED-VEL(K))/(36.0*980.665)
      IF(SPEED-VEL(K))101,100,100
  101 TAVG(K)=0.0
  100 CONTINUE
      RETURN
      END
```

```
C  PROGRAM FINAL
C
C
      DIMENSION DIST(77),XKON(77),XK(77),DX(77),TEMP(77),
     1 TM(77),CX(6),CRYX(77)
      COMMON CV(6)
      EQUIVALENCE (CV(1),CV1),(CV(2),CV2),(CV(3),CV3),
     1 (CV(5),CV5),(CV(6),CV6),(CX(1),CX1),(CX(2),CX2),
     2 (CX(4),CX4),(CX(5),CX5),(CX(6),CX6),(CV(4),CV4),
     3 (CX(3),CX3)
      VEL(X)=(CV1*EXP(CV2*((X-CV3)/CV4)**CV5)+CV6)*5.0/3.0
      XTAL(X)=CX1*EXP(CX2*((X-CX3)/CX4)**CX5)+CX6
      DXDT(X)=(XTAL(X)-CX6)*(CX2*CX5/CX4)*((X-CX3)/CX4)**
     1 (CX5-1.0)*VEL(X)/XMAX
C
C  INPUT SECTION
C
    1 READ(2,3010)
      READ(2,2010)LIM
      IF(LIM)10,10,5
    5 READ(2,2020)(DIST(K),TEMP(K),K=1,LIM)
      READ(2,2030)CX,CV
C
C  LOCATE STARTING POINT
      XMAX = XTAL(373.38)
      DO  100 K=1,LIM
      KGO=K
      IF(ABS(DIST(K)-CX3)-1.0)200,100,100
  100 CONTINUE
C
C  CALCULATE REQUIRED DATA
C
  200 DO 700 K=KGO,LIM
      CRYX(K)=XTAL(DIST(K))
      DX(K)=DXDT(DIST(K))
  700 CONTINUE
      KA=KGO+1
      TM(KGO)=0.0
      DO 600 K=KA,LIM
  600 TM(K)=TIME(DIST(K-1),DIST(K))+TM(K-1)
      DO 500 J=1,4
      AVN=FLOAT(J)
      DO 400 K=KGO,LIM
      Z=1.0-CRYX(K)/XMAX
      XKON(K)=(DX(K)/(AVN*Z))*(-ALOG(Z))**((1.0-AVN)/AVN)
      XK(K)=XKON(K)**AVN
  400 CONTINUE
C
C  WRITE RESULTS
C
      WRITE(3,3050)
      WRITE(3,3010)
      WRITE(3,3020)AVN
```

```
      WRITE(3,3030)
      WRITE(3,3040)(DIST(K),TEMP(K),TM(K),CRYX(K),DX(K),
     1 XKON(K),XK(K),K=KGO,LIM)
  500 CONTINUE
 3010 FORMAT(80H
     1                                                              )
 2010 FORMAT(I3)
 2020 FORMAT(4X,F6.0,7X,F6.0)
 2030 FORMAT(6E13.6/6E13.6)
 3050 FORMAT(1H1)
 3020 FORMAT(1H0,'AVRAMI INDEX = ',F4.1)
 3030 FORMAT(1H0,4X,'LENGTH',10X,'TEMP',11X,'TIME',11X,
     1'CRYX',11X,'DX/DT',10X,'CAP K',12X,'K'/7X,'(CM)',9X,
     2'(DEG C)',9X,'(SEC)',10X,'(PCT)',9X,'(1/SEC)'//)
 3040 FORMAT(1H ,4X,F7.2,8X,F6.1,7X,E10.3,7X,F6.2,7X,E10.3,
     15X,E10.3,5X,E10.3)
      GO TO 1
   10 CALL EXIT
      END
```

```
      FUNCTION TIME(XA,XB)
C
C
      COMMON CV1,CV2,CV3,CV4,CV5,CV6
      VEL(X)=(CV1*EXP(CV2*((X-CV3)/CV4)**CV5)+CV6)*5.0/3.0
      SUM=0.5/VEL(XA)
      XSAVE=XA
      X=XA
    5 X=X+0.1
      IF(XB-X)20,20,40
   40 SUM=SUM+1.0/VEL(X)
      XSAVE=X
      GO TO 5
   20 TIME=0.10*SUM+(XB-XSAVE)*0.5/VEL(XB)
      RETURN
      END
```

APPENDIX C

EQUIPMENT OPERATING INSTRUCTIONS

A. INSTRUCTIONS FOR EXTRUDER-SPINNING MACHINE

Startup Procedure

The following procedure contains the minimum steps for starting the extruder to spin fiber.

1. Turn on cooling water to the extruder throat.

2. Turn on main switch at the switch box on the wall.

3. Turn on main switch on extruder control panel.

4. Set all four temperature controllers to desired temperatures and turn on heaters.

5. Turn temperature meter on and set selector switch to position one to read extruder discharge temperature.

6. Wait two and a half hours for the extruder to heat. Extruder and pump drive circuits will energize two and one half hours after all four heater circuits have been turned on. This delay is a built in safety feature to prevent damaging the spin pump or extruder by attempting to operate the equipment while it is filled with frozen polymer. While waiting for the equipment to reach its operating temperature, check the following items.

7. Fill the feed hopper with polymer pellets.

8. Swing the spinning head toward the wall to facilitate purging and wiping operations after extruder startup.

9. Check the hopper nitrogen purge to make sure there is a flow of gas.

CAUTION: The next step must always be observed to avoid damage to the spin pump.

10. Loosen the lock screw on the spline section of the spin pump drive shaft. Using a large crescent wrench on the flats in the pump shaft, rotate the pump shaft to be certain the polymer inside is molten. If the shaft will not turn, wait 30 minutes and repeat the procedure. If the shaft can be easily turned, reposition the shaft in its original location and tighten the locking screw. The pump is ready for operation.

11. Start the spin pump by pushing its start button.

CAUTION: The next step must always be followed to prevent breaking the extruder screw.

12. Place the extruder pressure cut off switch in the "HAND" mode to bypass the low pressure stop switch.

13. Set the extruder speed potentiometer on its maximum reading. (This gives the minimum extruder speed.)

14. "Bump" the extruder by pushing the START button and quickly pushing the STOP button. Watch the extruder motor pulley to see if it rotates and stops or rotates and kicks back in the opposite direction. If it kicks back, the extruder is still frozen. Stop the spin pump, wait 30 minutes and try again. If the motor rotates and stops, the polymer is molten, and the extruder may be safely operated.

15. Push the START button and adjust the speed potentiometer while watching the pressure gage mounted above the spinning head. Adjust the speed to give a screw discharge pressure of 50 to 70 kg/cm^2.

16. Change the pressure cutoff switch to "AUTOMATIC" mode.

The extruder is now spinning a fiber. If a different polymer flow rate is needed, make the following changes while the spin pump and extruder are both running.

1. Adjust the spin pump speed to the new value using the knob on the PIV gear box.

2. Readjust the extruder speed to give an extruder discharge pressure of 50 to 70 gm/cm^2.

While spinning fiber, occasionally check the extruder pressure to see if it stays within the range 50 to 70 kg/cm^2. Carefully adjust extruder speed, if necessary, to bring the pressure in range.

Calibration of Platinum Resistance Thermometers

The PT 100 thermometers, which measure polymer temperatures in the spinning head, must be correctly calibrated to assure a correct reading of temperature. The meter that indicates temperatures sensed by the thermometer originally could not be adjusted to give a correct reading. Also changes could not be made in the thermometers to allow adjusting the temperature indicated on the control panel meter.

Since it was desirable to know the exact temperature sensed by the thermometers, a change was made in the circuitry of the meter to provide an adjustable element suitable for easy calibration adjustments. This was achieved using a potentiometer of very high resistance. It was wired in parallel with another resistance element in the input leads from thermometer to meter.

After this change adjustment of the temperature measuring system was simple. The actual resistance of a thermometer was measured

using a precision resistance meter. Using the value measured and the known temperature versus resistance relationship of the PT 100 thermometer, the correct temperature at the thermometer bulb was calculated. After reconnecting the thermometer to the meter, the reading on the meter was adjusted to the calculated value by means of the adjustable potentiometer.

The potentiometer is located inside a small compartment covered by a bakelite panel on the right side of the meter housing when viewed from the back of the control panel.

Spin Pack Makeup

The following instructions give details of the procedure for making spin packs both with and without sand filtration.

Begin by having all the needed parts at hand, the required tools on hand, and the critical pack parts clean and ready for assembly. The parts needed are as follows:

1. Spinneret (four hole spinneret design is given in Figure 35),
2. Pack body,
3. Filter screen,
4. Sand (if used),
5. Pack nut,
6. Pack gasket,
7. Antiseize compound.

The only tools needed are the spanner wrench made especially for the pack, and the holding plate for the pack body while tightening the pack nut. A vise can be used if the holding plate is not available.

K&E 19 1153 1-71 77833•

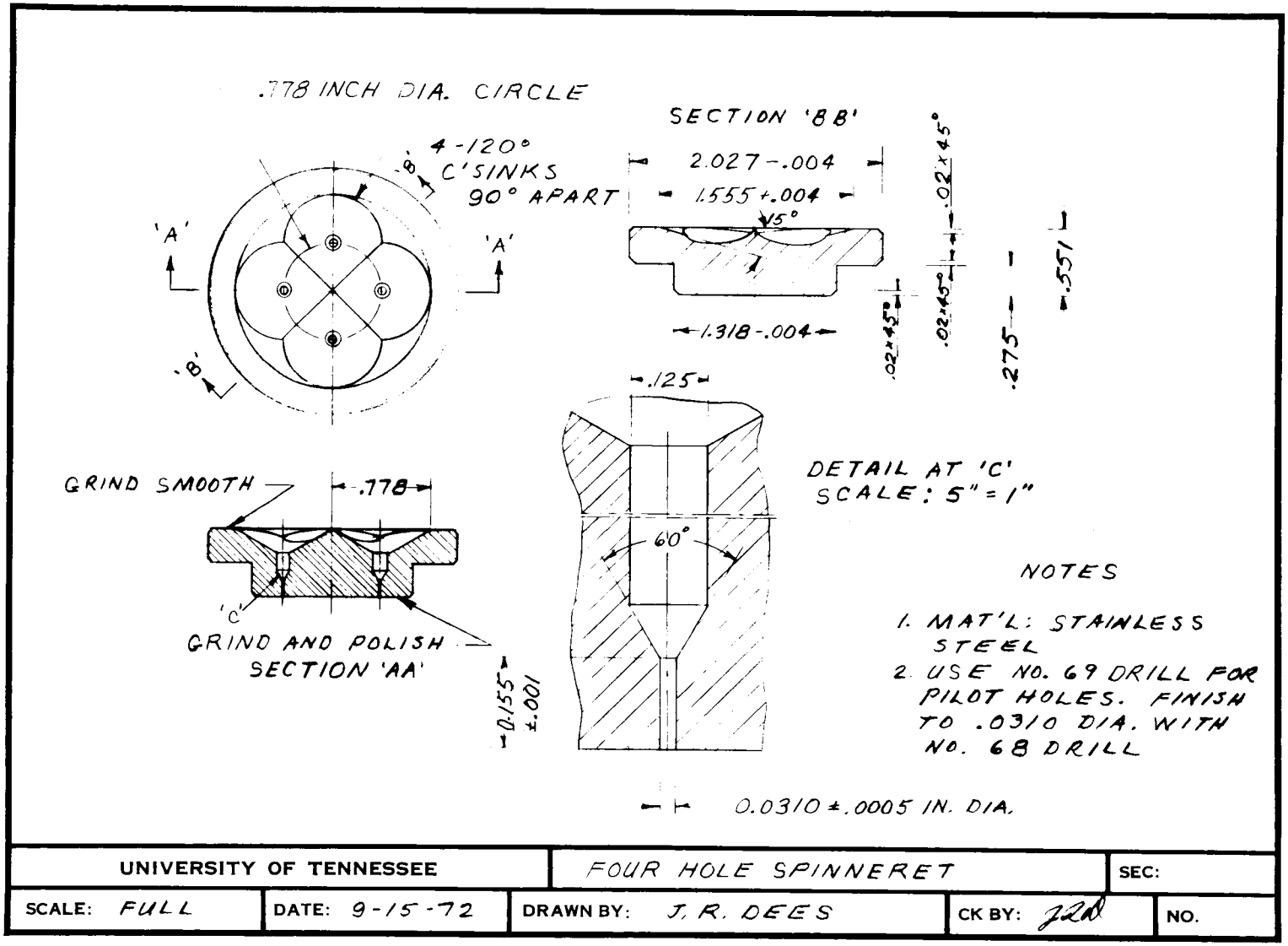

UNIVERSITY OF TENNESSEE	FOUR HOLE SPINNERET		SEC:
SCALE: FULL	DATE: 9-15-72	DRAWN BY: J. R. DEES	CK BY: JRD	NO.

Figure 35. Design Drawing for Four Hole Spinneret

Place the pack body on the holding plate with at least two bolts inserted through the holes in the holder and the pack. This will prevent the turning of the pack during tightening. Insert the spinneret in the pack body with the capillary positioned toward the outside (bottom) of the pack. Next place a support plate on the spinneret with the rimmed surface turned toward the spinneret and the flat surface up. Place a bound filtration screen on the support plate with the 50 mesh side (coarse mesh) down and the fine mesh side up. Coat the threads of the pack nut with antiseize compound, and screw the nut into the pack body as far as it will go. Use the spanner wrench to tighten the nut very tightly. (How tight this is will be learned only by experience. If the pack does not leak, then the nut is tight enough.) A note of caution is in order here. Always use the anti-seize compound on the nut threads. There is always the risk of stainless steel threads siezing in this type of service, and the best way to avoid this is to use the anti-sieze compound faithfully. If the threads seize, there is a strong possibility that the pack will be destroyed by trying to remove the nut with any type of mechanical assistance.

At this point the pack is suitable for use with non-gelling polymers. Place a gasket in the gasket recess around the inlet hole in the pack, and install the pack in the spinning machine. If the pack is to be used for a gel producing polymer, the proper sand fractions must be placed in the pack. Measure the required volumes of the proper grades of sand, and carefully pour each sand fraction into the pack

through the inlet hole. After each sand fraction gently tap the pack with a hammer on the side to level and settle the sand. This is very important to achieve uniformity from pack to pack. After all of the sand fractions have been placed in the pack, take care to avoid any sudden jolting of the pack. A sharp knock can disturb the sand layers and make the pack useless. Clean away any sand that may have spilled on the pack, place the inlet gasket in position, and the pack is ready for installation.

Changing a Spin Pack

CAUTION: This procedure requires handling hot pieces of apparatus. Wear asbestos gloves, safety goggles, and long sleeves.

1. Have a fresh spin pack ready for installation.

2. Place the pack holder in a vise so it will be ready for instant use.

3. Heat the spinning machine to operating temperature. This will require at least two and one-half hours unless the machine has already been in operation.

4. If the machine is running, stop the extruder and let the spin pump run until the extruder pressure drops to zero. Let the pump run about fifteen seconds longer to completely relieve any pressure between the extruder and spin pump.

5. Using the rachet with a six millimeter allen wrench, loosen all six spin pack bolts approximately one turn.

6. Remove four bolts completely, leaving two opposing ones to support the pack.

7. Loosen these bolts about three turns and dislodge the pack by tightening the jack screws located on the spin pack bolt circle.

8. Carefully remove the remaining two bolts while supporting the pack with a gloved hand and an asbestos pad. (Use an extra glove for a pad.)

9. When the pack drops out of the spinning head, immediately take it to the holding plate for disassembly.

10. The hot pack should be quickly disassembled before the polymer freezes.

11. Clean excess polymer out of the spinning head using brass wipe sticks.

12. Carefully slide the fresh spin pack into the spinning head being careful to keep the pack gasket in place.

13. Install two pack bolts to hold the pack in place.

14. Install the remaining bolts. Bolts threads should be coated with antiseize compound before installation in spinning head.

15. Tighten the bolts a little at a time, moving from one side of the pack to the opposite side until all bolts are tight.

16. Make a final tightening by moving from one bolt to the next around the circle.

17. Let the pack heat for two and one-half hours before attempting to spin.

Wiping the Spinneret

Polymer residues will periodically build up on the spinneret and interfere with the spinning process. When this occurs, the problem

can be eliminated by wiping the spinneret with a sharp, burr-free, wipe stick made of brass.

1. Spray a thin film of silicone mold release on the spinneret.

2. Place the sharp edge of the wipe stick squarely against the spinneret and move it across the orifice in a quick, smooth motion.

3. Repeat the procedure if further cleaning is needed.

4. If wiping does not eliminate the problem, look for other sources of trouble, possibly a dirty spin pack.

Meter Pump Change

At times it will be necessary to remove the meter pump because of a broken arbor or because of a need to change the pumping capacity. In these cases there are certain steps to be followed in making the change. First it should be noted that a pump can be removed either with a hot or a cold spinning head. In some cases it may be desirable to heat the spinning head to melt the polymer inside the pump and its adjoining passages. This will effectively break the otherwise stubborn connection made by the frozen polymer stream.

The first step is to remove the pump drive shaft. This is done by loosening the set screw holding the spline in its position and pulling the spline out of the pump arbor. Next, slide the drive shaft off of the shaft coming out of the gear reducer on the pump motor. This can be done in two ways. The set screw on the shaft can be removed and the entire shaft can then be slipped off; or the universal joint can be separated by swinging the pump shaft to a position ninety degrees from the axis of the gear reducer shaft. The universal joint will

then separate and the shaft can be placed out of the way during the ensuing work.

After removing the shaft, remove the aluminum block that covers the pump. Try pulling it out with a pair of pliers first. If it does not slip out easily, screw a bolt into the threaded hole in the block, and use that bolt to obtain a better grip and leverage on the block. It should come out with the use of a little force.

To remove the pump it is necessary to remove the four bolts that hold it in place in the spinning head. Use the allen wrench with the rachet. If there is sufficient clearance, the pump can be pulled out of the head with a minimum of difficulty. If the head is cold, there may be a problem in breaking the frozen polymer holding the pump in place. In that case heat the head above the melting point of the last polymer pumped through the extruder. After one hour the pump should slide out easily. When working with hot parts, use a pair of pliers and gloves and long sleeves. Polymer burns can be very serious and slow to heal.

If the pump is still tight in the head after heating, it will be necessary to loosen the stainless steel block that forms the left hand side of the pump cavity. Refer to the blue prints of the spinning head to get a clear picture of this block. It is held in place by only one bolt. However, that bolt is very hard to reach. To get to it, open the screw latches that hold the metal cowling around the spinning head and swing the cowling open across the pump cavity. Leave the other half of the cowling in place since it can be removed only after several electrical connections have been broken. Next, loosen

and open the latches that hold the heating band around the lower half of the spinning head. Carefully pull the heating band away from the pump cavity without making sharp bends in the band. It should now be possible to reach the bolt that holds the block next to the pump. Use the appropriate allen wrench and loosen the bolt as much as required to free the pump.

The pump mounts on a lapped face in the spinning head. This mounting plate should be carefully and thoroughly cleaned before installing another pump. Use brass tools when scraping polymer off the lapped surface. This will prevent scratches on the mounting and sealing surface of the wear plate. (If the lapped surface eventually becomes scratched to the point where polymer leaks appear, an effective seal can be made using flat gaskets of copper or hard aluminum between the pump and wear plate. The gasket should be cut to the exact configuration of the pump with inlet, outlet, and bolt holes correctly positioned.)

A new pump can be installed with the spinning head cold. Bolt the pump in its position first, and then reinstall the side block, heater, and cowling in that order. Next place the aluminum block over the pump. Reinstall the pump drive shaft on the gear reducer shaft. If it was originally removed by loosening the set screw, be sure the key is in the shaft before installing it on the reducer shaft. If the pump shaft was removed by separating it at the universal joint, reverse the procedure used to remove it. When done correctly, no force is required to separate and reconnect the shaft at the universal joint. Next slide the drive shaft tang into the pump arbor. If it does not

fit, the pump or the spline must be rotated to bring them into proper alignment. Once the tang is in the pump, use a pair of pliers to rotate the pump and spline together in order to line up the set screw and the set screw slot in the spline. If the pump will not turn easily, do not use excessive force. Wait until the extruder is heated for startup, and then check the pump rotation and make the final drive shaft connection as recommended in the extruder startup instructions.

Winder Gear Changes

The entire range of spinning speeds obtainable from the feed roll cannot be reached with a single set of gears in the Leesona winder. A chart of speed ranges and gear combinations was provided with the machine, and this should be consulted for the correct combination to use for any chosen speed. Gear changing is a relatively simple operation. The gears that determine the spindle speed are located on the drive motor and the end of the spindle. They are connected by a timing belt. To change gears, loosen the motor mount bolts and slide the motor toward the spindle gear to produce slack in the timing belt. Remove the belt. Loosen the set screws in the gears and slip them off their shafts. Be sure the keys are not lost during the change. Slide the new gears on the proper shafts and tighten the set screws. Replace the timing belt and slide the motor away from the spindle to tighten the belt. Tighten the motor mount bolts enough to hold the motor temporarily in place while testing the alignment of the gears, belt, and motor. Turn the motor on at a low speed and observe the tracking of the belt on the gears. If the belt tries to run off either of the gears, loosen the motor and slide it around until the

belt is tracking squarely on both gears. When this has been done, stop the motor and tighten the mounting bolts.

Spindle to traverse ratios of 4:1 and 2.5:1 are available on the winder. The higher ratio permits operation at high spinning speeds without damaging the traverse mechanism. The low ratio is actually not needed for the range of speeds normally used. There should be few if any occasions when the traverse ratio will need changing. Winder ratios and the gear combinations required to achieve them are given in the manufacturer's information. Examine the gears that are on hand to determine the exact ratio that can be reached and how the gears must be arranged to give that ratio. Five gears are involved in the change. One of them is located on the spindle shaft inside the winder head. The other four are positioned in two pairs on special mounting fixtures. To change gears, remove the gear from the spindle shaft and replace it with the new one. Remove the two clusters and replace them with the two new clusters. Adjust the positions of the clusters to give smooth meshing without excess pressure between gears. High noise from the winder head indicates the gears are too tight, while play between the traverse motion and the spindle indicates insufficient gear meshing. Adjust until a reasonable compromise is obtained.

Lubrication of Equipment

There are several pieces of operating equipment that should be lubricated at the proper intervals to assure satisfactory operation and extend the life of the equipment. The intervals specified here are for guides only. No damage will be done by lubricating more frequently

than specified herein, and the interval should be shortened if there is reason to think it is beneficial to the equipment.

There are two gear boxes on the spinning machine that should be drained and refilled with fresh oil every 2000 hours of operation. The gear box on the extruder should be filled with ninety weight automotive lubricant. The volume required is approximately 900 mls. The gear box on the meter pump drive should be filled to the mark on the sight glass with the Texaco Meropa lubricant that is stored in the lab.

Lubrication of the column of the spinning machine with twenty weight oil is recommended every two months. The oil can be applied by rubbing it on with a rag. Since the column is exposed to the air, it will collect dust and dirt on the oily surface. The column should be wiped clean with a solvent soaked rag once a year to remove the accumulated dirt and grit. The extruder must not be moved up or down the column without lubrication as there is a danger of seizure between the column and the bushing.

The Leesona winder has an oil sump in the winding head. This sump should always be filled with the lubricant recommended by the manufacturer. Addition of oil should be made as needed. Avoid overfilling the sump. Excess oil will eventually work its way out of the spinning head in several places, and there will be leakage as long as there is excess oil in the head.

Any points of contact between moving and stationary parts should periodically be lubricated with a light weight general purpose oil. Also any parts that appear to be rusting should be wiped occasionally with an oily rag.

B. RIGAKU ROTATING ANODE X-RAY GENERATOR

Modifications Made on the Machine

Two important modifications were made on the rotating anode x-ray machine when it was first readied for operation. One of these was a modification of the diffusion pump, and the other was the relocation of the anode drive motor. Pertinent details relating to each of these are discussed below.

The diffusion pump was modified by inserting a "spool piece" between the pump and the flange it mates with on the manifold valve. This spool piece is approximately four and a half inches long, and it is wrapped externally with copper tubing to permit circulation of cooling water. Internally there are three semicircular baffle plates located in staggered positions to cause tortuous flow of gases and minimize entrainment of droplets of diffusion pump oil. The flanges are sealed by o-ring gaskets. Cooling water is circulated through the spool piece in series with the normal diffusion pump. This piece provides an additional length of cooled wall for condensing diffusion oil vapors and stopping entrained mist. These features permit extended operation under vacuum without loss of oil and its attendant contamination of the interior surfaces of the high vacuum section of the machine.

The anode drive motor was moved to make a clear passage for fiber passing through a drilled hole in the top of the machine. This was accomplished with the aid of an idler pulley and a second v-belt. The belt to the anode was provided with a tension adjusting screw which can be reached on the machine's table top. Easy removal of the anode

v-belt is accomplished by loosening the belt, using the tensioning screw, and slipping the belt off the pulley and lifting it up between the pulley and the cathode housing. Belt installation is achieved by reversing the procedure. Final adjustment must be made while the anode motor is driving the anode. The belt should not be too loose since it will bump against the belt housing and wear the belt as well as make noise.

Input Voltage to the Rotating Anode X-Ray Machine

On a few occasions the Rigaku Rotating Anode X-Ray Generator presented problems that did not appear to arise from a known source. In all cases they went away without action by the machine operator or any maintenance personnel. However, the true cause of these problems was not found for a long time because these difficulties would disappear before a complete diagnosis could be made.

On one occasion the problem persisted with a variety of symptoms, and the trouble was traced to its source. First a brief description of the symptoms and then the problem and its solution will be discussed.

On the aforementioned occasion the vacuum system of the x-ray machine was operating, to all appearances, in a normal manner. Generation of x-rays was begun in the usual manner, but before any action was taken to stop the machine, it shut off the x-ray generating circuits. Upon trying to restart x-ray generation a buzzing sound could be heard when the "On" button was pressed, and there was no rotation of the anode, no x-ray generation, nothing except the buzzing. This sound was traced to a relay which, when activated, energized the high voltage circuits and the associated anode drive and regulating circuits.

During this same time of difficulty, the vacuum system was put out of service by shutting off the diffusion pump and the rotary pump. When an attempt was made to restart the vacuum pump, it would not run. It hummed and acted like it was in some state of electrical excitation, but it did not rotate. Upon making a systematic check of the problem using a voltmeter and the circuit diagram, it was found that low voltage existed on one phase of the three phase motor, and low voltage also existed across the energizing circuits of the high voltage relay. Further checks disclosed low voltage at several points in the machine. This was assumed to be the basic problem, and a few points will illustrate its severity.

In the case of the high voltage relay the activating coil was made to operate at 200 volts. It only received 170 volts from the auto-transformer. The entire machine was designed for 240 volts input from the line, but it was getting only 207 from a system that was nominally called a 220 volt system. Of course low voltages resulted from all transformer outputs as a result of the reduced input. It was postulated that the untimely stoppages of the machine were caused by fluctuations in the line voltage which was already lower than what the machine required. In particular the high voltage relay was operating at the lower limit of its range at 170 volts, and a decrease would easily cause the relay to open thus stopping all high voltage operations in the machine. Erratic cycling of the rotary pump motor also occurred at these times leading to a shutdown of all systems beyond the main switch.

To correct the problem a booster transformer was installed in the input line, and the machine was successfully operated with an input of 238 volts. Improvements in operation were immediately obvious. The diffusion pump reached operating temperature faster than before, the rotary pump motor rotated faster, the current overload system functioned properly, and the vacuum gage shifted its reading to higher pressure. Most of these changes were for the better. However, in the case of the vacuum gage a modification was eventually made to eliminate the deviation in its reading.

Elimination of Vacuum Gage Deviation

After increasing input voltage to the x-ray machine by installing a boosting transformer on the feed lines, it was found that the vacuum gage indicated a high pressure inside the vacuum system. A thorough check of the system revealed no leaks, and rotary pump and diffusion pump operation were improved enough by the voltage increase to be causes for pressure decrease rather than increase. The problem was found to be directly caused by increasing the input voltage. This change had also increased the voltage across the ionization gage, and the ionization of the same pressure of gas as was present before the voltage increase now produced an increase in current across the gage due to higher ionizing voltage. This change was shown as higher pressure on the vacuum gage, and this pressure was outside the operating ranges given in the instructions for the rotary pump and diffusion pump. Since the system pressure was actually the same as before and only the gage reading was different, it seemed reasonable to change the gage

voltage to give vacuum readings like those observed before the voltage increase. This was accomplished by installing a variable resistor in the primary circuit of the vacuum gage supply voltage transformer. Adjustment of the primary voltage to the ninety volts previously measured moved the vacuum reading to the same values observed in operations before installation of the booster transformer.

This variable resistor is mounted on the left distribution panel inside the machine. It can be adjusted from the front of the machine with ease. A voltmeter should be used to set the primary voltage to ninety volts if readjustment is ever required.

C. INSTRUCTIONS FOR DATA COLLECTION

Making Diameter Photographs

Use the 35 mm camera with a 135 mm lens and a bellows. A cable release and an eyepiece magnifier will help although they are not required. A shorter focal length lens can be used although it will also reduce the working distance from lens to subject. Use a photoflood lamp to illuminate the filament. Load the camera with Tri-x black and white film. Fasten the camera to a laboratory jack stand, and adjust the jack height as needed to focus on a particular subject. Extend the bellows to its full length to obtain the maximum magnification on the negatives, and adjust the lens focus to its infinity setting. Set the shutter speed at 1/500 second and the f stop to its lowest value. If the camera has a built in exposure meter, turn it off. It will not be used for taking filament photographs.

To take a picture of the fiber, position the flood light to give the maximum illumination of the filament. For best results make the final adjustment of the light while looking through the camera. Adjust the jack stand to the necessary height, aim the camera toward the fiber, and look through the camera while moving the camera back and forth until the fiber is in focus. Do not use the focus adjustment on the lens to focus on the fiber since this will change the magnification on that exposure. Focus only by moving the camera-bellows-lens assembly back and forth while looking through the camera at the fiber. Make a final adjustment on the light, cock the shutter, and take the picture.

After completing a roll of film, label the roll with suitable identifying information. This is best done by scratching on the emulsion side of the film leader with a sharp pointed object. This type of mark will remain on the film throughout the subsequent processing in the darkroom.

At the end of each roll of film take at least one picture of an accurate centimeter scale using the same bellows and focus adjustments as were used on the fiber photos. The exposure meter may be used to set the proper shutter speed and f stop. This scale will be used to compute a magnification factor for later determining the true filament diameters.

Reading the Diameter Photographs

After developing the diameter film, mount the negatives in 2 x 2 inch cardboard slide mounts for projection. Place these slides in a projector and project them onto a gridded screen. Position the

projector so there is no tilt. This will assure the same magnification and focus from top to bottom of the projected image. Project the scale negative, and measure the distance on the screen that is covered by a convenient unit of measure, for example, one centimeter. With this value a distance measured on the screen can be converted to the true dimension of the object photographed. From this point until the completion of the negatives on the roll the scale was on, do not change the position or focus of the projector as this will change the magnification of the image and require the calculation of a new scale factor. Project each diameter photograph and measure the diameter of the filament on the screen. Convert the projected diameter to actual filament diameter using the scale factor.

The projector should be positioned to give as high a magnification as is reasonable to provide the greatest accuracy. This often is not an exceptionally high magnification because the edges of the filament become more indistinct as the magnification is increased. A point is reached where there is nothing to be gained by using higher magnification. Again this is a matter of judgment.

Measuring Fiber Temperature

Fiber temperature measurements are made with the Hastings-Raydist Match-Temp Pyrometer. Position the instrument in a convenient location and plug the power cord into a 110 volt outlet. Connect a millivolt potentiometer to the recorder outlet of the instrument using the instructions provided with the potentiometer for connecting a thermocouple without a reference junction. (For accurate readings the

pyrometer potentiometer combination should be calibrated with known temperature baths such as ice, boiling water, and hot oil for higher temperatures.) The pyrometer probe can be hand held if necessary. However, if measurements are to be made at the same position each time it will be more convenient to clamp the probe on a laboratory ring stand and adjust it to the required height. Air currents will make measurement of fiber temperature difficult. This is especially a problem since the fiber drags air with it and creates quite a breeze at the filament surface when spinning at high takeup velocities. To eliminate this problem carefully place a small tuft of fine glass wool in the open space behind the thermocouple wires on the probe. Be very careful to avoid breaking any of the wires. Some adjustment of the glass wool may be needed to achieve the best elimination of air currents around the thermocouple.

To measure a filament temperature, allow the instrument to warm up for approximately twenty minutes and zero and adjust the potentiometer according to manufacturer's instructions. Switch the Hastings to the RECORD mode and use the potentiometer to measure the output voltage of the thermocouple. Use a table to convert volts to temperature for a chromel-alumel thermocouple. Using the heater adjusting knob on the Hastings, adjust the temperature of the thermocouple to a value estimated to be close to that of the fiber. Use only the potentiometer to determine the thermocouple temperature. After the temperature has been adjusted to the selected value, gently touch the probe to the fiber and note the deflection of the needle of the galvanometer on the potentiometer. A deflection of the needle indicates a difference between the fiber

temperature and the thermocouple temperature. Adjust the thermocouple heater to raise or lower the temperature as was indicated by the direction of the galvanometer deflection. Again contact the fiber and note the deflection. Repeat this procedure as often as necessary until a temperature is found where no galvanometer deflection occurs. At that point the fiber and thermocouple are at the same temperature, and this value can be read from the potentiometer and the table. This procedure is repeated for each measurement needed on the moving fiber.

When contacting the fiber, care should be taken to make the period of contact as short and gentle as possible. There are two good reasons for doing this. First, prolonged contact can lead to errors in temperature measurement due to friction heating of the thermocouple. Second, the use of extreme pressure in contacting the fiber will also increase the friction problem, and it may cause the fiber to break. This of course leads to a delay while the spinning machine is strung up and allowed to line out again. The duration and pressure of a good contact must be learned by experience. It should be as light as possible and as short as possible while still obtaining a readable signal on the potentiometer.

Tension Measurements

A tension measurement may be taken at any desired position on the filament as long as the filament does not break in the process. The most useful data are obtained at or near the takeup device. Follow the manufacturer's instructions for calibrating and using the instrument. Filament diameter does have an effect on the measurements made with this instrument. For best results the calibration should be checked at

the end of each spinning run using a piece of fiber made during that run.

Making X-Ray Diffraction Patterns on a Moving Filament

Follow manufacturer's instructions for startup of the rotating anode x-ray generator. Turn the generator on to produce a beam of low intensity. (20 kv and 15 ma is sufficient.) Turn off the room light. Using a fluorescent screen to observe the beam, place the filament in the guide mounted beneath the film holder track, and adjust the filament's position until it is in the beam. Turn off the x-ray beam. Turn on the room lights, and place the film cassette, with fresh film in it, on the track and move it to a position 3 cm away from the fiber. Place the portable shields around the radiation area and turn on the x-ray beam. Adjust the x-ray generator to the desired settings, set the timer for the desired time, and set the machine to turn off automatically. To minimize x-ray exposure, leave the spinning platform during the time of exposure.

After the machine shuts off, remove the film cassette and place the film in a secure place until it can be developed. Place fresh film in the cassette. Repeat the procedure for each pattern needed on a moving filament.

For a stationary sample, such as a sample from a bobbin of fiber, the procedure is essentially the same. A holder for a small piece of fiber is required and the filament guide used for spinning fiber is not used in this case.

VITA

John Robert Dees was born in Vernon, Alabama on October 17, 1940. He grew up in Birmingham, Alabama where he attended Woodlawn High School. In 1963 he graduated from Georgia Institute of Technology on the co-operative plan with a Bachelor of Chemical Engineering Degree. He accepted a job with Chemstrand Company, a subdivision of Monsanto Company, in Pensacola, Florida. From 1964 to 1966 he served in the Army Chemical Corps as Assistant Post Chemical Officer at Fort Benning, Georgia. Upon Completion of military service, he returned to employment with Monsanto Company at its Decatur, Alabama synthetic fiber plant.

He entered the University of Tennessee in September 1970 and received a Ph.D. in Chemical Engineering in June 1974. He is a member of the American Institute of Chemical Engineers, Tau Beta Pi, and Sigma Xi. He has been located at the Technical Center of Monsanto Textiles Company in Pensacola, Florida since January 1973.

He is married to the former Jo Ann Armstrong of Atlanta, Georgia; and they have two daughters, Sheron Rene' and Kathy Ellen.